



**Intercellular communication in
filamentous cyanobacteria**

Dennis J. Nürnberg

A thesis submitted for the degree of

Doctor of Philosophy

Statement of originality

I, Dennis J. Nürnberg, confirm that the research included within this thesis is my own work or that where it has been carried out in collaboration with, or supported by others, that this is duly acknowledged below and my contribution indicated. Previously published material is also acknowledged below.

I attest that I have exercised reasonable care to ensure that the work is original, and does not to the best of my knowledge break any UK law, infringe any third party's copyright or other Intellectual Property Right, or contain any confidential material.

I accept that the College has the right to use plagiarism detection software to check the electronic version of the thesis.

I confirm that this thesis has not been previously submitted for the award of a degree by this or any other university.

The copyright of this thesis rests with the author and no quotation from it or information derived from it may be published without the prior written consent of the author.

London, 25 August 2014

Work presented in this study has been partially published:

Nürnberg DJ, Mariscal V, Parker J, Mastroianni G, Flores E, Mullineaux CW (2014) Branching and intercellular communication in the Section V cyanobacterium *Mastigocladus laminosus*, a complex multicellular prokaryote. *Mol Microbiol* **91**: 935–949.

Abstract

Cyanobacteria represent one of the morphologically most diverse groups in the bacterial world, and one of the few where true multicellularity evolved. Their diversity ranges from single cells to branched filamentous forms. Some filamentous cyanobacteria are additionally able to undergo cell differentiation forming a two cell type system that represents the simplest model of multicellularity. *Anabaena* sp. PCC 7120 has been studied extensively in recent years as a model organism. Under nitrogen deprivation it differentiates photosynthetically-active vegetative cells into heterocysts, specialised cells for nitrogen fixation. Accordingly, true multicellularity of nitrogen-fixing cyanobacteria requires different forms of intercellular communication and mutual exchange of nutritional and regulatory compounds.

Although several studies could show that molecules are exchanged between cells in *Anabaena* sp. PCC 7120, little is known about the properties and routes that allow molecules to diffuse between adjacent cells. In this work, the transfer of several physiologically-important molecules was investigated, including the fluorescent sucrose analogue esculin, the fluorescent glucose derivatives 2-NBDG (2-(*N*-(7-Nitrobenz-2-oxa-1,3-diazol-4-yl)amino)-2-deoxyglucose) and 6-NBDG (6-(*N*-(7-Nitrobenz-2-oxa-1,3-diazol-4-yl)amino)-6-deoxyglucose), and the artificial fluorescent tracer BCECF (2',7'-Bis-(2-carboxyethyl)-5-(and-6-)carboxyfluorescein). Furthermore, the role of the septal proteins FraC, FraD and SepJ for the exchange of these molecules was examined in *Anabaena* sp. PCC 7120. Confocal microscopy and fluorescence recovery after photobleaching (FRAP) experiments reveal that cytoplasmic diffusion through channels between neighbouring cells is the primary route for molecular exchange. Loss of FraC, FraD and SepJ strongly reduced the movement of molecules between cells. Overexpression of *sepJ* altered the heterocyst

spacing pattern in *Anabaena* sp. PCC 7120, suggesting a role of SepJ for the diffusion of regulators.

Further, multicellularity in terms of intercellular communication was explored in *Mastigocladus laminosus*, a true branching cyanobacterium that is one of the morphologically most complex prokaryotes. FRAP analyses indicate the cytoplasmic continuity of the filament network and the dependency of molecular exchange on the morphology of the trichomes.

Acknowledgements

I am especially grateful to my supervisor Professor Conrad Mullineaux for his support and gentle guidance throughout my PhD project. I deeply appreciate his way of encouraging me to follow my research interests but also giving advice when needed. I am thankful for involving me into collaboration projects that gave me the opportunity to broaden my horizons. The meetings and discussions with him have always been a great source of motivation to me.

I also like to express my deepest gratitude to Professor Enrique Flores and Professor Antonia Herrero for their hospitality during my research stay in Seville and the fruitful collaboration that has evolved. Without their expertise this work would not have been possible. I am indebted to Professor Flores for his approachability during my entire PhD and for the inspiring discussions on several cyanobacterial research topics.

I am thankful to Dr Vicente Mariscal for introducing me into the ‘world of *Anabaena*’, his friendly way of explaining research techniques and methods are an inspiring example to me. It has been a great pleasure to work with him. I thank all people from the Flores and Herrero lab for making work and life in Seville so pleasant, in particular, Mireia, Laura, Silvia, Antonio, Sergio, Leticia, Victoria, Jose-Enrique, Ana, Dinka, Alvaro and Félix.

I thank Graham McPhail and Giulia Mastroianni for teaching me how to prepare samples for transmission electron microscopy and using the TEM. I am also grateful to Dr Jon Nield for his introduction to TEM and the support from Dr Zofia Luklinska at the NanoVision centre. I thank Anika Wiegard and Laura Corrales-Guerrero for

working together on the development of protocols for protein localisation by immunogold-labelling.

I am grateful to all people in the Mullineaux lab that helped to realise my PhD project and made working in the lab a real pleasure. In particular, Anja for introducing me to confocal microscopy and FRAP analyses, Sam for her support in generating mutants of *Synechocystis*, Luning and Tchern for their support in TIRF microscopy with Dr Liming Ying and Dr Ann Wheeler, Joanna, Thomasz, Sam, Petra and Gianna for their helpful discussions and Samiha, Mimi, Claudia, Jamie, Mahilini and Dorota for supporting my work with various experiments during their project studies.

I am indebted to all people I had the chance to collaborate with during my PhD. I am especially grateful to Professor Wolfgang Lockau, Dr Thomas Volkmer, Friederike Klemke and Dr Gabi Bayer for continuing the work on the cyanophycin and polyphosphate projects and Dr Norbert Krauß, Dr Bob Janes, Dr Soshichiro Nagano and Dr Kristina Zubow for becoming part of the team. I thank Professor Annegret Wilde for involving me into work on the motility of *Synechocystis*, Dr David Lea-Smith for working on the alkane project, Dr Raquel Cantos for investigating her ‘bombillo’ mutant, Dr Ron Cutler, Dr Hermine Mkrtychyan and Nan Wang for working on *Staphylococcus* biofilms, Dr Marianne Gründel for her support on the isolation of glycogen and Professor Jason Micklefield, Dr Anna-Winona Struck and Matthew Bennett for synthesising the fluorescent PatS pentapeptide. I am indebted to Professor Achilleas Frangakis for giving me the opportunity to work in his group on electron tomography and I am grateful to Dr Anja Seybert and Johnson Madrid for supporting my work in Frankfurt.

I am thankful to Professor Peter Wolk for providing plasmid pRL623 for conjugation, Professor Theodorus Gadella and Dr Joachim Goedhart for providing plasmid pmTurquoise2-C1 for protein localisation studies, and Professor Lockau and Thomas Volkmer for providing cyanophycin.

I thank the members of my PhD advisory panel Professor Richard Pickersgill and Dr Norbert Krauß for following my progress and giving advises.

I appreciate the helpful discussions with Dr Karina Stucken on identifying *sepJ* in *Mastigocladus laminosus*, Dr Iris Maldener on her fabulous nanopore assay, Dr Patricia Sanchez-Baracaldo on the evolution of cyanobacteria, and Professor Teresa Thiel, Professor Jim Golden, Professor Jack Meeks and Professor Peter Wolk on several aspects of cyanobacterial research.

I acknowledge Queen Mary University of London for the college studentship. I am also indebted to the University of London Central Research fund for supporting my research stays in Seville, and the Biochemical Society, the Society for General Microbiology, the British Broadcasting Company and the European Science Foundation for their financial support for attending conferences.

Finally, I thank my family and friends for their constant support. I am especially grateful to Christine for recognising and supporting my dreams even in difficult times, Jürgen for being always supportive and an example of willpower, Alexandra and Bernd for their helpful discussions, Franziska and Arne for being always there when needed and my beloved fiancée Nadine for filling my life with love and happiness. This thesis is dedicated to you.

Abbreviations

2-NBDG	2-(<i>N</i> -(7-Nitrobenz-2-oxa-1,3-diazol-4-yl)amino)-2-deoxyglucose
5-CFDA	5-carboxyfluoresceindiacetate
6-NBDG	6-(<i>N</i> -(7-Nitrobenz-2-oxa-1,3-diazol-4-yl)amino)-6-deoxyglucose
AM	acetoxymethylester
Amp	ampicilin
ANOVA	analysis of variance
APS	ammonium persulfate
ATCC	American Type Culture Collection
ATP	adenosine triphosphate
BCECF	2',7'-Bis-(2-carboxyethyl)-5-(and-6-)carboxyfluorescein
CC domain	coiled-coil domain
CCD	charge-coupled device
CCMEE	Culture Collection of Microorganisms from Extreme Environments
CCY	Culture Collection Yerseke
cfu	colony forming units
Chl <i>a</i>	chlorophyll <i>a</i>
CM	cytoplasmic membrane
Cm	chloramphenicol

CMOS	complementary metal-oxide semiconductor
CP	cyanophycin
CphA	cyanophycin synthetase
CTAB	cetyltrimethyl ammonium bromide
D	diffusion coefficient
DME family	drug/metabolite exporter family
DMSO	dimethyl sulfoxide
E	exchange coefficient
EDTA	ethylenediaminetetraacetic acid
EF	exoplasmic fracture face
Em	erythromycin
eYFP	enhanced yellow fluorescent protein
F	flux coefficient
FFEM	freeze-fracture electron microscopy
FRAP	fluorescence recovery after photobleaching
FWHM	full width at half-maximum
GFP	green fluorescent protein
GOE	Great Oxygenation Event
HEP-layer	heterocyst envelope polysaccharide layer
HGL-layer	heterocyst-specific glycolipid layer
HRP	horseradish peroxidase

I _F	immobile fraction
IMG database	Integrated Microbial Genomes database
IUCC	Indiana University Culture Collection of Algae
Km	kanamycin
L region	linker region
L-BMAA	β - <i>N</i> -methylamino-L-alanine
MBIC	Marine Biotechnology Institute Culture Collection, Japan
MCH	multiple contiguous heterocysts
M _F	mobile fraction
NBD	nitrobenzoxadiazole
Nm	neomycin
NTA	nitrilotriacetic acid
OM	outer membrane
orf	open reading frame
P domain	permease domain
PBS	phosphate buffered saline
PCC	Pasteur Culture Collection
PCR	polymerase chain reaction
PF	protoplasmic fracture face
PMT	photomultiplier
pO ₂	partial pressure of oxygen

R	recovery rate constant
ROI	region of interest
rpm	revolutions per minute
SAG	Sammlung von Algenkulturen Göttingen
SDS	sodium dodecyl sulphate
SDS-PAGE	sodium dodecyl sulphate polyacrylamide gel electrophoresis
Sm	streptomycin
Sp	spectinomycin
SUT	sucrose uptake transporters
TAT system	twin-arginine translocation system
Tc	tetracycline
TEM	transmission electron microscopy
TEMED	N,N,N',N'-tetramethylethylenediamine
TMH	transmembrane helix
UTEX	Culture Collection of Algae at the University of Texas at Austin

Table of contents

1	Introduction	25
1.1	Morphological diversity and classification of cyanobacteria	26
1.2	Nitrogen fixation as a prerequisite for intercellular communication.....	28
1.3	Routes of molecular exchange between cells	39
1.4	Distribution and structural characteristics of septal junctions and nanopores in cyanobacteria	47
1.5	Proteins forming septal junctions and nanopores	54
1.6	Aims and scope of the thesis	64
2	Materials and methods	66
2.1	Oligonucleotides	66
2.2	Strains and plasmids	66
2.3	Bioinformatics methods.....	73
2.3.1	Generation of plasmids and oligonucleotide primers.....	73
2.3.2	Amino acid sequence analyses	73
2.3.3	Blast search, sequence alignment and phylogenetic reconstruction.....	73
2.3.4	Physicochemical properties of molecules	73
2.4	Microbial methods	74
2.4.1	Growth of cyanobacteria	74
2.4.2	Growth of <i>Escherichia coli</i>	77
2.4.3	Cryopreservation and recovery	77

2.4.4	Preparation of chemical competent <i>E. coli</i> cells	78
2.4.5	Transformation of <i>E. coli</i> cells with plasmids.....	79
2.4.6	Conjugation of cyanobacteria.....	79
2.4.6.1	Conjugation of <i>Anabaena</i> sp. PCC 7120	79
2.4.6.2	Conjugation of <i>M. laminosus</i> SAG 4.84	81
2.4.7	Determination of Chlorophyll <i>a</i> concentration	81
2.5	Genetic methods	82
2.5.1	Genomic DNA isolation from cyanobacteria.....	82
2.5.2	Plasmid isolation	84
2.5.3	DNA quantification	85
2.5.4	Polymerase chain reaction (PCR).....	86
2.5.5	Purification of PCR products	87
2.5.6	Agarose gel electrophoresis.....	87
2.5.7	DNA extraction from agarose gels	88
2.5.8	Restriction digestion.....	88
2.5.9	Dephosphorylation of DNA	89
2.5.10	Ligation	89
2.5.11	DNA sequencing	89
2.6	Biochemical methods.....	89
2.6.1	Heterocyst isolation from <i>Anabaena</i> sp. strains.....	89
2.6.2	Membrane isolation from <i>Anabaena</i> sp. strains.....	90

2.6.3	SDS-PAGE.....	91
2.6.4	Western Blot and protein detection	93
2.7	Microscopy and spectroscopy.....	94
2.7.1	Bright-field microscopy	94
2.7.1.1	Alcian Blue Staining	94
2.7.2	Fluorescence and confocal microscopy.....	94
2.7.2.1	Fluorescent cell labelling	96
2.7.2.1.1	Labelling with fluorescent tracers for molecular exchange experiments.....	97
2.7.2.1.2	Fluorescent labelling of specific cell components.....	98
2.7.2.2	Visualisation and FRAP.....	98
2.7.2.3	Data analysis	99
2.7.3	Immunofluorescence localisation – sample preparation and fluorescence microscopy	100
2.7.4	Transmission Electron Microscopy (TEM).....	101
2.7.4.1	Sample preparation and visualisation of thin-sections.....	101
2.7.5	Fluorescence spectroscopy	103
3	Properties of transferred molecules between cells and their possible pathways in <i>Anabaena</i> sp. PCC 7120.....	104
3.1	Exchange of the sucrose analogue esculin in <i>Anabaena</i> sp. PCC 7120	105
3.1.1	Uptake of esculin by <i>Anabaena</i> sp. PCC 7120	106
3.1.2	Esculin as a fluorescent probe for intercellular communication	112

3.1.3	Intercellular diffusion of esculin in filaments of <i>Anabaena</i> sp. PCC 7120	113
3.1.4	Kinetics of esculin exchange and influence of the septal proteins SepJ, FraC and FraD on intercellular communication in <i>Anabaena</i> sp. PCC 7120.....	116
3.1.5	Loss of metabolic communication in senescent heterocysts	119
3.1.6	Conclusion.....	124
3.2	Exchange of fluorescent glucose analogues in <i>Anabaena</i> sp. PCC 7120..	124
3.2.1	Uptake of 2- and 6-NBDG by <i>Anabaena</i> sp. PCC 7120.....	125
3.2.2	Expression of a glucose uptake system from <i>Nostoc punctiforme</i> ATCC 29133 in <i>Anabaena</i> sp. PCC 7120.....	127
3.2.3	Intercellular diffusion of 2- and 6-NBDG in CSDN21	130
3.2.4	Kinetics of intercellular 2- and 6-NBDG diffusion in CSDN21	139
3.2.5	Influence of septal proteins FraC, FraD and SepJ on intercellular transfer of 2-NBDG.....	141
3.2.6	Conclusion.....	142
3.3	Exchange of BCECF in <i>Anabaena</i> sp. PCC 7120	143
3.3.1	Uptake of BCECF and kinetics of its transfer in <i>Anabaena</i> sp. PCC 7120	144
3.3.2	Influence of the septal proteins SepJ, FraC and FraD on the exchange of BCECF.....	147
3.3.3	Conclusion.....	147

3.4	Summary.....	148
4	Overexpression of <i>sepJ</i> in <i>Anabaena</i> sp. PCC 7120	154
4.1	Generation of mutants with increased <i>sepJ</i> expression in <i>Anabaena</i> sp. PCC 7120.....	154
4.2	Influence of <i>sepJ</i> overexpression on filament length	159
4.3	Influence of <i>sepJ</i> overexpression on diazotrophic growth and heterocyst spacing pattern	161
4.3.1	Influence of <i>sepJ</i> overexpression on intercellular communication	163
4.4	Influence of <i>sepJ</i> overexpression on protein localisation and molecular exchange of calcein and 5-CFDA.....	165
4.5	Conclusion	172
5	Regulation, redistribution and remodelling of intercellular communication in <i>Anabaena</i> sp. PCC 7120 after filament fragmentation.....	175
5.1	Filament fragmentation by sonication and its influence on cell viability..	176
5.2	Influence of filament fragmentation on molecular exchange of 5-CFDA.	177
5.3	Co-localisation of SepJ and 5-CFDA in <i>Anabaena</i> sp. PCC 7120.....	179
5.4	Influence of filament fragmentation on intercellular communication	184
5.5	Ultrastructure of fragmented filaments.....	185
5.6	Influence of fragmentation on the localisation of SepJ	186
5.7	Cell death in an aging culture of <i>Anabaena</i> sp. PCC 7120	187
5.8	Conclusion	190

6	Morphological complexity and intercellular communication in the	
	Section V cyanobacterium <i>Mastigocladus laminosus</i>	192
6.1	Development of different branching types in <i>M. laminosus</i>	195
6.2	Intercellular communication between branch and main trichome in <i>M. laminosus</i>	200
6.3	Visualisation of septal junctions in <i>M. laminosus</i>	201
6.4	Identification and composition of SepJ in <i>M. laminosus</i>	204
6.5	Localisation of SepJ in <i>M. laminosus</i>	208
6.6	Generation and characterisation of a <i>sepJ</i> inactivation mutant of <i>M. laminosus</i>	210
6.7	Characterisation of the <i>sepJ</i> inactivation mutant MLDN42.....	213
6.8	Intercellular communication between cells of different trichome types in <i>M. laminosus</i>	216
6.9	Barriers to cell-cell communication in the life cycle of <i>M. laminosus</i>	221
6.10	Conclusion	226
7	Summary and outlook	229
8	Appendix	238
9	Bibliography	242

List of figures

Figure 1. Morphological diversity of cyanobacteria.	28
Figure 2. Diazocytes in filaments of <i>Trichodesmium erythraeum</i> IMS101.	31
Figure 3. Two stage model for the establishment of the heterocyst spacing pattern in filamentous cyanobacteria.	34
Figure 4. Metabolites and regulators possibly being exchanged between vegetative cells and heterocysts in <i>Anabaena</i> sp. PCC 7120.	39
Figure 5. Outline of a FRAP experiment for a multicellular organism.	40
Figure 6. Presence of septal junctions and nanopores in cyanobacteria revealed by electron microscopy.	52
Figure 7. Predicted composition and topology of SepJ from <i>Anabaena</i> sp. PCC 7120.	55
Figure 8. Localisation of SepJ-GFP in <i>Anabaena</i> sp. PCC 7120.	59
Figure 9. Schematics of a fluorescence and confocal microscope.	95
Figure 10. Custom-built temperature-controlled sample holder for confocal microscopy.	99
Figure 11. Uptake of esculin by <i>Anabaena</i> sp. PCC 7120 filaments.	107
Figure 12. Sub-cellular distributions of esculin, chlorophyll and periplasmic GFP from confocal fluorescence images.	108
Figure 13. pH and oxygen dependence of esculin fluorescence.	110
Figure 14. Time-course for esculin uptake in <i>Anabaena</i> sp. PCC 7120 cells under different growth conditions and effect of sucrose competition.	111

Figure 15. Examples of FRAP experiments monitoring intercellular exchange of esculin in filaments of <i>Anabaena</i> sp. PCC 7120.	115
Figure 16. Testing for interaction of esculin and cyanophycin <i>in vitro</i>	117
Figure 17. Esculin labelling of <i>Anabaena</i> sp. PCC 7120 heterocysts.	121
Figure 18. Esculin labelling of heterocysts in an <i>Anabaena</i> sp. PCC 7120 mutant lacking cyanophycin synthetase CphA1.	123
Figure 19. Uptake of 2-NBDG by <i>Anabaena</i> sp. PCC 7120 and <i>N. punctiforme</i> ATCC 29133.	126
Figure 20. Sugar uptake properties of strain CSDN21.	129
Figure 21. Examples of FRAP experiments monitoring intercellular exchange of 2- NBDG in CSDN21.	131
Figure 22. Frequency of fluorescence recovery in FRAP experiments using 2-and 6-NBDG.	132
Figure 23. Labelling of heterocysts with 2-NBDG.	134
Figure 24. Influence of L-BMAA on uptake and transfer of 2- and 6-NBDG in CSDN21 and formation of NBDG-glycogen.	137
Figure 25. Degradation of 2-NBDG in filaments of CSDN21 and pH dependence of 2-NBDG fluorescence.	139
Figure 26. Example of FRAP experiments monitoring intercellular of BCECF exchange between vegetative cells in <i>Anabaena</i> sp. PCC 7120.	145
Figure 27. Comparison of molecular exchange in <i>Anabaena</i> sp. PCC 7120.	150
Figure 28. Construction of <i>sepJ</i> overexpression plasmids and genotypes of the corresponding strains.	156

Figure 29. SepJ protein levels in <i>Anabaena</i> sp. PCC 7120 wild-type and overexpression strains.....	158
Figure 30. Influence of <i>sepJ</i> overexpression on filament length in <i>Anabaena</i> sp. PCC 7120.....	161
Figure 31. Heterocyst formation in CSVM34-DN2A and CSDN2A.....	162
Figure 32. Construction of the <i>sepJ-gfp</i> overexpression mutant CSDN11.....	165
Figure 33. Fluorescent <i>E. coli</i> cells surrounding <i>Anabaena</i> sp. PCC 7120 during conjugation.....	167
Figure 34. Localisation of SepJ-GFP in <i>Anabaena</i> sp. PCC 7120 strains CSDN11 and CSAM137.....	169
Figure 35. Localisation of SepJ-GFP in CSVM34-DN11 and CSVM141-DN11...	171
Figure 36. Localisation of SepJ-GFP in <i>Anabaena</i> sp. PCC 7120 strains CSAM137 and CSDN11 48 h after nitrogen step down.....	172
Figure 37. Growth of <i>Anabaena</i> sp. PCC 7120 after fragmentation.....	177
Figure 38. 5-CFDA labelled filaments of <i>Anabaena</i> sp. PCC 7120 after fragmentation by sonication.....	178
Figure 39. Co-localisation of SepJ-mTurquoise2 and 5-CFDA in strain CSDN28. .	181
Figure 40. Co-localisation of SepJ-eYFP and 5-CFDA in strain CSDN7.....	182
Figure 41. Co-localisation of SepJ-mTurquoise2 and 5-CFDA in strain CSDN28 after fragmentation by sonication.....	183
Figure 42. Recovery of 5-CFDA in CSDN28 after filament fragmentation by sonication.....	184

Figure 43. Electron micrograph of an ultra thin section through the septal region of <i>Anabaena</i> sp. PCC7120 after fragmentation by sonication.	185
Figure 44. Redistribution of SepJ-GFP after fragmentation on strain CSAM137. .	187
Figure 45. Labelling of an aging culture of <i>Anabaena</i> sp. PCC 7120 with 5-CFDA.	189
Figure 46. Localisation of SepJ-GFP in an aging culture of CSAM137.....	190
Figure 47. Morphological complexity of <i>M. laminosus</i>	194
Figure 48. Different types of branching in <i>M. laminosus</i> , and their development revealed by confocal and transmission electron microscopy.....	196
Figure 49. Variations of branching in <i>M. laminosus</i>	198
Figure 50. Inhibition of terminal filament growth by remaining cell fragments.....	199
Figure 51. Intercellular transfer of 5-CFDA between branch and main trichome in a ‘T’-branch of <i>M. laminosus</i>	201
Figure 52. Electron micrographs of ultra thin sections through the septal region of <i>M. laminosus</i>	203
Figure 53. Design of primers for the identification of <i>sepJ</i> in <i>M. laminosus</i> based on sequence alignments using ClustalW 2.1.	205
Figure 54. 16S rRNA phylogenetic tree of <i>Mastigocladus/Fischerella</i> spp.	207
Figure 55. Localisation of SepJ by immunofluorescent labelling in <i>M. laminosus</i> .	209
Figure 56. Generation and verification of the <i>sepJ</i> inactivation mutant MLDN42.	212
Figure 57. Characterisation of mutant MLDN42.	215
Figure 58. Position of heterocysts in filaments of <i>M. laminosus</i>	219

Figure 59. Heterocyst-heterocyst connection in a narrow trichome of <i>M. laminosus</i> .	220
Figure 60. Function of necridia in intercellular communication, and their localisation in filaments of <i>M. laminosus</i> .	223
Figure 61. Appearance of necridia after filament release.	225
Figure 62. Uptake and diffusion of NBD-PatS5 in <i>Anabaena</i> sp. PCC 7120 grown in BG11.	232
Figure 63. Physiological importance of NBD-PatS-5.	233

List of tables

Table 1. Distribution and diameter of septal junctions among cyanobacteria studied by thin-section TEM.	48
Table 2. Distribution of septal junctions among cyanobacteria studied by FFEM. ..	51
Table 3. Distribution and characteristics of nanopores in the septa of cyanobacteria.	53
Table 4. Oligonucleotides used in this study.	66
Table 5. Strains and plasmids used in this study.	67
Table 6. Composition of BG11 ₀ medium.	75
Table 7. Composition of Castenholz D and Castenholz ND medium.	76
Table 8. Composition of LB medium, variation Miller.	77
Table 9. Composition of the solutions I, II and III for plasmid isolation.	85
Table 10. PCR cycling procedure	87
Table 11. Composition of electrophoresis buffers and loading dye.	88
Table 12. Composition of buffers for heterocyst isolation from <i>Anabaena</i> sp. strains.	90
Table 13. Composition of buffers for the isolation of membranes from <i>Anabaena</i> sp. species	91
Table 14. Composition of stacking gel and separation gel for SDS-PAGE.	92
Table 15. Composition of SDS loading dye and SDS running buffer.	92
Table 16. Fluorophores used in this study.	97

Table 17. Composition of phosphate buffer and Araldite resin for the preparation of samples for TEM.....	103
Table 18. Kinetics of esculin exchange from FRAP measurements on filaments of <i>Anabaena</i> sp. PCC 7120.	119
Table 19. Kinetics of 2- and 6-NBDG exchange from FRAP measurements on filaments of CSDN21 and related mutants.....	141
Table 20. Kinetics of BCECF exchange from FRAP measurements on filaments of <i>Anabaena</i> sp. PCC 7120 and septal mutants.....	146
Table 21. Recovery rate constants for calcein, BCECF, 5-CFDA, 2-NBDG and esculin under plus (BG11) and minus N (BG11 ₀) conditions.....	149
Table 22. Comparison of molecular exchange in <i>Anabaena</i> sp. PCC 7120.....	152
Table 23. Predicted physico-chemical properties of fluorophores used to probe intercellular communication in <i>Anabaena</i> sp. PCC 7120.	153
Table 24. Kinetics of calcein and 5-CFDA exchange from FRAP measurements on <i>Anabaena</i> filaments overexpressing <i>sepJ</i>	164
Table 25. Exchange (E) and flux coefficients (F) for 5-CFDA in <i>M. laminosus</i>	217
Table 26. Distribution and composition of SepJ-like proteins and DME-family permeases among cyanobacteria	238

1 Introduction

Cyanobacteria are the only known prokaryotes that are capable of oxygenic photosynthesis. Uptake and stable integration of one of these ancestral phototrophic prokaryotes into a eukaryotic organism by a process called primary endosymbiosis led to the evolution of the chloroplasts found today (Gould *et al.*, 2008). Cyanobacteria exhibit a great biochemical and morphological diversity and can be found in almost all habitats on our planet, including extreme environments such as hot springs (Castenholz, 1969) and polar regions (Vincent, 2007). Recent data suggest that cyanobacteria evolved around 3 billion years ago when first low but appreciable levels of atmospheric oxygen could be detected in rocks from the Pongola Supergroup in South Africa (Crowe *et al.*, 2013). Further proof for the early presence of cyanobacteria was obtained by phylogenetic analyses using 16S rRNA and fossil records (Schopf, 2012; Schirmermeister *et al.*, 2013). These studies date the existence of cyanobacteria to more than 2.7 billion years ago. Additional analyses using phylogenetic reconstructions and trait analyses indicate that these early cyanobacteria were presumably unicellular strains with small cell diameters that were restricted to freshwater ecosystems for several hundred million years until they started diversifying and moving into coastal brackish and marine environments at around 2.4 billion years ago (Blank and Sánchez-Baracaldo, 2010). This time point closely coincides with the ‘Great Oxygenation Event’ (GOE) (Bekker *et al.*, 2004), an event that led to a significant increase of the partial pressure of oxygen (pO_2) in the atmosphere from initially less than 0.002 atm to about 0.02 to 0.04 atm between 2.45 and 1.85 billion years ago (Holland, 2006).

The presence of multicellular cyanobacteria around the time of the GOE is well supported by recent phylogenetic studies (Tomitani *et al.*, 2006; Schirromeister *et al.*, 2011; Schirromeister *et al.*, 2013). The latest of these studies even suggests that multicellularity evolved earlier than the GOE and that multicellularity might have played a key role in triggering cyanobacterial evolution and diversification around the GOE (Schirromeister *et al.*, 2013). Although cyanobacteria were presumably already able to form heterocysts, specialised cells for nitrogen fixation, at this time (Tomitani *et al.*, 2006), it took more than a billion years until marine planktonic unicellular nitrogen fixing cyanobacteria evolved (850-635 million years ago) (Sánchez-Baracaldo *et al.*, 2014). The delayed evolution might be a result of the insufficient availability of trace elements such as molybdenum and vanadium in the open ocean at the time of the GOE which are essential co-factors of the nitrogenase, the nitrogen fixing enzyme (Sánchez-Baracaldo *et al.*, 2014).

1.1 Morphological diversity and classification of cyanobacteria

It is remarkable that multicellularity in cyanobacteria has evolved as early as the GOE and that the phylum reached its maximum morphological complexity around 2 billion years ago which remained almost unchanged until today (Damuth, 2001). According to their strong morphological variations, cyanobacteria have been divided into five sections, including unicellular forms (Section I and II), filamentous (Section III and IV) and filamentous-branching forms (Section V) (Rippka *et al.*, 1979). Cyanobacteria of Section I (formerly known as order Chroococcales) divide by binary fission while species of Section II (Pleurocapsales) exhibit a special mode of reproduction. Large cells undergo multiple fissions within the outer wall layer resulting in the release of small,

spherical daughter cells called baeocytes (Herdman and Rippka, 1988). Occasionally, cyanobacteria of the *Pleurocapsa* group (Section II) undergo binary fission which results in the formation of irregular cellular aggregates that resemble filaments but without plasmatic connections between these cells (pseudofilaments) (Rippka *et al.*, 1979). Real filaments of different complexity can only be observed in cyanobacteria of Sections III, IV and V. While filaments of cyanobacteria of Section III (Oscillatoriales) consist only of a single cell type, organisms of Section IV (Nostocales; including model organism *Anabaena* sp. PCC 7120) and Section V (Stigonematales; including the potential model organism *Mastigocladus laminosus*) show additionally the ability to undergo cell differentiation, forming specialised cells for nitrogen fixation (heterocysts), and sometimes also akinetes (resting cells) and hormogonia (motile filaments for dispersal and symbiosis competence) (Rippka *et al.*, 1979). Cyanobacteria of Section V exhibit further morphological complexity. Cellular division occurs in multiple planes, resulting in the formation of true branches. The morphological diversity of cyanobacteria is shown in Figure 1.

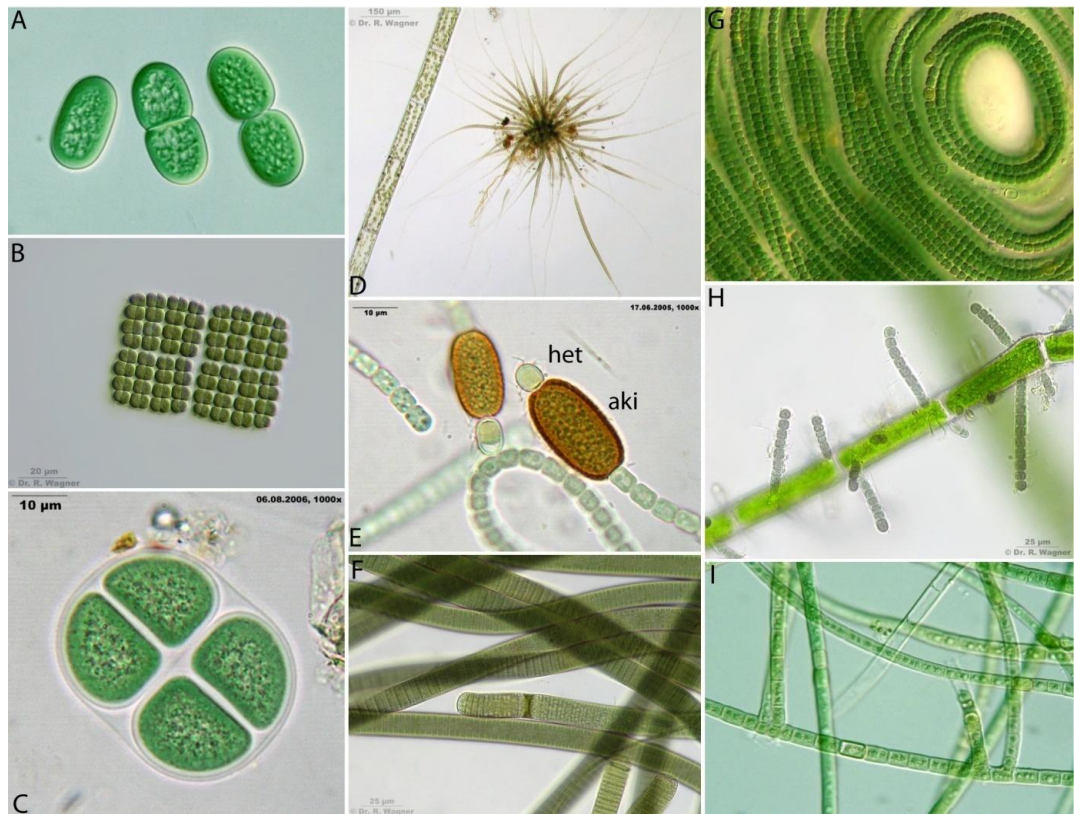


Figure 1. Morphological diversity of cyanobacteria.

(A) *Cyanothece aeruginosa* (Section I). (B) *Merismopedia* sp. (Section I) (C) *Chroococcus turgidus* (Section I). (D) *Gloeotrichia echinulata* (Section IV). (E) *Cylindrospermum* sp. (Section IV) with akinetes (aki) and heterocysts (het). (F) *Oscillatoria limosa* (Section III). (G) *Trichormus variabilis* (Section IV). (H) *Stichosiphon sansibaricus* (epiphytic with the green algae *Cladophora*) (Section III). (I) *Hapalosiphon hibernicus* (Section V). Photos A and I by Dr Yuuji Tsukii, Protist Information Server (protist.i.hosei.ac.jp), photos B - F and H by Dr Ralf Wagner (dr-ralf-wagner.de), and photo G by Dr Lira Gaysina.

1.2 Nitrogen fixation as a prerequisite for intercellular communication

Although nitrogen is the fifth most abundant element in our biosphere, it is only accessible for the incorporation into biological molecules such as proteins and DNA after its reduction to ammonium. The ability to fix nitrogen therefore limits

the productivity of the biosphere (Gruber and Galloway, 2008). Biological nitrogen fixation is a highly energy expensive process and requires the presence of the heterodimeric enzyme complex, nitrogenase. To fix one molecule of N_2 approximately 16 molecules of adenosine triphosphate (ATP) and 8 low-potential electrons (usually provided as reduced ferredoxin) are necessary (Canfield *et al.*, 2010). Cyanobacteria obtain this energy by oxygenic photosynthesis which seems paradoxically since the nitrogenase is extremely sensitive to oxygen. A pO_2 as low as 0.001 atm already starts inhibiting nitrogenase activity of *Plectonema boryanum* (Section III) and *Anabaena cylindrica* (Section IV) *in vitro* (Haystead *et al.*, 1970). In cyanobacteria various mechanisms evolved to allow both intrinsically incompatible processes to take place. According to Stal (1995) three strategies can be distinguished: (1) avoidance of O_2 , (2) temporal separation of oxygenic photosynthesis and nitrogen fixation, and (3) spatial separation of both processes.

Cyanobacteria using the strategy of oxygen avoidance can be either filamentous or unicellular and are found in a wide range of different environments. They fix nitrogen only under anaerobic (or microaerobic) conditions while oxygenic photosynthesis is inhibited. For example, the filamentous cyanobacterium *P. boryanum* fixes nitrogen at a pO_2 below 0.005 atm (Weare and Benemann, 1974). Particularly favourable are sulphide-rich environments as they are anaerobic and inhibit photosystem II activity. Organisms living in this environment, such as the filamentous cyanobacterium *Oscillatoria limnetica* (Section III), replace oxygenic photosynthesis by an effective sulphide-dependent photosynthesis, driven by photosystem I (Cohen *et al.*, 1975; Cohen *et al.*, 1986).

Cyanobacteria showing temporal separation of oxygenic photosynthesis and nitrogen fixation are able to fix nitrogen aerobically and can be either filamentous or unicellular. Cultures grown under an alternating light-dark cycle usually confine nitrogen fixation to the dark period when oxygen production is low or absent, a mechanism which is well described for the unicellular cyanobacteria *Cyanothece* sp. ATCC 51142 (Section I) (Reddy *et al.*, 1993), *Crocospaera watsonii* WH 8501 (Section I) (Tuit *et al.*, 2004) and for species of the genus *Gloeotheca* (Section I) (Stephens *et al.*, 2003). Also the filamentous species *Lyngbya aestuarii* (Section III) fixes nitrogen preferably during the dark period when grown under alternating light-dark cycles (Stal and Krumbein, 1985).

However, most organisms which are able to fix nitrogen aerobically still show optimum nitrogen-fixing activity only under low oxygen concentrations, e.g. between 25 and 80 μM O_2 for *Gloeotheca* sp. PCC 6919 depending on the age of the culture (exponential and stationary growth phase respectively) (Maryan *et al.*, 1986). An exception is the filamentous cyanobacterial genus *Trichodesmium* (Section III) which fixes nitrogen maximally at a pO_2 of 0.1 atm (Ohki and Fujita, 1988). Interestingly, *Trichodesmium* spp. fix nitrogen exclusively during the day and inactivate and degrade the nitrogenase during the night (Capone *et al.*, 1990). Although nitrogen fixation occurs during the time of oxygenic photosynthesis both processes are more or less temporally separated as nitrogen fixation occurs around mid-day when the oxygen production is reduced and oxygen-scavenging mechanisms are enhanced (Berman-Frank *et al.*, 2001). However, temporal separation is not the only mechanism that allows nitrogen fixation and oxygenic photosynthesis to occur under aerobic conditions in *Trichodesmium* spp. Bergman and Carpenter (1991) could show by immunogold labelling that the nitrogenase is

localised in subsets of specialised cells, called diazocytes (Figure 2), thus separating nitrogen fixation and oxygenic photosynthesis spatially.

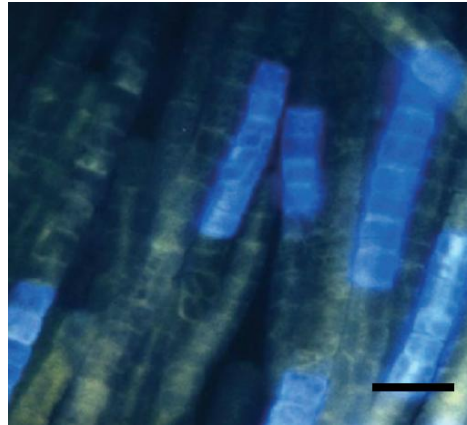


Figure 2. Diazocytes in filaments of *Trichodesmium erythraeum* IMS101.

Immunolocalisation of the NifH protein reveals the presence of the nitrogenase in subsets of cells named diazocytes (blue). Scale bar, 10 μm . (adapted from Bergman *et al.*, (2013))

However, the most prominent example for spatial separation is the localisation of the nitrogenase to specialised cells called heterocysts, while oxygenic photosynthesis and carbon fixation occur simultaneously in adjacent vegetative cells. In 1968 Peter Fay and co-workers proposed for the first time that heterocysts are the sites of nitrogen fixation (Fay *et al.*, 1968) and shortly afterwards Stewart *et al.* (1969) could experimentally confirm their hypothesis. The ability to form heterocysts is a main feature for the classification of cyanobacteria. Organisms which are capable of fixing nitrogen by the formation of heterocysts were grouped in Section IV and V (Rippka *et al.*, 1979). Heterocyst differentiation has been studied extensively in species of the genera *Anabaena* and *Nostoc* (both Section IV). In *Anabaena* spp. removal of combined nitrogen from the growth medium induces the formation of heterocysts at regular intervals of 10 to 20 cells along the filament (Wilcox *et al.*, 1973). Several stages can be

distinguished during the development from a vegetative cell towards a mature heterocyst (Sherman *et al.*, 2000). In order to establish a regular heterocyst spacing pattern transfer of regulators between cells is required. Gordon Elliot Fogg (1949) was the first who proposed that the spacing pattern is a result of periodic concentrations of an inhibitor along the filament that allows heterocyst formation only at the position of the lowest concentration. A prime candidate for such a diffusible inhibitor is the product of the gene *patS* (Yoon and Golden, 1998). Under nitrogen deprivation *patS* is expressed early in differentiating proheterocysts, potential heterocysts which represent an intermediate between a vegetative cell and a heterocyst (Yoon and Golden, 1998). Inactivation of *patS* in *Anabaena* sp. PCC 7120 results in the formation of heterocysts in the presence of combined nitrogen and in the formation of multiple contiguous heterocysts (MCH) under nitrogen deprivation (Yoon and Golden, 1998), whereas overexpression of the gene inhibits heterocyst differentiation (Liu and Golden, 2002). The *patS* gene encodes a polypeptide of just 17 amino acids of which the N-terminal amino acids are important for the proper processing and self-immunity of the producing cell while the C-terminal amino acids are essential for the suppression of heterocyst differentiation (Corrales-Guerrero *et al.*, 2013). A shortened PatS variant of only the 5 C-terminal residues RGSGR (PatS5) is sufficient to inhibit heterocyst differentiation when added to the external medium (Yoon and Golden, 1998; Huang *et al.*, 2004; Wu *et al.*, 2004). Another protein possessing the RGSGR motif named HetN is additionally needed to establish the heterocyst spacing pattern. Deletion of HetN (Black and Wolk, 1994; Callahan and Buikema, 2001) or deletion of the internal RGSGR sequence of HetN (Corrales-Guerrero *et al.*, 2014) led to MCH in *Anabaena* sp. PCC 7120. Both

proteins are likely to inhibit heterocyst differentiation in neighbouring cells by interacting with HetR, the positively-acting master regulator of heterocyst differentiation (Huang *et al.*, 2004; Risser and Callahan, 2009; Feldmann *et al.*, 2011; Higa *et al.*, 2012), and possibly also a regulator of other cellular processes in non-heterocystous cyanobacteria (El-Shehawy *et al.*, 2003; Zhang *et al.*, 2009). A recent study by Risser and Callahan (2009) confirmed the presence of HetR concentration gradients along filaments in *Anabaena* sp. PCC 7120 that respond to the expression of PatS and HetN. Deletion of both *patS* and *hetN* prevents the formation of HetR concentration gradients. Immunofluorescence localisation studies by Corrales-Guerrero *et al.* (2013) furthermore showed that RGSGR-containing peptides such as PatS and HetN accumulate in cells adjacent to the differentiating proheterocysts, suggesting that those peptides are transferred between cells. However direct transfer of the potential inhibitors has not been visualised yet. Whether PatS diffuses from differentiating proheterocysts to adjacent vegetative cells via the contiguous periplasmic space as suggested by Yoon and Golden (1998) or through channels linking the cytoplasm of adjacent cells remains to be investigated.

In order to establish the regular heterocyst spacing pattern along the filament some cells need to have initially the ability to differentiate. In *N. punctiforme* ATCC 29133 the protein PatN seems to determine which subset of cells is biased to differentiate (Risser *et al.*, 2012; and commentary by Flores (2012)). Inactivation of *patN* results not only in an increase in heterocyst frequency but also in shorter but still regularly spaced intervals of vegetative cells between two heterocysts (Risser *et al.*, 2012). Interestingly, the protein is distributed unevenly between cells. After cell division usually only one of the two daughter cells

possesses PatN while the other cell does not. The cell lacking PatN is transiently poised to undergo cell differentiation after nitrogen depletion, thus establishing a rudimentary pattern of subsets of potential heterocysts along the filament (Risser *et al.*, 2012). This initial pattern is later resolved into a single spaced heterocyst pattern by the diffusion of inhibitors such as PatS and HetN and their interaction with the transcription activator HetR (Risser *et al.*, 2012) (Figure 3).

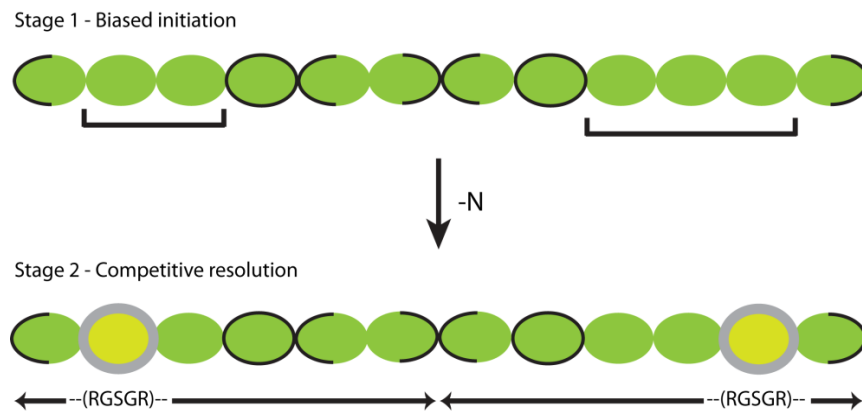


Figure 3. Two stage model for the establishment of the heterocyst spacing pattern in filamentous cyanobacteria.

During cell division PatN is localised at the half of the cell that contains the most recently formed septum (black cell lines). After cell division only one of the two daughter cells possesses PatN in the cytoplasmic membrane, resulting in subsets of cells that are devoid of PatN and are poised to differentiate after nitrogen depletion. Diffusion of inhibitors containing the pentapeptide RGSGR along the filament results in the formation of single heterocysts (yellow) separated by a regular number of vegetative cells in between (green) (adapted from Risser *et al.* (2012)).

The development of subsets of cells that potentially differentiate into heterocysts after nitrogen step-down is similar to the subset of diazocytes found in *Trichodesmium* spp. (Bergman *et al.*, 2013). Similar to the initial subsets of cells in heterocyst-forming cyanobacteria, diazocytes are not terminally differentiated

cells, they retain their ability to divide and regress into vegetative cells (Wilcox *et al.*, 1973; Fredriksson and Bergman, 1997). Based on this observation it has been proposed that heterocysts and diazocytes may have developed from a common non-heterocystous filamentous cyanobacterial ancestor (Bergman *et al.*, 2013). Keeping the initial stage of nitrogen fixing cells in *Trichodesmium* spp. (diazocytes) might be beneficial for the survival of the organism in the open ocean as it offers more flexibility to adapt to a rapidly changing environment (Bergman *et al.*, 2013). The similarity of regulatory mechanisms that determine diazocyte formation in *Trichodesmium* spp. to the earlier described mechanism in *Anabaena/Nostoc* spp. has not yet been resolved. A BlastP search revealed that there are no PatN similar proteins present in *Trichodesmium* spp.

Once the heterocyst pattern is established it allows filaments to survive nitrogen stress condition. While vegetative cells retain their metabolic and morphological characteristics, such as photosynthetic activity and carbon fixation, heterocysts undergo extensive changes in order to allow nitrogen fixation. Mature heterocysts provide a microoxic cytoplasm by synthesising a distinctive multilayered envelope. Additional to the outer membrane heterocysts have an inner laminated layer composed of heterocyst-specific glycolipids (also named heterocyst-specific glycolipid (HGL) layer)) that are highly specific for certain families or even genera of cyanobacteria, and an outer homogenous layer formed of polysaccharides (heterocyst envelope polysaccharide (HEP) layer) (Wildon and Mercer, 1963a; Lang and Fay, 1971; Bauersachs *et al.*, 2009). Both layers function as a gas diffusion barrier by limiting the entrance of O₂ into heterocysts (Walsby, 1985). The HEP-layer is additionally thought to protect the underlying HGL-layer and to support its formation as a scaffold (Nicolaisen *et al.*, 2009a). To

diminish oxygen concentration in heterocysts further, heterocysts reduce O₂ production and increase O₂ consumption by dismantling photosystem II and activating respiration (Fay and Walsby, 1966; Thomas, 1970; Donze *et al.*, 1972). These mechanisms enable heterocysts to retain a minimal O₂ concentration inside the heterocysts (ca. 600 nM O₂ for *Anabaena* sp. PCC 7120 (Tomitani *et al.*, 2006)) even in the presence of O₂ concentrations as high as 300 µM O₂ (Jensen and Cox, 1983). On the other hand heterocysts require atmospheric N₂. Anthony E. Walsby (2007) proposed that N₂ mainly enters heterocysts by diffusing from neighbouring vegetative cells into heterocysts rather than passing the heterocysts' envelope. Inside heterocysts N₂ is reduced by the nitrogenase to ammonia which is immediately incorporated into glutamine (Wolk *et al.*, 1976). As heterocysts contain high levels of glutamine synthetase (GS) which catalyses the ATP-dependent amidation of glutamate to produce glutamine, but lack the enzyme glutamine-2-oxoglutarate amidotransferase (GOGAT; also known as glutamate synthase) which catalyses the reductive transfer of the amide group from glutamine to 2-oxoglutarate to produce two glutamate molecules, it has been suggested that glutamate is transferred into heterocysts while glutamine is transferred into vegetative cells (Wolk, 1968; Wolk *et al.*, 1976; Thomas *et al.*, 1977; Jüttner, 1983; Martín-Figueroa *et al.*, 2000). Additionally, other amino acids might play a role in intercellular transfer. It has been shown by ¹⁴C labelling experiments that alanine is likely to be transferred from vegetative cells into heterocysts (Jüttner, 1983) which was verified by gene inactivation and localisation studies of the alanine dehydrogenase Alr2355 in *Anabaena* sp. PCC 7120 (Pernil *et al.*, 2010). Inactivation of the enzyme led to a substantially reduced nitrogenase activity and a bisected rate of diazotrophic growth. Moreover,

it has been suggested that the sulphur-containing amino acids cysteine and methionine are transported into heterocysts as their synthesis stops during heterocyst development (Omairi-Nasser *et al.*, 2014). Early microscopy studies furthermore revealed the presence of distinct granules in the neck region of heterocysts to adjacent vegetative cells which have been termed ‘cianoficina’ (Borzi, 1887) and later cyanophycin granules. Cyanophycin is a unique polymer in the sense that it consists only of the two amino acids arginine and aspartic acid in a nearly 1:1 ratio (Simon, 1971). Its synthesis is catalysed by the enzyme cyanophycin synthetase (CphA) that adds the single amino acids in two separate ATP dependent steps (Ziegler *et al.*, 1998; Berg *et al.*, 2000). The final product consists of a polyaspartic acid backbone with arginine side residues (Simon and Weathers, 1976). Although cyanophycin is not directly required for diazotrophic growth (Ziegler *et al.*, 2001), it seems to play an important role as a dynamic nitrogen reservoir to balance the nitrogen state of the cells, acting as a kind of ‘nitrogen buffer’ (Carr, 1988). It is likely that cyanophycin and its subunits are also involved in intercellular transfer of nitrogen molecules between cells. Beside the single amino acids, arginine and aspartic acid, the dipeptide β -aspartyl-arginine seems to be the main nitrogen vehicle from heterocysts into vegetative cells (Richter *et al.*, 1999; Ke and Haselkorn, 2013; Burnat *et al.*, 2014).

As heterocysts lack ribulose 1,5-bisphosphate carboxylase–oxygenase and do not fix CO₂, they depend on the supply of carbon skeletons from adjacent vegetative cells for the generation of energy for nitrogen fixation. Carbon skeletons are most likely provided by vegetative cells in form of sugars. Most studies so far, have focussed on the role of sucrose as carbon carrier (Schilling and Ehrnsperger, 1985; Wolk *et al.*, 1994; Curatti *et al.*, 2002; Cumino *et al.*, 2007; Marcozzi *et al.*,

2009; López-Igual *et al.*, 2010; Vargas *et al.*, 2011), but also the transfer of glucose or fructose has been suggested (Haury and Spiller, 1981; Jüttner, 1983).

Sucrose is known as a key molecule in plants, where it is probably the major vehicle for long distance transport of photosynthates, being involved in growth, development, storage, signal transduction and acclimation to environmental stress conditions (Salerno and Curatti, 2003). In cyanobacteria the importance of sucrose for diazotrophic growth has been shown by studies on the localisation and function of the sucrose hydrolysing invertase *InvB* in *Anabaena* sp. PCC 7120 (Schilling and Ehrnsperger, 1985; Curatti *et al.*, 2002; López-Igual *et al.*, 2010; Vargas *et al.*, 2011). Inactivation mutants of *invB* were unable to grow under diazotrophic conditions and accumulated ten times more sucrose than the wild type after nitrogen step-down while glycogen was less abundant in the mutant under this condition (López-Igual *et al.*, 2010; Vargas *et al.*, 2011).

In summary, nitrogen fixation via heterocysts requires exchange of various types of molecules and gases between cells. In order to establish the regular heterocyst spacing pattern, inhibitors containing the RGSGR pentapeptide need to diffuse from proheterocysts into neighbouring vegetative cells. Furthermore, N₂ needs to be transferred into heterocysts where it is fixed by the nitrogenase, and is returned to vegetative cells in form of amino acids. As heterocysts are unable to fix CO₂, carbon skeletons are provided by adjacent vegetative cells as sugars including sucrose. A summary of all potential metabolites and regulators that are likely to be exchanged between heterocysts and vegetative cells is given in Figure 4.

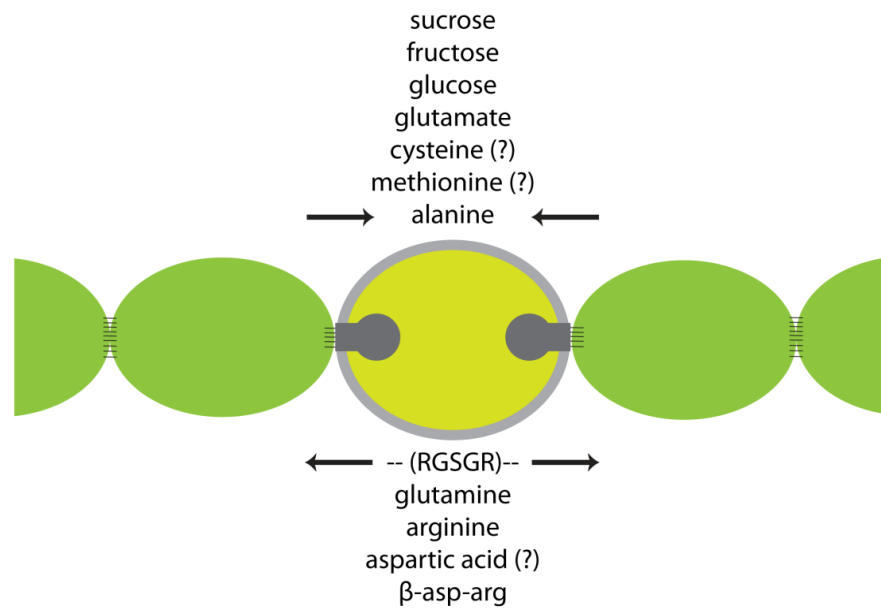


Figure 4. Metabolites and regulators possibly being exchanged between vegetative cells and heterocysts in *Anabaena* sp. PCC 7120.

1.3 Routes of molecular exchange between cells

First evidence for intercellular transfer of molecules between cyanobacterial cells was obtained by staining experiments with methylene blue and ruthenium red using different species of *Oscillatoria* (Section III) (see review by Wolk, 1973). The experiments show that the dyes move more rapidly across many septa than through a single outer wall.

In 1968 Peter Wolk made a ground breaking experiment in this field. By using radioactive labelled carbon he showed that part of the carbon fixed by vegetative cells moves through the filament into heterocysts. Shortly afterwards Stewart *et al.* (1969) confirmed his result and suggested additionally that there is rapid transfer of fixed nitrogen from heterocysts into neighbouring vegetative cells. However, little was known about possible routes of communication at this time.

In *Anabaena* sp. PCC 7120 (Section IV), there are currently two possible routes of metabolite exchange under discussion (Haselkorn, 2008; Flores and Herrero, 2010). One favours the transport of molecules via a continuous periplasm (Mariscal *et al.*, 2007), the other the diffusion of molecules from cytoplasm to cytoplasm via cell-cell connections termed septal junctions (Mullineaux *et al.*, 2008; Mariscal, 2014). Both pathways of intercellular communication have been studied using Fluorescence Recovery after Photobleaching (FRAP). The outline of a typical FRAP experiment for filamentous cyanobacteria is shown in Figure 5.

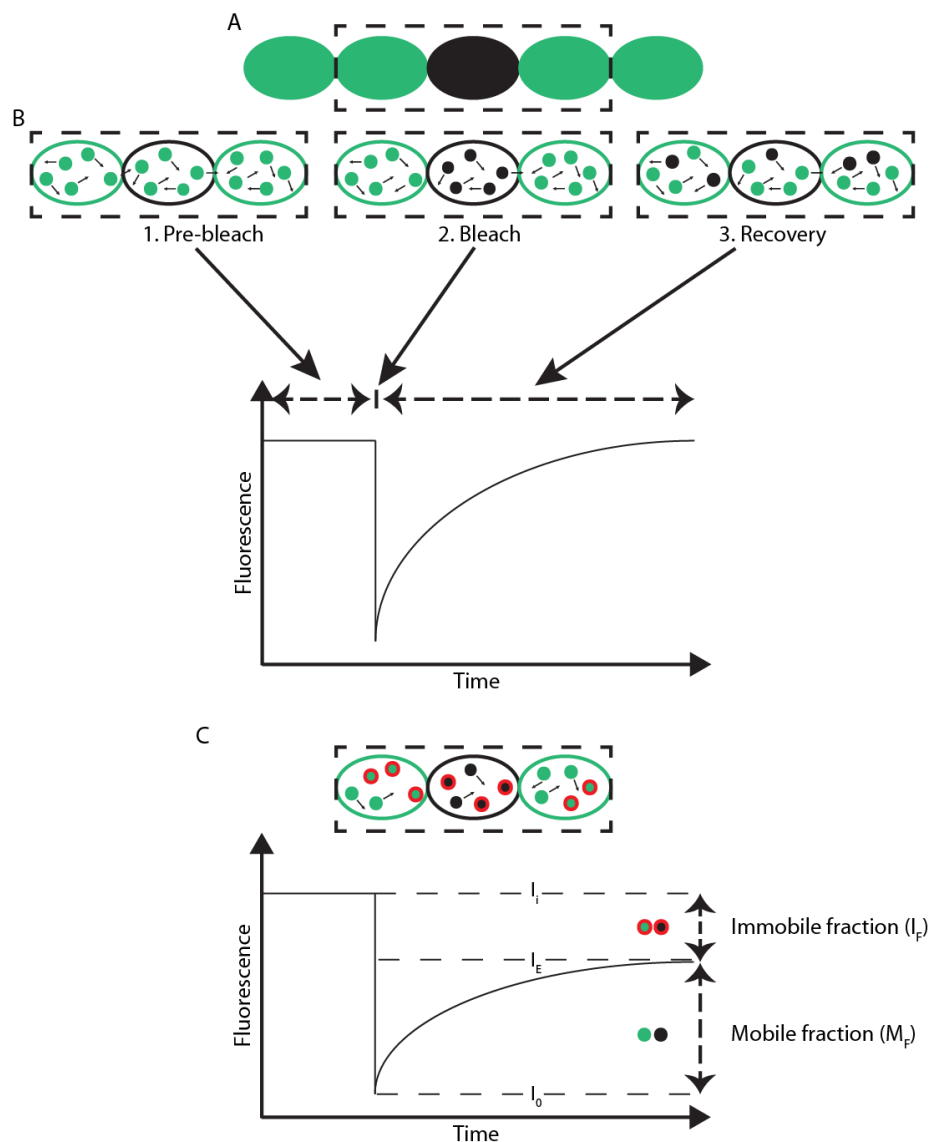


Figure 5. Outline of a FRAP experiment for a multicellular organism.

Figure 5

(A) The cytoplasm of all cells within a filament are labelled with a mobile fluorescent dye (green). The region of interest (ROI) is highlighted by a dashed rectangle. The bleached cell is marked black. (B) FRAP experiments consist of three phases. During the pre-bleach phase (1) mobile dye molecules (green) move randomly within the cytoplasm and establish a concentration equilibrium along the filament. By increasing the laser intensity in the cell highlighted in black (A) the fluorescence of the dye molecules is irreversibly bleached (2; black). As a result of the continuous movement of fluorescent molecules into the cell, and bleached molecules into the neighbouring cells the fluorescence intensity of the bleached cell recovers (3). Note that the displayed cell has not reached full recovery yet. The change of fluorescence intensity during the FRAP experiment is shown in the graph below. The bleach results in a sudden drop in intensity, followed by recovery. If the dye molecules are freely mobile and the filament is formed of many cells, with the result that the number of fluorescent molecules is considerable larger in comparison to the dye molecules present in the bleached cell, the overall loss of fluorescence is negligible. (C) When immobile fluorophores are present (red outline) the fluorescence intensity does not reach the initial fluorescence (I_i) after the bleach (I_0) and remains at a plateau value (I_E). The resulting immobile fraction (I_F) can be calculated by $[(I_i - I_E)/(I_i - I_0)]$. Accordingly, the mobile fraction (M_F) is defined by $1 - I_F$. (Figure modified after Staras *et al.* (2013))

A prerequisite for FRAP studies is the introduction of a suitable fluorescent tracer into the appropriate cell compartment. Periplasmic communication was studied by expressing Green Fluorescent Protein (GFP; 27 kDa) (Mariscal *et al.*, 2007; Zhang *et al.*, 2008a) or the smaller fluorescent protein iLOV (13 kDa) (Zhang *et al.*, 2013) fused to a signal sequence which is recognised by the twin-arginine translocation (TAT) system that exports the protein to the periplasm. To locate the expression of GFP to heterocysts of *Anabaena* sp. PCC 7120, Mariscal *et al.* (2007) used the promoter of the *patS* gene which is active specifically in

developing heterocysts (Yoon and Golden, 1998; 2001). After nitrogen depletion the GFP signal was present in the periphery of both cell types, heterocysts and neighbouring vegetative cells. In contrast, if the GFP was anchored to the cytoplasmic membrane of the producing heterocysts, the fluorophore would have been confined to the periplasm of these cells and would not have moved into neighbouring vegetative cells. These experiments suggest that molecules as big as GFP can move along the filament through the continuous periplasm. On the other hand, the results from Zhang's laboratory (2008, 2013) indicate that neither GFP nor the smaller molecule iLOV move within the periplasm from cell to cell. In their first approach Zhang *et al.* (2008) fused GFP to the signal sequence of the trimethylamine N-oxide reductase TorA from *Escherichia coli* which is one of the best-characterised substrates of the TAT system (Chanal *et al.*, 2003). To locate the expression of GFP into heterocysts or vegetative cells respectively they used three different promoters. While the *hepA* and *patB* promoters are exclusively active in heterocysts (Holland and Wolk, 1990; Jones *et al.*, 2003) the *rbcL* promoter is only active in vegetative cells (Yoon and Golden, 1998). Their results show that GFP is able to diffuse freely within the periplasmic space of a producing cell, but does not diffuse from heterocysts into adjacent vegetative cells or vice versa, suggesting that diffusion barriers exist in the periplasm for molecules as big as GFP. These results are contradictory to the results obtained by Mariscal *et al.* (2007). As it is unknown whether the *E. coli* signal is processed properly in *Anabaena* sp. PCC 7120 it has been suggested that the immobility of GFP might be a result of its interaction with the plasma membrane or the peptidoglycan layer (Nicolaisen *et al.*, 2009a). In their subsequent study Zhang *et al.* (2013) proved by immunoblotting that the TAT signal from *E. coli* is correctly

recognised and processed in *Anabaena* sp. PCC 7120. Furthermore, they fused the fluorescent protein iLOV to the signal sequence of All3333, a putative homologue of the nitrate transporter NrtA in *Anabaena* sp. PCC 7120 and expressed the protein cell-specifically by using the *nifHDK* promoter for the expression of iLOV in heterocysts and the *rbcL* promoter for the expression in vegetative cells. Fluorescence microscopy indicated that iLOV is neither transferred from the periplasm of heterocysts to vegetative cells nor in the periplasmic space from vegetative cells into heterocysts, confirming the presence of diffusion barriers for molecules bigger than 13 kDa. The reasons for the different results obtained by Mariscal *et al.* (2007) and Zhang *et al.* (2008; 2013) remain unknown. Further experiments are necessary to clarify whether the periplasm is continuous and can be considered as a possible route of molecular exchange.

Alternatively, intercellular communication between cells could be achieved via cytoplasmic bridges linking the cytoplasm of neighbouring cells. Although neither GFP nor iLOV diffuse between the cytoplasm of heterocysts and vegetative cells (Yoon and Golden, 1998; Mariscal *et al.*, 2007; Zhang *et al.*, 2008; Cheng-Cai Zhang, personal communication), it could be shown that the smaller fluorescent tracer molecules calcein and 5-carboxyfluoresceindiacetate (5-CFDA) are transferred cytoplasmically between cells (Mullineaux *et al.*, 2008; Mariscal *et al.*, 2011). Both molecules are available as an acetoxymethylester (AM) derivative that is non-fluorescent and hydrophobic enough to enter the cell. Hydrolysis of the ester groups by cytoplasmic esterases converts the precursor molecule to a fluorescent form which is trapped in the cytoplasm because it is too hydrophilic to traverse lipid bilayers (Mullineaux *et al.*, 2008; Mariscal *et al.*, 2011). Uptake of calcein into the cytoplasm was shown for different

cyanobacterial strains of Section III (*Oscillatoria terebriformis*) and IV (*Anabaena cylindrica* PCC 7122, *Anabaena variabilis* ATCC 29413 and *Anabaena* sp. PCC 7120) (Mullineaux *et al.*, 2008). FRAP experiments reveal transfer of calcein and 5-CFDA between the cytoplasm of adjacent cells in these organisms by passive diffusion (Mullineaux *et al.*, 2008; Mariscal *et al.*, 2011; Merino-Puerto *et al.*, 2011b). There is no indication of active transport. After bleaching out the fluorescence of single cell within a filament, fluorescence of the entire filament changes following the concentration gradient. The fluorescence of the bleached cell recovers while the fluorescence of neighbouring cells decreases (Mullineaux *et al.*, 2008). The diffusion of calcein along the filament differs from ‘classical diffusion’ in that it is not spatially homogeneous. The rate-limiting step for the diffusion of calcein from cell to cell is the cell-cell interface. In order to quantify the kinetics of dye exchange between cells Mullineaux *et al.* (2008) introduced the ‘exchange coefficient’ (E), a parameter which relates the rate of molecular flux between adjacent cells to the difference in dye concentration between the cells. For the pairwise exchange of molecules between two adjacent cells, the net rate of exchange is given by $E (C_1 - C_2)$ where C_1 and C_2 are the dye concentrations in cell 1 and 2. However, cyanobacterial filaments usually consist of dozens of connected cells, making the calculation difficult. Under the assumption that E is identical for every cell junction, the actual E value can be determined by fitting a predicted recovery curve for the cell of interest onto the experimentally determined recovery curve. For the prediction of redistribution of calcein within the filament Mullineaux *et al.* (2008) used an iterative model in which the neighbouring cells determine the incremental change in dye concentration in any cell within the filament (δC_n) within a time increment δt ,

resulting in $\delta C_n = E\delta t[(C_{n+1} - C_n) + (C_{n-1} - C_n)] = E\delta t(C_{n+1} + C_{n-1} - 2C_n)$. Using this approach it was shown that calcein and 5-CFDA are transferred between vegetative cells of *Anabaena* sp. PCC 7120, *Anabaena cylindrica* PCC 7122 and *Anabaena variabilis* ATCC 29413 (Mullineaux *et al.*, 2008; Mariscal *et al.*, 2011). Interestingly, no significant molecular exchange of calcein was observed in the filamentous non-heterocystous cyanobacterium *Oscillatoria terebriformis* (Section III), suggesting that the connections are specific for metabolite exchange in differentiating cyanobacteria (Mullineaux *et al.*, 2008). However, it is likely that other molecules are transferred between cells of *Oscillatoria* species as they possess pores in the cross-walls between cells (Metzner, 1955; Drawert and Metzner, 1956) and are highly motile, being even able to change the direction of movement (Halfen and Castenholz, 1971). Further investigations are required to identify a possible route of communication in the genus *Oscillatoria*.

The importance of the connections for the exchange of metabolites is further strengthened by a significant increase of the exchange coefficient between vegetative cells under nitrogen deprivation in comparison to growth in the presence of combined nitrogen. In *A. cylindrica* PCC 7122 and *A. variabilis* ATCC 29413 the E value for calcein for vegetative cells is approximately 3 to 10 times faster 72 h after nitrogen depletion (Mullineaux *et al.*, 2008).

As heterocysts and vegetative cells are mutually dependent on metabolite transfer with vegetative cells providing fixed carbon and heterocysts providing fixed nitrogen, FRAP experiments should also reveal insights into the kinetics of exchange between vegetative cells and heterocysts. Mullineaux *et al.* (2008)

showed that fluorescence recovery occurs in heterocysts but at a much slower rate than in vegetative cells. During recovery of the heterocyst's fluorescence the concentration of dye remains nearly constant in the adjacent vegetative cells. Hence, recovery in heterocysts follows a simple exponential model. For an intercalary heterocyst the fluorescence in the heterocysts is defined by $C_H = C_0 + C_R(1 - e^{-2Et})$ where C_0 is the initial fluorescence intensity immediately after the bleach and tending towards $(C_0 + C_R)$ during time t . A similar equation applies for a terminal heterocyst: $C_H = C_0 + C_R(1 - e^{-Et})$. FRAP results indicate that exchange between heterocysts and vegetative cells is approximately 13 times slower than between vegetative cells (Mullineaux *et al.*, 2008). The reduction of molecular exchange may be necessary to maintain the functionality of the nitrogenase by keeping the influx of oxygen low enough to be reduced by the terminal oxidases in the heterocysts. Mullineaux *et al.* (2008) also showed that the presence of cyanophycin plugs in the neck region of heterocysts reduces the exchange of calcein with neighbouring vegetative cells. A $\Delta cphA1$ mutant of *A. variabilis* ATCC 29413 which is unable to form cyanophycin (Ziegler *et al.*, 2001) shows an approximately three times higher E value for heterocysts than wild-type heterocysts.

In summary, both cell types, heterocysts and vegetative cells, show cytoplasmic transfer of calcein and 5-CFDA. Whether the periplasm is an additional route of metabolite and regulator transfer in *Anabaena* sp. PCC 7120 remains to be clarified.

1.4 Distribution and structural characteristics of septal junctions and nanopores in cyanobacteria

Cytoplasmic exchange requires the presence of septal junctions or pores penetrating the cross-walls. The occurrence of such structures has been studied extensively in cyanobacteria by electron microscopy. Various methods including conventional thin-section TEM, freeze-fracture EM and electron tomography revealed insights into the distribution and dimension of these structures among cyanobacteria. Electron micrographs of thin sections through the septal regions between adjacent cells show clearly structures pervading the septa (Figure 6). These structures have been named initially ‘microplasmodesmata’ although they lack cytoplasmic membrane connections and hence do not resemble the structure of plasmodesmata of plants (Bell and Oparka, 2011).

Thin-section TEM on cyanobacteria of Sections III, IV and V reveal that all filamentous species possess junctions at the septa between neighbouring cells of similar dimensions although their metabolisms and morphologies vary (Table 1). Septal junctions are present in both vegetative-vegetative and vegetative-heterocyst septa (Wildon and Mercer, 1963a; Lang and Fay, 1971; Omairi-Nasser *et al.*, 2014). According to electron micrographs the diameter of septal junctions in cyanobacteria is approximately 5 to 15 nm, making them wider than gap junctions in animals (2 to 3 nm) but narrower than plasmodesmata in plants (20 to 50 nm) and simple pores (50 to 500 nm) and Dolipores in fungi (100 to 200 nm) (see review by Bloemendal and Kück, 2013).

Table 1. Distribution and diameter of septal junctions among cyanobacteria studied by thin-section TEM.

	strain	diameter [nm]	reference
Section III	<i>Microcoleus vaginatus</i>	10-15 (core)	Lamont, 1969
	IUCC 621	5-10 (wall)	
	<i>Oscillatoria limosa</i>	15	Hagedorn, 1961
	<i>Symploca muscorum</i>	5 (core)	Pankratz and Bowen, 1963
	IUCC B617	2 (wall)	
Section IV	<i>Anabaena catenula</i>		Wilcox <i>et al.</i> , 1973
	<i>Anabaena cylindrica</i>		Wilcox <i>et al.</i> , 1973
		<5	Lang and Fay, 1971
			Haselkorn, 1978
	<i>Anabaena cylindrica</i> Lemm		Giddings and Staehelin, 1978
	<i>Anabaena</i> mutant	5	Haselkorn, 2008
	<i>Anabaena</i> sp. L14		Wildon and Mercer, 1963
	<i>Anabaena</i> sp. PCC 7120	14 ± 1 (Ru)*	Wilk <i>et al.</i> , 2011
		5.5 ± 0.7 (K)*	
		12 ± 1 (veg)#	Omairi-Nasser <i>et al.</i> , 2014
		14 ± 1 (het)#	
		$\Delta sepJ$	Wilk <i>et al.</i> , 2011
	<i>Anabaena variabilis</i>	10-13	Golecki and Drews, 1974
			Palinska and Krumbein, 2000
	<i>Anabaenopsis</i> sp. 51		Peat and Whitton, 1968
	<i>Cyanospira rippkae</i>		Palinska and Krumbein, 2000
	Florenzano		

	strain	diameter [nm]	reference
	<i>Nostoc commune</i>	25	Palinska and Krumbein, 2000
	<i>Nostoc muscorum</i> N52		Wildon and Mercer, 1963b
	<i>Nostoc shaericum</i> Vaucher		Bisalputra <i>et al.</i> , 1975
	<i>Nostoc</i> sp. F. Blasia		Gorelova and Baulina, 2009
	<i>Nostoc</i> sp. IUCB 756		Bisalputra <i>et al.</i> , 1975
	<i>Nostoc punctiforme</i> ATCC 29113		Lehner <i>et al.</i> , 2011
	<i>Fischerella ambigua</i>		Thurston and Ingram, 1971
	<i>Fischerella muscicola</i> LB1427/1		Butler and Allsopp, 1972
	<i>Geitleria calcarea</i>		Couté, 1982
	<i>Loriellopsis cavernicola</i>		Lamprinou <i>et al.</i> , 2011
Section V	<i>Loriella</i> populations		Hernández-Mariné <i>et al.</i> , 1999
	<i>Mastigocladus laminosus</i> SAG 4.84		Nürnberg <i>et al.</i> , 2014
	<i>Mastigocladopsis repens</i> BCF 172-6		Merino <i>et al.</i> , 1994
	<i>Stigonema hormoides</i>		Butler and Allsopp, 1972
	<i>Stigonema mamillosum</i>		Butler and Allsopp, 1972

* Ru – ruthenium red; K – KMnO₄

het – heterocyst; veg – vegetative cell

The presence of septal junctions was confirmed by freeze-fracture electron microscopy (FFEM) (Table 2). FFEM is a powerful method for revealing the distribution and organisation of membrane proteins at macromolecular resolution (Severs, 2007). During the freeze-fracture process a frozen membrane is split into

two half-membrane leaflets, a leaflet close to the (inner) cytoplasm (protoplasmic fracture face (PF)) and a leaflet close to the (outer) exoplasmic space (exoplasmic fracture face (EF)) (Branton *et al.*, 1975). Septal junctions appear as protrusions on the PF face and pits on the EF face (Giddings and Staehelin, 1978; Giddings and Staehelin, 1981) (Figure 6.). According to Giddings and Staehelin (1978, 1981) the number of septal junctions between cells of different species is quite variable. In general, filamentous heterocyst-forming species (Section IV) show a higher number of connecting structures than filamentous species (Section III) (Table 2). It has been suggested that a higher number of septal junctions in Section IV cyanobacteria is required for the exchange of metabolites, especially under nitrogen deprivation, while the lower number in cyanobacteria of Section III might be sufficient to coordinate phototactic responses and motility (Giddings and Staehelin, 1981). Although the number of septal junctions between vegetative cells remains nearly constant in the presence and absence of a combined nitrogen source (ca. 175 to 300), the number of these structures is greatly reduced in septa between heterocysts and vegetative cells under nitrogen deprivation (ca. 50) (Table 2). As the formation of septal junctions occurs during cell division (Peat and Whitton, 1968; Giddings and Staehelin, 1978), the differentiation process requires a yet unknown mechanism of septal remodelling.

Table 2. Distribution of septal junctions among cyanobacteria studied by FFEM.

	strain	number	reference
Section III	<i>Phormidium luridum</i> var. olivaceae	30-40	Giddings and Staehelin, 1981
	<i>Plectonema boryanum</i> IUC 5944	30-40	Giddings and Staehelin, 1981
Section IV	<i>A. cylindrica</i>	200-300 (v)*	Giddings and Staehelin, 1978
		50 (h)*	Giddings and Staehelin, 1978
		175-250	Giddings and Staehelin, 1981
	<i>A. variabilis</i> ATCC 29413	100-140*	Giddings and Staehelin, 1981
	<i>A. variabilis</i> UTEX B377	200-300*	Giddings and Staehelin, 1981
	<i>Nostoc muscorum</i> UTEX 1038	200-300*	Giddings and Staehelin, 1981

* Cells grown in the absence of combined nitrogen; h – heterocyst; v - vegetative cell

Although Giddings and Staehelin (1978) suggested a proteinaceous character of the septal junctions based on the assumption that the outer diameters of these structures are too small (< 20 nm) to be made of a stable lipid bilayer (> 20 nm), a final proof was missing. Wilk *et al.* (2011) addressed the question of composition by another approach. They used two different methods of sample preparation for electron tomography and compared the obtained staining patterns with those of gap junctions whose proteinaceous character is proven. As the structures appear positively stained in a KMnO₄-based preparation method and negatively stained in an OsO₄/Ruthenium red-based preparation, they concluded that the septal junctions of cyanobacteria consist of proteins and suggested naming them ‘septosomes’ in analogy to desmosomes. However, this nomenclature is ambiguous as the term septosome is used frequently to describe the prokaryotic

protein complex machinery during cytokinesis (e.g. Di Lallo *et al.*, 2003). In the following work the term ‘septal junction’ will be used to describe the cell-cell joining structures which has been recently suggested by (Mariscal, 2014). However, a revision of the naming is necessary.

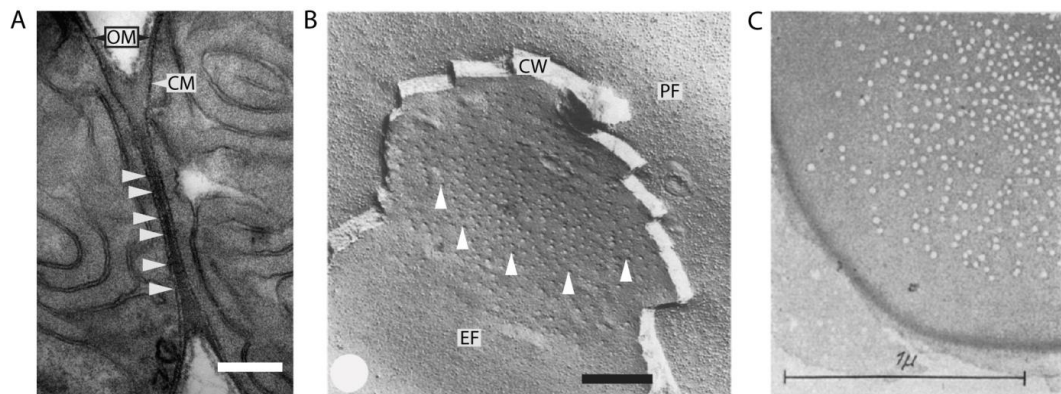


Figure 6. Presence of septal junctions and nanopores in cyanobacteria revealed by electron microscopy.

(A) Septal junctions visualised by thin-section TEM in *Anabaena* sp. PCC 7120. Structures linking two neighbouring cells are visible as black lines at the septum (white arrowheads). Note that only the cytoplasmic membrane (CM) of each cell enters the septum and not the outer membrane (OM). Cells were fixed with glutaraldehyde and KMnO_4 . Scale bar, 200 nm. (B) Septal junctions of *A. variabilis* IUCB B377 visualised by FFEM. More than 300 complexes (white arrowheads) are visible as pits on the exoplasmic fracture face (EF) of the plasma membrane. Cell wall (CW). Protoplasmic fracture face (PF). Scale bar, 250 nm. Image modified after Giddings and Staehelin (1981). (C) Nanopores in isolated peptidoglycan sacculi of *Tolypothrix tenuis*. (Micrograph from Metzner (1955)).

In order to connect the cytoplasm of neighbouring cells via septal junctions, nanopores need to be formed in the cross-walls. The presence of such pores has been demonstrated by TEM on isolated peptidoglycan sacculi of cyanobacteria of all filamentous sections (Section III, IV and V) (Table 3; Figure 6). The diameters

of these pores vary between 10 and 20 nm (Table 3) and are accordingly in the range of the diameters observed for septal junctions by thin-section TEM (Table 1) and FFEM (< 20 nm; Giddings and Staehelin, 1978). Interestingly, the number of nanopores determined for cross-walls of *Nostoc punctiforme* ATCC 29133 (155 ± 13 ; Table 3) is similar to the number of septal junctions observed for other organisms of Section IV by FFEM (Table 3) and electron tomography (Omairi-Nasser *et al.*, 2014), suggesting that the nanopores constitute a framework for the proteins of the septal junctions to penetrate the cell wall (Lehner *et al.*, 2013). However, it has to be noted that the frequency of nanopores might also be strain-specific, e.g. *Nostoc punctiforme* ATCC 29133 shows approximately 155 nanopores while in the closely related strain *Anabaena* sp. PCC 7120 only about 77 nanopores are present (Table 3), a finding which confirms earlier observations by FFEM (Giddings and Staehelin, 1978; 1981).

Table 3. Distribution and characteristics of nanopores in the septa of cyanobacteria.

	strain	diameter [nm]	number	reference
	<i>Lyngbya aerugineo-coerulea</i>	13-16		Metzner, 1955
Section III	<i>Microcoleus paludosus</i>	15		Drawert and Metzner, 1956
	<i>Oscillatoria limosa</i>	13		Drawert and Metzner, 1956
				Hagedorn, 1961*
	<i>Oscillatoria okeni</i>	13-16		Metzner, 1955
	<i>Oscillatoria sancta</i>	13-16		Metzner, 1955
	<i>Phormidium unicatum</i>			Frank <i>et al.</i> , 1962

	strain	diameter [nm]	number	reference
Section IV	<i>Anabaena</i> sp. PCC 7120	15 ± 0.1	77 ± 12	Iris Maldener, unpublished Drews and Weckesser, 1982 Golecki, 1988
	<i>Anabaena variabilis</i>			
	<i>Cylindrospermum</i> <i>licheniforme</i>	20		Drawert and Metzner, 1956
	<i>Cylindrospermum stagnale</i>	20		Drawert and Metzner, 1956
	<i>Gloeotrichia natans</i>	20		Metzner, 1955
	<i>N. punctiforme</i> ATCC 29133	20 ± 1.8	155 ± 13	Lehner <i>et al.</i> , 2013
	<i>Scytonema julianum</i>	10-15		Metzner, 1955
	<i>Tolypothrix tenuis</i>	17		Metzner, 1955
V	<i>Mastigocladus laminosus</i> Cohn	11-18		Marcenko, 1962

* revealed by thin-section TEM

1.5 Proteins forming septal junctions and nanopores

Giddings and Staehelin (1978) already hypothesised that septal junctions in cyanobacteria might be composed of protein subunits. Several proteins have been identified in recent years and suggested to be involved in the formation of the septal junctions. Key players might be the proteins SepJ (or FraG) (Flores *et al.*, 2007; Nayar *et al.*, 2007; Mariscal *et al.*, 2011), FraC and FraD (Bauer *et al.*, 1995; Merino-Puerto *et al.*, 2010; 2011b). Analyses of deletion mutants show the importance of these proteins for filament integrity, diazotrophic growth, and intercellular communication in *Anabaena* sp. PCC 7120 (Bauer *et al.*, 1995; Flores *et al.*, 2007; Nayar *et al.*, 2007; Mullineaux *et al.*, 2008; Merino-Puerto *et*

al., 2010; Mariscal *et al.*, 2011; Merino-Puerto *et al.*, 2011b). All mutants show also a reduced number of nanopores penetrating the peptidoglyan layer of cross-walls, thus providing further evidence for the involvement of the septal proteins SepJ, FraC and FraD in the formation of septal junctions (Iris Maldener, unpublished).

In *Anabaena* sp. PCC 7120 SepJ is encoded by the open reading frame (orf) *alr2338* which is located upstream of the *hetR* gene, a master regulator of heterocyst differentiation (Flores *et al.*, 2007; Nayar *et al.*, 2007). The 751-amino acid long protein is likely to be composed of three domains, including an approximately 200-amino acid long N-terminal coiled-coil domain (CC), a highly repetitive internal linker region (L) of 211 amino acids and an approximately 340-amino acid long C-terminal permease domain (P) that is predicted to show high similarity with cytoplasmic membrane proteins of the drug/metabolite exporter (DME) family of bacteria and archaea (Figure 7) (Flores *et al.*, 2007).

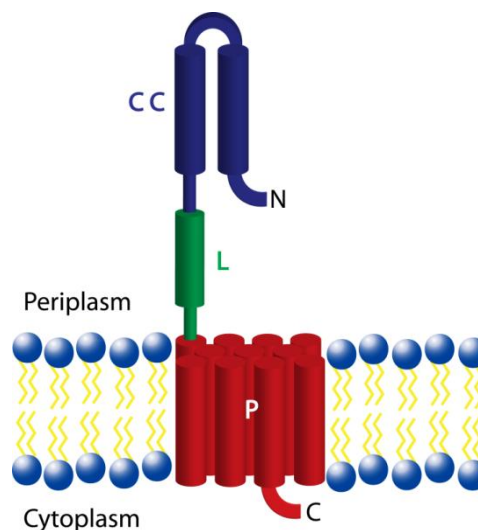


Figure 7. Predicted composition and topology of SepJ from *Anabaena* sp. PCC 7120.

Figure 7

The protein shows potentially three domains: a permease domain (P) with 11 predicted transmembrane helices (TMHs) spanning the cytoplasmic membrane, and an external part composed of the highly repetitive linker region (L) that is rich in proline and serine and a predicted coiled-coil domain (CC). Positions of the N- and C-terminus are indicated.

Proteins which possess either two or three domains [(CC+P) or (CC+L+P)] are considered to be SepJ-like proteins, whereas proteins showing only similarity to the permease domain are considered as DME-family permeases. A recent BlastP search with the amino acid sequence of SepJ from *M. laminosus* SAG 4.84 as query against all cyanobacterial sequences available from the Integrated Microbial Genomes (IMG) database (Markowitz *et al.*, 2012), and against the recently published sequences by Dagan *et al.* (2013) revealed the wide distribution of SepJ-like proteins among cyanobacteria (Appendix, Table 26; Nürnberg *et al.*, 2014). A SepJ variant is present in 62 from 139 cyanobacterial species (45 %) while only 28 cyanobacterial species (20 %) possess a DME family permease, of which 16 (12 %) can be found additionally in cyanobacteria possessing a SepJ-like protein (Nürnberg *et al.*, 2014). While all cyanobacteria of Sections IV and V (20 and 12 species respectively), and most species of Section III (32 from 34 species (94 %)) possess a SepJ-like protein, a SepJ variant is absent from unicellular species of Sections I and II, indicating the importance of SepJ for filamentous cyanobacteria (Nürnberg *et al.*, 2014). A closer look at the composition of the SepJ-like proteins in the different cyanobacterial sections revealed that filamentous species of Section III mostly possess a two domain protein (CC+P) (23/32 species; 72 %), and nearly all filamentous, heterocyst-forming (and branching) cyanobacteria of Sections IV and V exhibit a three-

domain (CC+L+P) SepJ variant (20/20 species (100 %); and 11/12 species (92 %) respectively). Hence, SepJ-like proteins containing a coiled-coil domain and a highly repetitive linker region of various lengths can be attributed to filamentous heterocystous cyanobacteria (Nürnberg *et al.*, 2014). Based on the distribution of SepJ proteins among cyanobacteria it has been suggested that the evolution of the three domain SepJ protein (CC+L+P) might have started from the DME-family protein and evolved by adding first the coiled-coil domain and finally the linker region (Mariscal *et al.*, 2011).

So far the physiological function of SepJ has been mainly characterised in *Anabaena* sp. PCC 7120 (Section IV). A *sepJ* deletion mutant shows filament fragmentation which increases in the absence of a combined nitrogen source, resulting in very short filaments and single cells (Flores *et al.*, 2007; Nayar *et al.*, 2007; Mariscal *et al.*, 2011). Additionally, a $\Delta sepJ$ mutant of *Anabaena* sp. PCC 7120 is inhibited in the formation of mature heterocysts and the synthesis of heterocyst-specific glycolipids, and is unable to fix nitrogen under any condition (Fix⁻ phenotype) (Flores *et al.*, 2007; Nayar *et al.*, 2007; Mariscal *et al.*, 2011). Higher expression levels of *sepJ* in *Anabaena* sp. PCC 7120 wild-type under nitrogen deprivation support the importance of the protein for the acclimation to diazotrophic growth conditions (Flores *et al.*, 2007; Nayar *et al.*, 2007). On basis of the observed phenotype Nayar *et al.* (2007) named the product of *alr2338 fraG* (**f**ragmentation, **g**lycolipid). However, in this work the suggested term *sepJ* is preferred as it better reflects the subcellular localisation of the protein at the septal region (Flores *et al.*, 2007). A SepJ-GFP fusion protein forms distinct fluorescent spots at the poles at the septa between neighbouring vegetative cells and between vegetative cells and heterocysts in the corresponding mutant strain of *Anabaena* sp.

PCC 7120 (CSAM137; Figure 8; Flores *et al.*, 2007). Its localisation is already determined during cell division when the protein forms a ring-like structure similar to that observed for FtsZ (Meier and Goley, 2014). It is notable that also the positioning of the septal junctions occurs during cell division (Peat and Whitton, 1968; Giddings and Staehelin, 1978), suggesting a connection of SepJ with the transport of molecules between cells. FRAP analyses revealed that transfer of calcein is strongly impaired in a $\Delta sepJ$ mutant of *Anabaena* sp. PCC 7120, being approximately 7 to 30 times slower than in the wild-type (Mullineaux *et al.*, 2008; Mariscal *et al.*, 2011). However, as exchange of the smaller fluorescent tracer 5-CFDA is only inhibited by approximately 54 % in comparison to the wild-type (Mariscal *et al.*, 2011; Merino-Puerto *et al.*, 2011b) and septal junctions are still present (Wilk *et al.*, 2011) other proteins are likely to be involved in the formation of structures for intercellular communication. Interestingly, functional dissection analyses of the SepJ protein from *Anabaena* sp. PCC 7120 revealed that the linker region of the protein is dispensable (Mariscal *et al.*, 2011). Mutants lacking this part of the protein are able to grow diazotrophically again and transfer high levels of 5-CFDA but not calcein, suggesting that transfer of molecules smaller than calcein is sufficient for diazotrophic growth and that the linker region might influence only the effective size of the channel connecting neighbouring cells (Mariscal *et al.*, 2011). However, Mariscal *et al.* (2011) also showed that the permease domain of *Anabaena* sp. PCC 7120 has an important role for diazotrophic growth of the organism. The replacement of SepJ by a chimeric SepJ composed of the CC from *Anabaena* sp. PCC 7120 and the P domain from the filamentous, non-heterocystous cyanobacterium *Trichodesmium erythraeum* does not allow

heterocyst formation and diazotrophic growth while a combination of CC domain from *T. erythraeum* and a P domain from *Anabaena* sp. PCC 7120 does.

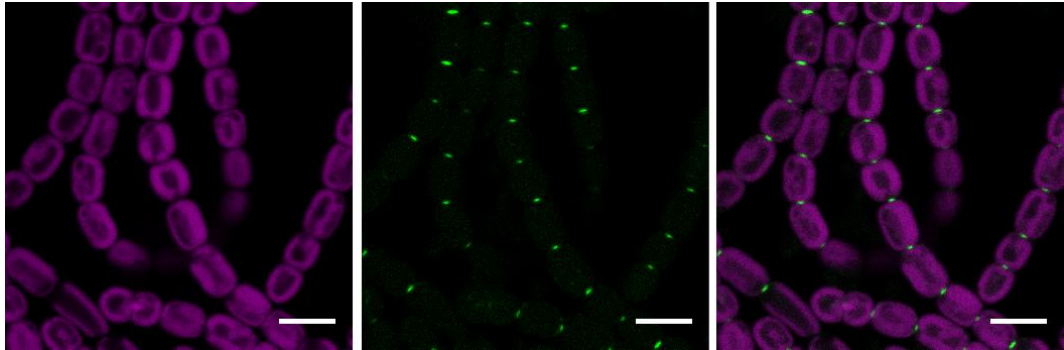


Figure 8. Localisation of SepJ-GFP in *Anabaena* sp. PCC 7120.

SepJ-GFP is localised in distinct spots in the intercellular septa. Images show chlorophyll fluorescence (magenta; 670-730 nm), GFP fluorescence (green; 500-527 nm), and an overlay of both images. Cells were visualised with a laser-scanning confocal microscope (Leica SP5) using a $\times 63$ oil-immersion objective (Leica HCX PL APO lambda blue 63.0 \times 1.40 OIL UV), and an excitation wavelength of 488 nm. Emission wavelengths for the detection are mentioned above. The pinhole was set to 95 μm , giving a resolution of 0.8 μm in the z-direction. Scale bars, 5 μm .

Several other mutants of *Anabaena* sp. PCC 7120 were isolated which are unable to grow diazotrophically and show extensive filament fragmentation (Buikema and Haselkorn, 1991; Ernst *et al.*, 1992). Two genes, namely *fraC* (*alr 2392*) and *fraD* (*alr2393*) were identified as being important for multicellularity and therefore likely to be involved in the formation of channels linking neighbouring cells (Bauer *et al.*, 1995; Merino-Puerto *et al.*, 2010; Merino-Puerto *et al.*, 2011b). Both genes are part of the *fraC* operon, including another gene named *fraE* that is important for filament integrity, formation of mature heterocysts and nitrogenase activity but probably not for intercellular communication (Merino-Puerto *et al.*, 2010). Just recently, an additional gene upstream of the *fraC* operon named *fraF*

(*aln* 2395) was identified in *Anabaena* sp. PCC 7120; it forms the *fraC-fraD-fraE*←*fraF* gene cluster (Merino-Puerto *et al.*, 2013). FraF negatively affects filament length and thus, has an effect opposite to that of the *fraC* operon (Merino-Puerto *et al.*, 2013). It seems that the *fraC* operon is widely conserved in filamentous cyanobacteria and is present in all heterocyst-forming species of which 60 % possess the entire *fraC-fraD-fraE*←*fraF* gene cluster (Merino-Puerto *et al.*, 2013). However, the constitutive expression of the *fraC* operon occurs at relative low levels (Merino-Puerto *et al.*, 2010)

fraC of *Anabaena* sp. PCC 7120 encodes a 179-amino acid long, phenylalanine-rich (13 %) protein with three predicted transmembrane helices spanning the cytoplasmic membrane (Bauer *et al.*, 1995; Merino-Puerto *et al.*, 2010; Merino-Puerto *et al.*, 2011b). FraD of *Anabaena* sp. PCC 7120 is slightly shorter (167 amino acids) but is also localised in the cytoplasmic membrane (Merino-Puerto *et al.*, 2010; Merino-Puerto *et al.*, 2011b). The protein is predicted to possess 5 TMHs and a periplasmic segment composed of two coiled-coil motifs which seem to be important in sustaining filament integrity by protein-protein interactions as suggested for the CC domain of SepJ (Flores *et al.*, 2007; Merino-Puerto *et al.*, 2010; Mariscal *et al.*, 2011; Merino-Puerto *et al.*, 2011b). The localisation of both proteins at the septa was determined by GFP-labelling and for FraD additionally by immunogold labelling (Merino-Puerto *et al.*, 2010; Merino-Puerto *et al.*, 2011b). Although FraC and FraD are located at the septa and their positioning occurs already during cell division, the proteins are less focussed than SepJ which forms distinct spots in the centre between two cells. Under nitrogen deprivation, for example, FraC can be even found in the periphery of the cell away from the septa (Merino-Puerto *et al.*, 2010). Furthermore, immunogold

labelling revealed that the positioning of FraD depends on FraC but not SepJ, suggesting a role for FraC in the normal localisation of FraD (Merino-Puerto *et al.*, 2011b). In frame deletion of *fraC* and *fraD* in *Anabaena* sp. PCC 7120 results not only in extensive filament fragmentation in the absence of combined nitrogen but also in a less focussed position of SepJ at the septa and a strongly hampered transfer of calcein and 5-CFDA (Bauer *et al.*, 1995; Merino-Puerto *et al.*, 2010; Merino-Puerto *et al.*, 2011b). As transfer of 5-CFDA is much less impaired in the *sepJ* deletion mutant, Merino-Puerto *et al.* (2011) suggested that a second route of intercellular molecular exchange that depends on FraC and FraD but not on SepJ is present in *Anabaena* sp. PCC 7120. This meets the prediction of Robert Haselkorn (1978) that not all channels are identical and that there exist subsets of channels for specialised transport of molecules. Interestingly, both mutants are still able to form mature heterocysts under nitrogen deprivation which differ, however, from heterocysts found in the wild-type by a greater distance between the cytoplasmic membranes of both cell types and by their mainly terminal localisation (Bauer *et al.*, 1995; Merino-Puerto *et al.*, 2010; Merino-Puerto *et al.*, 2011b).

In summary, FRAP experiments with calcein and 5-CFDA revealed the presence of two systems for molecular exchange in *Anabaena* sp. PCC 7120, one mediated by SepJ, the other by FraC and FraD. However, it is notable that septal junctions can be observed in all tested mutants by electron microscopy and tomography (Bauer *et al.*, 1995; Merino-Puerto *et al.*, 2011b; Wilk *et al.*, 2011). Furthermore, all deletion mutants still show molecular exchange between cells (Mullineaux *et al.*, 2008; Merino-Puerto *et al.*, 2010; Mariscal *et al.*, 2011; Merino-Puerto *et al.*,

2011b), suggesting that in addition to SepJ, FraC and FraD, other proteins are also involved in intercellular communication in *Anabaena* sp. PCC 7120.

The inactivation of the *fraH* gene (*alr1603*) in *Anabaena* sp. PPC 7120 results in filament fragmentation and hence suggests a possible influence of the protein on cell-cell communication (Bauer *et al.*, 1995; Merino-Puerto *et al.*, 2010; Merino-Puerto *et al.*, 2011a). However, FRAP analyses using the fluorescent tracers calcein and 5-CFDA indicated no or only partially impaired transfer of both molecules (Merino-Puerto *et al.*, 2011a). Another candidate is the gene *conR* (*all0187*) which encodes a LytR-CpsA-Psr domain protein that is associated with cell wall maintenance, the development of normal septa and diazotrophic growth (Fan *et al.*, 2006; Mella-Herrera *et al.*, 2011). Mella-Herrera *et al.* (2011) hypothesised that the diazotrophic growth defect might be a result of the inability to transport fixed nitrogen from heterocysts into neighbouring vegetative cells. Whether transfer is affected remains to be investigated.

In order to establish the presence of fully functional channels linking the cytoplasm of neighbouring cells the septal peptidoglycan layer needs to be penetrated by nanopores. Such modification requires the activity of specific enzymes. In *E. coli* three N-acetylmuramyl-L-alanine amidases, AmiA, AmiB and AmiC were found to play an important role in septation and the following separation of the daughter cells (Heidrich *et al.*, 2001). Deletion of the *ami* genes results in the formation of long cell chains as cell wall cross-links cannot be destroyed by cleaving the amide bond between the N-terminal L-alanine residue and the N-acetylmuramic acid backbone (Heidrich *et al.*, 2001). Just recently the function of these amidases was investigated in the filamentous, heterocyst-

forming cyanobacteria *Anabaena* sp. PCC 7120 (Zhu *et al.*, 2001; Berendt *et al.*, 2012) and *N. punctiforme* ATCC 29133 (Lehner *et al.*, 2011; Lehner *et al.*, 2013). Both organisms possess two adjacent copies of the *amiC* gene homologue, *amiC1* and *amiC2*. Localisation studies with GFP-labelled variants revealed the presence of the amidases in young septa of freshly divided vegetative cells, cells of hormogonia and in the polar region of developing heterocysts (Lehner *et al.*, 2011; Berendt *et al.*, 2012; Lehner *et al.*, 2013). In *N. punctiforme* ATCC 29113 the gene *amiC2* (NpF1846) is pivotal for filament morphology, intercellular communication, cell differentiation and the formation of nanopores in the cross-walls (Lehner *et al.*, 2011; Lehner *et al.*, 2013). An *amiC2* deletion mutant of *N. punctiforme* ATCC 29113 forms irregular clusters of twisted cells which lack nanopores at the septal peptidoglycan layer and cell-cell connecting structures, and are accordingly unable to transfer calcein between cells within the filament (Lehner *et al.*, 2011; Lehner *et al.*, 2013). Interestingly, *amiC2* (*alr0093*) seems to be less important for maintaining cell and filament morphology in *Anabaena* sp. PCC 7120 (Zhu *et al.*, 2001; Berendt *et al.*, 2012). Results obtained for the importance of AmiC2 (or HcwA (**h**eterocyst **c**ell **w**all formation protein **A**)) (Zhu *et al.*, 2001) are contradictory. While Zhu *et al.* (2001) showed that the gene is essential for growth on N₂, the deletion mutant generated by Berendt *et al.* (2012) did not show any altered phenotype in the absence of a combined nitrogen source in comparison to the wild-type. Inactivation of *amiC1* (*alr0092*) in *Anabaena* sp. PCC 7120 however, resulted in a mutant which was unable to grow diazotrophically and transfer calcein between cells (Berendt *et al.*, 2012). Whether the mutant is also affected in the formation of nanopores remains to be investigated. It is not known whether AmiC1 has a similar function in

N. punctiforme ATCC 29113. Attempts to inactivate the gene have so far failed, suggesting that *amiC1* (NpF1845) is essential for growth of the organism even in the presence of a combined nitrogen source (Lehner *et al.*, 2011).

In summary, remodelling of the peptidoglycan layer is required for the formation of functional heterocysts and normal intercellular septa in the filamentous, heterocyst-forming cyanobacteria *Anabaena* sp. PCC 7120 and *N. punctiforme* ATCC 29133. AmiC proteins possibly drill holes into the cross-walls which could provide the framework for cell-joining proteins such as SepJ, FraC and FraD (Lehner *et al.*, 2013). Additionally, they might increase the permeability of the peptidoglycan layer of developing heterocysts in order to transfer glycolipids and polysaccharides across the cell wall for the formation of the heterocyst envelope (Zhu *et al.*, 2001).

1.6 Aims and scope of the thesis

This work aims to deepen our knowledge of intercellular communication in filamentous heterocyst-forming cyanobacteria by using the well-established model organism *Anabaena* sp. PCC 7120 (Section IV; chapter 3, 4 and 5) and the potential model organism for cyanobacteria of Section V, *Mastigocladus laminosus* (chapter 6).

Although previous FRAP studies revealed that molecules diffuse via channels connecting the cytoplasm of neighbouring cells in *Anabaena* sp. PCC 7120 little is still known about the selectivity of the channels for different kinds of molecules. All studies so far used artificial fluorescent tracers that are related members of a family of fluorescein derivatives. In chapter 3, the transfer of

molecules with different properties including artificial but also molecules which are similar to physiological-important metabolites is investigated. These molecules include the fluorescent sucrose analogue esculin (chapter 3.1), the fluorescent glucose derivatives 2- and 6-NBDG (chapter 3.2) and the artificial fluorescent tracer BCECF (chapter 3.3). Furthermore, the role of the septal proteins FraC, FraD and SepJ for the exchange of these molecules is examined.

Chapter 4 addresses the question of the function of SepJ by overexpressing the gene and investigating its influence on filament length, heterocyst spacing pattern and molecular exchange. By fusing SepJ to the fluorescent protein GFP the localisation of the additional proteins was visualised in the background of various mutants and the wild-type.

In another approach, insights into the properties of the septal junctions were revealed by inducing filament breakage by sonication and investigating its influence on molecular exchange and the localisation of SepJ (chapter 5). The question, whether filament breakage results in the death of the entire filament or individual cells possess the ability to close their open ends, is addressed.

In the final chapter 6, multicellularity in terms of intercellular communication is explored in *Mastigocladus laminosus*, a true branching cyanobacterium of Section V. FRAP experiments and SepJ localisation studies are performed in order to reveal insights into differences and similarities in intercellular communication between *Anabaena* sp. PCC 7120 and *Mastigocladus laminosus*.

2 Materials and methods

2.1 Oligonucleotides

Oligonucleotides for PCR and sequencing were obtained from Sigma-Aldrich and Eurofins. Lyophilised primers were solubilised in nuclease-free water to a final concentration of 10 μ M. Table 4 summarises oligonucleotides used in this study.

Table 4. Oligonucleotides used in this study

primer	sequence (5' \rightarrow 3')
alr2338_7	atacaggaaattagagtgagc
fw_d_sepJ_ML_down_BamHI	cccaacagtcacggatcccgccgatg
fw_d_sepJ_ML_up_SpeI	ttaactagtgtcagaaaactcacgagc
fw_mlam_sepJ	atggggcgcattgagaagcg
Fw_mTq2_EcoRV	gatatcatggtgagcaagggcgag
fw_neo	ctgcttgccgaatatcatggtg
pRL500_1	ataggcgtatcacgaggc
rv_d_sepJ_ML_down_PstI	taactgcagtataggagctaaaacc
rv_d_sepJ_ML_up_BamHI	catcggcgggatccgatgactgttggg
rv_mlam_hetR	gttcggctgcatctaaaaa
rv_mlam_sepJ_seq	gctgtcctgatgataagctgg
rv_mTq2	gtccggactgtacagctcgtc
YFP-1	gatatcatggtgagcaagggcga
YFP-2	ttaaacacctgtacagctcgtc

2.2 Strains and plasmids

Microbial strains and plasmids used in this study are listed in Table 5.

Table 5. Strains and plasmids used in this study.

strain or plasmid	genotype or relevant characteristics	resistance*	source or reference
<i>Anabaena</i> sp. strains			
PCC 7120	wild-type		PCC
CSAM137	<i>sepJ-gfp</i>	Sm ^R Sp ^R	Flores <i>et al.</i> (2007)
CSDN1A	Φ(C.K1(+)- <i>sepJ</i>)	Km ^R	This study
CSDN1B	Φ(C.K1(-)- <i>sepJ</i>)	Km ^R	This study
CSDN2A	Φ(C.K1(+)- <i>sepJ</i>) in pCSAM200	Sm ^R Sp ^R	This study
CSDN2B	Φ(C.K1(-)- <i>sepJ</i>) in pCSAM200	Sm ^R Sp ^R	This study
CSDN7	<i>sepJ-eYFP</i>	Sm ^R Sp ^R	This study
CSDN11	Φ(C.K3(+)- <i>sepJ-gfp</i>)	Km ^R	This study
CSDN21	Npun_R5320-R5323 in pRL25C	Km ^R	This study
CSDN24	<i>sepJ-cfp</i>	Sm ^R Sp ^R	This study
CSDN28	<i>sepJ-mTurquoise2</i>	Sm ^R Sp ^R	This study
CSS7	<i>cphA1 (all3879)::C.S3</i>	Sm ^R Sp ^R	Picossi <i>et al.</i> (2004)
CSVM18	P _{patS} promoter- <i>gfp</i>	Sm ^R Sp ^R	Mariscal <i>et al.</i> (2007)

strain or plasmid	genotype or relevant characteristics	resistance [*]	source or reference
Anabaena sp. strains			
CSVM34	$\Delta sepJ$		Mariscal <i>et al.</i> (2011)
CSVM34-DN11	$\Delta sepJ$; $\Phi(C.K3(+)-sepJ-gfp)$	Km ^R	This study
CSVM34-DN21	$\Delta sepJ$; Npun_R5320-R5323 in pRL25C	Km ^R	This study
CSVM141	$\Delta sepJ \Delta fraC \Delta fraD$		Vicente Mariscal, unpublished
CSVM141-DN11	$\Delta sepJ \Delta fraC \Delta fraD$; $\Phi(C.K3(+)-sepJ-gfp)$	Km ^R	This study
CSVM141-DN21	$\Delta sepJ \Delta fraC \Delta fraD$; Npun_R5320-R5323 in pRL25C	Km ^R	This study
CSVT22	$\Delta fraC \Delta fraD$		Merino-Puerto <i>et al.</i> (2011)
CSVT22-DN21	$\Delta fraC \Delta fraD$; Npun_R5320-R5323 in pRL25C	Km ^R	This study
Other cyanobacterial strains			
<i>M. laminosus</i> MLDN42	$sepJ::C.K1(-)$	Km ^R	This study
<i>Mastigocladus laminosus</i> SAG 4.84	wild-type		SAG
<i>Nostoc punctiforme</i> ATCC 29113-S (UCD 153)	spontaneous derivative that grows more homogenously and rapidly than wild-type		Campbell <i>et al.</i> (2007; 2008)

strain or plasmid	genotype or relevant characteristics	resistance*	source or reference
<i>Escherichia coli</i> K-12 strains			
DH5 α	F ⁻ ϕ 80 <i>lacZ</i> Δ M15 Δ (<i>lacZYA-argF</i>) U169 <i>recA1 endA1</i> <i>hsdR17</i> (r _K ⁻ , m _K ⁺) <i>phoA supE44</i> λ^- <i>thi-1 gyrA96 relA1</i> versatile cloning strain		Bethesda Research Laboratories (1986)
ED8654	F ⁻ <i>lacY1 hsdR514</i> (r _K ⁻ , m _K ⁻) <i>supE44 supF58 recA56 mcrA1</i> <i>metB1 galK2 galT22 trpR55 tyrT58</i> λ^-		Borck <i>et al.</i> (1976)
HB101	F ⁻ <i>hsdS20</i> (r _B ⁻ , m _B ⁻) <i>leuB6 supE44 ara14 galK2 lacY1</i> <i>proA2 rpsL20</i> (Sm ^R) <i>xyl-5 mtl-1 recA13 mcrBC</i>	Sm ^R	Boyer and Roulland-Dussoix (1969)
NEB5 α	DH5 α derivative; versatile cloning strain		NEB
plasmids			
pCSAM135	<i>sepJ-C-gfp</i> cloned in pGEM [®] T-Easy	Amp ^R	Flores <i>et al.</i> (2007)
pCSAM200	replicative vector	Sm ^R Sp ^R	Ionescu <i>et al.</i> (2010)
pCSDN1A	C.K1(+)- <i>sepJ</i> cloned in pCSV3	Km ^R Sm ^R Sp ^R	This study
pCSDN1B	C.K1(-)- <i>sepJ</i> cloned in pCSV3	Km ^R Sm ^R Sp ^R	This study
pCSDN2A	C.K1(+)- <i>sepJ</i> cloned in pCSAM200	Km ^R Sm ^R Sp ^R	This study

strain or plasmid	genotype or relevant characteristics	resistance[*]	source or reference
pCSDN2B	C.K1(-)- <i>sepJ</i> cloned in pCSAM200	Km ^R Sm ^R Sp ^R	This study
pCSDN3	<i>sepJ</i> cloned in pRL278 with C.K3 cassette upstream of gene	Km ^R	This study
pCSDN5	<i>eyfp</i> cloned in pSPARK [®]	Amp ^R	This study
pCSDN6	<i>sepJ-C-eyfp</i> cloned in pGEM [®] T-Easy	Amp ^R	This study
pCSDN7	<i>sepJ-C-eyfp</i> cloned in pCSV3	Sm ^R Sp ^R	This study
pCSDN10	<i>sepJ-gfp</i> cloned in pSPARK [®]	Amp ^R	This study
pCSDN11	<i>sepJ-gfp</i> cloned in pRL278	Km ^R	This study
pCSDN21	Npun_R5320-23 cloned in pRL25C	Km ^R	This study
pCSDN24	<i>sepJ-C-cfp</i> cloned in pCSV3	Sm ^R Sp ^R	This study
pCSDN27	<i>mTurquoise2</i> cloned in pGEM [®] T-Easy	Amp ^R	This study
pCSDN28	<i>sepJ-C-mTurquoise2</i> cloned in pCSV3	Sm ^R Sp ^R	This study
pCSV3	positive selection vector	Sm ^R Sp ^R	Valladares <i>et al.</i> (2011)
pCSV58	source of <i>sepJ</i>	Amp ^R	Vicente Mariscal, unpublished

strain or plasmid	genotype or relevant characteristics	resistance*	source or reference
pCSV59A	source of C.K1(+)- <i>sepJ</i>	Amp ^R Km ^R	Vicente Mariscal, unpublished
pCSV59B	source of C.K1(-)- <i>sepJ</i>	Amp ^R Km ^R	Vicente Mariscal, unpublished
pCSVT10	<i>cfp</i> cloned in pMBL-T	Amp ^R	Victoria Merino-Puerto, unpublished
pDN40	<i>sepJ</i> (<i>M. lamosus</i>) with inserted BamHI site cloned in pRL271	Cm ^R Em ^R	This study
pDN42	pDN40 with inserted C.K1 in BamHI	Cm ^R Em ^R Km ^R	This study
71 pGEM [®] -T Easy	cloning vector	Amp ^R	Promega
pmTurquoise2-C1	source of <i>mTurquoise2</i>	Km ^R	Goedhart <i>et al.</i> (2012)
pRL25C	cargo plasmid; carries pDU1 replicon	Km ^R	Wolk <i>et al.</i> (1988)
pRL161	source of C.K1 cassette	Km ^R	Elhai and Wolk (1988)
pRL271	suicide vector containing <i>sacB</i> for the selection of double recombination events	Cm ^R Em ^R	Black <i>et al.</i> (1993)
pRL278	suicide vector containing <i>sacB</i> for the selection of double recombination events	Km ^R	Black <i>et al.</i> (1993)

strain or plasmid	genotype or relevant characteristics	resistance[*]	source or reference
pRL443	conjugative plasmid	Amp ^R Km ^R Tc ^R	Elhai <i>et al.</i> (1997)
pRL623	helper plasmid; carries mob and DNA methylases M.AvaI, M.Eco47II, and M.EcoT22I	Cm ^R	Elhai <i>et al.</i> (1997)
pSKS3-cph2(1-6)-eYFP	source of <i>eyfp</i>	Amp ^R Cm ^R	Annegret Wilde, unpublished
pSPARK [®]	cloning vector	Amp ^R	Canvax, Biotech SL
pUC19	transformation efficiency test vector	Amp ^R	Yanisch-Perron <i>et al.</i> (1985)

* Amp – ampicilin; Cm – chloramphenicol; Em - erythromycin; Km – kanamycin (determinants also confer resistance to neomycin (Nm)); Sm – streptomycin; Sp – spectinomycin; Tc - tetracycline

2.3 Bioinformatics methods

2.3.1 Generation of plasmids and oligonucleotide primers

Serial Cloner (SerialBasics) was used to develop cloning strategies and to draw plasmid maps. Properties of generated oligonucleotides were calculated using OligoCalc (Kibbe, 2007).

2.3.2 Amino acid sequence analyses

DNA sequences were translated into the corresponding amino acid sequences using the ExPASy translate tool (<http://web.expasy.org/translate/>). Further sequence analyses were performed using the TMHMM server 2.0 (<http://www.cbs.dtu.dk/services/TMHMM/>) in order to predict the localisation of transmembrane helices, TRUST (Szklarczyk and Heringa, 2004) for the detection of internal repeats, and Coils/PCoils (<http://toolkit.tuebingen.mpg.de/pcoils>) for the identification of potential coiled-coiled regions in proteins.

2.3.3 Blast search, sequence alignment and phylogenetic reconstruction

BlastP (Altschul *et al.*, 1997) and BlastN (Zhang *et al.*, 2000) searches were performed to identify orthologous sequences. Sequences were aligned using ClustalW 2.1 (Larkin *et al.*, 2007) and phylogenetic reconstructions were performed using the Phylogeny.fr platform (Dereeper *et al.*, 2008).

2.3.4 Physicochemical properties of molecules

Molecular properties and structures were predicted by using tools at chemicalize.org and Marvin 6.0.2 (ChemAxon).

2.4 Microbial methods

2.4.1 Growth of cyanobacteria

N. punctiforme ATCC 29113-S was grown in liquid BG11₀ medium (Rippka *et al.*, 1979) supplemented with 2.5 mM NH₄Cl and 5 mM TES-NaOH buffer (pH 7.5) at 30°C under constant agitation (100 rpm) and under illumination with white light of approximately 20 μE m⁻² s⁻¹, or on agar plates with 1 % (w/v) Bacto agar (BD).

Anabaena sp. strains were grown in liquid BG11 medium (BG11₀ medium supplemented with 17.6 mM NaNO₃) (Rippka *et al.*, 1979) under the conditions stated above. Mutants were cultivated in the presence of antibiotics when indicated. Neomycin was added to liquid medium in a final concentration of 10 μg ml⁻¹ and of 40 μg ml⁻¹ to agar plates. Spectinomycin and streptomycin were used in a final concentration of 2.5 μg ml⁻¹ for both liquid medium and agar plates. Heterocyst differentiation was induced by growth in BG11₀ medium under the conditions described above. The cells were first harvested by centrifugation (3,000xg; 5 min) and then washed three times in BG11₀ medium. The composition of BG11₀ medium is given in Table 6.

Table 6. Composition of BG11₀ medium.

BG11 ₀	
component	concentration (mg l ⁻¹)
MgSO ₄ * 7 H ₂ O	75
CaCl ₂ * 2 H ₂ O	36
Citric acid	6
Ferric ammonium citrate	6
Na ₂ -EDTA	0.93
Na ₂ CO ₃	20
H ₃ BO ₃	2.86
MnCl ₂ * 4 H ₂ O	1.81
ZnSO ₄ * 7 H ₂ O	0.222
Na ₂ MoO ₄ * 2 H ₂ O	0.39
CuSO ₄ * 5 H ₂ O	0.079
CoCl ₂ * 6 H ₂ O	0.0494
K ₂ HPO ₄	34.8

Mastigocladus laminosus SAG 4.84 was grown in liquid Castenholz D medium (Castenholz, 1988) at 40°C, under constant white light at approximately 20 $\mu\text{E m}^{-2} \text{s}^{-1}$. To provide constant agitation cultures were bubbled with sterile air or shaken (100 rpm). Heterocyst differentiation was induced by removal of combined nitrogen and incubation in liquid Castenholz ND medium (Castenholz, 1988), under the above described conditions. For growth on solid medium 1.5 % (w/v) agar was added to the media. The composition of Castenholz D and Castenholz ND medium is given in Table 7.

Table 7. Composition of Castenholz D and Castenholz ND medium.

component	concentration (mg l ⁻¹)	
	Castenholz D	Castenholz ND
nitrilotriacetic acid (NTA)*	100	100
NaNO ₃	700	
KH ₂ PO ₄		36
Na ₂ HPO ₄	110	70
KNO ₃	100	
MgSO ₄ * 7 H ₂ O	100	100
CaSO ₄ * 2 H ₂ O	60	60
NaCl	8	8
FeCl ₃ * 6 H ₂ O	0.25	0.25
<u>micronutrients</u>		
MnSO ₄ * H ₂ O	1.14	1.14
H ₃ BO ₃	0.25	0.25
ZnSO ₄ * 7 H ₂ O	0.25	0.25
CuSO ₄ * 5 H ₂ O	0.0125	0.0125
Na ₂ MoO ₄ * 2 H ₂ O	0.0125	0.0125
CoCl ₂ * 6 H ₂ O	0.0225	0.0225
H ₂ SO ₄ (conc.)	0.25 µl	0.25 µl

* NTA was first dissolved by adjusting the pH to 6.5 with KOH. After adding the remaining components the pH was adjusted to 7.5 and the solution sterilised by autoclaving.

2.4.2 Growth of *Escherichia coli*

Cells of *Escherichia coli* were grown in liquid lysogeny broth (LB) medium (Table 8) or on 1.5 % (w/v) LB agar at 37°C. Liquid cultures were agitated with 180 to 250 rpm. In order to select for bacterial cells bearing plasmids antibiotics were added as follows: 100 µg ml⁻¹ ampicilin, 30 µg ml⁻¹ chloramphenicol, 50 µg ml⁻¹ kanamycin, 50 µg ml⁻¹ spectinomycin and 25 µg ml⁻¹ streptomycin.

Table 8. Composition of LB medium, variation Miller.

LB medium, Miller	
component	concentration (g l ⁻¹)
trypton	10
yeast extract	5
NaCl	10

2.4.3 Cryopreservation and recovery

For long-term storage microbial cells were harvested from late log or early stationary growth phases by centrifugation (3,000xg; 3 min) and resuspended in the corresponding growth medium supplemented with either 20 % (w/v) glycerol (*E. coli*) or 8 % (v/v) dimethyl sulfoxide (DMSO) (cyanobacteria). Cells were immediately flash frozen in liquid nitrogen and stored at -80°C.

For short-term storage *E. coli* cells were frozen in LB medium supplemented with 20 % (w/v) glycerol and stored at -20°C.

Viable cells of *E. coli* were recovered by transferring a small amount of the frozen culture into liquid LB medium or by restreaking cells on LB agar plates supplemented with appropriate antibiotics.

Cyanobacterial cultures of *Anabaena* sp. strains and *N. punctiforme* ATCC 29133 were recovered by transferring a drop of a thawed culture to a BG11 agar plate and keeping the plate at room temperature until the media was fully absorbed. The culture was then spread away from the original place to avoid inhibition of growth by DMSO. Cells of *M. laminosus* were revived by transferring 'cell clumps' directly to liquid growth medium and incubating the culture under the conditions described above.

2.4.4 Preparation of chemical competent *E. coli* cells

Chemical competent cells of *E. coli* were prepared after a slightly modified protocol by Inoue *et al.* (1990). 3 ml of LB medium supplemented with 20 mM glucose were inoculated with a single colony of *E. coli* and grown over day at 37°C and 200 rpm. 0.5 ml of the culture was transferred to 25 ml fresh LB – 20 mM glucose medium and grown at 25°C and 200 rpm overnight. 50 ml LB medium supplemented with 20 mM glucose were then inoculated with 2.5 ml of the pre-culture and grown at 25°C and 200 rpm until the OD₆₀₀ reached 0.5 to 0.6. Cells were placed on ice for 20 min before harvesting by centrifugation (3,000xg; 5 min; 4°C). The supernatant was discarded and the cell pellet resuspended in 12.5 ml ice-cold transformation buffer (10 mM HEPES, pH 6.7; 55 mM MnCl₂; 15 mM CaCl₂; 150 mM KCl). After centrifugation for 5 min at 3,000xg and 4°C the cell pellet was resuspended in 5 ml ice-cold transformation buffer and 7 % (v/v) DMSO was added. Cells were mixed gently and placed on ice for 30 min.

Flash frozen aliquots of 200 µl were stored at -80°C. Transformation efficiency was tested by adding 100 pg of plasmid pUC19. Cells with a transformation efficiency greater than $1 * 10^5$ cfu µg⁻¹ DNA were used for further transformations.

2.4.5 Transformation of *E. coli* cells with plasmids

Transformation of *E. coli* cells with plasmids was performed according to Hanahan (1983). 200 µl of competent cells were thawed on ice for 20 min. 10 µl of ligation mixture or approximately 50 ng of plasmid DNA were added, the suspension gently mixed and further incubated on ice. After 20 min of incubation cells were heat shocked for 90 s at 42°C (water bath) and chilled for 5 min on ice. 800 µl of LB medium was added and the tubes were incubated for 1 h at 37°C and 200 rpm. Cells were harvested by centrifugation (10,000xg; 30 s), the supernatant was decanted and the cells were resuspended in the remaining liquid. Cells were then spread on LB agar plates supplemented with appropriate antibiotics and incubated at 37°C overnight.

2.4.6 Conjugation of cyanobacteria

2.4.6.1 Conjugation of *Anabaena* sp. PCC 7120

Constructs generated in this work (see Table 5) were transferred to *Anabaena* sp. PCC 7120 strains by conjugation as described by Elhai and Wolk (1988). Cargo plasmids were transferred to *E. coli* HB101 cells containing the helper plasmid pRL623 (Elhai *et al.*, 1997) which encodes mobilisation proteins (mob) from ColK that allow the mobilisation of plasmids carrying the oriT of pMB1 such as the derivatives of pBR322 used in this study. Additionally, pRL623 encodes three

DNA methylases M.AvaI, M.Eco47II, and M.EcoT22I which protect the plasmid against digestion by the restriction enzymes of *Anabaena* sp. PCC 7120. A second *E. coli* strain containing the conjugative plasmid pRL443 (Elhai *et al.*, 1997), a RP4 derivative that lost its kanamycin resistance and allows the usage of cargo plasmids for the generation of mutants which contain a kanamycin resistance cassette was used in this study for conjugation. Both strains HB101 [pRL623 + cargo plasmid] and ED8654 [pRL443] were grown in 3 ml liquid LB medium supplemented with the appropriate antibiotics overnight at 37°C. 250 µl ED8654 [pRL443] and 350 µl of HB101 [pRL623 + cargo plasmid] were added to 10 ml of LB medium supplemented with appropriate antibiotics and were grown for 2.5 h at 37°C. Antibiotics were removed by washing the cells three times with 10 ml LB medium (3,000xg; 3 min). After the final centrifugation, the cell pellets were resuspended in approximately 60 µl of LB medium and both cultures mixed. The cell mixture was left for 1.5 h at room temperature before adding cells of *Anabaena* sp. strains corresponding to 10 µg of chlorophyll *a*. Cells were spotted on Immobilon-NC membrane (Millipore) on 1 % (w/v) agar BG11 plates supplemented with 5 % (v/v) LB medium, and incubated for 3 h in the dark at 30°C before exposing to normal light conditions. After 24 h of incubation the membrane was transferred to a 1 % (w/v) agar BG11 plate, and for selection every 48 h to 72 h transferred to a 1 % (w/v) agar BG11 plate supplemented with up to 5 µg ml⁻¹ streptomycin and spectinomycin or up to 200 µg ml⁻¹ neomycin. Colonies were picked and restreaked on 1 % (w/v) agar BG11 plates supplemented with antibiotics until strains were fully segregated.

2.4.6.2 Conjugation of *M. laminosus* SAG 4.84

For the transfer of plasmids to *M. laminosus* SAG 4.84 a similar approach was used as described for *Anabaena* sp. PCC 7120. Prior to the conjugation a *M. laminosus* culture was homogenised by several passages through a syringe needle of 0.8 mm in diameter, and the disrupted filaments were washed four times with Castenholz D medium. Cells were resuspended by vortexing, and harvested by centrifugation (5,000xg; 5 min). Before adding *M. laminosus*, the *E. coli* strain HB101 bearing plasmid pRL623 and the construct for genomic modification and *E. coli* strain ED8654 bearing plasmid pRL443 were mixed, and incubated for 2 h at RT. The amount of *M. laminosus* cells was adjusted to 15µg of chlorophyll *a* per plate. Cells were spotted on Immobilon-NC membrane (Millipore) on 1 % (w/v) agar Castenholz D plates supplemented with 5 % (v/v) LB medium, and incubated for 3 h in the dark at 35°C before exposing to normal light conditions. After 24 h the membrane was transferred to a 1 % (w/v) agar Castenholz D plate, and for selection every 48 h to 72 h transferred to a 1 % (w/v) agar Castenholz D plate supplemented with antibiotics. For selection of strains bearing a kanamycin resistance cassette 60 µg ml⁻¹ neomycin was added to the plates. Colonies were picked and restreaked three times on 1 % (w/v) agar Castenholz D plate supplemented with 30 µg ml⁻¹ neomycin before growing in liquid Castenholz D medium with 10 µg ml⁻¹ neomycin at 40°C.

2.4.7 Determination of Chlorophyll *a* concentration

Chlorophyll *a* (Chl *a*) concentrations were used to estimate culture growth and to standardise conjugation of *Anabaena* sp strains and *M. laminosus*. Chl *a* was extracted from cyanobacterial cells by adding methanol to a final concentration of

90 % (v/v) and vortexing the suspension for 1 min at RT. After removing cell fragments by centrifugation (16,100xg; 1 min) the absorption of the supernatant was measured at 665 nm with a Jenway 6300 spectrophotometer. The final concentration of Chl *a* was calculated in terms of the formula $\text{Chl } a \text{ } [\mu\text{g ml}^{-1}] = 13.43 * A_{665 \text{ nm}} * \text{dilution factor}$ (Porra *et al.*, 1989).

2.5 Genetic methods

2.5.1 Genomic DNA isolation from cyanobacteria

Depending on the cyanobacterial strain various methods for the extraction of genomic DNA were used.

Genomic DNA from *Anabaena* sp. strains and *N. punctiforme* ATCC 29133-S

was isolated by phenol-chloroform extraction as described by Cai and Wolk (1990). Cells were harvested by centrifugation (4,000xg; 5 min) and resuspended in 400 μl 10 mM Tris - 0.1 mM EDTA, pH 7.5. To break cells 150 μl sterile glass beads (212 - 300 μm diameter; Sigma-Aldrich), 20 μl of a 10 % sodium dodecyl sulphate (SDS) solution and 450 μl phenol-chloroform (1:1 (v/v)) were added and the suspension vigorously vortexed for 1 min at RT before cooling on ice for 1 min. This cycle was repeated 4 to 6 times. The final suspension was centrifuged for 15 min at 15,000xg and 4°C, and the supernatant was transferred to a new microcentrifuge tube. The supernatant was extracted once with phenol, once with phenol:chloroform (1:1 (v/v)) and twice with chloroform with centrifugation steps in between (15,000xg; 1 min). DNA was precipitated by adding 1/10 volume of 3 M sodium acetate pH 5.2 and 2.5 volumes ethanol. After overnight incubation at -20°C the suspension was centrifuged for 15 min at 15,000xg and 4°C. The DNA

pellet was washed once in 70 % (v/v) ethanol and dried on air before resuspending in 30 μ l 10 mM Tris - 0.1 mM EDTA, pH 7.5. Genomic DNA samples were stored at 4°C.

Genomic DNA from *M. laminosus* was extracted using the protocol of Morin *et al.* (2010) with a cell homogenisation step prior cell lysis. The cells were harvested by centrifugation (3,000xg, 5 min) and resuspended in fresh growth medium. Homogenisation of the culture was achieved by multiple passages through a 0.8 mm needle with the help of a syringe. The cells were collected by centrifugation (3,000xg, 5 min), resuspended in 0.5 ml in 0.15 M NaCl, 0.1 M EDTA, pH 8.0 and transferred to a 2 ml cryogenic vial (Nalgene®) for three freeze-thawing cycles, alternating freezing in liquid nitrogen and thawing in a water bath at 37°C. Cells were harvested by centrifugation (7,000xg; 2 min) and resuspended in 0.5 ml TE buffer (10 mM Tris-HCl, 1 mM EDTA, pH 8.0) for the subsequent enzymatic cell lysis by adding 100 μ l of a 50 mg ml⁻¹ of lysozyme solution (Sigma-Aldrich) and incubating the suspension for 30 min at 37°C. Protein degradation was achieved by adding 12.5 μ l of 20 mg ml⁻¹ proteinase K (Qiagen) and SDS to a final concentration of 2 % (v/v) and incubating the mixture for 1 h at 37°C. To remove proteins and polysaccharides which are highly abundant in cultures of *M. laminosus*, forming thick sheaths surrounding the filaments, and have been shown to inhibit enzymes such as DNA polymerases (Fang *et al.*, 1992) 0.1 volume of cetyltrimethylammonium bromide (CTAB; AppliChem) and 150 μ l of 5 M NaCl were added to the solution. After 10 min of incubation at 65°C 1 volume of chloroform:isoamyl alcohol (24:1 (v/v)) was added and the tubes placed on ice for 30 min to allow precipitation of CTAB-protein and -polysaccharide complexes. After centrifugation (12,000xg; 10 min)

the supernatant was transferred to a new microcentrifuge tube and 0.6 volume of 2-propanol was added to precipitate DNA. The tubes were centrifuged for 10 min at 12,000xg and the DNA pellet was washed once in 70 % (v/v) ethanol. After a final centrifugation step (12,000xg; 10 min) the supernatant was discarded and the pellet was dried at air before resuspending in 50 µl TE buffer. Purified genomic DNA was stored at 4°C.

Alternatively, genomic DNA from all cyanobacterial organisms used in this study was successfully extracted by using the ZR Fungal/Bacterial DNA MiniPrep™ kit (Zymo Research).

2.5.2 Plasmid isolation

Plasmid isolation was generally performed with commercially available kits from Qiagen (QIAprep Spin Miniprep Kit), Machery-Nagel (NucleoSpin Plasmid), peqlab (peqGOLD Plasmid Miniprep Kit I) and Thermo Scientific (GeneJET Plasmid Miniprep Kit) according to the manufacturer's protocols.

Alternatively, plasmids were extracted from *E. coli* by classical alkaline lysis with SDS (Sambrook and Russel, 2001). 3 ml of an *E. coli* overnight culture were harvested by centrifugation (3,000xg; 3 min) and cells were resuspended in 100 µl of ice-cold solution I (Table 9). Alkaline lysis was initiated by adding 200 µl of freshly prepared solution II (Table 9), mixing the solutions by inverting the tube rapidly for 5 times and adding 150 µl of ice-cold solution III (Table 9). Tubes were inverted until the sample was homogenously mixed and centrifuged for 5 min at 16,100xg and 4°C. The supernatant was transferred to a new microcentrifuge tube and nucleic acids were precipitated by adding 2 volumes of

ethanol and leaving the tube for 2 min at room temperature. Precipitated nucleic acids were collected by centrifugation (16,100xg; 5 min), washed once in 70 % (v/v) ethanol and finally resuspended in 50 μ l of 10 mM Tris – 1 mM EDTA, pH 8.0 containing 10 μ g ml⁻¹ RNase A. Plasmid DNA was stored at – 20°C for further analyses.

Table 9. Composition of the solutions I, II and III for plasmid isolation.

solution I	solution II	solution III
50 mM glucose	0.2 N NaOH	60 ml 5 M potassium acetate
25 mM Tris-HCl pH 8.0	1 % (w/v) SDS	11.5 ml glacial acetic acid
10 mM EDTA pH 8.0		28.5 ml H ₂ O

2.5.3 DNA quantification

DNA was quantitated by using different strategies. Nucleic acids absorb ultraviolet radiation. At 260 nm the optical density of a 50 μ g ml⁻¹ solution of double strand DNA equals 1.0. To get an indication of the purity of the DNA solution the OD₂₆₀:OD₂₈₀ ratio was calculated; solutions possessing a ratio above 1.8 were considered as pure. Absorption was measured with a NanoVue Plus spectrophotometer (GE Healthcare). Alternatively, DNA concentrations were determined by using a fluorescent dye that is specific for double-stranded DNA and becomes highly fluorescent after binding to its target molecule (Qubit system, Thermo Fisher Scientific Inc.). The fluorescence is then detected with a fluorometer and converted into a DNA concentration by comparing the signal with that of samples of known DNA concentrations. In comparison to UV absorbance measurements the Qubit system allows distinguishing between DNA,

RNA, free nucleotides and proteins and thus provides an accurate way to determine the actual double-stranded DNA concentration in the sample.

2.5.4 Polymerase chain reaction (PCR)

DNA fragments from cyanobacterial genomes or plasmids were amplified using the polymerase chain reaction (PCR) technique. For the amplification of DNA fragments for cloning and sequencing DNA polymerases were used that possess a 3' → 5' proofreading exonuclease activity which excises mismatched nucleotides and thus reduces the error rate. In this study the high-fidelity DNA polymerases iProof (Bio-Rad) and Phusion (NEB) and the Expand High Fidelity PCR System (Roche) were used for high quality DNA amplification. For the determination of the optimal annealing temperature and to identify mutants, *Taq* polymerases were used from Bioline (BioTaq) and Promega (PCR Master Mix). A standard PCR mixture contained 1-10 ng plasmid DNA or 50-150 ng genomic DNA as template, 200 μM of each desoxynucleoside triphosphate (dNTP), including dATP, dCTP, dGTP and dTTP, 0.5 μM of each primer (forward and reverse) and 1-2 U of DNA polymerase per 50 μl reaction. For colony PCRs single colonies of *E. coli* or cyanobacteria were resuspended in the DNA-free PCR reaction mixture after restreaking the culture on a new agar plate. Table 10 summarises the general PCR cycling procedure for the different enzymes used in this study. Reactions were carried out in a C1000 Thermal Cycler (Bio-Rad) and a MyCycler (Bio-Rad).

Table 10. PCR cycling procedure

		iProof/Phusion	BioTaq
denaturation		98°C; 30 s	95°C; 3 min
25-30 cycles	denaturation	98°C; 10 s	95°C; 30 s
	annealing*	45-72°C; 30 s	60-65°C; 30 s
	elongation	72°C; 1 kb 30 s ⁻¹	72°C; 1 kb 30 s ⁻¹
final elongation		72°C; 10 min	72°C; 10 min

* Annealing temperatures were generally 5°C below the lowest melting temperature of the pair of primers used

2.5.5 Purification of PCR products

To remove oligonucleotides, unspecific DNA fragments and the DNA polymerase, and to exchange the buffer for further downstream applications, PCR products were purified either by separation on agarose gels and subsequent DNA extraction or by using the commercially available purification kits from GE Healthcare (illustra GFX PCR DNA and Gel Band Purification Kit) and Qiagen (QIAquick PCR Purification Kit).

2.5.6 Agarose gel electrophoresis

PCR products, digested plasmids or other DNA fragments were separated according to their size by agarose gel electrophoresis. Agarose (type 2; Sigma-Aldrich) was dissolved in either 0.5x Tris-borate-EDTA (TBE; Table 11) or 1x Tris-acetate-EDTA (TAE; Table 11) buffer to a final concentration of 0.8 to 2.0 % (w/v), depending on the size of the DNA fragments to be separated. When required, loading dye (Table 11) was added to the DNA sample prior

electrophoresis. For the separation of bands a voltage of 3 to 6 V per centimetre electrode distance was applied. DNA was visualised by adding the stains SYBR safe (Thermo Fisher Scientific) or GelRed (Biotium) to the gels and using either blue light (Dark reader transilluminator; Clare Chemical Research) or UV light excitation. Images were taken with the gel doc systems G:BOX (Syngene) or Gel-Doc XR⁺ (Biorad). Sizes of DNA bands were determined by comparing with bands from a marker with DNA fragments of known sizes (1kb DNA ladder blue (iNtRON Biotechnology) and peqGOLD DNA-ladder mix (peqlab)).

Table 11. Composition of electrophoresis buffers and loading dye.

50x TAE	10x TBE	10x loading dye
2M Tris	0.9 M Tris	50 % (v/v) glycerol
2 M acetic acid	0.9 M boric acid	0.4 % (w/v) bromphenol blue
50 mM EDTA, pH 8.3	20 mM EDTA, pH 8.0	0.4 % (w/v) xylene cyanol FF

2.5.7 DNA extraction from agarose gels

DNA from agarose gels was extracted by using purification kits from Fermentas (GeneJet Gel Extraction Kit) and GE Healthcare (illustra GFX PCR DNA and Gel Band Purification Kit) according to the manufacturer's protocol.

2.5.8 Restriction digestion

For restriction digestion, DNA was treated with restriction endonucleases from NEB and Thermo Scientific according to the manufacturer's protocol. The incubation time for the FastDigest restriction enzymes from Thermo Scientific was elongated to 30-60 min to achieve a higher percentage of digested plasmids

and PCR products. Standard restriction digests were generally incubated for 2 h at 37°C before separation on agarose gels or dephosphorylation.

2.5.9 Dephosphorylation of DNA

In order to prevent self-ligation of linearised vectors phosphate groups were removed by adding the FastAP Thermosensitive Alkaline Phosphatase (Thermo Scientific) or the rAPid Alkaline Phosphatase (Roche) directly to the restriction digest, incubating the mixture for 10 min at 37°C and inactivating the phosphatase by subjecting the mixture to 75°C for 7 min. Dephosphorylated and linearised vectors were separated by agarose gel electrophoresis prior to ligation.

2.5.10 Ligation

DNA fragments were ligated by using the T4 DNA ligases from Dominion-MBL or Promega or the Quick Ligase from NEB which reduces the incubation time from generally 2 h to 5 min at room temperature. The molar ratio of insert to vector was approximately 3:1.

2.5.11 DNA sequencing

Correctness of nucleotide sequences of generated plasmids and PCR products was verified by sequencing using the service provided by Secugen and Eurofins.

2.6 Biochemical methods

2.6.1 Heterocyst isolation from *Anabaena* sp. strains

Heterocysts of *Anabaena* sp. strains were isolated as described by Golden *et al.* (1991) with minor modifications. Filaments grown in BG11₀ medium were

harvested by centrifugation at 3,000xg for 10 min, washed twice in BG11₀ medium and finally resuspended in ice-cold STET buffer (Table 12) containing 1 mg ml⁻¹ lysozyme (Sigma-Aldrich) by vigorous vortexing for 2-3 min at room temperature. The suspension was subjected to mild sonication on ice using a Vibra-Cell VC 130 ultrasonic processor (Sonics & Materials, Inc.) until only heterocysts were visible in a light microscope (Olympus CH20). Heterocysts were collected by centrifugation (3,000xg; 5 min; 4°C) and washed three times in SET buffer (Table 12).

For esculin uptake studies sucrose was omitted from all buffers.

Table 12. Composition of buffers for heterocyst isolation from *Anabaena* sp. strains.

component	concentration	
	STET	SET
sucrose	8 % (w/v)	8 % (w/v)
Triton X-100	5 % (v/v)	
EDTA, pH 8.0	50 mM	50 mM
Tris-HCl pH 8.0	50 mM	50 mM

2.6.2 Membrane isolation from *Anabaena* sp. strains

Cells of *Anabaena* sp. cultures were collected by filtration using cellulose membranes with a pore diameter of 0.45 µm (Millipore). Filaments were washed once with 25 ml buffer A (Table 13) and stored at -20°C until further treatment. Cells were resuspended in 10 ml buffer A supplemented with protease inhibitor

(*Complete Mini EDTA-free*, Roche) and broken by two passages through a SLM Aminco French pressure cell at 10,000 psi. After centrifugation at 32,000xg for 15 min at 4°C the supernatant was subjected to ultra centrifugation (120,000xg; 90 min; 4°C) in order to sediment membranes. Membranes were washed once in 10 ml phosphate buffered saline (PBS; Table 13) and finally resuspended in 0.5 ml PBS. Isolated membranes were stored at -20°C for analyses by SDS-PAGE and Western blot.

Table 13. Composition of buffers for the isolation of membranes from *Anabaena* sp. species

buffer A	PBS, pH 7.4
20 mM HEPES-NaOH pH 8.0	137 mM NaCl
10 mM MgCl ₂	2.7 mM KCl
5 mM CaCl ₂	10 mM Na ₂ HPO ₄
10 % (w/v) glycerol	1.8 mM KH ₂ PO ₄

2.6.3 SDS-PAGE

Proteins were separated by sodium dodecyl sulphate polyacrylamide gel electrophoresis (SDS-PAGE) according to their molecular mass. As migration of the proteins through the gel depends on the porous character of the gel a polyacrylamide concentration of 8 % (w/v) was used to obtain an ideal separation range for SepJ. SDS-PAGE was performed according to Sambrook and Russel (2001). The composition of the resolving separation gel and the overlying stacking gel are given in Table 14.

Table 14. Composition of stacking gel and separation gel for SDS-PAGE.

Volumes of the solutions are indicated in ml to prepare gels of 10 ml.

component	stacking gel (5 %)	separation gel (8 %)
30% acrylamide/0.8% bisacrylamide	1.7	2.7
1 M Tris-HCl pH 6.8	1.25	
1.5 M Tris-HCl pH 8.8		1.25
10 % (w/v) SDS	0.1	0.1
10 % (w/v) APS	0.1	0.1
TEMED	0.01	0.006
H ₂ O	6.8	4.6

Samples were incubated for 5 min at 95°C in 1x SDS loading dye (Table 15), centrifuged for 3 min at 16,100xg and loaded onto the gel. Electrophoresis was carried out at a constant voltage of 15 V cm⁻¹ in SDS running buffer (Table 15).

Gels were either stained with Imperial Protein Stain (Thermo Scientific) which is a staining solution on the basis of coomassie brilliant blue R-250 to visualise proteins or subjected to Western blotting.

Table 15. Composition of SDS loading dye and SDS running buffer.

SDS loading dye	SDS running buffer
50 mM Tris-HCl pH 6.8	25 mM Tris
100 mM DTT	190 mM glycine
2 % (w/v) SDS	0.05 % (w/v) SDS
0.1 % (w/v) bromphenol blue	
10 % (v/v) glycerol	

2.6.4 Western Blot and protein detection

Proteins were transferred from polyacrylamide gels to PVDF membranes (Hybond-P; Amersham Biosciences) using a semi-dry electroblotting system (Novex, Life technologies) and an ethanol based transfer buffer (25 mM Tris; 192 mM glycine; 20 % (v/v) ethanol). The PVDF membranes were prepared by soaking briefly in ethanol and then in transfer buffer. Transfer was carried out by applying a constant voltage of 20 V for 30 min. The success of protein transfer was validated by staining the PVDF membrane with Ponceau S solution (0.1 % (w/v) Ponceau S; 5 % (w/v) acetic acid) that can easily be removed by subsequent washing in H₂O.

To detect specific proteins, membranes were blocked with 5 % (w/v) skimmed milk powder dissolved in PBS with 0.1 % (v/v) Tween-20 (PBS-T) for 1 h under gentle shaking. The membranes were washed three times in PBS-T (1x 15min; 2x 5min) before adding a mouse anti-GFP antibody (Life technologies) in a concentration of 1:5,000 for 1 h at RT or over night at 4°C. To remove surplus antibody solution the membranes were washed three times in PBS-T (1x 15min; 2x 5min). After 1 h of incubation with the horseradish peroxidase (HRP) - conjugated antibody anti-rabbit IgG HRP (Promega) in a concentration of 1:10,000, the membranes were washed three times in PBS-T (1x 15min; 2x 5min). Alternatively, the two step antibody staining protocol was replaced by a one step procedure using the monoclonal antibody anti-GFP-HRP (Miltenyi Biotec Ltd) for 1 h at RT. The protein bands were visualised using the enhanced chemiluminescence (ECL) kit (Amersham Biosciences) according to the manufacturer's protocol. X-ray films were developed manually.

2.7 Microscopy and spectroscopy

In this study various methods of microscopy were used to reveal insights into the morphology and ultrastructure of cyanobacterial cells and filaments. Furthermore, these techniques allowed the localisation of fluorescent molecules and the kinetics of their diffusion between cells.

2.7.1 Bright-field microscopy

Bright field images were taken with a Leica laser-scanning confocal microscope SP5, a Leica DM6000B fluorescence microscope or a Leica DM RA2 microscope connected to a digital CCD camera (QImaging Retiga EXi IEEE 1394) using a x40 objective and the imaging software Velocity (PerkinElmer). Images were processed with ImageJ software (Abràmoff *et al.*, 2004).

2.7.1.1 Alcian Blue Staining

To highlight developing (pro-) and mature heterocysts the polysaccharide stain Alcian Blue was added as described by Borthakur *et al.* (2005). 5 µl of 0.5 % (w/v) Alcian Blue 8GX solution in 50 % (v/v) ethanol (Acros Organics) was added to 500 µl of culture and the solution incubated for 30 min at 30°C. Access stain was removed by washing the cells three times in BG11₀ medium (4,000xg; 1 min) prior to examination by bright field microscopy.

2.7.2 Fluorescence and confocal microscopy

Confocal and fluorescence microscopy were used to visualise fluorescent molecules in both living and fixed specimen. Chlorophyll of cyanobacterial cells is fluorescent on its own (autofluorescence), but most proteins and molecules do

not show any fluorescence when excited with visible light. Thus, fluorescent molecules were introduced into living cells either by uptake or expression as proteins such as green fluorescent proteins (GFP) (see results chapter for details on the generation of fluorophore-tagged proteins in *Anabaena* sp. PCC 7120). The localisation of proteins in fixed specimen was additionally studied by immunofluorescent labelling of the protein of interest with a fluorophore-tagged antibody (see chapter 2.7.3). As two types of microscopes have been used extensively in this work, they are described briefly in the following Figure 9.

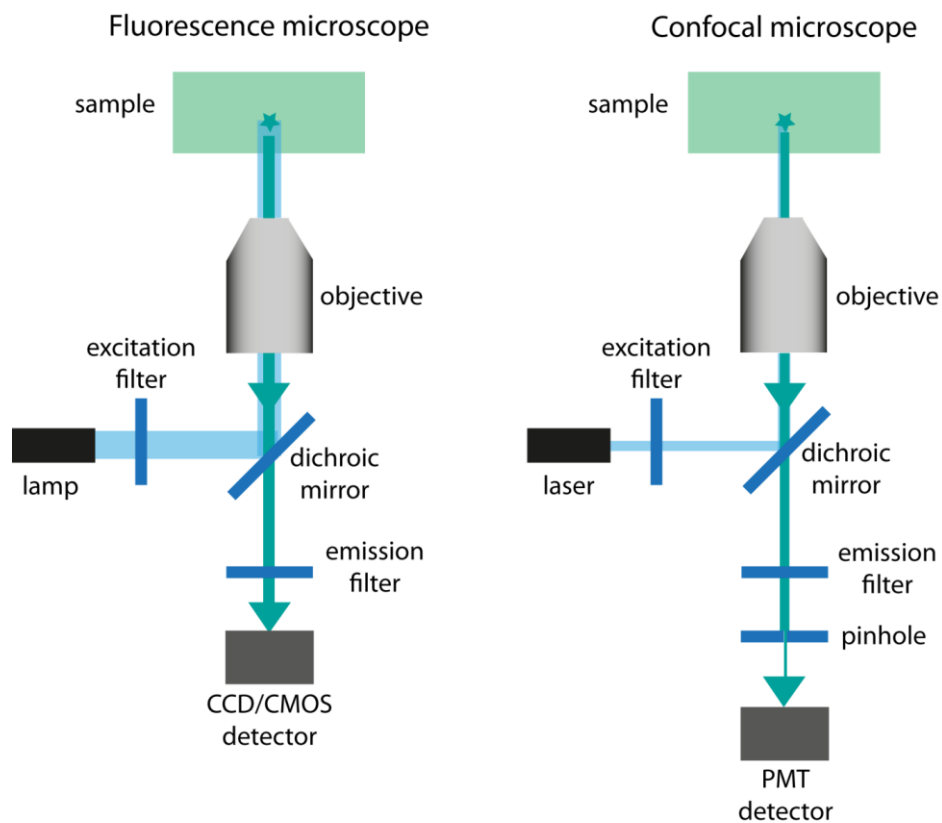


Figure 9. Schematics of a fluorescence and confocal microscope.

Figure 9.

Fluorescence and confocal microscopes consist of a light source, an excitation filter that selects for a specific excitation wavelength, a dichroic mirror which allows the separation of emission and excitation photons, an emission filter that

selects for a specific emission wavelength and a sensitive imaging device. Main differences between both devices are in the way of exciting the fluorophore and detecting its emission. While fluorescence microscopes consist of broad spectrum light sources such as mercury-vapor lamps or xenon arc lamps and detect photons by charge-coupled device (CCD) or complementary metal-oxide semiconductor (CMOS) cameras, confocal microscopes excite fluorophores by a laser beam of a specific wavelength that systematically scans the sample in a point-by-point fashion and detects fluorescence signals with a photomultiplier (PMT) after passing through a pinhole which rejects out-of-focus light. Thus, confocal microscopy allows collecting fluorescence emission light only from the focal plane or ‘optical section’ of a thick specimen. By capturing images from different focal planes (z-stacking) it is possible to reconstruct the three-dimensional structure of a sample. However, image acquisition usually takes longer than in fluorescence microscopy.

2.7.2.1 Fluorescent cell labelling

For molecular exchange experiments and localisation studies of cell components cyanobacterial cells were labelled with various fluorescent tracers summarised in Table 16.

Table 16. Fluorophores used in this study

fluorophore	usage	excitation wavelength [nm]	emission wavelength [nm]	supplier
BCECF	molecular exchange	488	500-527	Molecular Probes
calcein	molecular exchange	488	500-527	Molecular Probes
5-CFDA	molecular exchange	488	500-527	Molecular Probes
esculin hydrate	molecular exchange	355	443-490	Sigma-Aldrich
FM1-43FX	cytoplasmic membrane stain	488	570-595	Molecular Probes
Hoechst 33258	DNA stain	355	455-495	AppliChem
2-NBDG	molecular exchange	476	520-560	Molecular Probes; Cayman Chemical
6-NBDG	molecular exchange	476	520-560	Molecular Probes
GFP	fluorescent protein tag	488	500-527	
mTurquoise2	fluorescent protein tag	458	460-490	
YFP	fluorescent protein tag	514	520-535	

2.7.2.1.1 Labelling with fluorescent tracers for molecular exchange experiments

Cyanobacterial cells were harvested by centrifugation (4000xg, 1 min), washed twice in fresh growth medium and resuspended in 1 ml medium. Fluorescent tracers were added as follows: 12 μl of a 1 mg ml^{-1} calcein or 5-CFDA solution in DMSO, 10 μl of a 1 mg ml^{-1} 2- or 6-NBDG solution in ultra-pure water, 30 μl of a saturated esculin hydrate solution in ultra-pure water (ca. 5 mM) and 5 μl of a 10 mM BCECF solution in DMSO. The suspensions were incubated for 20 min

(2- and 6-NBDG), 30 min (BCECF, 5-CFDA and esculin hydrate) and 90 min (calcein) in the dark at optimal growth temperature and under gentle shaking (80 rpm). To remove the fluorescent dyes, cells were washed three times in growth medium, and incubated for another 15-30 min in 1 ml of medium at optimal growth temperature in the dark under gentle shaking (80 rpm). After a final washing step, cells were spotted onto growth medium agar plates, and excess solution was removed. To maintain the growth conditions throughout the experiment media and plates were preheated to optimal growth temperature.

2.7.2.1.2 Fluorescent labelling of specific cell components

Two additional fluorescent dyes, FM1-43FX and Hoechst 33258, were used to visualise specific cellular components. FM1-43FX stains the cytoplasmic membranes of cyanobacteria (Schneider *et al.*, 2007), while Hoechst 33258 interacts with DNA. For labelling, cells were washed once in fresh growth medium, and 1 μl Hoechst 33258 (1 mg ml^{-1} ; Bisbenzimidazole H33258) and/or 2.5 μl FM1-43FX (0.1 mg ml^{-1}) was added to 0.5 ml of culture. The suspension was incubated for 10 min at room temperature and washed twice with growth medium prior mounting on growth medium agar plates. Surplus medium was removed.

2.7.2.2 Visualisation and FRAP

For confocal microscopy, small blocks of agar were placed in a custom-built temperature-controlled sample holder covered with a glass coverslip (Figure 10). FRAP and time-lapse experiments were performed at the optimal growth temperature of the organism by attaching a water bath to the sample holder and pumping water through the metal body.

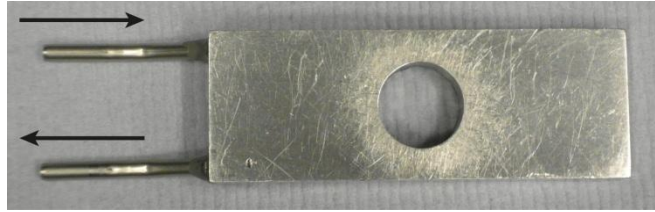


Figure 10. Custom-built temperature-controlled sample holder for confocal microscopy.

The sample was placed on a cover slip inside the well and the temperature adjusted by pumping water through the sample holder (arrows).

Cells were visualised with the Leica laser-scanning confocal microscope SP5 using a x63 oil immersion objective (Leica HCX PL APO lambda blue 63.0×1.40 OIL UV). Excitation and emission wavelengths for the different dyes and fluorescent proteins were chosen according to Table 16. Chlorophyll fluorescence (autofluorescence) was imaged usually simultaneously by using an emission detection range from 670 to 720 nm.

For imaging, a 95 μm confocal pinhole was used which corresponds to a resolution of approximately 0.7 to 0.8 μm in the z-direction, whereas for FRAP measurements the pinhole was maximally opened (600 μm , resulting in an optical section thickness of ca. 4.0 - 4.2 μm).

FRAP experiments were performed as follows: After taking an initial image (pre-bleach), the region of interest (ROI) was bleached by increasing laser intensity and zooming into the ROI. Recovery was then recorded.

2.7.2.3 Data analysis

Images were prepared and analysed with ImageJ software (Abràmoff *et al.*, 2004).

FRAP data were analysed as described by Mullineaux *et al.* (2008) and Merino-Puerto *et al.* (2011) to estimate the ‘exchange coefficient’ E and the ‘recovery rate’ constant R, using Image Pro Plus 6.3 (Media Cybernetics) and SigmaPlot 10.0 (Systat Software).

2.7.3 Immunofluorescence localisation – sample preparation and fluorescence microscopy

For immunofluorescence localisation of SepJ in cells of *M. laminosus*, filaments were harvested by centrifugation (3000xg; 2 min) and resuspended in fresh growth medium. Cultures were transferred onto 0.2 µm Nucleopore membranes, which were subsequently placed onto poly-L-lysine-coated slides. For fixation the slides were incubated in 50 ml plastic Falcon tubes containing 70 % (v/v) chilled (−20°C) ethanol for 30 min at −20°C. After three washing steps for 2 min with PBS-T, the samples were immersed in 3 % (w/v) milk powder, diluted in PBS-T, and incubated for 15 min at room temperature. Afterwards, the slides were directly incubated with the primary antibody, rabbit anti-*Anabaena* sp. PCC 7120 SepJ (Mariscal *et al.*, 2011), diluted 1:250 in PBS-T, and stored for 3 h at 30°C in a moisture chamber. After incubation, the samples were washed three times in PBS-T for 2 min, and then incubated with the secondary antibody for 45 min at 30°C. The secondary antibody was an anti-rabbit immunoglobulin G conjugated with Alexa Fluor 488 (Life technologies) diluted 1:500 in PBS-T. After three washing steps with PBS-T for 2 min each, the slides were mounted with a coverslip using FluorSave™ Reagent (Calbiochem), and sealed with nail varnish.

Immunolabelled cells were examined with a Leica DM6000B fluorescence microscope, using a $\times 63$ oil immersion objective and an ORCA-ER camera (Hamamatsu). Alexa Fluor 488 fluorescence was monitored using a fluorescein isothiocyanate (FITC) L5 filter (excitation, band-pass (BP) 480/40 filter; emission, BP 527/30 filter), and autofluorescence was detected using a Texas Red TX2 filter (excitation, BP 560/40; emission, BP 645/75). Images were convolved with the Leica Application Suite Advanced Fluorescence software.

2.7.4 Transmission Electron Microscopy (TEM)

In contrast to light, fluorescence and confocal microscopy transmission electron microscopy (TEM) can be used to reveal structural characteristics of cells with much higher spatial resolution by illuminating the thin section of a specimen with a high voltage electron beam (short wavelength) instead of visible light. However, due to the power of the electron beam and the vacuum inside the microscope biological samples cannot be visualised alive but need to be prepared in a complex process, including the fixation of the sample and further steps, described in detail in the following paragraph.

2.7.4.1 Sample preparation and visualisation of thin-sections

Cultures were harvested by centrifugation (3000xg; 2 min) and chemically fixed for 2 h at room temperature with 4 % (w/v) glutaraldehyde in 100 mM phosphate buffer pH 7.3 (Table 17) to preserve the biological structure of the cells. To remove the fixative, samples were washed three times with 100 mM phosphate buffer. After embedding in 2 % (w/v) low-gelling temperature agarose (Sigma-Aldrich), samples were cut in 1–2 mm cubic blocks, and post-fixed with 2 % (w/v) potassium permanganate dissolved in distilled water overnight at 4°C.

2 Materials and methods

Addition of KMnO_4 as fixative has been shown to increase the contrast of membranes (Luft, 1956). Samples were washed with distilled water until the supernatant remained clear, and dehydrated through a graded ethanol series (1×15 min 30 %, 1×15 min 50 %, 1×15 min 70 %, 1×15 min 90 % and 3×20 min 100 %). Two washes for 5 min with propylene oxide were performed prior infiltration with Araldite (Table 17) for 1 h and with fresh Araldite overnight. Polymerisation was achieved by incubation at 60–65°C for 48 h. Alternatively, cells were fixed for 2 h at room temperature in 100 mM phosphate buffer pH 7.3 containing 3 % (w/v) glutaraldehyde, 1 % (w/v) formaldehyde and 0.5 % (w/v) tannic acid, washed with phosphate buffer, and incubated in 2 % (w/v) OsO_4 in phosphate buffer overnight. Dehydration was performed using a graded acetone series as described for ethanol prior to embedding in Araldite. Thin sections were cut with a glass knife prepared with a LKB 7800B KnifeMaker (LKB-Produkter AB) at a Reichert Ultracut E microtome. Areas of interest were identified by visualising cells with 2.5 % (w/v) toluidine blue in 0.5 % (w/v) sodium tetraborate on semi-thin sections. Ultra-thin sections (ca. 70 nm) were collected on uncoated, 300 mesh copper grids (Agar Scientific). High contrast was obtained by poststaining with saturated aqueous uranyl acetate and lead citrate (Reynolds, 1963) for 4 min each. The grids were examined in a JOEL JEM-1230 transmission electron microscope at an accelerating potential of 80 kV.

Table 17. Composition of phosphate buffer and Araldite resin for the preparation of samples for TEM.

Phosphate buffer, pH 7.3	Araldite resin*
450 ml 0.2 M Na ₂ HPO ₄	40 ml Araldite CY212
150 ml 0.2 M KH ₂ PO ₄	60 ml dodecanyl succinic anhydride
381 ml H ₂ O	2 ml methyl nadic anhydride
	1 ml benzyl dimethylamine

* all chemicals were obtained from Agar Scientific

2.7.5 Fluorescence spectroscopy

Fluorescence emission spectra for esculin and 2-NBDG were recorded in a Perkin-Elmer LS55 luminescence spectrometer at room temperature at different pH. Esculin was excited at 360 nm and emission detected from 400 to 600 nm (slit-widths 2.5 nm). For 2-NBDG an excitation wavelength of 465 nm and an emission range from 500 to 600 nm (slit-widths 5 nm) was used. Data were analysed using SigmaPlot 12.5.

Interaction of cyanophycin and esculin was tested by dissolving esculin to a final concentration of 300 nM in 10 mM KH₂PO₄/K₂HPO buffer at pH 6.0, pH 7.0 and pH 10.0 and adding cyanophycin to a final concentration of 1 mg ml⁻¹, corresponding to approximately 30 to 40 μM assuming a molecular weight of 25 to 35 kDa. Suspensions were incubated for 0.5 - 3 h with gentle shaking at RT, and cyanophycin was then removed from the suspension by centrifugation (1 min; 16,100xg).

3 Properties of transferred molecules between cells and their possible pathways in *Anabaena* sp. PCC 7120

As heterocysts lack ribulose 1,5-bisphosphate carboxylase–oxygenase and do not fix CO₂, they depend on the supply of carbon skeletons from adjacent vegetative cells for the generation of energy for nitrogen fixation (Wolk, 1968) but provide in turn combined nitrogen compounds for neighbouring vegetative cells. Until now it has remained unclear which metabolites in particular are exchanged between the two cell types. It has been suggested that ammonia or a substance derived from it such as glutamine (Fogg, 1949; Wolk *et al.*, 1976; Thomas *et al.*, 1977) and/or the amino acids which form the storage compound cyanophycin, i.e. aspartate, arginine, or its smallest subunit β -aspartyl-arginine (Carr, 1988; Richter *et al.*, 1999; Ke and Haselkorn, 2013; Burnat *et al.*, 2014), could function as nitrogen vehicles between heterocysts and vegetative cells. In the other direction, it is likely that carbon metabolites are exchanged as sugars. Most studies so far, have focussed on the role of sucrose as carbon carrier (Schilling and Ehrnsperger, 1985; Wolk *et al.*, 1994; Curatti *et al.*, 2002; Cumino *et al.*, 2007; Marcozzi *et al.*, 2009; López-Igual *et al.*, 2010; Vargas *et al.*, 2011) but also the transfer of glucose or fructose has been suggested (Haury and Spiller, 1981; Jüttner, 1983). Additionally, some amino acids such as glutamate, alanine, methionine and cysteine may be transferred from vegetative cells into heterocysts (Wolk, 1968; Wolk *et al.*, 1976; Jüttner, 1983; Pernil *et al.*, 2010; Omairi-Nasser *et al.*, 2014). A summary of potential metabolites being exchanged between heterocysts and vegetative cells is displayed in Figure 4.

3 Properties and pathways of transferred molecules

Although it has been shown that fluorescent molecules are transferred between cells either via a continuous periplasm (Mariscal *et al.*, 2007) or from cytoplasm to cytoplasm via cell-cell connections in *Anabaena* sp. PCC 7120 (Mullineaux *et al.*, 2008), these studies are based on using fluorophores that are not directly comparable to physiologically-important metabolites. In the following chapter, the role of various fluorescent molecules in intercellular communication is investigated, including molecules that are similar to metabolites such as the sucrose analogue esculin and the glucose derivatives 2- and 6-NBDG. Furthermore, an additional ‘artificial’ molecule, BCECF, is introduced. The possible routes of transfer and the influence of the septal proteins FraC, FraD and SepJ on molecular exchange are explored by confocal microscopy and FRAP measurements. Finally, the physico-chemical properties of the molecules are compared with previously used fluorescent tracers and a conclusion about the properties of the complexes mediating the molecular transfer is drawn.

3.1 Exchange of the sucrose analogue esculin in *Anabaena* sp.

PCC 7120

Sucrose is not only a key metabolite in cyanobacteria but also in plants where it is probably the major product of photosynthesis and long distance transport, being involved in growth, development, storage, signal transduction and acclimation to environmental stress conditions (Salerno and Curatti, 2003). It has been shown for plants that sucrose uptake transporters (SUTs) are important for loading sucrose into vascular tissues (phloem) and for the uptake of sucrose into sink tissues, such as flowers and seeds (Reinders *et al.*, 2012a). An efficient way to study type I SUTs in plants has been recently developed by using the fluorescent coumarin

3 Properties and pathways of transferred molecules

β -glucoside esculin and detecting its fluorescence using microscopy and spectroscopy (Gora *et al.*, 2012; Reinders *et al.*, 2012b). Uptake of esculin in *Saccharomyces cerevisiae* could be specifically induced by the heterologous expression of the potato sucrose transporter StSUT1 (Gora *et al.*, 2012; Reinders *et al.*, 2012b). Furthermore, the rate of esculin import by the type I SUTs, AtSUC2 and AtSUC9 from *Arabidopsis thaliana* is similar to that of sucrose (Sivitz *et al.*, 2007; Reinders *et al.*, 2012a), indicating that esculin is recognised and transported in a similar way to sucrose. However, it remains unknown whether cells of *Anabaena* sp. PCC 7120 take up esculin or related fluorescent sucrose analogues.

3.1.1 Uptake of esculin by *Anabaena* sp. PCC 7120

Several fluorescent sucrose analogues which have been used to follow sucrose uptake in plants such as rutin, quercetin, esculin (Sivitz *et al.*, 2007), and hesperidin were tested for their ability to be taken up into cells of *Anabaena* sp. PCC 7120. Confocal images reveal that esculin was significantly incorporated and retained in filaments of *Anabaena* sp. PCC 7120 (Figure 11).

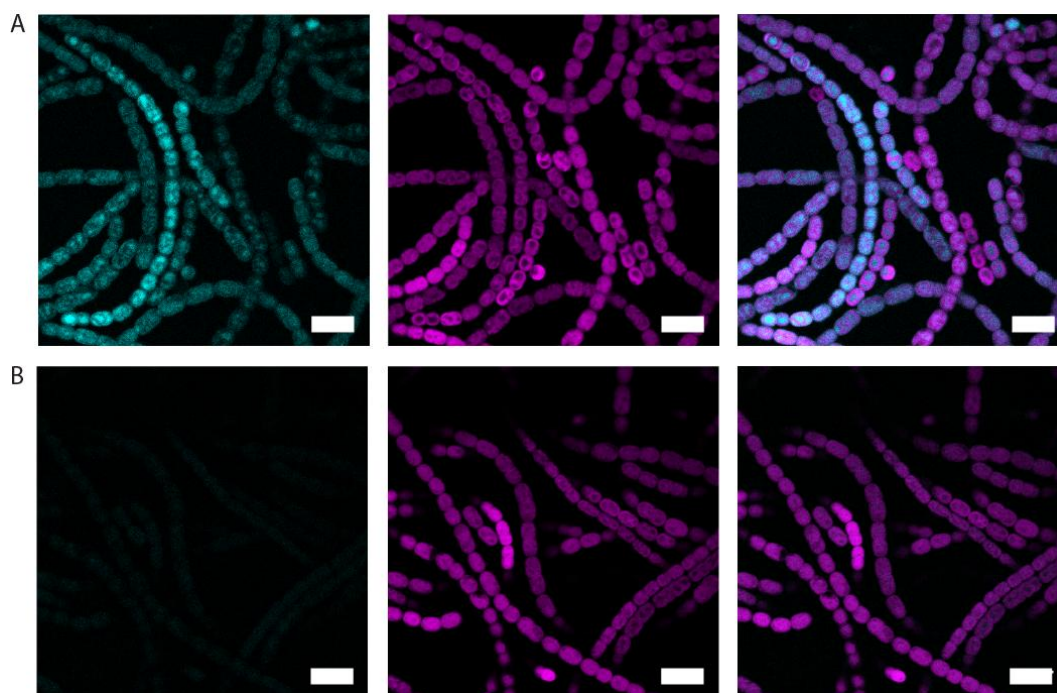


Figure 11. Uptake of esculin by *Anabaena* sp. PCC 7120 filaments.

(A) Esculin-labelled cells (grown in BG11). (B) Control with unlabeled cells. Images show esculin fluorescence (cyan), autofluorescence (magenta) and an overlay of both channels. Scale bars, 10 μm .

Comparison of the distributions of esculin and chlorophyll fluorescence from the thylakoid membranes shows that esculin fluorescence originates from the cytoplasm (Figure 11A). Esculin fluorescence could not be detected in the periplasm, where fluorophores such as GFP and iLOV make a fluorescent halo outside the thylakoid membranes (Mariscal *et al.*, 2007; Zhang *et al.*, 2008a; Zhang *et al.*, 2013). An additional comparison of the distributions of esculin fluorescence with chlorophyll and periplasmic GFP in *Anabaena* sp. PCC 7120 strain CSV18 (Mariscal *et al.*, 2007) did not show significant esculin fluorescence in the periplasm (Figure 12). However, since the periplasm is a thin compartment, the presence of some esculin in the periplasm cannot be excluded, but it is clear that at least the vast majority of esculin must be in the cytoplasm. Although nearly all cells show esculin fluorescence in the cytoplasm, significant

3 Properties and pathways of transferred molecules

variation in fluorescence intensity (Figure 11A) indicates variation in competence for esculin uptake.

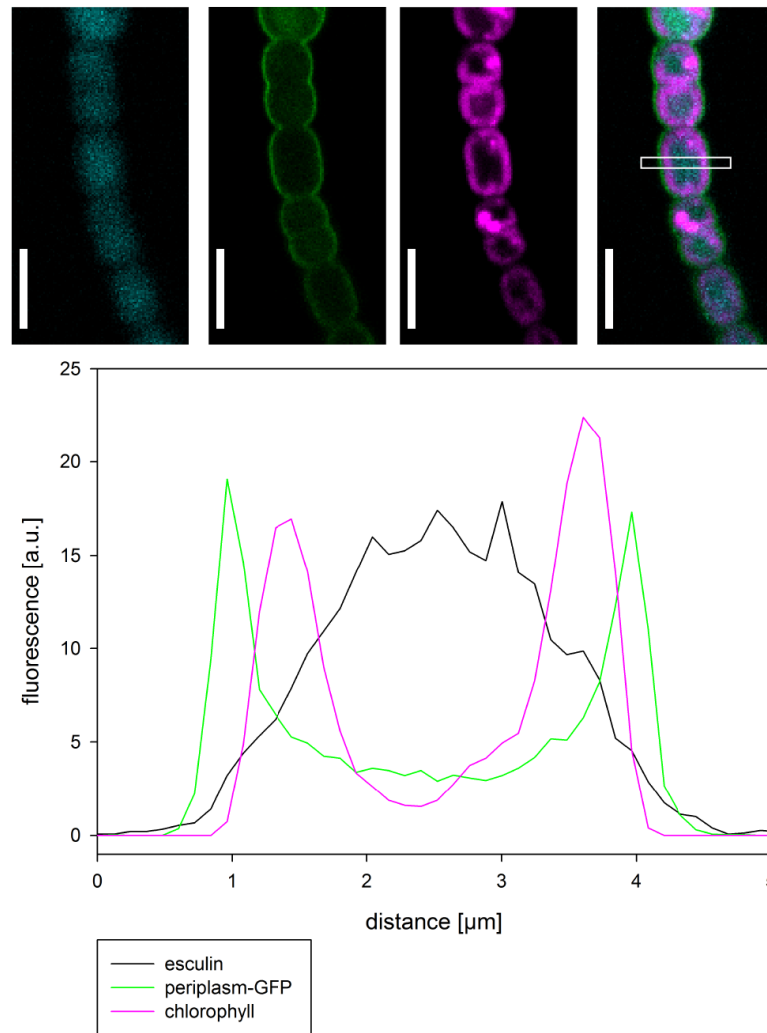


Figure 12. Sub-cellular distributions of esculin, chlorophyll and periplasmic GFP from confocal fluorescence images.

Esculin fluorescence visualised in cells of CSV18, an *Anabaena* sp. PCC 7120 mutant that expresses GFP fused to a signal sequence that is recognised by the TAT system, resulting in GFP export to the periplasm (Mariscal *et al.*, 2007). Cells were grown for 24 h in BG11₀ medium to induce GFP expression (Mariscal *et al.*, 2007). Images show esculin fluorescence (cyan), GFP fluorescence (green), chlorophyll fluorescence (magenta) and a merged image. Scale bars, 5 μm. Fluorescence profiles taken across a cell in the region marked by the white box in the merged image is shown underneath.

3 Properties and pathways of transferred molecules

As it has been reported that esculin fluorescence depends on pH (Yin *et al.*, 1996) it was investigated to which extent esculin fluorescence is influenced by pH. Fluorescence emission spectra were recorded at pH 4.5 to 10.0 (Figure 13A). Assuming that the cytoplasmic pH in *Anabaena* sp. PCC 7120 is about 7.0 (Blanco-Rivero *et al.*, 2005) and assuming that the pH in other cell compartments falls within the range 6.5 to 8.0 esculin fluorescence yield would be similar within a factor of approximately 0.8 to 1.3 (Figure 13A). Therefore, the effect of pH on esculin fluorescence intensity is negligible under physiological conditions. Another key factor which might influence esculin fluorescence is the difference in oxygen concentration between oxic vegetative cells and nearly anoxic heterocysts. Fluorescence spectroscopy revealed that esculin fluorescence yield was unaffected by oxygen concentration (Figure 13B), thus making esculin a suitable fluorophore to investigate fluorescence changes within different compartments of *Anabaena* sp. PCC 7120.

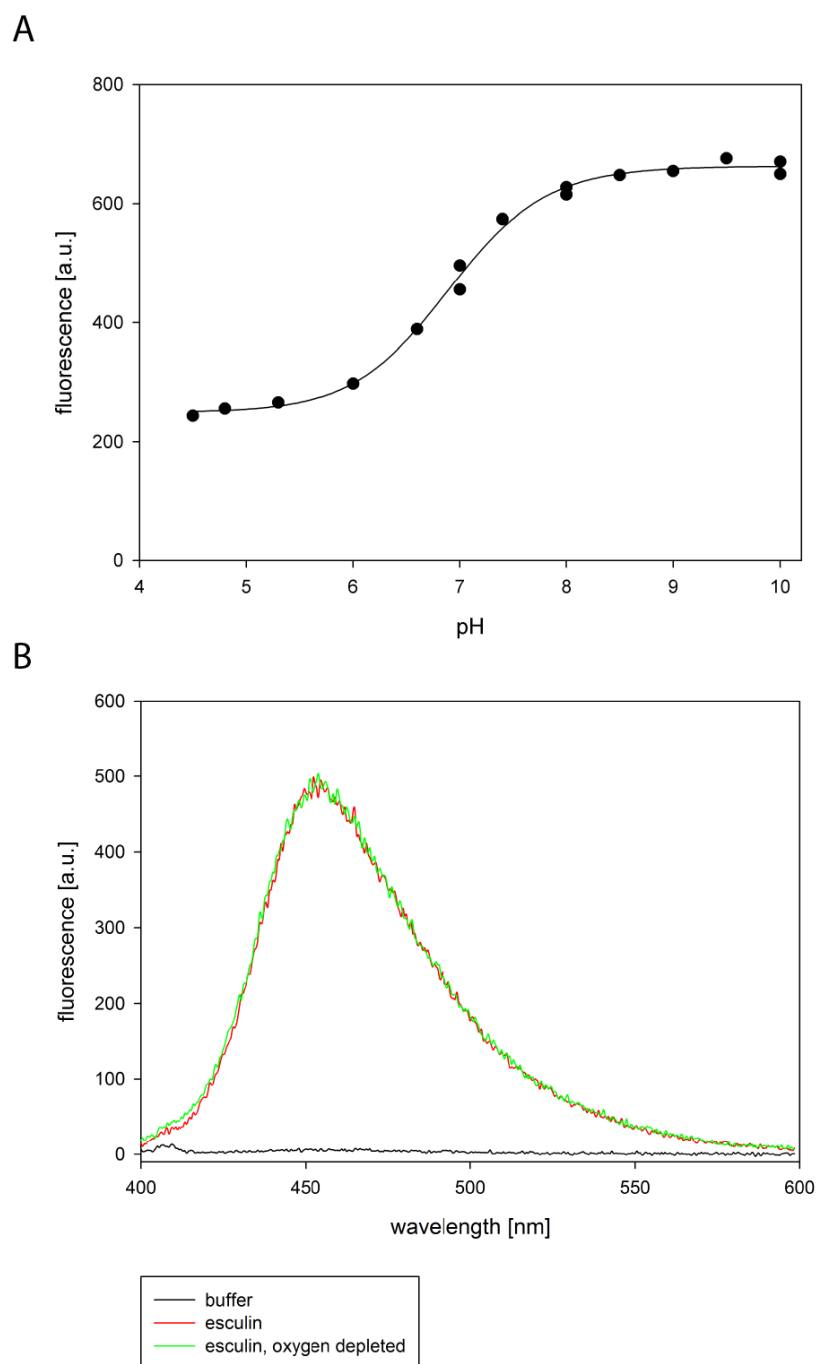


Figure 13. pH and oxygen dependence of esculin fluorescence.

(A) pH dependence. Emission of esculin at the peak wavelength of 453 nm is plotted vs. pH from 4.5 to 10.0. (B) Oxygen dependence. Fluorescence emission spectra for a 330 nM esculin solution at pH 7.0, either in solution equilibrated with atmospheric O_2 or after purging by bubbling with N_2 . A similar treatment carried out in a Clarke-type oxygen electrode (OxyLab 2; Hansatech) confirmed that purging with N_2 decreases the O_2 concentration in the solution from 0.213 mM to 0.013 mM.

3 Properties and pathways of transferred molecules

To test whether esculin is taken up by a specific sucrose transporter a fluorometric assay was developed that allowed following esculin fluorescence over time (Figure 14). The results indicate that esculin was taken up linearly for at least 70 min. Addition of sucrose significantly reduced the rate of esculin uptake, suggesting that both molecules compete for the same uptake mechanism and possess similar properties. This applies under both diazotrophic and non-diazotrophic growth conditions.

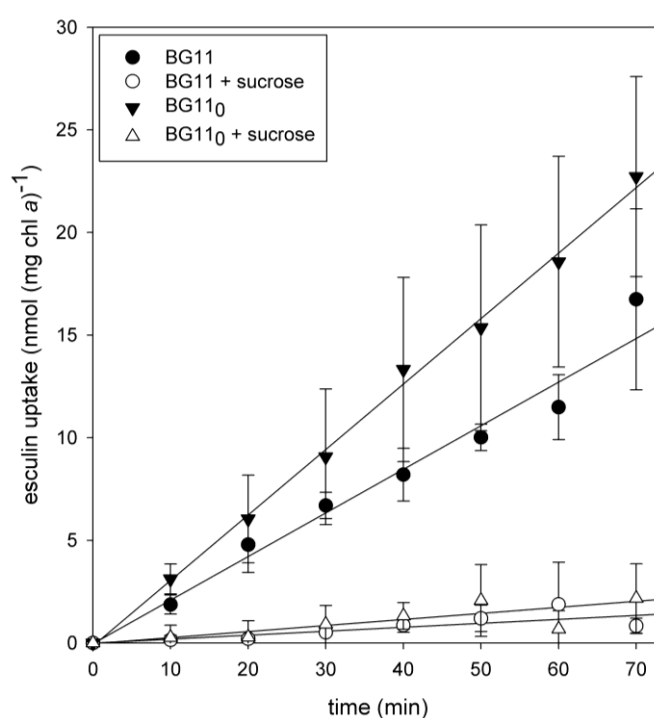


Figure 14. Time-course for esculin uptake in *Anabaena* sp. PCC 7120 cells under different growth conditions and effect of sucrose competition.

Cells were grown either with (BG11) or without combined nitrogen (BG11₀). Uptake of esculin (100 μ M) was measured in the presence or absence of sucrose at 10 mM. Error bars represent standard deviations (number of biological replicates $n = 3-5$). Student's t -tests show that rates of uptake differed significantly for: BG11 \pm sucrose ($p = 0.00003$); BG11₀ \pm sucrose ($p = 0.002$); BG11 vs. BG11 sucrose) ($p = 0.05$). Absolute values for esculin uptake assume that the intracellular fluorescence yield is similar to that in the buffer. (Data were kindly provided by Mercedes Nieves-Mori3n.)

3.1.2 Esculin as a fluorescent probe for intercellular communication

In contrast to FRAP experiments with calcein as fluorescent tracer (Mullineaux *et al.*, 2008), experiments with esculin were more difficult to perform for the following reasons:

- Cells of *Anabaena* sp. PCC 7120 show a weak but detectable background autofluorescence at the wavelengths used for esculin detection (Figure 11).
- Esculin fluorescence is easily bleached while recording image series. To diminish the effect of photobleaching the laser power was reduced and the pin hole maximally opened. This approach allowed image recording with negligible photobleaching but less resolution in the z -direction.
- Esculin shows spontaneous recovery from photobleaching. When fluorescence of an entire filament is bleached out no recovery is possible due to redistribution of the fluorophore but only by spontaneous recovery. About 7.5 % of the initial fluorescence recovered spontaneously (Table 18).
- Esculin possesses a high immobile fraction (I_F) of about 50-75 % (Table 18). Similar to 5-CFDA in *Anabaena* sp. PCC 7120 (Merino-Puerto *et al.*, 2011b) esculin always showed incomplete recovery. Esculin binds to proteins such as human serum albumin (Zhang *et al.*, 2008b) and possibly to specific sucrose-binding factors. Once bound it is likely that esculin becomes trapped inside a cell. Neither GFP (27 kDa) (Yoon and Golden, 1998; Mariscal *et al.*, 2007) nor iLOV (13 kDa) (Zhang, personal communication) diffuse between adjacent cells. To quantitate intercellular transfer Mullineaux *et al.* (2008) introduced the ‘exchange coefficient’ E

3 Properties and pathways of transferred molecules

which relates the rate of dye movement between two adjacent cells to the difference in dye concentration between the cells. However, the high immobile fraction prevents calculation of E as this requires fitting of the simulated time-development of dye distribution in the filament to the experimental data (Mullineaux *et al.*, 2008). Alternatively, kinetics of esculin transfer between vegetative cells can be quantified by determining the ‘recovery rate constant’ R as previously described by Merino-Puerto *et al.* (2011). To allow valid comparison of terminal cells (with one cell junction) with cells in the middle of filaments (with two cell junctions), R values were divided by 2 in the latter case. However, E is easier to estimate for exchange at vegetative cell:heterocyst junctions, provided that exchange at such junctions is significantly slower than exchange among vegetative cells. Then it can be assumed that the dye re-equilibrates among a large pool of vegetative cells on a faster time-scale than it exchanges with the heterocyst (Mullineaux *et al.*, 2008). Under these conditions E simply approximates to R for the heterocyst (Mullineaux *et al.*, 2008).

3.1.3 Intercellular diffusion of esculin in filaments of *Anabaena* sp.

PCC 7120

In order to quantitate intercellular transfer of esculin in filaments of *Anabaena* sp. PCC 7120 FRAP experiments were performed. Esculin fluorescence in a single cell was bleached out and its recovery monitored over time (Figure 15). Experiments were carried out in filaments grown with or without a combined nitrogen source. In the later case, both cell types, vegetative cells and heterocysts, were analysed. FRAP measurements indicate that esculin transfer is present

3 Properties and pathways of transferred molecules

between vegetative cells (Figure 15A,B) and from vegetative cells into heterocysts (Figure 15C,D). As the extent of fluorescence recovery is considerably greater than the spontaneous recovery of esculin fluorescence (Table 18), the observed recovery is due to molecular exchange of the fluorophores between cells. To test whether esculin also diffuses from heterocysts into vegetative cells, fluorescence of all vegetative cells neighbouring a terminal heterocyst was bleached out and the fluorescence intensity of the heterocyst monitored over time. A control experiment using the same visualisation settings as for recording the images after the initial bleach did not show a bleaching effect (Figure 15E). Subsequently, the observed decay of heterocyst fluorescence indicates that esculin can be transferred from heterocysts to vegetative cells. Transfer in both directions occurs at similar timescales (Figure 15D,E), suggesting that transfer of esculin in *Anabaena* sp. PCC 7120 is due to simple diffusion rather than active transport. Because no esculin fluorescence was detected in the periplasm (Figure 11; Figure 12) intercellular communication from cytoplasm to cytoplasm appears to be the main route of communication in *Anabaena* sp. PCC 7120. This is in good agreement with previous studies using calcein (Mullineaux *et al.*, 2008) and 5-CFDA (Mariscal *et al.*, 2011; Merino-Puerto *et al.*, 2011b).

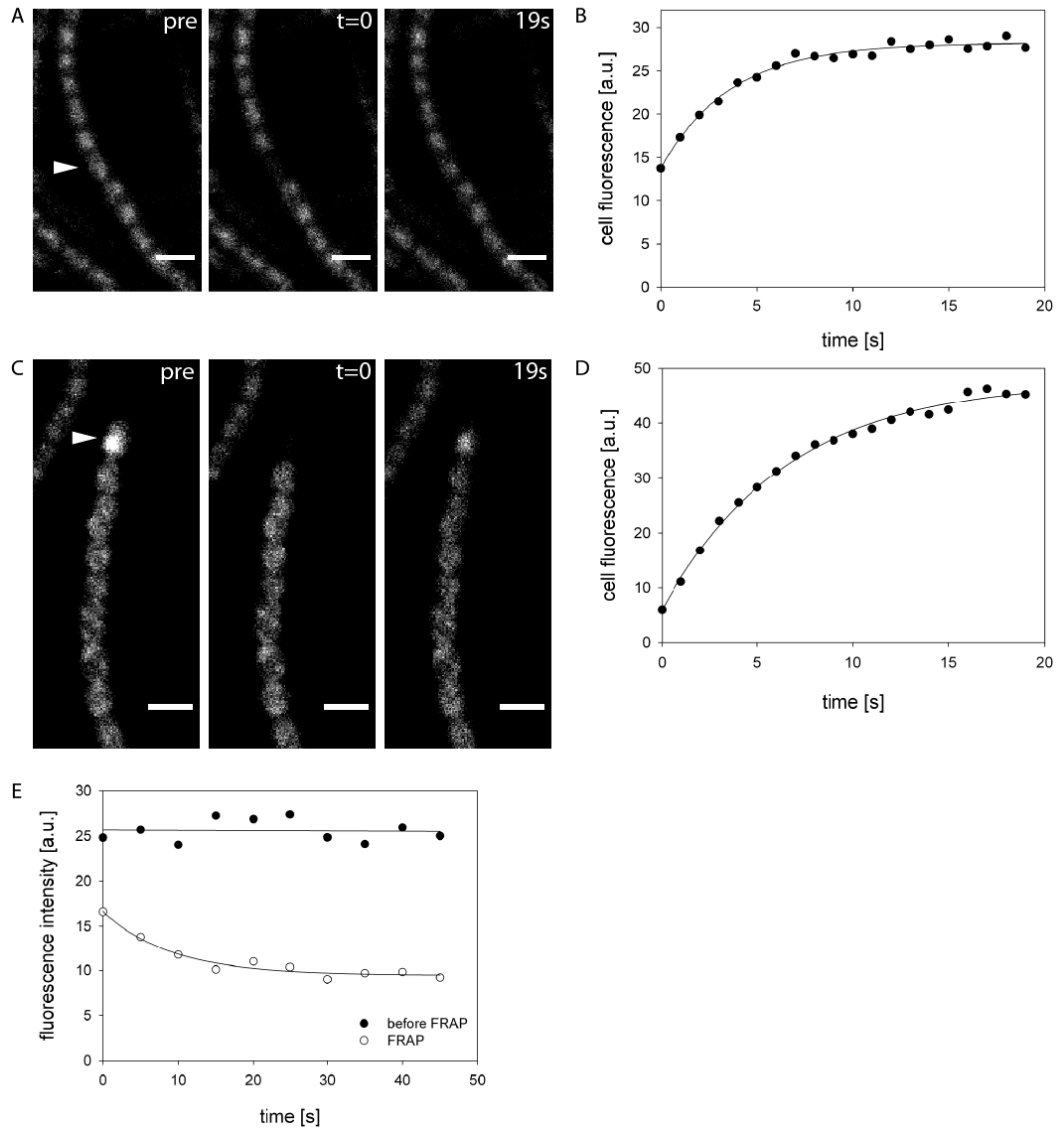


Figure 15. Examples of FRAP experiments monitoring intercellular exchange of esculin in filaments of *Anabaena* sp. PCC 7120.

(A,B) Esculin exchange among vegetative cells. (C,D) Esculin exchange from vegetative cells to a terminal heterocyst. (A,C) Fluorescence images from FRAP time-series showing esculin fluorescence prior to the bleach (pre), immediately after bleaching out fluorescence in the highlighted cell ($t = 0$), and 19 s later. Scale bars, 5 μm . (B,D) Fluorescence recovery curves for the bleached cells. (E) Esculin transfer from a terminal heterocyst to neighbouring vegetative cells. The graph shows heterocyst fluorescence over time prior FRAP (filled circles) and after bleaching out the fluorescence of all vegetative cells (open circles). Heterocyst fluorescence at $t = 0$ is already lowered by diffusion of esculin out of the heterocyst during the bleach.

3.1.4 Kinetics of esculin exchange and influence of the septal proteins SepJ, FraC and FraD on intercellular communication in *Anabaena* sp. PCC 7120

In order to quantitate esculin exchange recover rate constants (Merino-Puerto *et al.*, 2011b) were determined for different cell types and growth conditions. They revealed that exchange of esculin is significantly faster among vegetative cells than between vegetative cells and heterocysts (Table 18), following the same pattern as with calcein (Mullineaux *et al.*, 2008). However, esculin transfer into heterocysts is faster than that of calcein by a factor of about 1.7.

In contrast to previous observations with calcein (Mullineaux *et al.*, 2008; Mariscal *et al.*, 2011), rates of exchange of esculin among vegetative cells did not significantly increase following combined nitrogen step-down (Table 18) and the presence of cyanophycin plugs in the neck region of heterocysts did not influence molecular exchange of esculin. Esculin influx into heterocysts remained similar in an *Anabaena* sp. PCC 7120 mutant lacking the cyanophycin synthetase CphA1 for the synthesis of cyanophycin plugs (strain CSS7; Picossi *et al.*, 2004) (Table 18). Consistent with this finding, no interaction between esculin and cyanophycin was detected *in vitro* (Figure 16). Different pH were tested to exclude the possibility of charge mediated interaction between esculin and cyanophycin. Neither neutral esculin (pH 6.0) nor negatively charged esculin (pH 10.0) showed binding of esculin to cyanophycin (Figure 16). No interaction at physiological conditions (pH 7.0; Blanco-Rivero *et al.*, 2005) was detected.

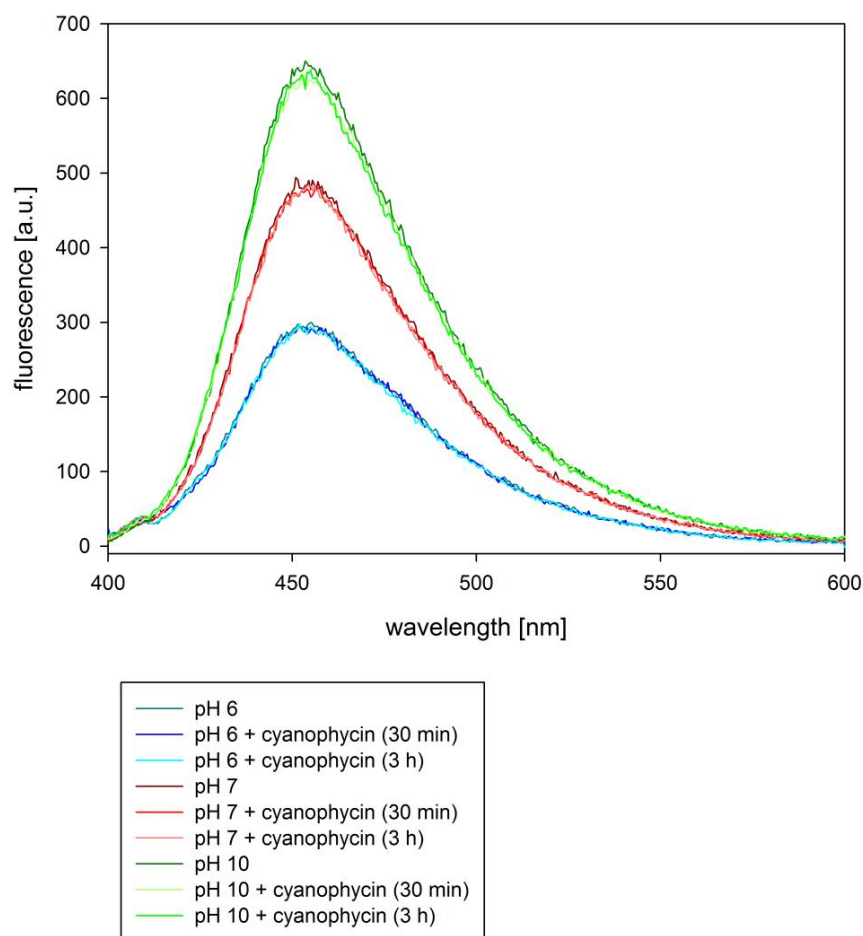


Figure 16. Testing for interaction of esculin and cyanophycin *in vitro*.

Fluorescence emission spectra for esculin at pH 6.0, pH 7.0 and pH 10.0 in buffer and after adding cyanophycin for 0.5 h and 3 h. Binding of esculin to cyanophycin is not detectable at any pH tested, as cyanophycin treatment did not lead to any detectable loss of fluorescence.

As previous work showed that the septal proteins FraC, FraD and SepJ are important for the intercellular exchange of the fluorescent tracers calcein and 5-CFDA (Mullineaux *et al.*, 2008; Mariscal *et al.*, 2011; Merino-Puerto *et al.*, 2011b) the influence of these proteins on the intercellular transfer of esculin was investigated using the deletion mutants CSVM34 ($\Delta sepJ$; Mariscal *et al.* (2011)), CSVT22 ($\Delta fraC \Delta fraD$; Merino-Puerto *et al.* (2011)) and CSVM141 ($\Delta sepJ$

3 Properties and pathways of transferred molecules

$\Delta fraC \Delta fraD$; Vicente Mariscal, unpublished). In the presence of combined nitrogen, all three mutants showed significantly reduced fluorescence recovery rates compared to the wild type (Table 18), suggesting that these proteins are involved in intercellular exchange of esculin among vegetative cells. Deletion of FraC and FraD reduced the rate of esculin exchange between vegetative cells by about 50 % (Table 18). Interestingly, additional loss of SepJ did not reduce the rate of molecular transfer further (Table 18). It is likely that recovery rates remain similar between the two mutants as deletion of *fraC* and *fraD* strongly influences SepJ at the septa (Merino-Puerto *et al.*, 2010). However, slower residual esculin exchange was still observed in the triple mutant (Table 18) suggesting that additional yet unknown proteins are involved in intercellular communication.

Determining the influence of FraC, FraD and SepJ on molecular exchange between heterocysts and vegetative cells is difficult. Mutants lacking SepJ such as CSVM43 ($\Delta sepJ$; Mariscal *et al.* (2011)) and CSVM141 ($\Delta sepJ \Delta fraC \Delta fraD$; Vicente Mariscal, unpublished) do not grow diazotrophically and do not form heterocysts after nitrogen depletion and thus do not allow further investigations. Although strain CSVT22 ($\Delta fraC \Delta fraD$) is also incapable of sustained diazotrophic growth, it survives nitrogen depletion for more than 48 hours and produces well-developed heterocysts during this time (Merino-Puerto *et al.*, 2011b), enabling to test for the involvement of FraC and FraD in esculin exchange between heterocysts and vegetative cells. FRAP experiments revealed that the transfer of esculin into CSVT22 heterocysts is slower than in the wild-type by a factor of greater than 3 (Table 18).

Table 18. Kinetics of esculin exchange from FRAP measurements on filaments of *Anabaena* sp. PCC 7120.

Measurement (number of replicates)	R [s ⁻¹] (± s.d.)	E [s ⁻¹] (± s.d.)	I _F (± s.d.)
1. Vegetative cells in presence of nitrate			
a) <i>Anabaena</i> sp. PCC 7120 (n = 29)	0.137 ± 0.050 ^a		0.518 ± 0.143
b) CSV34 ($\Delta sepJ$) (n = 25)	0.099 ± 0.042 ^b		0.571 ± 0.145
c) CSV22 ($\Delta fraC \Delta fraD$) (n = 30)	0.069 ± 0.029 ^c		0.605 ± 0.072
d) CSV141 ($\Delta sepJ \Delta fraC \Delta fraD$) (n = 21)	0.069 ± 0.030 ^c		0.671 ± 0.068
2. Vegetative cells 48 h after nitrogen deprivation			
<i>Anabaena</i> sp. PCC 7120 (n = 38)	0.142 ± 0.046 ^a		0.507 ± 0.110
3. Heterocysts 48 h after nitrogen deprivation			
a) <i>Anabaena</i> sp. PCC 7120 (n = 33)	0.060 ± 0.054 ^c	0.060 ± 0.054	0.757 ± 0.069
b) CSV22 ($\Delta fraC \Delta fraD$) (n = 18)	0.017 ± 0.024 ^d	0.017 ± 0.024	0.736 ± 0.097
c) CSS7 (<i>cphA1::C.S3</i>) (n = 24)	0.074 ± 0.069 ^e	0.074 ± 0.069	0.640 ± 0.160
4. Spontaneous fluorescence recovery			
<i>Anabaena</i> sp. PCC 7120 (n = 21)			0.925 ± 0.049

Mean exponential recovery rate constants (R), exchange coefficients (E) and immobile fractions (I_F) for filaments grown ± combined nitrogen. R values were standardised by dividing by 2 for cells with 2 connecting junctions. I_F is defined by $[(I_i - I_E)/(I_i - I_0)]$, where I_i = initial fluorescence intensity before bleaching, I₀ = fluorescence intensity immediately after the bleach, I_E = final fluorescence intensity. Extent of spontaneous fluorescence recovery in (4.) is given by (1 - I_F). Different letters indicate statistically significant differences between R values based on a ANOVA test followed by Fisher LSD pair-wise comparison. R values for cells showing recovery less than 7.5 % (equivalent to the spontaneous fluorescence recovery in the absence of diffusion) were considered as being 0.

3.1.5 Loss of metabolic communication in senescent heterocysts

When cultures of *Anabaena* sp. PCC 7120 were grown diazotrophically for 48 hours, not all heterocysts showed esculin fluorescence, although neighbouring

3 Properties and pathways of transferred molecules

vegetative cells remained fluorescent (Figure 17A,B). This suggests that some heterocysts are deficient in esculin exchange with their vegetative neighbours. To quantify esculin equilibration between heterocysts and vegetative cells, esculin fluorescence intensity in each heterocyst was divided by the mean fluorescence intensity in its vegetative neighbours (I_H/I_V). While I_H/I_V should be close to 1 for ‘communicating’ heterocysts as esculin fully equilibrates across the cell junctions, I_H/I_V should be close to zero for heterocysts that are deficient in esculin exchange and also incapable of direct esculin uptake. A frequency distribution of I_H/I_V within a population confirms the bimodal distribution with two peaks close to zero and 1 (Figure 17C). Fluorescence from the ‘non-communicating’ heterocysts was not significantly above the background seen in unlabelled cells. Sometimes ‘communicating’ and ‘non-communicating’ heterocysts were present in the same filament (Figure 17B). The frequency of ‘communicating’ heterocysts was almost 100 % 24 hours after combined nitrogen step-down, but then dropped to about 70 % at 48 hours and subsequently remained at this level (Figure 17B). Therefore young heterocysts are virtually all capable of esculin exchange, but during continued diazotrophic growth a population of about 30 % of ‘non-communicating’ heterocysts builds up. A *cphA1* deficient mutant which is unable to synthesise cyanophycin (Picossi *et al.*, 2004) showed a similar frequency of ‘non-communicating’ heterocysts (Figure 18) indicating that cyanophycin plugs are not the cause of heterocyst non-communication.

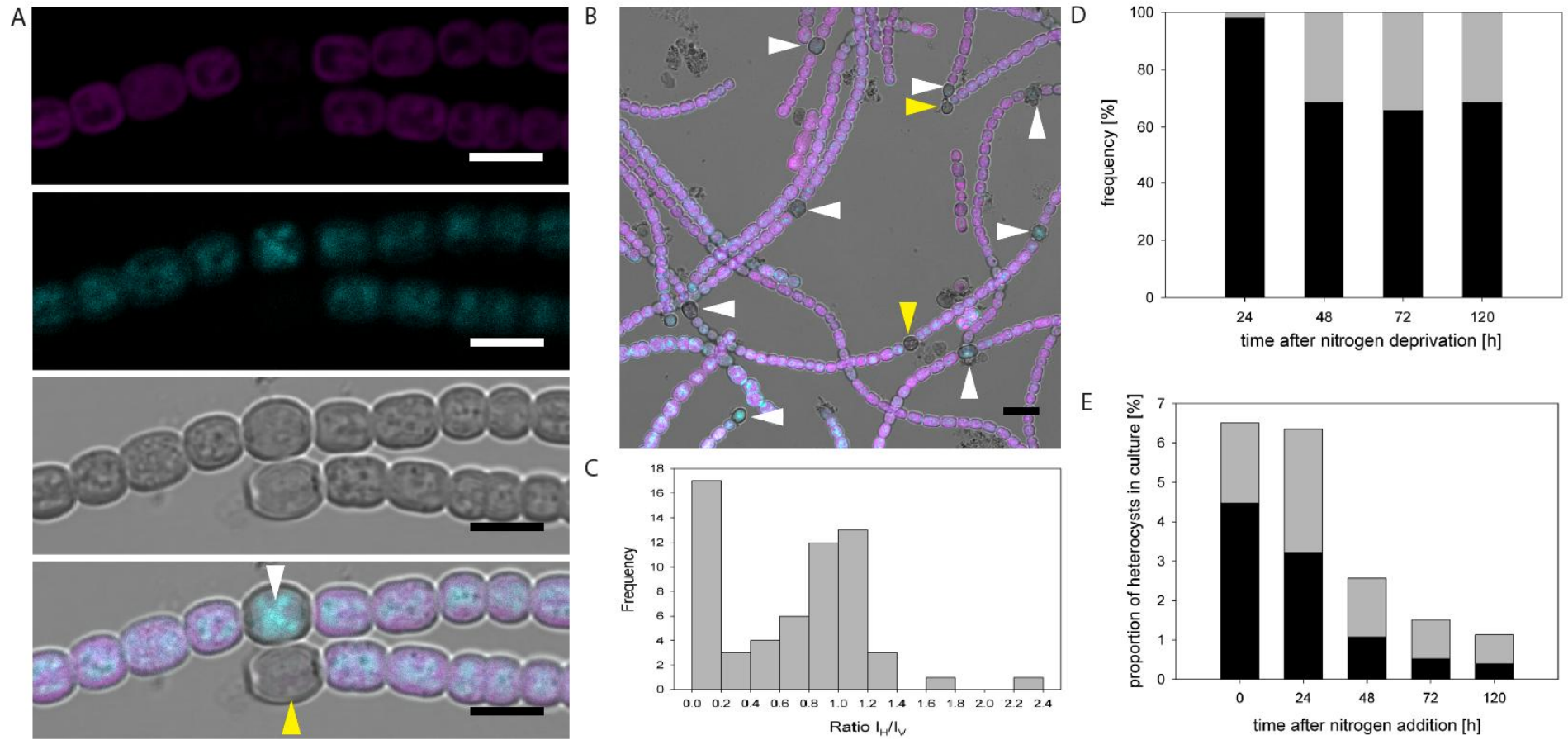


Figure 17. Esculin labelling of *Anabaena* sp. PCC 7120 heterocysts.

Figure 17

(A,B) Fluorescence micrographs show esculin-labelled filaments 48 h after nitrogen step-down. ‘Communicating’ heterocysts are highlighted by white arrows and ‘non-communicating’ heterocysts (defined by $I_H/I_V < 0.2$) by yellow arrows. I_H = esculin fluorescence intensity in the heterocyst; I_V = mean esculin fluorescence intensity in the immediately neighbouring vegetative cells. Images show chlorophyll fluorescence (magenta), esculin fluorescence (cyan) and bright-field images (grey). (A) (bottom) and (B) are merged images. Scale bars, 5 μm in (A) and 10 μm in (B). (C) Frequency distribution of I_H/I_V for heterocysts in esculin-labelled filaments as in (A,B). (D,E) Frequencies of ‘communicating’ (black) and ‘non-communicating’ (gray) heterocysts vs. time following combined nitrogen step-down (D) and after addition of combined nitrogen to a diazotrophic culture (E). Detached heterocysts are not included in the statistics.

As heterocysts are incapable of further cell division and have a limited lifetime before they senesce and die (Meeks *et al.*, 2002) the ‘non-communicating’ heterocysts may represent a senescent population. To test this possibility, nitrate was added to a diazotrophic culture, a procedure which prevents the generation of new heterocysts and must therefore lead to the gradual disappearance of heterocysts from the culture (Meeks *et al.*, 2002). The results indicate that heterocyst frequency decreases following combined nitrogen addition, with a simultaneous decrease in the proportion of communicating heterocysts (Figure 17E) suggesting that senescent heterocysts are indeed characterised by loss of communication with their vegetative neighbours. This occurs prior to any obvious morphological changes (Figure 17A) suggesting that it is an early event in heterocyst senescence. As heterocysts can consume about 50 % of the filament's photosynthates (Wolk, 1996) supply of only fully-functional heterocysts seems logical. Furthermore, loss of communication before cell lyses avoids leakage of

molecules from the entire filament. Insights into channel closure in *Anabaena* sp. PCC 7120 are given in chapter 5.

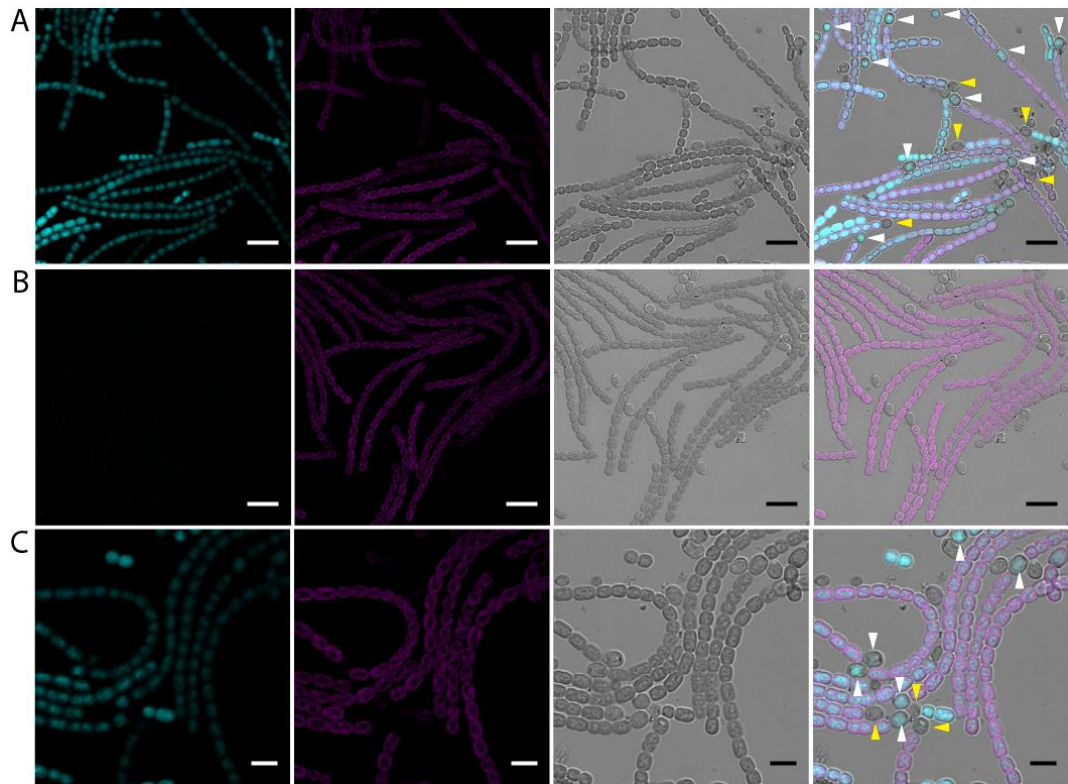


Figure 18. Esculin labelling of heterocysts in an *Anabaena* sp. PCC 7120 mutant lacking cyanophycin synthetase CphA1.

Strain CSS7 (*cphA1::C.S3*) is unable to form polar plugs of cyanophycin in the neck region of heterocysts (Picossi *et al.*, 2004). Fluorescence micrographs show esculin-labelled filaments 72 h after nitrogen step-down (A,C) and an unlabelled control (B). ‘Communicating’ heterocysts are highlighted by white arrows and ‘non-communicating’ heterocysts by yellow arrows. ‘Non-communicating’ heterocysts are defined as those for which $I_H/I_V < 0.2$, where I_H = esculin fluorescence intensity in the heterocyst; I_V = mean esculin fluorescence intensity in the immediately neighbouring vegetative cells. Images show autofluorescence (magenta), esculin fluorescence (cyan) and a bright-field image (gray). Right-hand images are merged. Scale bars, 10 μm in (A, B) and 5 μm in (C).

3.1.6 Conclusion

The fluorescent sucrose analogue esculin is incorporated into the cytoplasm of *Anabaena* sp. PCC 7120 by a sucrose import system. Addition of sucrose reduces the rate of esculin uptake significantly. FRAP experiments revealed that esculin diffuses from cytoplasm to cytoplasm between vegetative cells and between heterocysts and vegetative cells. In comparison to the diffusion of sucrose in water (Table 23) the diffusion of esculin between cells is slow. Assuming sucrose diffuses with a diffusion coefficient D of $0.52 \text{ cm}^2 \text{ s}^{-1}$ a distance x of one cell in *Anabaena* sp. PCC 7120 which is approximately $5 \text{ }\mu\text{m}$, the required time $t = \frac{x^2}{4D} = 12 \text{ ms}$.

Loss of the septal proteins FraC, FraD and SepJ strongly impairs transfer of esculin between cells. However, a triple mutant still shows transfer of esculin between vegetative cells, suggesting the involvement of other proteins which remain to be identified. In conclusion, the major pathway for supplying heterocysts with sucrose is via intercellular diffusion from cytoplasm to cytoplasm via septal junction complexes. Interestingly, intercellular communication is lost in a significant fraction of older heterocysts, suggesting that molecular exchange is controlled to prevent the death of the entire filament when a heterocyst dies.

3.2 Exchange of fluorescent glucose analogues in *Anabaena* sp.

PCC 7120

In comparison to earlier studies based on isotope glucose analogues the usage of fluorescent derivatives enables the measurement of data of high temporal and spatial resolution for living cells such as the exact localisation of glucose and the

3 Properties and pathways of transferred molecules

kinetics of its transfer and turn-over (Kim *et al.*, 2012). In the following subchapter two fluorescent tagged glucose molecules, 2-NBDG (2-(N-(7-Nitrobenz-2-oxa-1,3-diazol-4-yl)Amino)-2-Deoxyglucose) and 6-NBDG (6-(N-(7-Nitrobenz-2-oxa-1,3-diazol-4-yl)amino)-6-Deoxyglucose) are used to label filaments of *Anabaena* sp. PCC 7120 and their role in intercellular communication is investigated. Both fluorophores have been studied extensively for eukaryotic cell systems in the background of cancer and diabetes research but only little for microorganisms (Kim *et al.*, 2012).

3.2.1 Uptake of 2- and 6-NBDG by *Anabaena* sp. PCC 7120

It is known from *E. coli* that 2-NBDG can enter the cells but 6-NBDG cannot be incorporated (Yoshioka *et al.*, 1996). Uptake of 2-NBDG in *E. coli* is mediated by the phosphoenolpyruvate (PEP):carbohydrate phosphotransferase system (PTS) which immediately phosphorylates 2-NBDG into 2-NBDG-6-phosphate after uptake (Yoshioka *et al.*, 1996). Interestingly, both glucose derivatives accumulated in the cytoplasm of *Anabaena* sp. PCC 7120 filaments (Figure 19), suggesting a different route of uptake in *Anabaena* sp. PCC 7120 than found in *E. coli*. However, the efficiency of cell labelling was nominal and not suited for FRAP measurements. Only a fraction of filaments were labelled with 2-NBDG (Figure 19A).

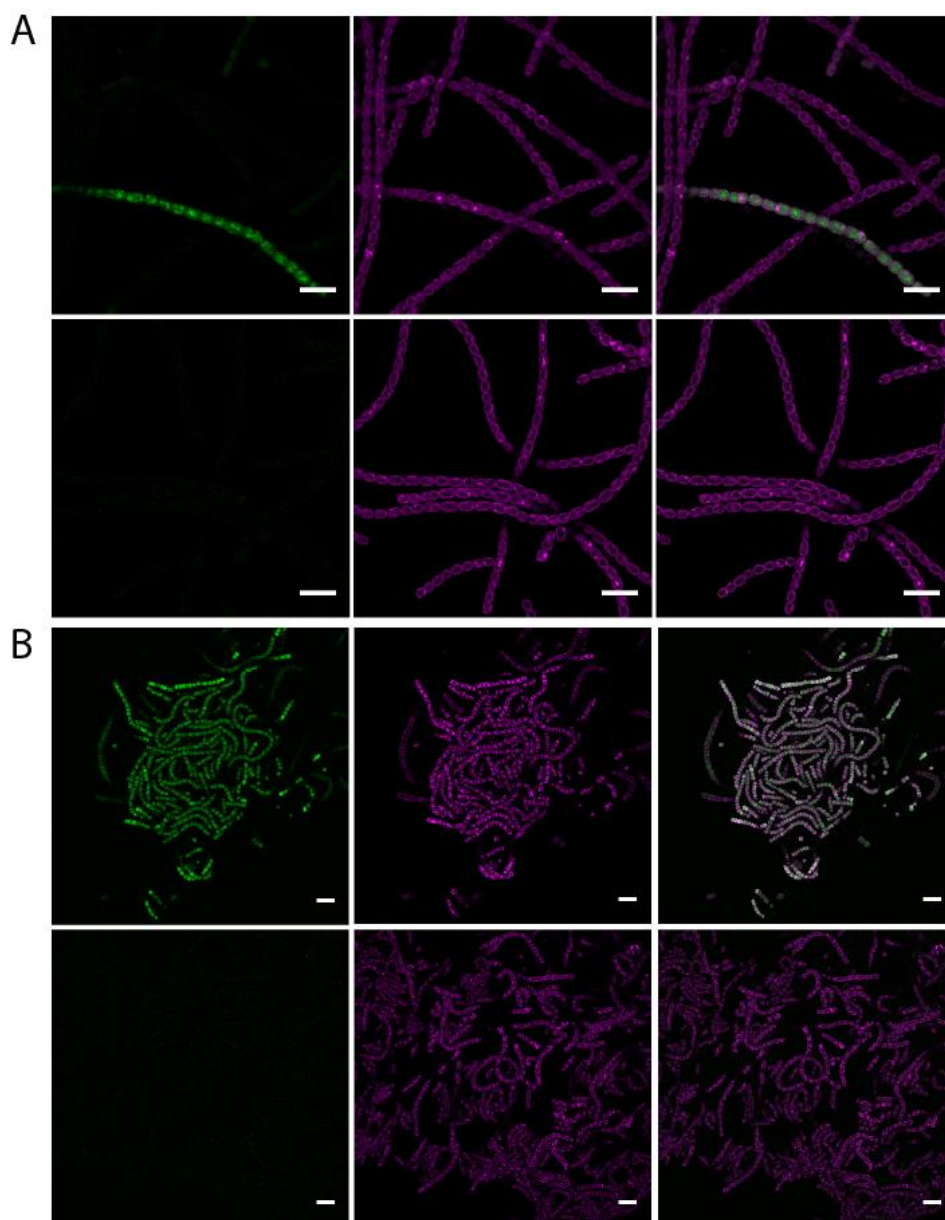


Figure 19. Uptake of 2-NBDG by *Anabaena* sp. PCC 7120 and *N. punctiforme* ATCC 29133.

(A) *Anabaena* sp. PCC 7120 grown in BG11. (B) *N. punctiforme* ATCC 29133 grown in BG11₀ supplemented with ammonia. Images show 2-NBDG fluorescence (green) and chlorophyll fluorescence (magenta). Right-hand images are merged. Control images with unlabeled cells are shown at the bottom of each panel. Scale bars, 10 μm .

3.2.2 Expression of a glucose uptake system from *Nostoc punctiforme* ATCC 29133 in *Anabaena* sp. PCC 7120

Confocal images reveal that 2-NBDG was to a significant degree incorporated and retained in filaments of the closely related cyanobacterium *Nostoc punctiforme* ATCC 29133-S (also known as UCD 153; Campbell *et al.*, 2007; 2008) (Figure 19B). On the basis of an earlier study by Ekman *et al.* (2013), showing that the OprB-like porin Npun_R5320 and the glucose permease GlcP (Npun_R5323) are important for the uptake of glucose in *N. punctiforme* ATCC 29133, mutants of *Anabaena* sp. PCC 7120 were generated which express both genes from the replicative vector pRL25C (Wolk *et al.*, 1988). The gene region Npun_R5320-Npun_R5323 was amplified by PCR using primers f_Npun_R5320-23 and r_Npun_R5320-23 and DNA of *N. punctiforme* ATCC 29133-S as template. The DNA fragment was digested with the restriction endonuclease BamHI and inserted into the BamHI-site of plasmid pRL25C, resulting in construct pCSDN21. The correctness of the inserted sequence was verified by sequencing. Construct pCSDN21 was transferred to *Anabaena* sp. PCC 7120, CSVM34 ($\Delta sepJ$; Mariscal *et al.*, 2011), CSVM141 ($\Delta sepJ \Delta fraC \Delta fraD$; Vicente Mariscal, unpublished) and CSVT22 ($\Delta fraC \Delta fraD$; Merino-Puerto *et al.*, 2011) by conjugation as described by Elhai and Wolk (1988), resulting in strains CSDN21, CSVM34-CSDN21, CSVM141-CSDN21 and CSVT22-CSDN21 respectively.

Uptake studies using the ^{14}C -labelled sugar molecules glucose, fructose and sucrose revealed enhanced uptake by CSDN21 for glucose but not fructose and sucrose (Figure 20A), strengthening the importance of Npun_R5320 and Npun_R5323 as specific glucose transporters. Further studies using confocal

3 Properties and pathways of transferred molecules

microscopy on NBDG labelled filaments of CSDN21 show the presence of both fluorescent tracers 2- and 6-NBDG in the cytoplasm (Figure 20B,C) while unlabelled cells remain non-fluorescent under the same visualisation settings (Figure 20D). The increase of NBDG uptake in strain CSDN21 remains to be quantitated. The fluourometric assay described for esculin (see chapter 3.1.1) could resolve this question.

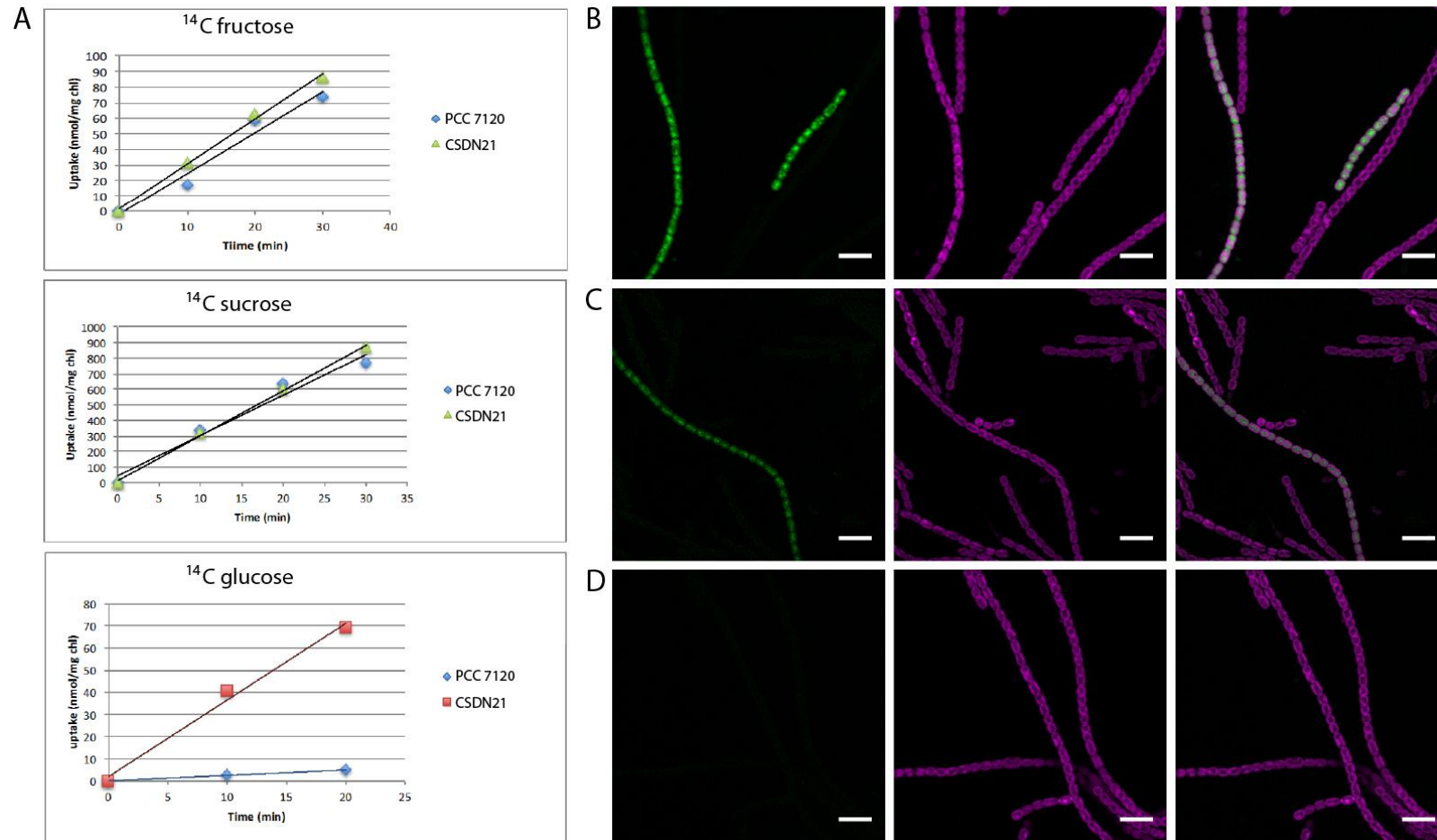


Figure 20. Sugar uptake properties of strain CSDN21.

Figure 20

Cells grown in BG11. (A) Time-course for uptake of ^{14}C labelled glucose, fructose and sucrose. All substrates were used at 100 μM . (Data and graphs were kindly provided by Vicente Mariscal and Mercedes Nieves-Mori3n) (B) 2-NBDG labelled cells. (C) 6-NBDG labelled cells. (D) Control with unlabelled cells using the same settings as for (B,C). Images show NBDG fluorescence (green), chlorophyll fluorescence (magenta) and overlays. Scale bars, 10 μm .

3.2.3 Intercellular diffusion of 2- and 6-NBDG in CSDN21

In order to investigate the role of the fluorescent glucose derivatives in intercellular communication, FRAP experiments were performed as previously described by Mullineaux *et al.* (2008). After labelling cells with either 2- or 6-NBDG the fluorescence of a specific cell was bleached out by increased laser intensity and zooming into the ROI, and its recovery followed over time. FRAP measurements revealed that NBDG fluorescence recovers within 25 s for both glucose derivatives.

Figure 21 shows exemplary fluorescence recovery of 2-NBDG in vegetative cells and heterocysts. These experiments indicate that 2- and 6-NBDG are transferred between adjacent vegetative cells and between vegetative cells and heterocysts via cytoplasmic bridges.

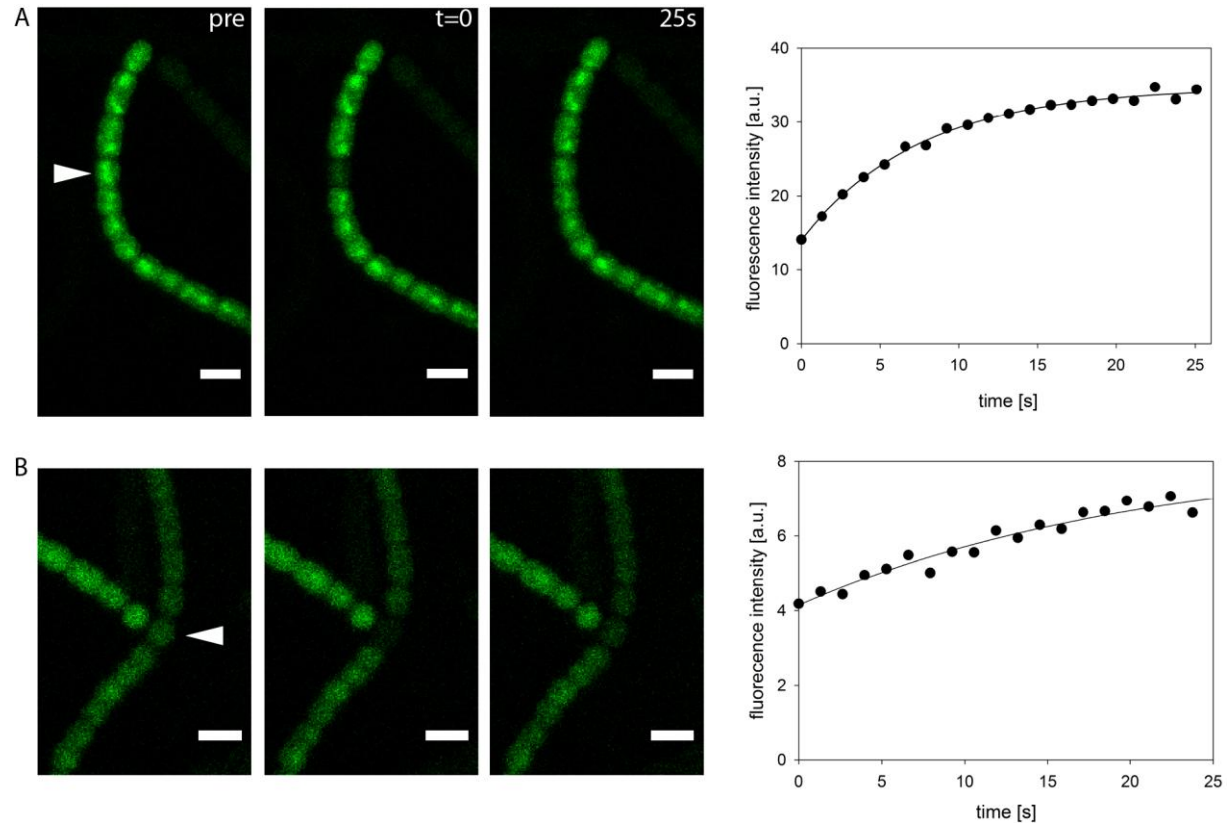


Figure 21. Examples of FRAP experiments monitoring intercellular exchange of 2-NBDG in CSDN21.

Exchange between vegetative-vegetative cells (A) and vegetative cells-heterocysts (B). Fluorescence images from FRAP time-series show 2-NBDG fluorescence prior to the bleach (pre), immediately after bleaching out fluorescence in the highlighted cell ($t = 0$), and 25 s later. Scale bars, 5 μm . Fluorescence recovery curves for the bleached cells are displayed on the right-hand site.

3 Properties and pathways of transferred molecules

However, not all cells show fluorescence recovery after bleaching. The frequency of non-communicating cells ranges from 10 % for 6-NBDG to 41 % for 2-NBDG (Figure 22). It is likely that the lack of molecular transfer results from immobilisation of the NBDG molecules within the cell. Similar to 5-CFDA (Merino-Puerto *et al.*, 2011b) and esculin (see chapter 3.1) 2- and 6-NBDG always showed incomplete recovery. When incubating filaments of CSDN21 for 24 h in BG11 medium supplemented with either 2- or 6-NBDG the frequency of non-communicating cells dramatically increased to 90 % for 2-NBDG and 100 % for 6-NBDG (Figure 22).

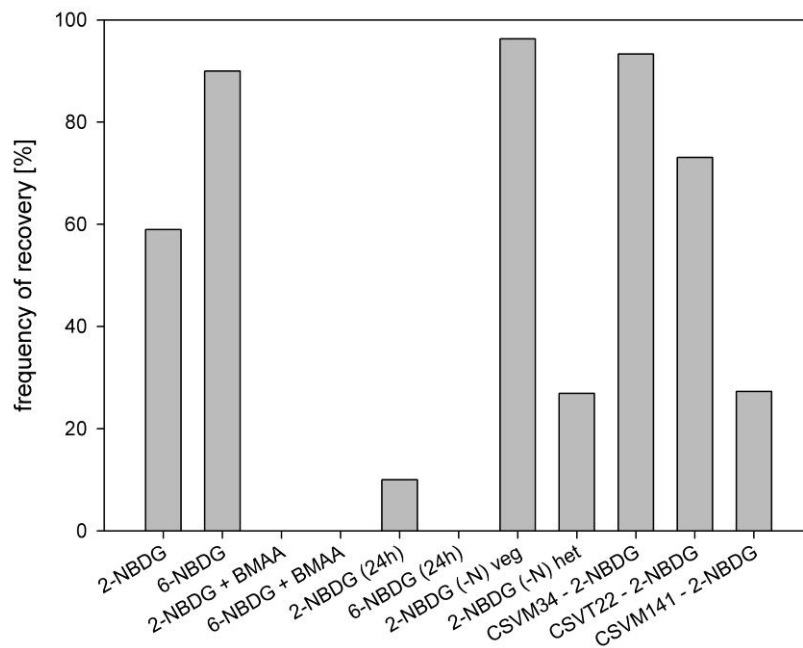


Figure 22. Frequency of fluorescence recovery in FRAP experiments using 2- and 6-NBDG.

Number of performed measurements: 39 (2-NBDG), 20 (6-NBDG), 20 (2-NBDG+BMAA), 21 (6-NBDG+BMAA), 20 (2-NBDG (24h)), 20 (6-NBDG (24h)), 27 (2-NBDG (-N) veg), 26 (2-NBDG (-N) het), 30 (CSV34-2-NBDG), 26 (CSV22-2-NBDG) and 33 (CSV141-2-NBDG). het - heterocyst; veg - vegetative cell.

3 Properties and pathways of transferred molecules

Interestingly, the frequency of immobilised 2-NBDG in vegetative cells was significantly lower under nitrogen depletion than in cells grown with nitrate as nitrogen source (5 % and 41 % respectively) (Figure 22). In contrast to vegetative cells, heterocysts showed a high frequency of 2-NBDG immobilisation (73 %; Figure 22). Further investigation by confocal microscopy revealed a high variability of heterocyst labelling with both 2- and 6-NBDG with some cells showing fluorescence and others being non-fluorescent (Figure 23A). Variation in heterocyst labelling has been also observed for esculin (see chapter 3.1). However, labelling with NBDG molecules was in general less efficient with less cells being labelled in comparison to the labelling with esculin. Sometimes only heterocysts were labelled within a filament (Figure 23A). To further investigate whether heterocysts are capable of taking up 2-NBDG, heterocysts were purified and the fluorescent glucose derivative added. Isolated heterocysts did not show any fluorescence (Figure 23B) suggesting that 2-NBDG is not taken up directly by heterocysts but diffuses from neighbouring vegetative cells into the cell where degradation processes might be slower or missing. To prove that isolated heterocysts are viable calcein-AM was added to isolated heterocysts. Calcein-AM becomes only fluorescent inside living cells after hydrolysis by intracellular esterases. Isolated heterocysts showed fluorescence (Figure 23C) indicating the suitability of the used purification method to obtain viable heterocysts.

3 Properties and pathways of transferred molecules

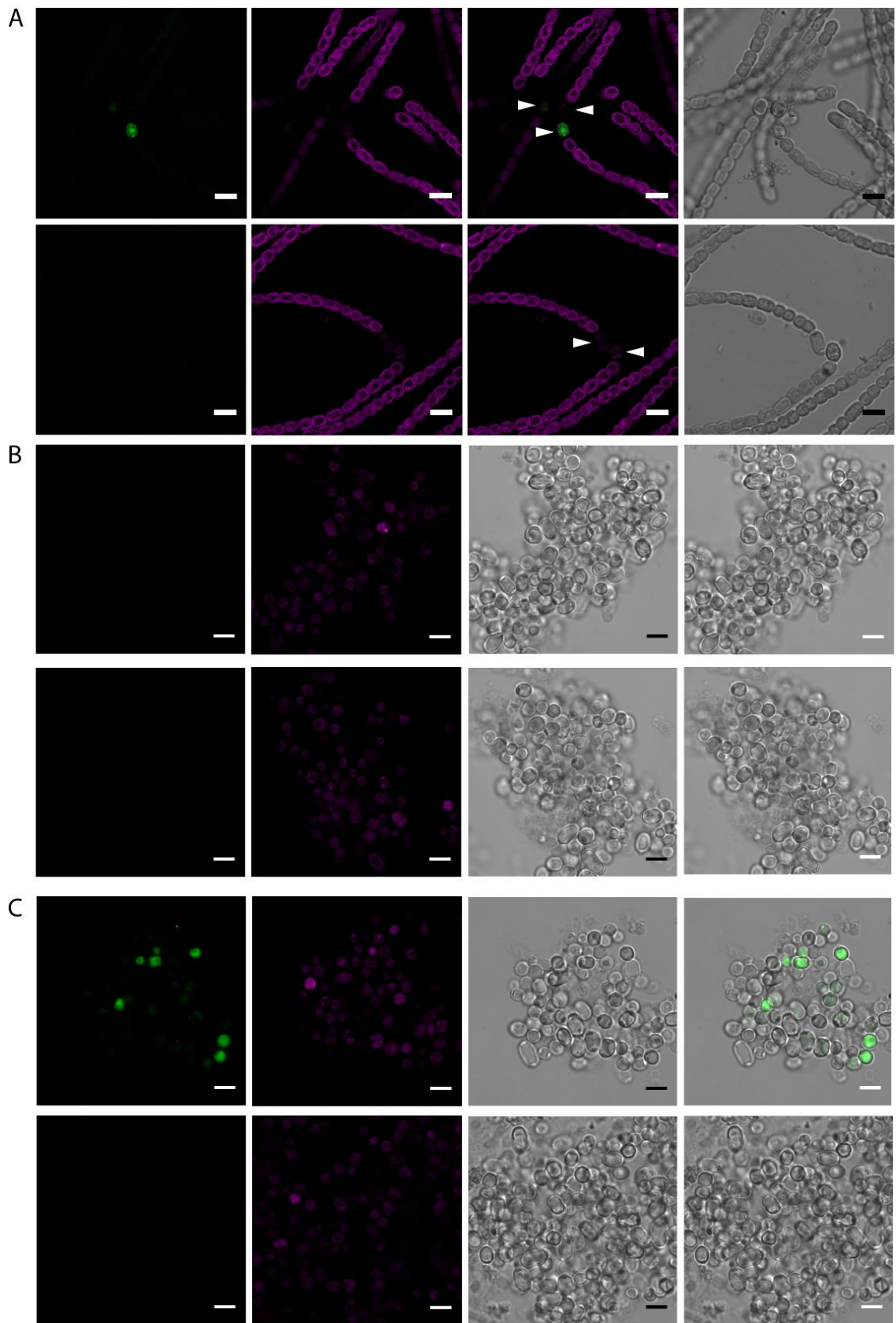


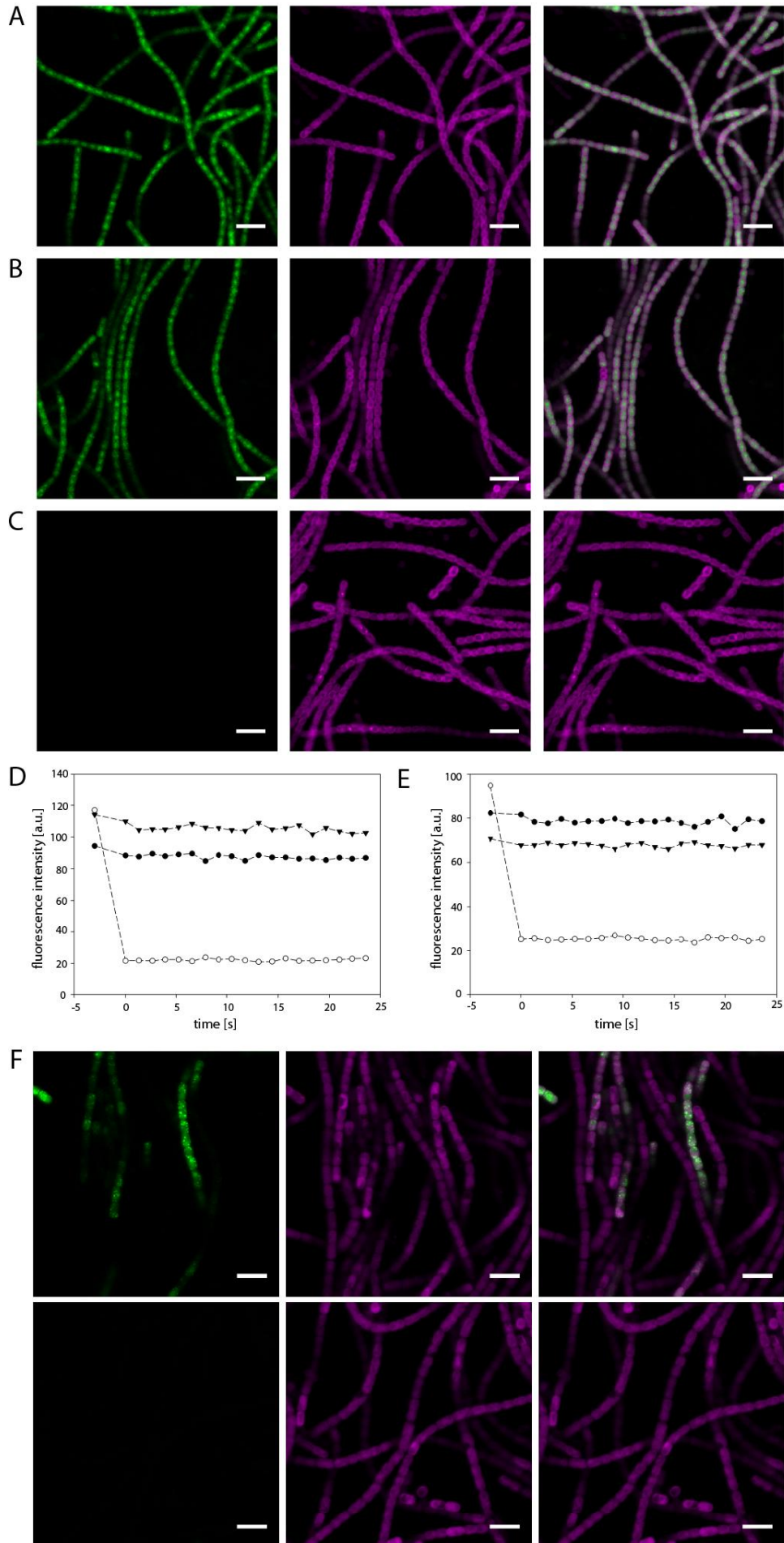
Figure 23. Labelling of heterocysts with 2-NBDG.

Figure 23

(A) Fluorescence micrographs showing filaments 48 h after nitrogen step-down. Heterocysts of interest are indicated by white arrows. Images show 2-NBDG fluorescence (green), chlorophyll fluorescence (magenta), overlays of both channels and bright-field images (grey). Control with unlabelled cells (bottom panel). Scale bars, 10 μm . (B,C) Uptake of 2-NBDG (B) and calcein (C) by purified heterocysts. Images show 2-NBDG fluorescence (green), chlorophyll fluorescence (magenta), bright-field images (grey) and overlays of 2-NBDG fluorescence and bright-field. Controls without dye are displayed in the bottom row of each panel. Scale bars, 5 μm .

Louzao *et al.* (2008) reported that 2-NBDG accumulates in glycogen in living cells and cell-free systems. In order to test whether the immobilisation of the fluorescent glucose derivatives coincides with the formation of glycogen, the non-proteinogenic amino acid β -N-methylamino-L-alanine (L-BMAA) was added. In *Anabaena* sp. PCC 7120 the addition of L-BMAA strongly influences the metabolic pathways of the organism by rapidly inhibiting nitrogenase activity and massively accumulating glycogen (Berntzon *et al.*, 2013). Addition of L-BMAA results in extensive accumulation of both fluorophores in filaments of CSDN21 (Figure 24A,B) and complete immobilisation of both NBDG molecules (Figure 22, Figure 24D,E). NBDG fluorescence of a bleached vegetative cell did not recover, consistent with the constant fluorescence intensity of neighbouring vegetative cells (Figure 24D,E). These results suggest that incorporation of 2- and 6-NBDG into glycogen could be the main cause for the loss of mobility. However, immobilisation due to interactions with other cell components such as proteins and lipids is possible. The model in Figure 24G shows that both molecules can be incorporated into glycogen. Although incorporation of 6-NBDG does not allow the formation of $\alpha(1\rightarrow6)$ linkages, it is likely that glycogen formation is still possible using unlabelled glucose molecules instead.

3 Properties and pathways of transferred molecules



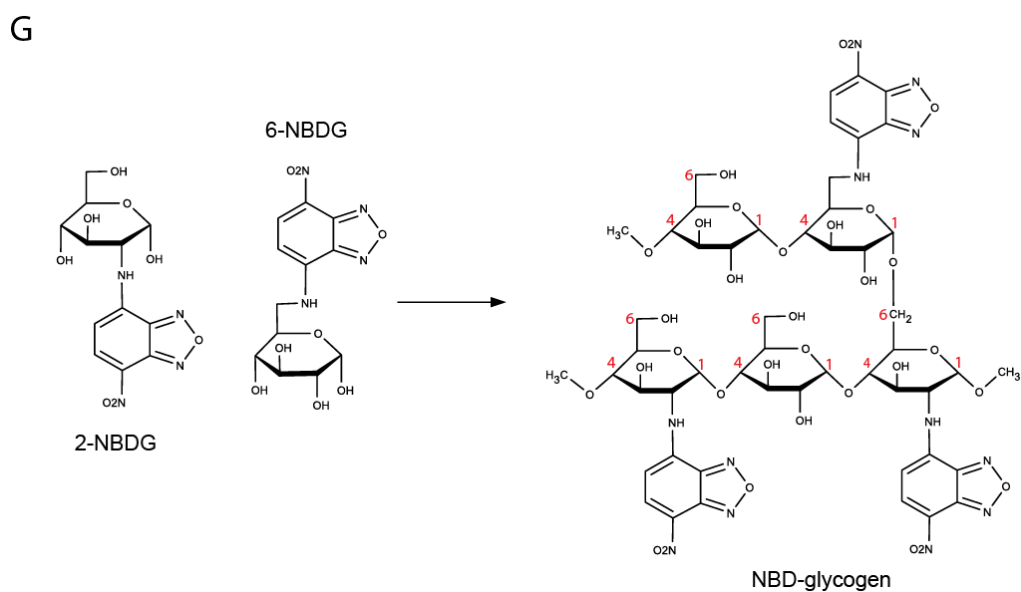


Figure 24. Influence of L-BMAA on uptake and transfer of 2- and 6-NBDG in CSDN21 and formation of NBDG-glycogen.

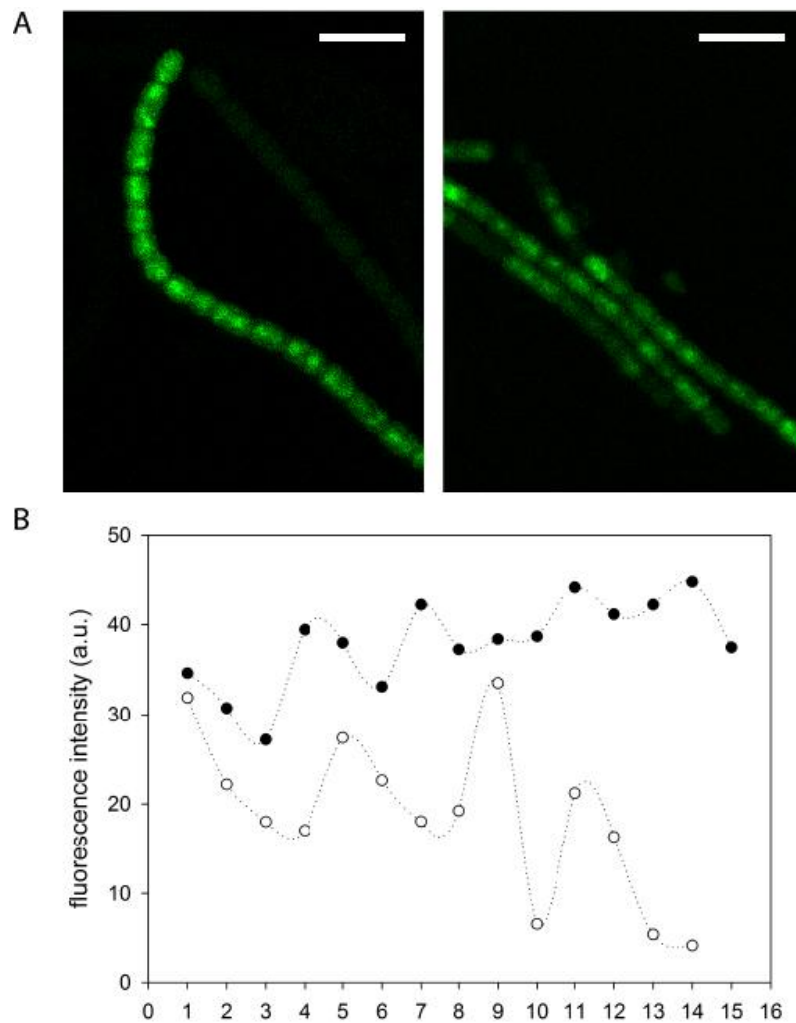
Filaments of CSDN21 incubated for 24 h with 2-NBDG (A) and 6-NBDG (B). (C) Control without dye. Images show NBDG fluorescence (green), chlorophyll fluorescence (magenta) and overlays. Scale bars, 10 μ m. (D,E) Fluorescence recovery curves for 2-NBDG (D) and 6-NBDG (E). NBDG fluorescence for the bleached cell (cell 2 (open circle)) and neighbouring vegetative cells (cell 1 (filled circle) and cell 3 (filled triangle)) vs. time. (F) Fluorescent 2-NBDG granules in filaments of CSN21. Images show 2-NBDG (green), chlorophyll fluorescence (magenta) and overlays. Control with unlabeled cells (bottom row). Scale bars, 10 μ m. (G) Hypothetical structure for NBD-glycogen based on incorporation of 2- and 6-NBDG. Glycogen is formed of glucose molecules which are covalently linked via $\alpha(1\rightarrow4)$ and $\alpha(1\rightarrow6)$ bonds. Carbon atoms which are involved in formation of the linkages are numbered in red.

Interestingly, after removal of both L-BMAA and the fluorescent glucose derivative and further incubation for 24 h, filaments of CSDN21 showed a highly variable fluorescence within the same filament (Figure 25A,B), suggesting that single cells within the same filament exhibit different metabolic characteristics. The variation in fluorescence along the filaments of CSDN21 also indicates that once immobilised

3 Properties and pathways of transferred molecules

NBDG molecules do not retain mobility and cannot diffuse freely between neighbouring cells until reaching the concentration equilibrium.

To test whether NBDG fluorescence is dependent on pH, fluorescence emission spectra were recorded at pH 4.5 to 10.0 (Figure 25C). Assuming that the cytoplasmic pH in *Anabaena* sp. PCC 7120 is about 7.0 (Blanco-Rivero *et al.*, 2005) and assuming that the pH in other cell compartments falls within the range 6.0 to 8.0 NBDG fluorescence yield would be nearly constant (Figure 25C). Therefore, the effect of pH on 2-NBDG fluorescence intensity is negligible under physiological conditions.



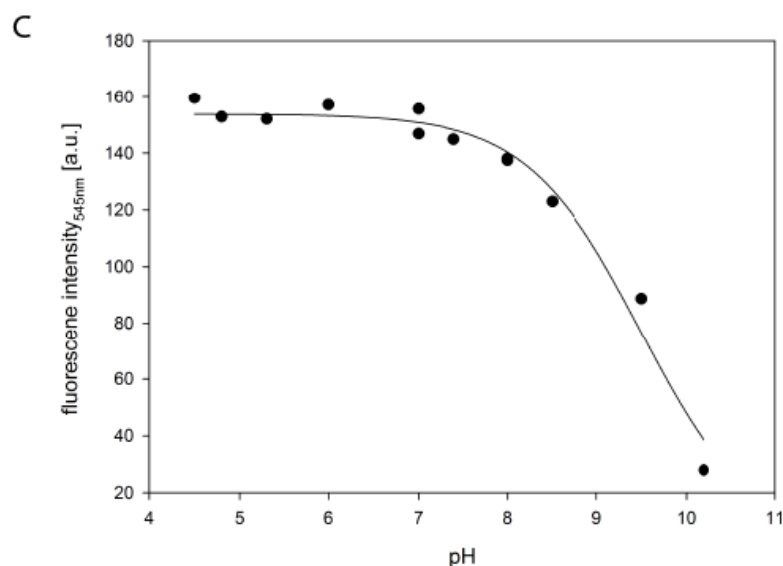


Figure 25. Degradation of 2-NBDG in filaments of CSDN21 and pH dependence of 2-NBDG fluorescence.

(A) Fluorescence images of CSDN21 after incubation for 24 h with 2-NBDG and L-BMAA (upper left) and 24 h after removal of 2-NBDG and L-BMAA (upper right). 2-NBDG fluorescence shown in green. Scale bars, 10 μ m. (B) Fluorescence intensity plot using cells displayed in (A). Filled circles - 24 h after addition of 2-NBDG and L-BMAA; open circles - 24 h after removal of 2-NBDG and L-BMAA. (C) pH dependence of 2-NBDG fluorescence. Emission of 2-NBDG at the peak wavelength of 545 nm is plotted vs. pH from 4.5 to 10.

3.2.4 Kinetics of intercellular 2- and 6-NBDG diffusion in CSDN21

To quantify the kinetics of intercellular exchange for the different fluorophores, Mullineaux *et al.* (2008) introduced the ‘exchange coefficient’ E that relates the rate of dye movement between two neighbouring cells to the difference in dye concentration between these cells. After short incubation of CSDN21 with the fluorescent glucose variants the majority of cells shows fluorescence recovery after the initial bleach (Figure 22) indicating that NBDG molecules remain mobile. However, as even recovering cells never showed full recovery, E can only be

3 Properties and pathways of transferred molecules

determined for heterocysts but not for vegetative cells (see esculin 3.1.2 for discussion). Therefore, the 'recovery rate constant' R was used for quantitation of molecular transfer between vegetative cells (Merino-Puerto *et al.*, 2011).

In the presence of a combined nitrogen source exchange of 2- and 6-NBDG was similar between vegetative cells in strain CSDN21 (Table 19). For simplicity the following FRAP experiments were performed with 2-NBDG only.

Under nitrogen depletion the need for intercellular communication becomes substantial. Filaments of *Anabaena* sp. PCC 7120 differentiate photosynthetically-active vegetative cells into photosynthetically-inactive heterocysts which provide fixed nitrogen but depend on the provision of fixed carbon from neighbouring cells. In contrast to calcein (Mullineaux *et al.*, 2008) but similar to esculin (see chapter 3.1) exchange for 2-NBDG between vegetative cells was not significantly faster under this condition (Table 19). Intercellular transfer of 2-NBDG between vegetative cells and heterocysts was significantly slower by about 76 % than between vegetative cells under nitrogen deprivation (Table 19). A result which could be attributed to the reduced number of septal junctions identified by freeze-fracture electron microscopy (Giddings and Staehelin, 1978) and electron tomography (Omairi-Nasser *et al.*, 2014).

Table 19. Kinetics of 2- and 6-NBDG exchange from FRAP measurements on filaments of CSDN21 and related mutants.

Measurement (number of replicates)		R [s ⁻¹] (± s.d.)		E [s ⁻¹] (±s.d.)
		6-NBDG	2-NBDG	2-NBDG
1. vegetative cells in presence of nitrate				
a) CSDN21	(n=18)	0.095 ± 0.048 ^a		
b)	(n=23)	0.126 ± 0.083 ^a		
c) CSVM34 ($\Delta sepJ$)-DN21	(n=28)	0.082 ± 0.044 ^b		
d) CSVT22 ($\Delta fraC \Delta fraD$)-DN21	(n=19)	0.042 ± 0.026 ^c		
e) CSVM141($\Delta sepJ \Delta fraC \Delta fraD$)- DN21	(n=9)	0.042 ± 0.023 ^c		
2. vegetative cells 48 h after nitrogen deprivation				
CSDN21	(n=26)	0.100 ± 0.058 ^a		
3. heterocysts 48 h after nitrogen deprivation				
CSDN21	(n=7)	0.024 ± 0.014 ^d	0.024 ± 0.014	

Mean recovery rate constants (R) and exchange coefficients (E) for filaments grown in the presence and absence of combined nitrogen. R values were standardised by dividing by 2 for cells with 2 connecting junctions (i.e. all cells except those at the terminus of the filament). Different letters indicate statistically significant differences between R values. ANOVA followed by Fisher LSD pair-wise comparison.

3.2.5 Influence of septal proteins FraC, FraD and SepJ on intercellular transfer of 2-NBDG

As previous work showed that the septal proteins FraC, FraD and SepJ are important for the intercellular exchange of the fluorescent tracers calcein, 5-CFDA (Mullineaux *et al.*, 2008; Mariscal *et al.*, 2011; Merino-Puerto *et al.*, 2011b) and esculin (see chapter 3.1), the influence of these proteins on the intercellular transfer of 2-NBDG

3 Properties and pathways of transferred molecules

was investigated by FRAP. To increase glucose uptake in mutants CSVM34 ($\Delta sepJ$; Mariscal *et al.* (2011)), CSVT22 ($\Delta fraC \Delta fraD$; Merino-Puerto *et al.* (2011)) and CSVM141 ($\Delta sepJ \Delta fraC \Delta fraD$; Vicente Mariscal, unpublished) plasmid pCSDN21 was introduced, resulting in strains CSVM34-DN21, CSVT22-DN21 and CSVM141-DN21. Deletion of *fraC*, *fraD* and *sepJ* significantly reduces molecular transfer between vegetative cells to about 33 % in comparison to CSDN21 (Table 19). While in CSVM34-DN21 ($\Delta sepJ$) the recovery rate constant remains at about 65 %, deletion of *fraC* and *fraD* results in reduction of molecular exchange to about 33 % (Table 19). The similarity of recovery rate constants in CSVM141-DN21 and CSVT22-DN21 is likely due to the importance of FraC and FraD for the correct localisation of SepJ at the septa (Merino-Puerto *et al.*, 2010). It is notable that both mutants still show intercellular exchange of 2-NBDG suggesting that other proteins are likely involved in mediating diffusion between cells.

3.2.6 Conclusion

Uptake of glucose by *Anabaena* sp. PCC 7120 can be significantly increased by expressing the genes *oprB* (Npun_R5320) and *glcP* (Npun_R5323) from *N. punctiforme* ATCC 29133 from the self-replicating plasmid pRL25C. OprB and GlcP together provide the capability of specific transport of glucose but not fructose or sucrose in *Anabaena* sp. PCC 7120. Generated mutants show uptake of two fluorescent glucose derivatives, 2- and 6-NBDG that diffuse in the cytoplasm between adjacent vegetative cells and vegetative cells and heterocysts. Septal proteins FraC, FraD and SepJ are important factors for molecular transfer. Deletion of the three genes reduces exchange to a third. Furthermore, a high frequency of immobilised fluorophore was observed likely due to their incorporation into

glycogen. Different degradation velocities of the fluorescent glucose derivatives suggest that single cells within a filament possess different metabolic characteristics.

3.3 Exchange of BCECF in *Anabaena* sp. PCC 7120

2',7'-Bis-(2-carboxyethyl)-5-(and-6-)carboxyfluorescein (BCECF) was first introduced in 1982 to measure the cytoplasmic pH of lymphocytes (Rink *et al.*, 1982) and has since then become the most widely used intracellular pH indicator for mammalian and plant cells (see review by Han and Burgess, 2010) but also bacteria (e.g. Corvini *et al.*, 2000). The technique is based on pH dependent changes in fluorescence intensities when exciting the molecule at different wavelengths (Slavík, 1997). Similar to calcein and 5-CFDA the fluorescent tracer BCECF is a fluorescein derivative that is added as acetoxymethylester (AM) to the cultures. BCECF-AM is hydrophobic enough to enter the cell. Once inside the cytoplasm the ester groups are hydrolysed by esterases and the molecule converted to its fluorescent form. As BCECF is too hydrophilic to traverse lipid bilayers it is retained in the cytoplasm. Thus, fluorescence recovery after photobleaching can only be observed when fluorophores diffuse into the bleached cell from neighbouring cells. In comparison to calcein and 5-CFDA, BCECF exhibits some specific physico-chemical properties, allowing the investigation of the effect of size and charge on molecular transfer via septal junctions. While BCECF is strongly negatively charged, similar to calcein, its size is more comparable to that of 5-CFDA (Table 23). In the following subchapter the role of BCECF in intercellular communication is investigated by FRAP measurements. Results are compared with transfer of 5-CFDA and calcein. Furthermore, the influence of the septal proteins FraC, FraD and SepJ on BCECF transfer is examined.

3.3.1 Uptake of BCECF and kinetics of its transfer in *Anabaena* sp. PCC 7120

Cells of *Anabaena* sp. PCC 7120 were successfully labelled with BCECF after 30 min of incubation with the dye. Confocal images reveal the presence of the fluorophore in the cytoplasm (Figure 26) and FRAP experiments indicate that BCECF is transferred between vegetative cells (Figure 26) and between vegetative cells and heterocysts (data not shown). As cells did not show full fluorescence recovery after bleaching, molecular exchange was quantitated by the method of Merino-Puerto *et al.* (2011) by determining the recovery rate constant R . For comparison purposes cells of the same culture were labelled in separate experiments with the fluorescein derivatives 5-CFDA and calcein as described in the materials and methods section 2.7.2.1. Table 20 summarises the results.

Both fluorophores, BCECF and calcein exhibited similar recovery rates in the presence of a combined nitrogen source while exchange of 5-CFDA is significantly faster under this condition, indicating that the negative charge of the molecule might be a key feature beside its size reducing transfer between vegetative cells. When cells of *Anabaena* sp. PCC 7120 were deprived of combined nitrogen, exchange between vegetative cells increases for BCECF and calcein and became similar to the value determined for 5-CFDA. Accordingly, nitrogen step-down allows faster exchange of molecules that are negatively charged and slightly bigger. How molecular transfer is increased remains speculative. It is possible that either new channels between cells are formed or the properties of existing structures are altered e.g. by structural modifications or by adding new components/proteins. According to the FFEM studies by Giddings and Staehelin (1981) the number of septal junctions between vegetative cells remains nearly constant in the presence and absence of combined

3 Properties and pathways of transferred molecules

nitrogen in the closely related strain *Anabaena cylindrica*, suggesting that existing structures are modified for molecular exchange.

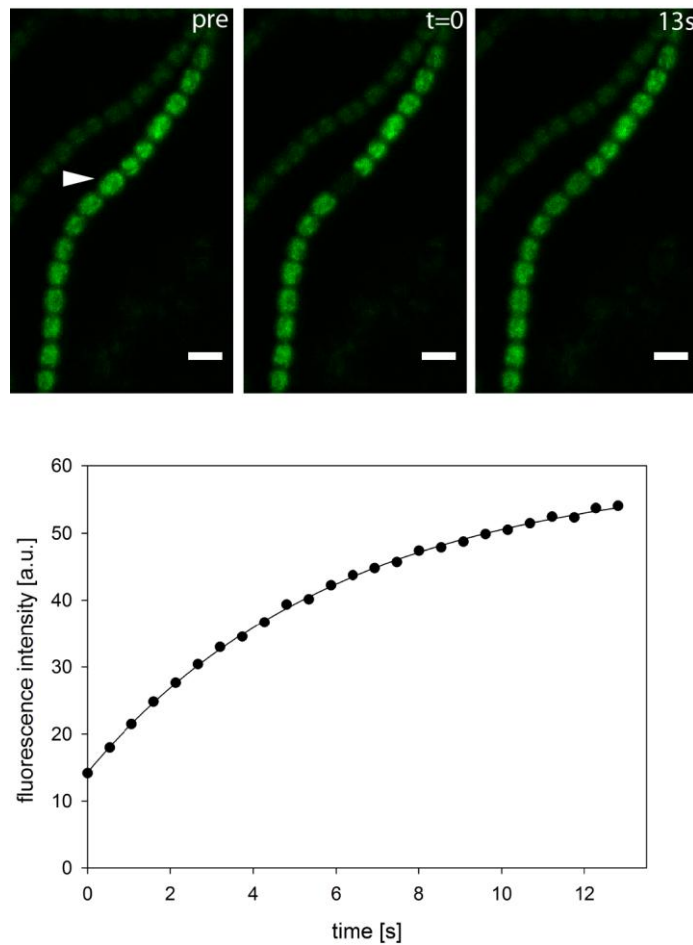


Figure 26. Example of FRAP experiments monitoring intercellular of BCECF exchange between vegetative cells in *Anabaena* sp. PCC 7120.

Fluorescence images from FRAP time-series show BCECF fluorescence prior to the bleach (pre), immediately after bleaching out fluorescence in the highlighted cell ($t = 0$), and 13 s later. Scale bars, 5 μm . Fluorescence recovery curve for the bleached cell is displayed underneath.

Exchange of BCECF between vegetative cells and heterocysts was significantly slower than between vegetative cells. This is in good agreement with earlier studies on the exchange of calcein in *Anabaena* sp. PCC 7120 (Mullineaux *et al.*, 2008) and is possibly the result of the reduced number of septal junctions found in septa

3 Properties and pathways of transferred molecules

between heterocysts and vegetative cells (Giddings and Staehelin, 1981; Omairi-Nasser *et al.*, 2014). Furthermore, it is notable that the exchange coefficients for heterocysts are highly variable with several cells showing no recovery, indicated by the high standard deviation in Table 20.

Table 20. Kinetics of BCECF exchange from FRAP measurements on filaments of *Anabaena* sp. PCC 7120 and septal mutants.

Measurement	R [s ⁻¹] (± s.d.) (number of replicates)		
	BCECF	5-CFDA	Calcein
1. vegetative cells in presence of nitrate			
a) <i>Anabaena</i> sp. PCC 7120	0.079 ± 0.050 (n=48) ^a	0.094 ± 0.054 (n=57) ^{A*}	0.072 ± 0.042 (n=39) ^{B*}
b) CSVM34 ($\Delta sepJ$)	0.049 ± 0.032 (n=66) ^b		
c) CSVT22 ($\Delta fraC \Delta fraD$)	0.007 ± 0.008 (n=23) ^c		
d) CSVM141($\Delta sepJ \Delta fraC \Delta fraD$)	0.004 ± 0.007 (n=24) ^c		
2. vegetative cells after nitrogen deprivation			
a) <i>Anabaena</i> sp. PCC 7120 - 48 h	0.095 ± 0.035 (n=14) ^a	0.088 ± 0.034 (n=13) ^A	0.105 ± 0.039 (n=10) ^C
b) <i>Anabaena</i> sp. PCC 7120 - 72 h	0.085 ± 0.033 (n=26) ^a	0.101 ± 0.048 (n=10) ^A	0.111 ± 0.054 (n=4) ^C
3. heterocysts after nitrogen deprivation			
a) <i>Anabaena</i> sp. PCC 7120 - 48 h	0.010 ± 0.019 (n=6) ^c		
b) <i>Anabaena</i> sp. PCC 7120 - 72 h	0.010 ± 0.020 (n=4) ^c		

Mean recovery rate constants (R) for filaments grown in the presence and absence of combined nitrogen. Different letters indicate statistically significant differences between R values for a specific dye under minus or plus N conditions. Significant differences for R values for different dyes are indicated by "*". ANOVA followed by Fisher LSD pair-wise comparison.

3.3.2 Influence of the septal proteins SepJ, FraC and FraD on the exchange of BCECF

Exchange of 5-CFDA and calcein depends on the presence of FraC, FraD and SepJ in *Anabaena* sp. PCC 7120. Loss of these proteins strongly reduced transfer between vegetative cells (Mullineaux *et al.*, 2008; Mariscal *et al.*, 2011; Merino-Puerto *et al.*, 2011b). Similar results were obtained for transfer of BCECF in strains CSV34 ($\Delta sepJ$; Mariscal *et al.* (2011)), CSV22 ($\Delta fraC \Delta fraD$; Merino-Puerto *et al.* (2011)) and CSV141 ($\Delta sepJ \Delta fraC \Delta fraD$; Vicente Mariscal, unpublished) (Table 20). Deletion of *fraC*, *fraD* and *sepJ* (CSV141) and deletion of *fraC* and *fraD* (CSV22) nearly inhibited molecular transfer between vegetative cells completely, while recovery in the *sepJ* deletion mutant (CSV34) remains at 62 % of the level determined in the wild-type (Table 20).

3.3.3 Conclusion

BCECF is a suitable fluorescent probe to investigate intercellular communication in *Anabaena* sp. PCC 7120. Both, vegetative cells and heterocysts can be labelled with the dye. FRAP results reveal that BCECF diffuses within the cytoplasm of different cell types. Exchange of BCECF is similar to the molecular diffusion determined for calcein, suggesting that charge and size of the molecules passing the channels are important characteristics. Loss of the septal proteins FraC, FraD and SepJ significantly reduces transfer of BCECF.

3.4 Summary

Several new fluorescent dyes were introduced in this chapter to study intercellular communication in *Anabaena* sp. PCC 7120, including molecules that are similar to physiologically-important molecules such as the sucrose analogue esculin and the glucose derivatives 2- and 6-NBDG but also a new fluorescein derivative that is highly negatively charged (Table 23). Confocal microscopy and FRAP experiments revealed cytoplasmic transfer via septal junction complexes as the main route of exchange for all tested molecules. This is in good agreement with earlier studies, showing cytoplasmic transfer of calcein and 5-CFDA in *Anabaena* sp. PCC 7120 (Mullineaux *et al.*, 2008; Merino-Puerto *et al.*, 2010; Mariscal *et al.*, 2011; Merino-Puerto *et al.*, 2011a; 2011b; Berendt *et al.*, 2012). However, it cannot be excluded at this stage that a small fraction of molecules diffuses additionally from cell to cell via the continuous periplasm (Mariscal *et al.*, 2007).

Little is known about the selectivity of septal junction complexes. The expansion of the range of molecular probes for intercellular communication described in this chapter, allows a first comparison. In the presence of combined nitrogen (BG11 medium), calcein and BCECF exhibited significantly different recovery rates than 5-CFDA, 2-NBDG and esculin (Table 21) suggesting that bigger and more negatively charged molecules diffuse slower between vegetative cells. Accordingly, charge and size can be considered as important properties of molecules passing septal junction complexes (Figure 27).

When cultures of *Anabaena* sp. PCC 7120 were deprived of combined nitrogen (BG11₀ medium), exchange of calcein increases significantly in comparison to conditions when combined nitrogen source abundant (Table 21). As no significant

3 Properties and pathways of transferred molecules

differences were observed between plus and minus combined nitrogen conditions for BCECF, 5-CFDA, 2-NBDG and esculin (Table 21) this result suggests that nitrogen step-down leads to a change of septal junction complexes, allowing bigger molecules to diffuse faster between vegetative cells in the absence of combined nitrogen than in its presence. Charge of the molecules does not influence transfer. Comparison of the recovery rates of the different molecules under minus N conditions revealed that the smallest molecule, esculin is exchanged fastest between vegetative cells (Table 21).

Table 21. Recovery rate constants for calcein, BCECF, 5-CFDA, 2-NBDG and esculin under plus (BG11) and minus N (BG11₀) conditions.

fluorophore (number of replicates)	R [s ⁻¹] (± s.d.)	
	BG11	BG11 ₀
calcein (74/31)	0.077 ± 0.037 ^{a*}	0.103 ± 0.030 ^{A*}
BCECF (48/14)	0.079 ± 0.050 ^a	0.095 ± 0.035 ^A
5-CFDA (98/32)	0.110 ± 0.055 ^b	0.096 ± 0.045 ^A
2-NBDG (23/26)	0.126 ± 0.083 ^{b,c}	0.100 ± 0.058 ^A
esculin (29/38)	0.137 ± 0.050 ^c	0.142 ± 0.046 ^B

Mean recovery rate constants (R) for filaments grown in the presence and absence of combined nitrogen. Different letters indicate statistically significant differences ($p \leq 0.05$) between R values under minus or plus N conditions. Significant differences for R values for a specific dye under different growth conditions are indicated by "*". ANOVA followed by Fisher LSD pair-wise comparison.

3 Properties and pathways of transferred molecules

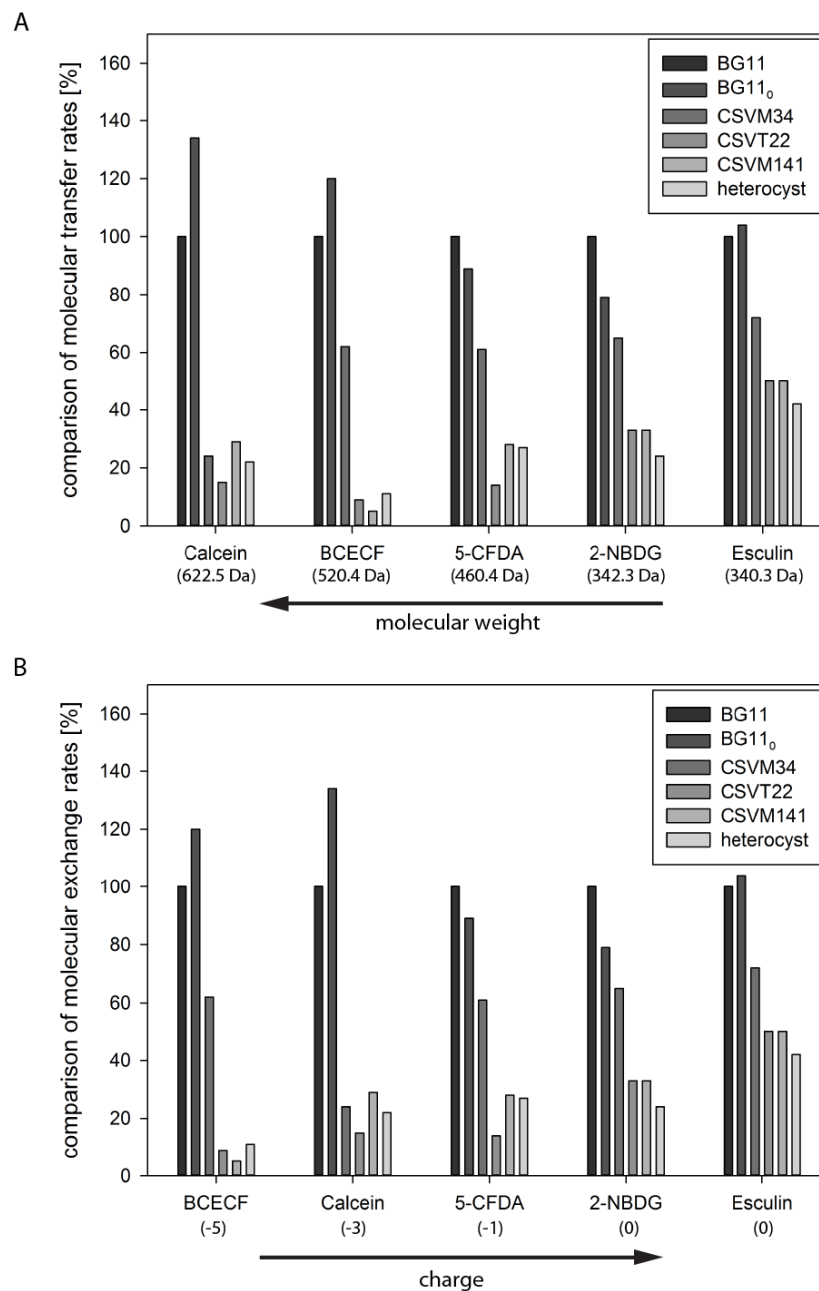


Figure 27. Comparison of molecular exchange in *Anabaena* sp. PCC 7120.

Influence of molecular weight (A) and charge (B) on transfer of fluorescent tracers. Graphs are based on R and E values presented in this work and by Mullineaux *et al.* (2008), Merino-Puerto *et al.* (2010; 2011a; 2011b) and Mariscal *et al.* (2011). The E value for 5-CFDA in *Anabaena* sp. PCC 7120 under nitrogen deprivation determined by Mariscal *et al.* (2011) and the E value for calcein in *Anabaena* sp. PCC 7120 under nitrogen deprivation determined by Mullineaux *et al.* (2008) were excluded as outliers.

3 Properties and pathways of transferred molecules

In *Anabaena* sp. PCC 7120 the septal proteins FraC, FraD and SepJ are important components mediating intercellular transfer of calcein and 5-CFDA (Mullineaux *et al.*, 2008; Mariscal *et al.*, 2011; Merino-Puerto *et al.*, 2011b). Furthermore, Merino-Puerto *et al.* (2011b) suggested the existence of a FraC/FraD-dependent intercellular exchange route that does not require SepJ. In order to investigate the importance of FraC, FraD and SepJ for the transfer of specific molecules further, the determined E and R values were compared with data previously published by Mullineaux *et al.* (2008); Merino-Puerto *et al.* (2010; 2011a; 2011b) and Mariscal *et al.* (2011). However, as the two parameters cannot be compared directly, a different approach was taken. Differences were determined by comparing the E and R values for each mutant strain to the value determined for the wild-type. Loss of SepJ (CSVM34) strongly reduces transfer of calcein (ca. 24 % of wild-type; Table 22) but transfer of BCECF, 5-CFDA, 2-NBDG and esculin to much less extent (ca. 61 - 72 %; Table 22), suggesting that SepJ is a key protein for transfer of bigger molecules independent of their charge. Loss of FraC and FraD (CSVT22) reduces transfer of all molecules dramatically with smaller and neutral molecules being less impaired in diffusion. Additional loss of SepJ (CSVM141) does not reduce transfer of molecules further. As deletion of *fraC* and *fraD* influences localisation of SepJ (Merino-Puerto *et al.*, 2010) it is likely that both mutants possess a similar septal composition.

Diffusion of all tested molecules into heterocysts was always much slower than between vegetative cells (Table 22). Differences were determined by comparing R values for heterocysts and for vegetative cells in the absence of combined nitrogen. Exchange of calcein, 5-CFDA and 2-NBDG remained at around 25 % while exchange of BCECF was slightly slower and exchange of esculin was slightly faster (Table 22). According to Giddings and Staehelin (1978) the number of septal

junctions is reduced between vegetative cells and heterocysts by 80 % which is in good agreement with the observed reduction of intercellular transfer.

Table 22. Comparison of molecular exchange in *Anabaena* sp. PCC 7120.

Differences in molecular exchange in mutant strains under different conditions are given in percentage. For vegetative cells exchange was compared to wild-type cells grown in BG11 medium. Exchange between vegetative cells and heterocysts was compared to wild-type vegetative cells after nitrogen step-down (BG11₀).

	vegetative cells					heterocyst
	wild-type					
	BG11	BG11 ₀	CSVM34	CSVT22	CSVM141	
calcein	100	134	24	15	29	22
BCECF	100	120	62	9	5	11
5-CFDA	100	89	61	14	28	27
2-NBDG	100	79	65	33	33	24
esculin	100	104	72	50	50	42

In summary, both charge and size influence molecular diffusion between cells in filaments of *Anabaena* sp. PCC 7120. The importance of these properties for transport has also been shown for eukaryotic plasmodesmata (Tucker, 1982) and gap junction channels (Elfgang *et al.*, 1995). However, the size exclusion limit for molecules in cyanobacteria remains to be determined. Analyses could reveal interesting insights whether small proteins diffuse through septal junctions.

Table 23. Predicted physico-chemical properties of fluorophores used to probe intercellular communication in *Anabaena* sp. PCC 7120.Properties are predicted for pH 7.0, corresponding to the pH in the cytoplasm of vegetative cells (Blanco-Rivero *et al.*, 2005).

property	calcein	BCECF	5-CFDA	2-NBDG	6-NBDG	esculin	sucrose
molecular mass (Da)	622.5	520.4	460.4	342.3	342.3	340.3	342.3
polar surface area (Å ²)	231.7	195.7	125.4	184.2	184.2	145.9	189.5
molecular surface area, solvent accessible (Å ²)	794.8	618.9	575.8	413.8	411.8	414.6	456.5
van der Waals volume (Å ³)	510.4	427.4	372.4	266.5	266.5	278.0	289.0
min. projection area (Å ²)	67.0	73.9	79.7	42.9	41.7	45.8	57.1
length perpendicular to min. projection area (Å)	19.7	18.0	13.3	14.4	14.7	14.8	11.5
max. projection area (Å ²)	139.1	133.4	111.2	78.6	84.1	90.1	78.0
length perpendicular to max. projection area (Å)	10.4	10.7	11.0	8.0	7.9	7.0	9.2
charge at pH 7.0 (with % abundances of different charged species)	-3 (48 %)	-5 (84 %)	-1 (100 %)	0 (100 %)	0 (100 %)	0 (93 %)	0 (100 %)
	-2 (25 %)	-4 (16 %)				-1 (7 %)	
	-4 (25 %)						
	-5 (2 %)						
diffusion coefficient in water at 25°C (10 ⁻⁵ cm ² s ⁻¹)*							0.52*

*CRC Handbook of Chemistry and Physics. 95th ed. CRC Press: Boca Raton, FL, 2014-2015.

4 Overexpression of *sepJ* in *Anabaena* sp. PCC 7120

Although it has been shown by deletion mutants that the septal protein SepJ is important for filament integrity, heterocyst formation (Flores *et al.*, 2007; Nayar *et al.*, 2007; Mariscal *et al.*, 2011) and intercellular transfer of fluorescent tracers such as calcein (Mullineaux *et al.*, 2008), 5-CFDA (Mariscal *et al.*, 2011), BCECF (chapter 3.3), esculin (chapter 3.1) and NBD-glucose derivatives (chapter 3.2) the exact function of the protein is still unknown. To reveal further insights into the role of SepJ for multicellularity in cyanobacteria mutants of *Anabaena* sp. PCC 7120 were generated that possess an increased level of *sepJ* expression. These mutants were analysed with respect to filament length, heterocyst spacing pattern and molecular transfer of calcein and 5-CFDA. Furthermore, the additional SepJ proteins in *Anabaena* sp. PCC 7120 were localised by confocal microscopy using a GFP-tagged version of SepJ.

4.1 Generation of mutants with increased *sepJ* expression in *Anabaena* sp. PCC 7120

To increase the level of *sepJ* expression in *Anabaena* sp. PCC 7120, various constructs with promoters of different strength were generated (

Figure 28). Constructs pCSDN1 and pCSDN2 possess C.K1 cassettes with a constitutive promoter upstream of *sepJ* that has been used in earlier studies to increase the level of transcription and expression in *Synechococcus elongatus* PCC 7942 (Espinosa *et al.*, 2010; Moronta-Barrios *et al.*, 2013). In order to avoid making observations caused by polar effects, both constructs were generated with the two

possible orientations of the C.K1 cassette upstream of the target gene, resulting in plasmids pCSDN1A and pCSDN2A with the C.K1 in the same orientation as *sepJ* and pCSDN1B and pCSDN2B with the C.K1 cassette in opposite orientation. While the pCSDN1A/B constructs were integrated into the chromosome of *Anabaena* sp. PCC 7120 by single recombination resulting in strains CSDN1A and CSDN1B respectively, vectors pCSDN2A/B were maintained as replicative plasmids in strains CSDN2A and CSDN2B that are derivatives of pCSAM200 (Ionescu *et al.*, 2010). These plasmids contain the pDU1 replicon from *Nostoc* sp. PCC 7524 that replicates in various cyanobacteria of different sections including *Anabaena* spp. and *Nostoc* spp. (Section IV; Schmetterer and Wolk, 1988), *Fischerella muscicola* PCC 7414 and *Chlorogloeopsis fritschii* PCC 6912 (Section V; Stucken *et al.*, 2012) and *Chroococcidiopsis* spp. (Section II; Billi *et al.*, 2001), and it has been shown for a similar plasmid to be present in *Anabaena* sp. PCC 7120 at approximately 17 copies per chromosome (Lee *et al.*, 2003). Accordingly, expression of *sepJ* would be at medium level. In a third approach, the *sepJ* gene was inserted downstream of the C.K3 cassette in plasmid pRL278 (Black *et al.*, 1993) and the resulting construct pCSDN3 integrated into the chromosome of *Anabaena* sp. PCC 7120 by single recombination. In the C.K3 cassette the strong constitutive promoter P_{psbA} from the chloroplast of *Amaranthus hybridus* (Hirschberg and McIntosh, 1983; Dzelzkalns *et al.*, 1984; Elhai and Wolk, 1988b) is present which has been shown to highly increase expression of genes in *Nostoc punctiforme* ATCC 29133 (Ekman *et al.*, 2013).

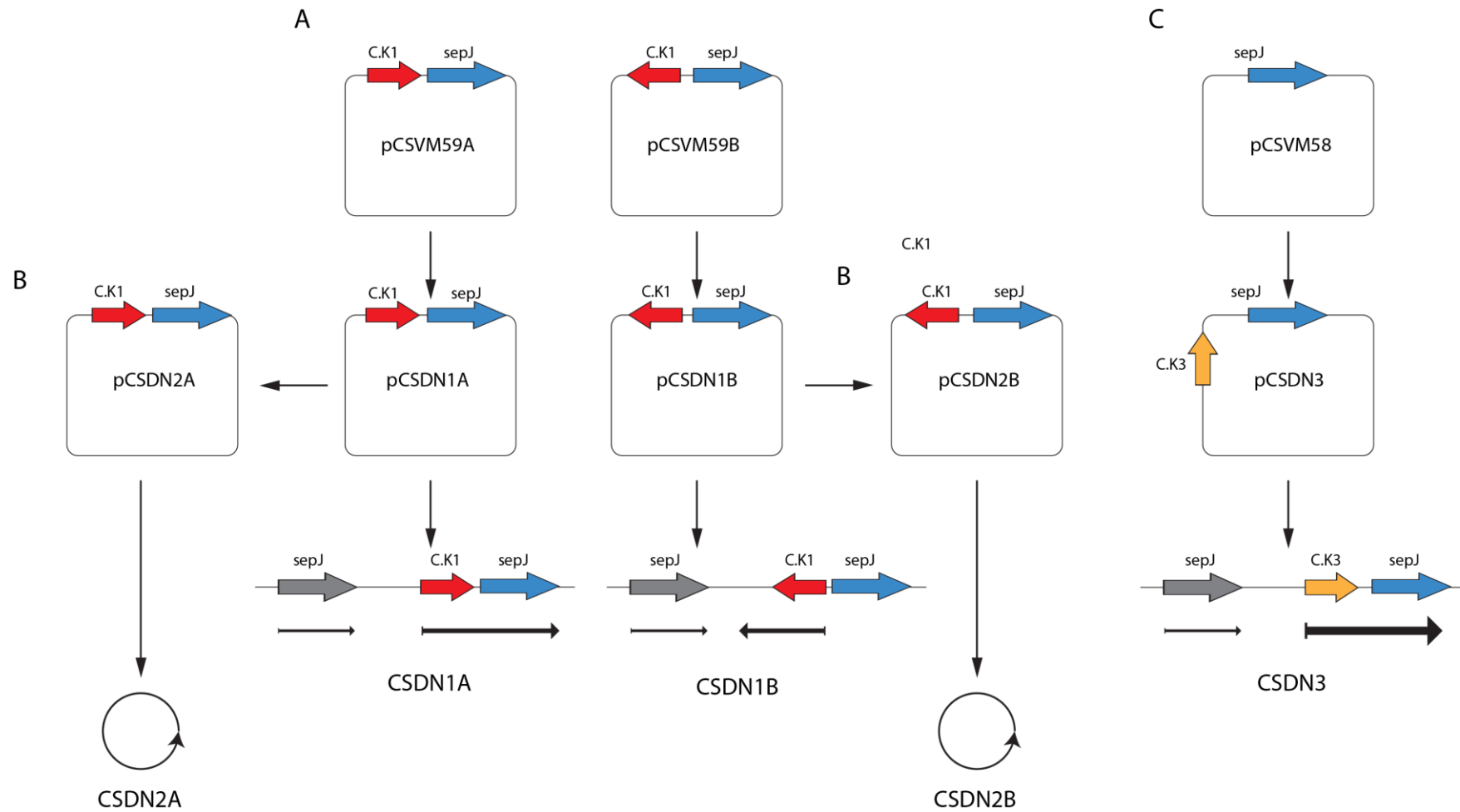


Figure 28. Construction of *sepJ* overexpression plasmids and genotypes of the corresponding strains.

Figure 28

DNA fragments of C.K1-*sepJ* were obtained from plasmids pCSVM59A and pCSVM59B depending on the orientation of the C.K1 cassette upstream of *sepJ*. While in plasmid pCVM59A the C.K1 cassette is orientated in the same direction as *sepJ*, plasmid pCSVM58B bears the C.K1 cassette in opposite orientation. C.K1-*sepJ* was extracted from plasmids pCSVM58A/B using the restriction sites XhoI and Sall and inserted into plasmid pCSV3 via Sall, resulting in constructs pCSDN1A/B (A). To generate plasmids pCSDN2A/B the C.K1-*sepJ* fragments were then restricted from pCSDN1A/B and inserted into the self-replicating vector pCSAM200 via EcoRI (B). The C.K3 based expression vector pCSDN3 was generated by inserting *sepJ* derived from pCSVM58 by Sall and XhoI digestion into the XhoI-restricted plasmid pRL278 (C). Constructs pCSDN1A, pCSDN1B and pCSDN3 were integrated into the chromosome by single recombination. The resulting genetic modifications are displayed, including the expected level of transcription, indicated by the thickness of the arrows below the genes. pCSDN2A and pCSDN2B are self-replicating plasmids that are maintained in *Anabaena* sp. PCC 7120.

All constructs were introduced into *Anabaena* sp. PCC 7120 by conjugation. To test whether the $\Delta sepJ$ phenotype can be complemented by plasmid pCSDN2A, the plasmid was transferred into the *sepJ* deletion mutant CSVM34, resulting in strain CSVM34-DN2A. Additionally, plasmid pCSDN2B was transferred into CSVM34 as a negative control, resulting in strain CSVM34-DN2B.

All mutants were restreaked for at least three times on BG11 plates supplemented with appropriate antibiotics. While mutants CSDN1A, CSDN1B, CSDN2A, CSDN2B, CSVM34-DN2A and CSVM34-DN2B could be successfully generated, the generation of mutant CSDN3 failed. It is likely that over-expression of *sepJ* or the resistance cassette gene became lethal for the cells. Thus, mutant CSDN3, which is expected to show the highest level of expression, is unable to survive.

To test the generated mutants for increased levels of SepJ protein, membranes were isolated and Western Blotting with an anti-SepJ antibody carried out (Mariscal *et al.*, 2011). Although earlier studies revealed that transcription and protein level could be increased by adding the C.K1 cassette with its constitutive promoter upstream of the target gene in *Synechococcus elongatus* PCC 7942 (Espinosa *et al.*, 2010; Moronta-Barrios *et al.*, 2013) a higher level of SepJ protein in the *Anabaena* sp. PCC 7120 mutant CSDN1A could not be detected (Figure 29). However, the level of SepJ protein in CSDN2A was approximately 4.3 times higher than in the wild-type (Figure 29). Hence, plasmid pCSDN2A is suitable to increase the level of gene expression in cells of *Anabaena* sp. PCC 7120, allowing study of the effects of higher levels of SepJ protein on multicellularity. However, it is also notable that the amount of SepJ in CSDN2B was approximately 2.3 times higher than in the wild-type (Figure 29).

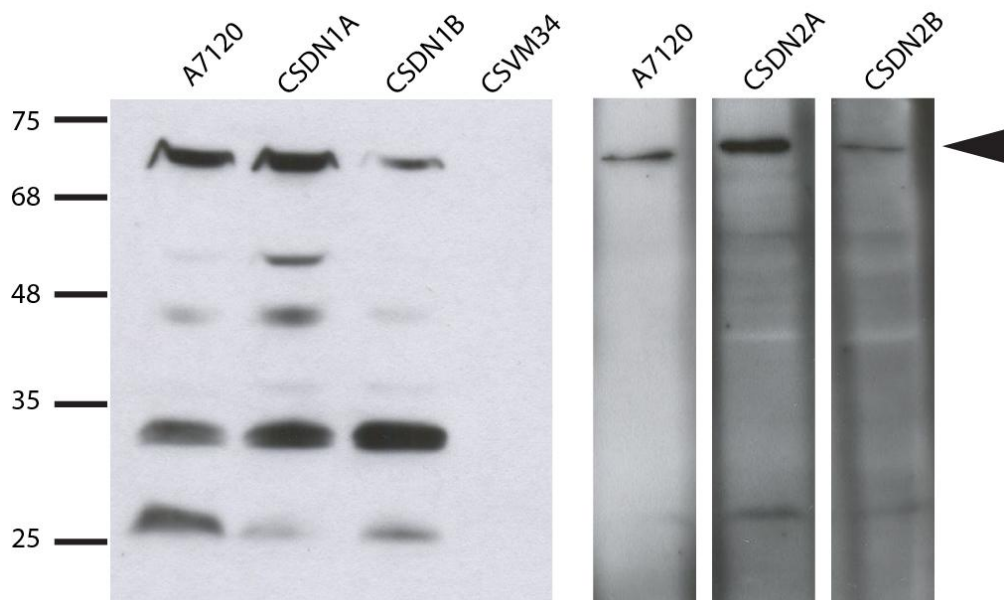


Figure 29. SepJ protein levels in *Anabaena* sp. PCC 7120 wild-type and overexpression strains.

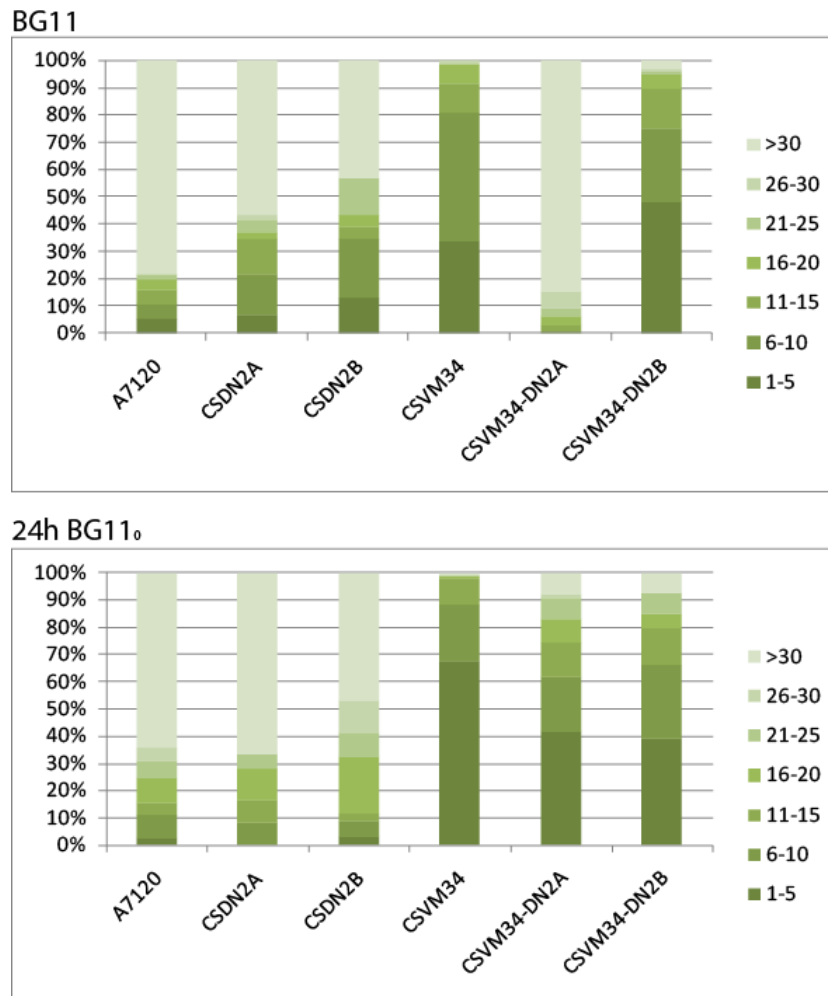
Figure 29. Western Blotting with an anti-SepJ antibody on isolated membranes. Same amount of protein from membrane fractions loaded. Molecular masses of a protein marker are displayed in kDa (left). The *sepJ* deletion mutant CSVM34 does not show any band. The black arrow indicates the position of SepJ on the gel of approximately 72 kDa. (Western blotting was performed by Vicente Mariscal.)

4.2 Influence of *sepJ* overexpression on filament length

It has been shown earlier for *Anabaena* sp. PCC 7120 that septal protein SepJ is important for filament integrity (Flores *et al.*, 2007; Nayar *et al.*, 2007; Mariscal *et al.*, 2011). Deletion of *sepJ* results in extensive filament fragmentation with an average filament length of about 7 cells in BG11 medium and approximately 2 cells following nitrogen depletion (Mariscal *et al.*, 2011). The filament fragmentation phenotype of CSVM34 was complemented by adding plasmid pCSDN2A. Strain CSVM34-DN2A reveals a similar filament length distribution as the wild-type and significantly longer filaments as CSVM34 when grown in presence of nitrate while strain CSVM34-DN2B does not show increased filament length (Figure 30). When grown in the absence of combined nitrogen CSVM34-DN2A shows stronger filament fragmentation than the wild-type but filaments remain initially longer than for the $\Delta sepJ$ mutant (Figure 30). However, filament fragmentation becomes obvious after prolonged incubation in BG11₀ medium, suggesting that the level of intracellular SepJ protein is not sufficient to maintain filament integrity. It remains unknown whether the C.K1 promoter leads to overexpression of *sepJ* under nitrogen limiting conditions or whether plasmid loss occurs during the prolonged incubation. Additional studies using either Western or Northern blotting are required to answer this question.

4 Overexpression of *sepJ*

Further studies using CSDN2A, CSDN2B and *Anabaena* sp. PCC 7120 wild-type revealed no obvious influence of SepJ on filament length. Filaments of all three strains exhibit similar filament lengths under all tested conditions. In conclusion, plasmid pCSDN2A is suitable to complement the phenotype of mutant CSV34 by increasing filament length but enhanced expression of *sepJ* in *Anabaena* sp. PCC 7120 does not alter filament length.



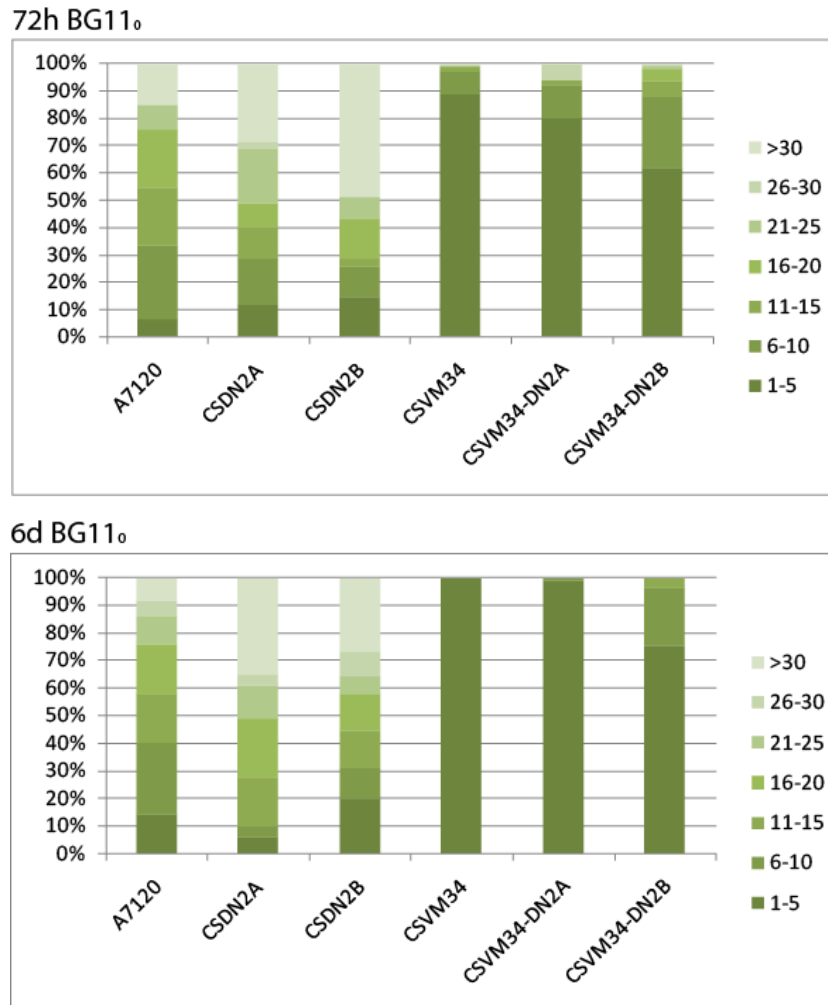


Figure 30. Influence of *sepJ* overexpression on filament length in *Anabaena* sp. PCC 7120.

Filament length in the presence of nitrate (BG11) and at different time points after nitrogen step-down (BG11₀), Colour intensities indicate the number of cells per filament. Images were taken with a light microscope and analysed manually. 30 to 100 filaments were counted per condition and strain.

4.3 Influence of *sepJ* overexpression on diazotrophic growth and heterocyst spacing pattern

Inactivation of *sepJ* in *Anabaena* sp. PCC 7120 results not only in intensive filament fragmentation but also in impaired heterocyst formation and consistently in a failure of the organism to grow diazotrophically (Flores *et al.*, 2007; Nayar *et al.*, 2007;

Mariscal *et al.*, 2011). When introducing plasmid pCSDN2A into CSV34 the strain is able to grow in the absence of combined nitrogen by differentiating heterocysts in a regular spacing pattern (Figure 31). These results are in good agreement with our earlier observation that filament integrity can be restored in CSV34-DN2A. Thus, plasmid pCSDN2A is capable of complementing the phenotype of CSV34 by expression of *sepJ* in BG11 and the initial phase after nitrogen step-down.

Interestingly, when the level of SepJ protein is further increased an altered heterocyst spacing pattern was observed with more vegetative cells between two heterocysts. In CSDN2A the number of vegetative cells between two heterocysts increases to 15.95 ± 5.90 after incubation for 18 h in BG11₀ and after 96 h to 18.69 ± 10.06 while in filaments of *Anabaena* sp. PCC 7120 heterocysts are separated by 10.64 ± 3.63 cells (18 h) and 14.33 ± 6.51 cells (96 h) respectively (data were kindly provided by Vicente Mariscal).

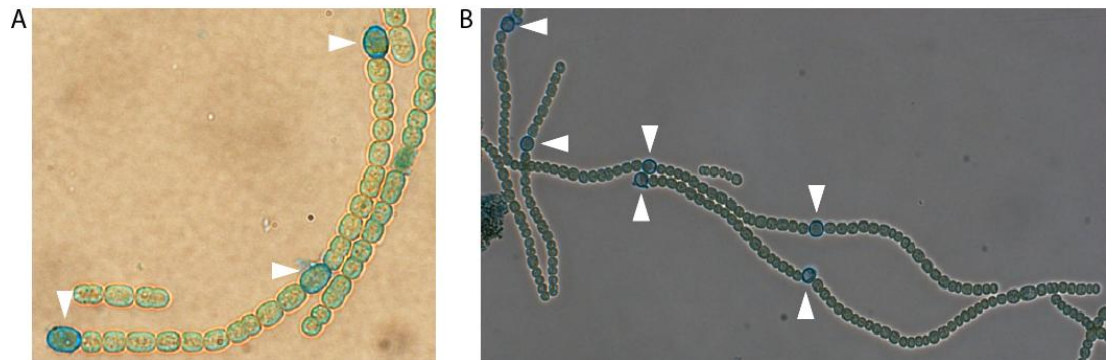


Figure 31. Heterocyst formation in CSV34-DN2A (A) and CSDN2A (B).

Cells were visualised with a conventional light microscope. Heterocysts were labelled with Alcian Blue and are highlighted with white arrows.

4.3.1 Influence of *sepJ* overexpression on intercellular communication

In order to test whether the increase of SepJ molecules in the cell could generate the altered heterocyst spacing pattern by influencing molecular exchange between cells, FRAP experiments with the fluorescent tracers calcein and 5-CFDA were performed. Calcein and 5-CFDA are taken up into the cytoplasm of the filaments, enabling quantitation of the kinetics of the diffusion between adjacent cells by bleaching out the fluorescence of a specific cell, following its recovery over time and determining the recovery rate constant R as previously described by Merino-Puerto *et al.* (2011). No significant difference for molecular exchange of both fluorophores between vegetative cells in *Anabaena* sp. PCC 7120 wild-type and strain CSDN2A was observed (Table 24). The R values remain similar for adjacent vegetative cells in the presence and absence of nitrate as nitrogen source. However, exchange of calcein is significantly faster between heterocysts and vegetative cells 48 h after nitrogen depletion while exchange for 5-CFDA remains similar (Table 24).

Considering that SepJ is a key protein for the molecular transfer of calcein in *Anabaena* sp. PCC 7120 (Mullineaux *et al.*, 2008; Mariscal *et al.*, 2011), it is notable that additional SepJ molecules do not increase the rate for molecular transfer between vegetative cells. Although Western Blot analyses revealed an increased level of SepJ protein in membranes of CSDN2A (Figure 29) it is possible that the additional proteins are not localised at the septa of neighbouring cells and thus, do not contribute to intercellular transfer. In order to determine the specific localisation of additional SepJ molecules, a mutant that overexpresses a fluorescent-labelled *sepJ* variant was generated.

Table 24. Kinetics of calcein and 5-CFDA exchange from FRAP measurements on *Anabaena* filaments overexpressing *sepJ*.

Measurement (number of replicates)	Calcein		5-CFDA	
	R [s ⁻¹] (± s.d.)	E [s ⁻¹] (± s.d.)	R [s ⁻¹] (± s.d.)	E [s ⁻¹] (± s.d.)
1. vegetative cells in presence of nitrate				
a) <i>Anabaena</i> sp. PCC 7120 (35/41)	0.083 ± 0.032		0.133 ± 0.049	
b) CSDN2A (34/18)	0.075 ± 0.031		0.110 ± 0.052	
c) CSAM137 (16/15)	0.097 ± 0.043		0.117 ± 0.050	
d) CSDN11 (15/20)	0.099 ± 0.028		0.116 ± 0.056	
2. vegetative cells 48 h after nitrogen deprivation				
a) <i>Anabaena</i> sp. PCC 7120 (21/19)	0.102 ± 0.025		0.101 ± 0.052	
b) CSDN2A (24/18)	0.109 ± 0.039		0.094 ± 0.033	
3. heterocysts 48 h after nitrogen deprivation				
a) <i>Anabaena</i> sp. PCC 7120 (15/5)	0.022 ± 0.013	0.022 ± 0.013	0.027 ± 0.012	0.027 ± 0.012
b) CSDN2A (10/10)	0.038 ± 0.021	0.038 ± 0.021	0.030 ± 0.024	0.030 ± 0.024

Mean exponential recovery rate constants (R) and exchange coefficients (E) for filaments grown ± combined nitrogen. R values were standardised by dividing by 2 for cells with 2 connecting junctions. Student's t-test show R is significantly different for calcein between (3a) and (3b) ($p = 0.021$). No significant differences were detected for calcein and 5-CFDA between (1a) and (1b); (1c) and (1d); (2a) and (2b); and for 5-CFDA between (3a) and (3b).

4.4 Influence of *sepJ* overexpression on protein localisation and molecular exchange of calcein and 5-CFDA

In order to determine the specific localisation of additional SepJ molecules, *sepJ* was fused to *gfp* and the expression level increased by using the strong constitutive promoter P_{psbA} (Figure 32).

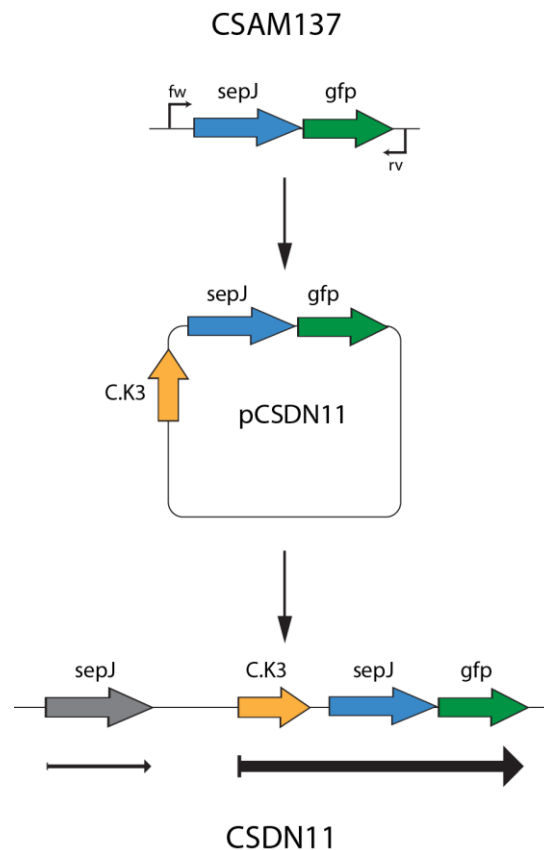


Figure 32. Construction of the *sepJ-gfp* overexpression mutant CSDN11.

The DNA fragment *sepJ-gfp* was amplified from genomic DNA of strain CSAM137 (Flores *et al.*, 2007) by PCR using primer alr2338_7 (fw) and pRL500_1 (rv) and directly cloned into vector pSPARK[®], resulting in plasmid pCSDN10. Correctness of the inserted sequence was verified by sequencing. pCSDN10 contains additional restriction sites that were present in the multiple cloning site of the pSpark[®] vector. *sepJ-gfp* was cut from pCSDN10 using the restriction endonuclease SalI and inserted into the XhoI-restricted pRL278 plasmid. The resulting plasmid pCSDN11 bears the C.K3 cassette upstream of *sepJ-gfp* in the same orientation as the target gene.

Construct pCSDN11 was transferred into *Anabaena* sp. PCC 7120 by conjugation using triparental mating (Elhai and Wolk, 1988a). During this process the *E. coli* helper strain carrying the conjugative plasmid pRL443 (Elhai *et al.*, 1997) and the *E. coli* donor strain carrying the mobilisable plasmid pCSDN11 and the methylases encoding plasmid pRL663 (Elhai *et al.*, 1997) are mixed with the recipient strain *Anabaena* sp. PCC 7120. When checking the cultures at an early stage of the segregation process fluorescent *E. coli* cells were observed by confocal microscopy surrounding *Anabaena* sp. PCC 7120 filaments (Figure 33). The signal was specific for GFP indicating that expression of *sepJ-gfp* in *E. coli* cells is possible by using plasmid pCSDN11. However, the fluorescence signal was present throughout the entire cytoplasm of the cells suggesting that either SepJ-GFP cannot be localised in the membrane of *E. coli* or GFP is cleaved off SepJ resulting in free GFP in the cytoplasm. This question was approached by Western blotting using an anti-GFP antibody on cells of the *E. coli* strain carrying pCSDN11 and the native *E. coli* strain as a control. A specific band for free GFP with a molecular mass of approximately 29 kDa was detected (data not shown) suggesting that GFP is cleaved off SepJ when the fused gene is expressed in *E. coli*.

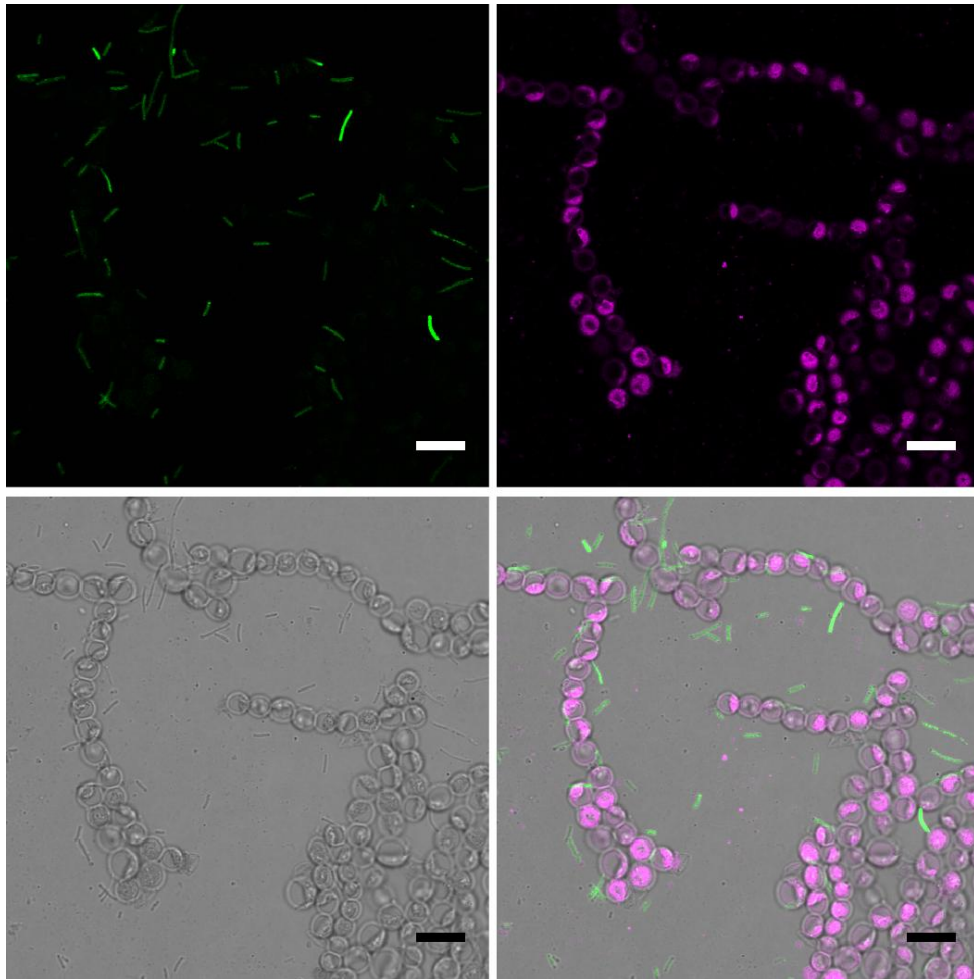


Figure 33. Fluorescent *E. coli* cells surrounding *Anabaena* sp. PCC 7120 during conjugation.

Images show GFP fluorescence of *E. coli* cells bearing plasmid pCSDN11 (green), autofluorescence of *Anabaena* sp. PCC 7120 (magenta), a bright field view (grey) and a merged image of all three channels. Scale bars, 10 μ m.

After several restreaks strain CSDN11 was visualised by confocal microscopy. Images revealed that additional SepJ proteins are localised in the membranes at the septa of neighbouring cells similar to the localisation of the protein under naturally occurring expression levels (Figure 34). However, additional SepJ molecules are not localised as distinctly as observed in strain CSAM137 (SepJ-GFP). While in CSAM137 SepJ is localised in distinct spots (Figure 34B), SepJ is spread over the full length of the septum in CSDN11 (Figure 34A). The difference in SepJ

distribution was further studied by plotting fluorescence intensity against the position of a defined rectangular region of interest at the septum and fitting a Gaussian model to the data. A representative example is displayed in Figure 34C. Based on the fit the full width at half-maximum (FWHM) was determined and compared between strains CSDN11 and CSAM137. The average values for the FWHM in both strains were significantly different as indicated by a Student's t-test. In CSDN11 SepJ is around two times more widely distributed than in CSAM137 with a FWHM value of $1.22 \pm 0.13 \mu\text{m}$ in comparison to $0.64 \pm 0.12 \mu\text{m}$ for CSAM137. The number of considered septa was 36. In order to determine the effect of the imaging system and the used settings on the spread of the recorded fluorescence signal observed for SepJ-GFP filaments of *Anabaena* sp. PCC 7120 wild-type were stained with the fluorescent dye FM1-43FX. According to Schneider *et al.* (2007) FM1-43FX highlights the cytoplasmic membrane in cyanobacteria and thus defines a distinct distance of approximately 45 nm in *Anabaena* sp. PCC 7120 (Nicolaisen *et al.*, 2009a). The fluorescence signal detected by confocal microscopy using the same settings as for the visualisation of SepJ-GFP revealed an average FWHM value of $0.32 \pm 0.06 \mu\text{m}$ for 36 measurements. To correct the estimate of SepJ-GFP distribution, the point spread value was subtracted off the FWHM for CSAM137 and CSDN11, resulting in a FWHM of $0.90 \pm 0.14 \mu\text{m}$ for CSDN11 and $0.32 \pm 0.13 \mu\text{m}$ for CSAM137.

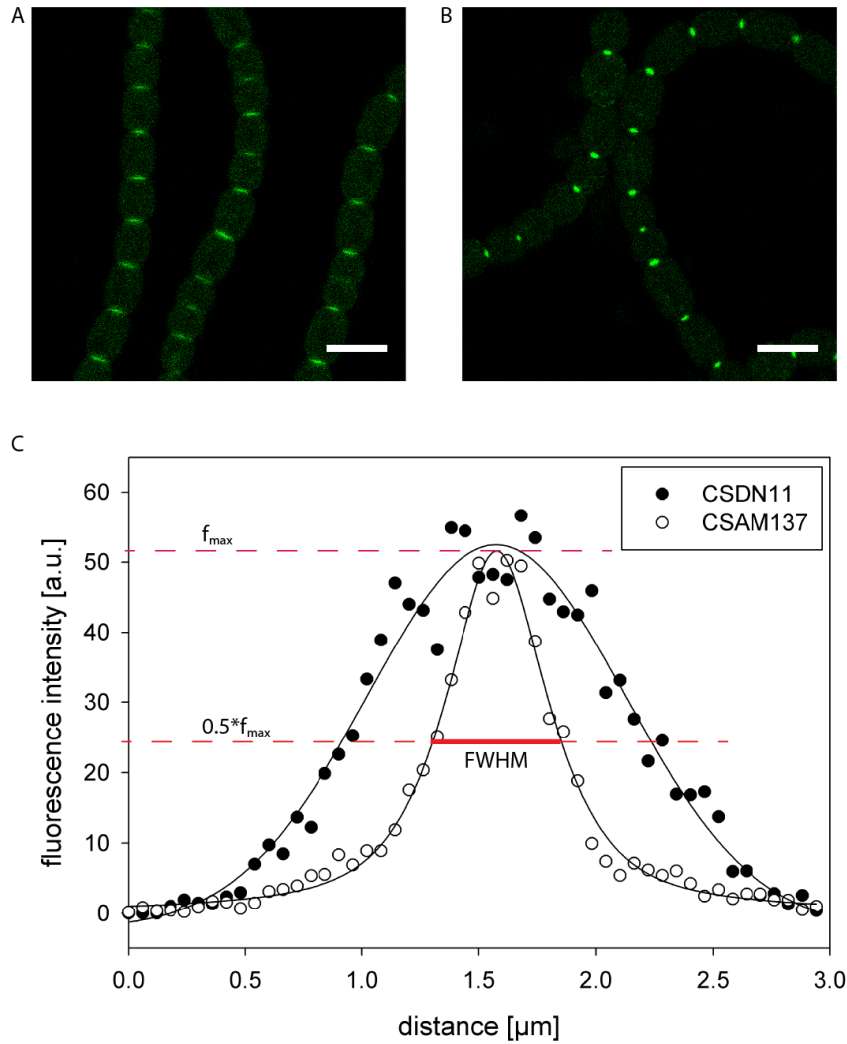


Figure 34. Localisation of SepJ-GFP in *Anabaena* sp. PCC 7120 strains CSDN11 and CSAM137.

SepJ-GFP fluorescence is shown in green for CSDN11 (A) and CSAM137 (B). Scale bars, 5 μm . The difference in distribution was analysed by plotting the fluorescence intensity against the position of the signal at the septum and fitting a Gaussian model to the data for which an example is shown in panel (C). The Gaussian model equation is given by $f(x) = y_o + a * \exp(-0.5 * (\frac{x-x_o}{b})^2)$. The definition of the full width at half maximum (FWHM) is shown for CSAM137 with f_{max} being the maximal fluorescence intensity. Following the Gaussian model the FWHM is defined by $2 \sqrt{2 \ln 2} b$.

Whether the additional SepJ-GFP proteins influence intercellular communication was investigated by FRAP experiments using calcein and 5-CFDA as fluorophores. No difference in molecular transfer was observed for both molecules between vegetative cells in strains CSAM137 and CSDN11 (Table 24) supporting the earlier results that additional SepJ molecules do not alter molecular diffusion between vegetative cells.

To test whether the generated construct pCSDN11 is capable of complementing the phenotype observed for *sepJ* deletion mutants, the plasmid was transferred to CSVM34 ($\Delta sepJ$) and CSVM141 ($\Delta sepJ \Delta fraC \Delta fraD$). Strain CSVM34-DN11 shows long filaments with SepJ being localised in distinct spots at the septum of neighbouring cells as observed in CSAM137 (Figure 35A) indicating the suitability of the construct for complementation. When *sepJ-gfp* is expressed in strain CSVM141 a slightly altered localisation was observed. GFP fluorescence was less focussed, being more spread at the septum rather than forming a distinct spot (Figure 35B). This is in good agreement with the study by Merino-Puerto *et al.* (2010), showing the influence of *fraC* and *fraD* on the localisation of SepJ-GFP. The loss of each protein caused a less focussed localisation of SepJ-GFP similar to what was observed for strain CSVM141-DN11. To conclude, plasmid pCSDN11 is suitable for expressing *sepJ-gfp*. Its product is localised in the ‘correct’ position at the septa.

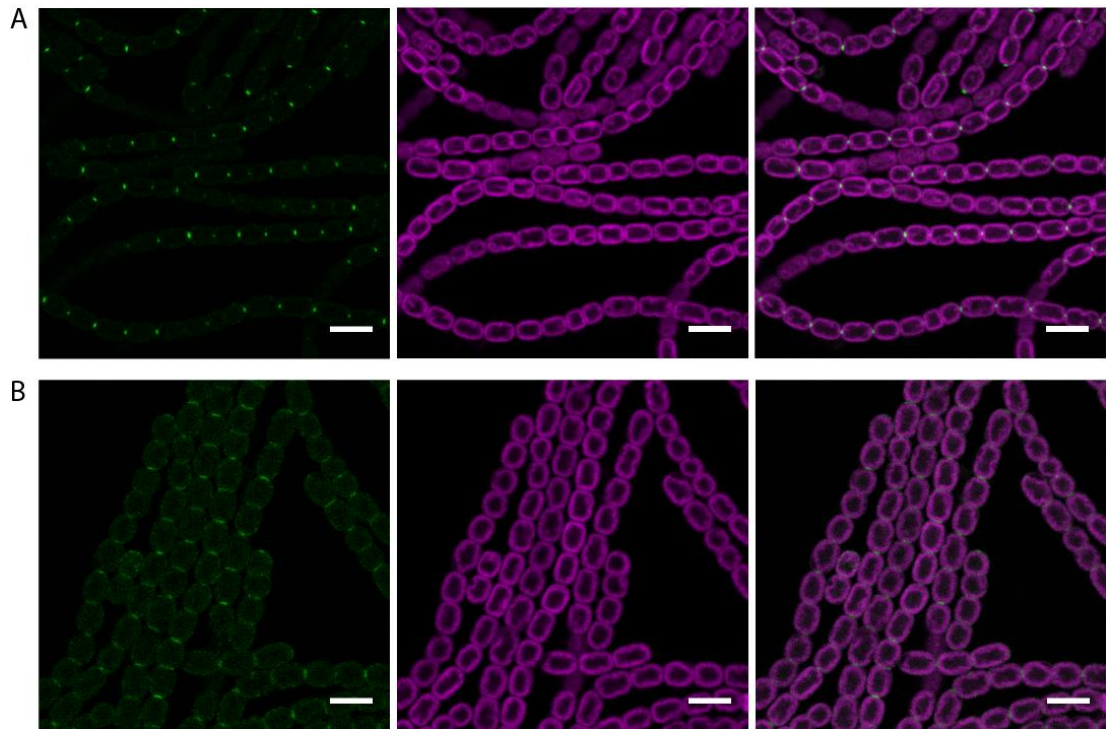


Figure 35. Localisation of SepJ-GFP in CSVM34-DN11 (A) and CSVM141-DN11 (B).

Images show GFP fluorescence (green), autofluorescence (magenta) and an overlay of both channels. Scale bars, 5 μm.

When cultures of *Anabaena* sp. PCC 7120 are deprived of combined nitrogen vegetative cells differentiate into heterocysts by undergoing extensive biochemical and morphological changes (Maldener and Muro-Pastor, 2010). To enable nitrogenase activity in the heterocysts the oxygen concentration is strongly reduced by increasing the activity of oxidases, synthesising additional layers around the cell as gas-diffusion barriers (known as envelope) and diminishing the entry of O₂ into heterocysts by reducing the area of cell-cell connection between vegetative cells and heterocysts to a small pore (Walsby, 2007). These changes require extensive modifications of the septa including proteins such as SepJ. Confocal microscopy revealed that SepJ-GFP in strain CSDN11 is localised in distinct spots at the septa of heterocyst and vegetative cells with some molecules spreading into the neck region

of the heterocyst 48 h after nitrogen step-down while SepJ-GFP proteins remain as widely distributed at the septa of adjacent vegetative cells as observed in the presence of combined nitrogen (Figure 36B). A similar localisation for SepJ-GFP at the septa of heterocysts and vegetative cells was observed in CSAM137 (Figure 36A; Flores *et al.* (2007)) suggesting that additional SepJ molecules undergo the same remodelling process.

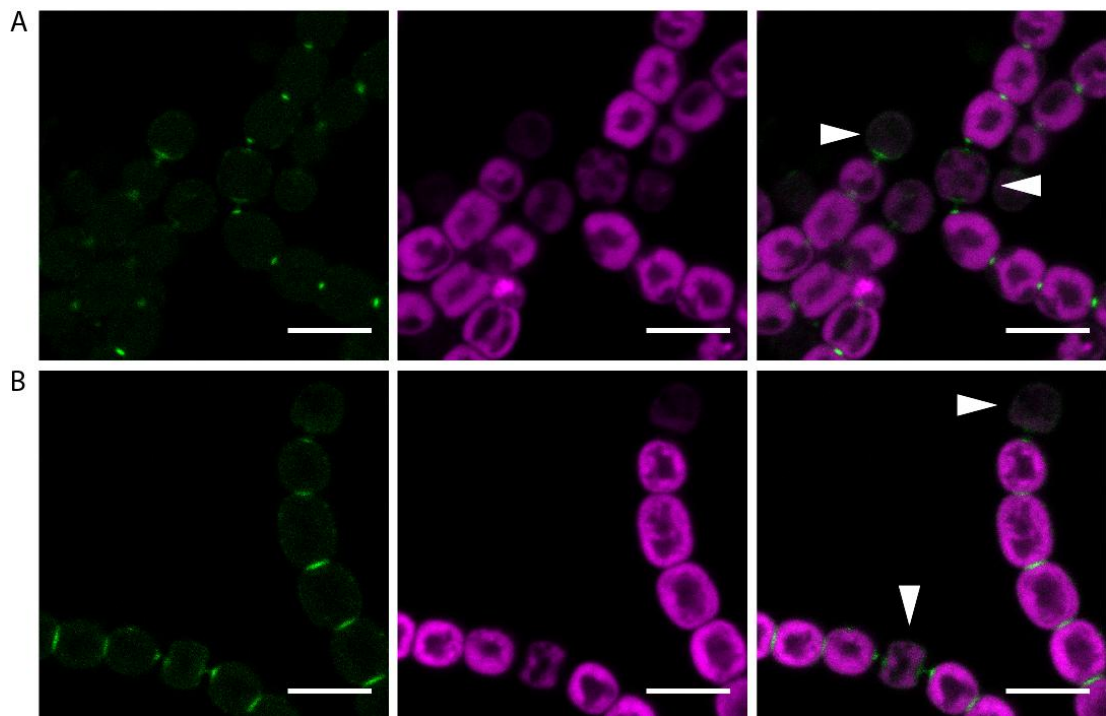


Figure 36. Localisation of SepJ-GFP in *Anabaena* sp. PCC 7120 strains CSAM137 (A) and CSDN11 (B) 48 h after nitrogen step down.

Images show GFP fluorescence (green), autofluorescence (magenta) and a merged image. Heterocysts are highlighted by white arrows. Scale bars, 5 μ m.

4.5 Conclusion

The data presented in this chapter reveal that overexpression of *sepJ* in *Anabaena* sp. PCC 7120 can be achieved by using the self-replicating plasmid pCSDN2A. When expressed in the background of the *sepJ* deletion mutant CSVM34 the generated

strain CSVM34-DN2A is capable of growing in long filaments that show cell differentiation under nitrogen depletion. Thus, pCSDN2A is suitable to complement the phenotype observed for CSVM34 (Mariscal *et al.*, 2011). When pCSDN2A is introduced in the *Anabaena* sp. PCC 7120 wild-type, the heterocyst spacing pattern is altered with more vegetative cells separating two heterocysts. As earlier studies could show that SepJ is important for the transfer of molecules between cells such as calcein (Mullineaux *et al.*, 2008) and 5-CFDA (Mariscal *et al.*, 2011), it is likely that additional SepJ molecules might increase diffusion of these molecules between neighbouring cells. However, no influence on the transfer of calcein or 5-CFDA was observed between vegetative cells, suggesting that the additional SepJ molecules might not contribute to the formation of septal junction complexes or nanopores. It remains to be investigated whether the number of nanopores in CSDN2A remains similar to that found in the wild-type. Alternatively, SepJ might change cell-cell adhesion. Localisation studies using a GFP-tagged SepJ fusion protein indicate that additional SepJ molecules are not as focussed at the septa of neighbouring vegetative cells as observed for a strain showing the natural expression level. Transmission electron microscopy experiments could reveal further insights into the influence of SepJ on the organisation of the septum. Further studies could also involve overexpression of the septal proteins FraC and FraD which have been shown to be important for filament integrity, intercellular communication and the proper localisation of SepJ in *Anabaena* sp. PCC 7120 (Merino-Puerto *et al.*, 2010; 2011b). An increased level of FraC and FraD proteins might accelerate molecular transfer.

However, it needs to be pointed out that additional SepJ molecules increase the rate of calcein exchange between heterocysts and vegetative cells, suggesting that the altered heterocyst spacing pattern could be a result of an enhanced rate of molecular

diffusion between heterocysts and vegetative cells. It has been shown by Yoon and Golden (1998) that the product of the *patS* gene is a main regulator for establishing the regular heterocyst spacing pattern in *Anabaena* sp. PCC 7120. Inactivation of *patS* results in formation of heterocysts in the presence of combined nitrogen and in the formation of multiple contiguous heterocysts (MCH) under nitrogen deprivation (Yoon and Golden, 1998), whereas overexpression of the gene suppresses heterocyst formation (Liu and Golden, 2002) presumably by interacting with HetR (Huang *et al.*, 2004; Risser and Callahan, 2009; Feldmann *et al.*, 2011; Higa *et al.*, 2012). It is likely that an enhanced diffusion of PatS occurs in CSDN2A which could result in a further diffusion of the peptide along the filament than in the wild-type and hitherto in a change of the heterocyst spacing pattern. However, this is just speculation at this stage and needs further investigation.

5 Regulation, redistribution and remodelling of intercellular communication in *Anabaena* sp. PCC 7120 after filament fragmentation

Filament fragmentation is a characteristic feature of all filamentous cyanobacteria that are associated with heterocyst formation and reproduction by hormogonia (Rippka *et al.*, 1979; Golubić *et al.*, 1996). Both processes are one of the few known developmental ‘dead ends’ among prokaryotes (Meeks *et al.*, 2002). While hormogonia formation mostly occurs by randomly localised dead cells that have been termed necridia (Kohl, 1903; Lamont, 1969; Rippka *et al.*, 1979) heterocyst differentiation follows a regular spacing pattern in most cyanobacteria such as *Anabaena* spp. (Wilcox *et al.*, 1973). As mature heterocysts are unable to divide, the filament fragments when these cells die (Meeks *et al.*, 2002). Accordingly, the death rate of cells is highest under nitrogen depletion conditions when heterocysts are abundant (Lee and Rhee, 1997). It has been suggested that filament fragmentation during nitrogen fixation might be unavoidable but could improve the efficiency of this process by forming dense mats where oxygen and nutrients could be more effectively managed (Fay, 1992; Bauer *et al.*, 1995). There are also other factors known that influence filament length. Adverse growth conditions such as long-term sulphate starvation usually reduce filament length and it has been proposed that this process might be a genetically programmed response in order to allow dispersal to favourable growth conditions (Bauer *et al.*, 1995). The presence of programmed cell death in *Anabaena* spp. has been strongly supported by later studies (Lee and Rhee, 1999; Ning *et al.*, 2002). However, it remained unknown how filament viability is maintained during the fragmentation process which exposes the cytoplasmic

5 Regulation, redistribution and remodelling of intercellular communication channels linking adjacent cells (see e.g. Giddings and Staehelin, 1978; Mullineaux *et al.*, 2008; Lehner *et al.*, 2013; Omairi-Nasser *et al.*, 2014). In the following part of this chapter the influence of filament fragmentation on intercellular communication is investigated by subjecting filaments of *Anabaena* sp. PCC 7120 to sonication and comparing the data to fragmentation occurring in old cultures.

5.1 Filament fragmentation by sonication and its influence on cell viability

In the presence of combined nitrogen *Anabaena* sp. PCC 7120 forms long filaments that can be composed of several hundreds of cells. In order to reduce filament length filaments of *Anabaena* sp. PCC 7120 were subjected to sonication, a method routinely used during the generation of mutants of *Anabaena* spp. (e.g. Mannan *et al.*, 1991; Wu *et al.*, 2007). To test whether this method is suitable for reducing filament length but also for maintaining cell viability filaments of *Anabaena* sp. PCC 7120 were fragmented by mild sonication; growth of the culture monitored over 24 h by confocal microscopy. The results indicate that mild sonication reduces filament length significantly with nearly all cells remaining alive and continuing to divide (Figure 37). Even unicellular cells start forming short filaments after 24 h of incubation under optimal growth conditions (Figure 37). Thus, sonication is a suitable method for filament fragmentation in *Anabaena* sp. PCC 7120 without influencing cell viability negatively.

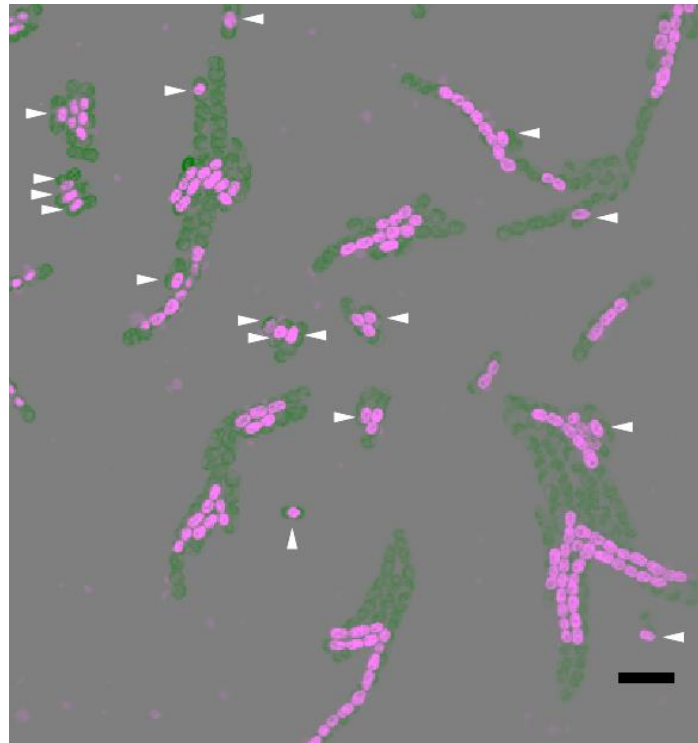


Figure 37. Growth of *Anabaena* sp. PCC 7120 after fragmentation.

The image shows an overlay of the autofluorescence shortly after fragmentation (magenta) and 24 h after incubation under optimal growth conditions (green). Note that even unicellular cells survive the fragmentation process and start dividing (white arrows). Scale bar, 15 μ m.

5.2 Influence of filament fragmentation on molecular exchange of 5-CFDA

In order to survive the fragmentation process it appears logical that efflux of molecules through the exposed channels at the new terminus of the filament needs to be prevented. However, a final proof has been lacking so far. Cytoplasmic transfer of molecules between neighbouring cells can be visualised by loading a fluorescent tracer into the cytoplasm of the filament, bleaching out the fluorescence of a single cell and monitoring its recovery over time. This method is known as FRAP and has been established for filamentous cyanobacteria by Mullineaux *et al.* (2008) to

5 Regulation, redistribution and remodelling of intercellular communication quantitate molecular exchange. Although several new fluorophores have been introduced for FRAP experiments within this work (see chapter 3) the best studied tracers are the fluorescein derivatives calcein and 5-CFDA (Mullineaux *et al.*, 2008; Merino-Puerto *et al.*, 2010; Lehner *et al.*, 2011; Mariscal *et al.*, 2011; Merino-Puerto *et al.*, 2011b; Berendt *et al.*, 2012; Nürnberg *et al.*, 2014). As 5-CFDA is slightly smaller than calcein, exhibiting a molecular mass of 460.4 Da in comparison to the 622.5 Da of calcein the molecule is more likely to leak into the surrounding medium if the channels stay open after filament breakage. Filaments of *Anabaena* sp. PCC 7120 were labelled with 5-CFDA, fragmented by sonication and visualised by confocal microscopy. These results indicate that short filaments remain fluorescent after fragmentation (Figure 38), supporting the hypothesis that efflux of molecules is prevented after the fragmentation event by channel closure. However, to be certain about the position of the filament breakage and accordingly to clarify whether the visualised filament is a fragmented one or just a short filament in general, a different approach was taken, based on the localisation of SepJ.

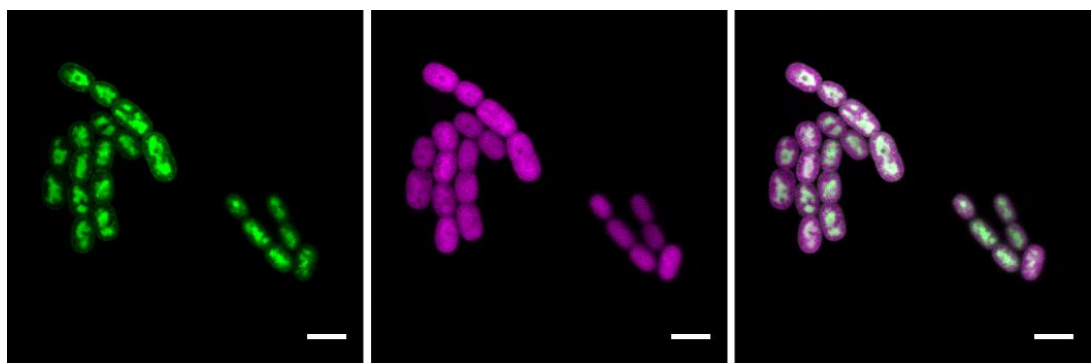


Figure 38. 5-CFDA labelled filaments of *Anabaena* sp. PCC 7120 after fragmentation by sonication.

Images show 5-CFDA fluorescence (green), autofluorescence (magenta) and an overlay of both channels. After filament fragmentation the dye remains in the cytoplasm indicating that channels are closed. Scale bars, 5 μ m.

5.3 Co-localisation of SepJ and 5-CFDA in *Anabaena* sp. PCC 7120

SepJ is localised in distinct spots at the septum of two adjacent cells but is not present at the terminus of a filament in *Anabaena* sp. PCC 7120 (Flores *et al.*, 2007). When filament breakage is induced in a strain of *Anabaena* sp. PCC 7120 that expresses a GFP-tagged version of *sepJ* (CSAM137; Flores *et al.* (2007)) the new terminus is highlighted by the presence of the distinct SepJ-GFP spot that is normally found in between two neighbouring cells (Figure 41). Thus, localisation of SepJ can be used as an indicator to determine whether a short filament was formed by fragmentation using sonication or whether it was formed naturally. However, GFP and 5-CFDA possess similar emission and excitation spectra which prevent the co-localisation of both fluorophores simultaneously in the same filaments. To overcome this difficulty an *Anabaena* sp. PCC 7120 mutant was generated that possesses an mTurquoise2-labelled SepJ protein. The fluorescent protein mTurquoise2 is an improved cyan variant of GFP from *Aequorea victoria* that has recently been designed by Goedhart *et al.* (2012). It exhibits high photostability, fast maturation and one of the highest quantum yield measured for a monomeric fluorescent protein making it ideal for localisation studies.

mTurquoise2 was amplified from plasmid pmTurquoise2-C1 (Goedhart *et al.*, 2012) by PCR using primer fw_mTq2_EcoRV and rv_mTq2 which generates an additional EcoRV restriction site upstream of *mTurquoise2*. The resulting DNA fragment was introduced into the multiple cloning site of the pGEM[®]-T Easy vector (Promega), resulting in construct pCSDN27. The correctness of the sequence of *mTurquoise2* was verified by sequencing. *mTurquoise2* was then introduced into pCSDN24 via EcoRV and PstI, generating plasmid pCSDN28. Plasmid pCSDN24 encodes a SepJ-CFP

5 Regulation, redistribution and remodelling of intercellular communication variant. The construct was generated by exchanging the *eyfp* gene downstream of *sepJ* from plasmid pCSDN7 (see below) by *cfp* from plasmid pCSV10 (Victoria Merino-Puerto, unpublished) using restriction sites EcoRV and ApaI. Construct pCSDN7 (*sepJ-eyfp*) was generated by amplifying *eyfp* from plasmid pSKS3-cph2(1-6)-eYFP (Annegret Wilde, unpublished) using primer YFP-1 and YFP-2. The resulting DNA fragment was introduced into the multiple cloning site of pSpark[®], producing plasmid pCSDN5. The correctness of the amplified sequence *eyfp* was verified by DNA sequencing. *eyfp* was then introduced into pCSAM135 (Flores *et al.*, 2007) by replacing the *gfp* gene downstream of *sepJ* using restriction sites EcoRV and ApaI. The generated construct was labelled as pCSDN6. Finally, *sepJ-eyfp* was transferred into pCSV3 via KpnI digestion, resulting in plasmid pCSDN7. Plasmid pCSDN7 was transferred into *Anabaena* sp. PCC 7120 resulting in strain CSDN7. Plasmid pCSDN28 was conjugated into *Anabaena* sp. PCC 7120, generating strain CSDN28.

Strain CSDN28 was labelled with 5-CFDA and tested for its co-localisation properties by confocal microscopy. Both fluorophores could be detected simultaneously by using a single exciting wavelength (Figure 39). While 5-CFDA is visible in the cytoplasm of the cells SepJ-mTurquoise2 forms distinct spots at the septa of adjacent cells (Figure 39). The overlap of both emission spectra appears marginal and does not influence the co-localisation. In comparison, co-localisation studies using strain CSDN7 could not resolve the different localisation of 5-CFDA and SepJ-eYFP clearly even when using separate and optimal excitation wavelengths for each fluorophore (Figure 40). When exciting with the optimal wavelength for eYFP strong emission was visible for 5-CFDA in the detection range (Figure 40).

5 Regulation, redistribution and remodelling of intercellular communication

Thus, localisation of SepJ-eYFP becomes visible only if filaments are weakly stained with 5-CFDA.

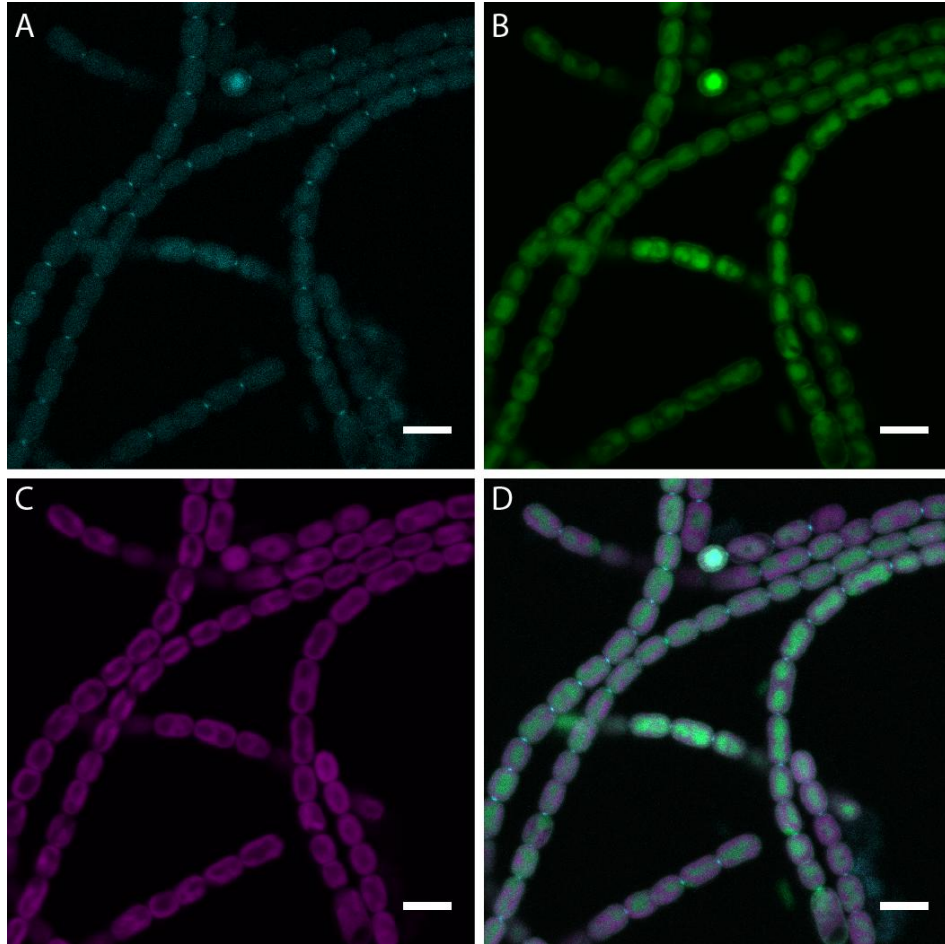


Figure 39. Co-localisation of SepJ-mTurquoise2 and 5-CFDA in strain CSDN28.

Cells were excited with a single wavelength of $\lambda_{\text{ex}} = 458$ nm. Images show SepJ-mTurquoise2 fluorescence (cyan; $\lambda_{\text{em}} = 460\text{-}490$ nm; A), 5-CFDA fluorescence (green; $\lambda_{\text{em}} = 500\text{-}530$ nm; B), autofluorescence (magenta, $\lambda_{\text{em}} = 670\text{-}720$ nm; C) and an overlay of all three channels (D). Scale bars, 5 μm .

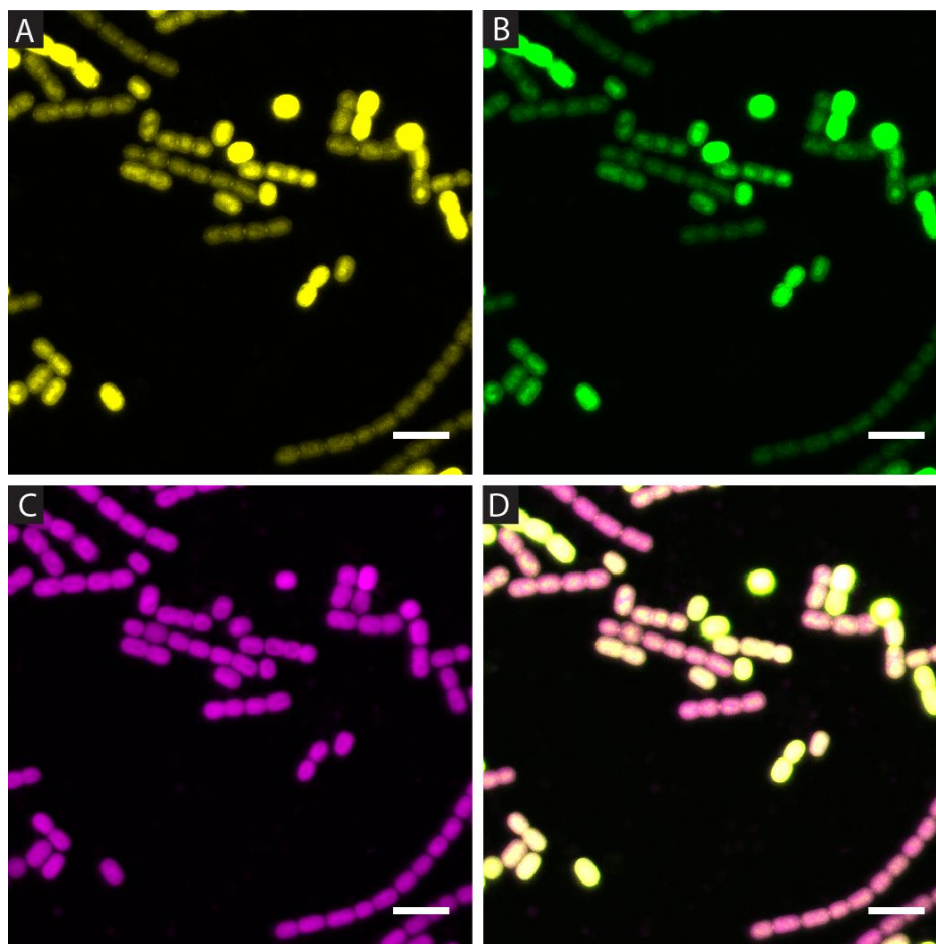


Figure 40. Co-localisation of SepJ-eYFP and 5-CFDA in strain CSDN7.

Cells were either excited with a wavelength of $\lambda_{\text{ex}} = 514$ nm (eYFP, autofluorescence) or $\lambda_{\text{ex}} = 488$ nm (5-CFDA). Images show SepJ-eYFP fluorescence (yellow; $\lambda_{\text{em}} = 520\text{-}535$ nm; A), 5-CFDA fluorescence (green; $\lambda_{\text{em}} = 500\text{-}520$ nm; B), autofluorescence (magenta, $\lambda_{\text{em}} = 670\text{-}720$ nm; C) and an overlay of all three channels (D). Scale bars, 10 μm .

Filaments of CSDN28 were then subjected to mild sonication and tested for their ability to retain the fluorescent tracer within the cells. Images indicate that filament fragmentation does not lead to efflux of 5-CFDA. Filaments showing a terminal SepJ-mTurquoise2 spot remained labelled with 5-CFDA (Figure 41), supporting the proposed channel closure after cell breakage.

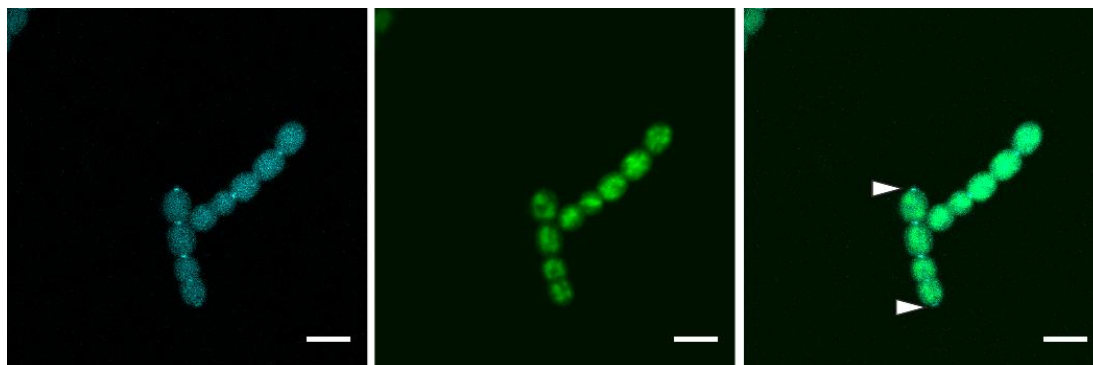


Figure 41. Co-localisation of SepJ-mTurquoise2 and 5-CFDA in strain CSDN28 after fragmentation by sonication.

Images show SepJ-mTurquoise2 fluorescence (cyan), 5-CFDA fluorescence (green), and an overlay of both channels. The terminal SepJ-mTurquoise2 spots are highlighted with white arrows. Scale bars, 5 μ m.

Interestingly, fragmentation studies by Nicolaisen *et al.* (2009) revealed that uptake of glutamate, aspartate, glutamine and sucrose was significantly higher for fragmented filaments than for untreated filaments of *Anabaena* sp. PCC 7120, and based on micrographs of these filaments the authors suggested that substrates diffuse through holes at the site of breakage into the periplasmic space and are then transported into the cytoplasm. Accordingly, when a filament breaks its viability can only be maintained if molecules remain in the cytoplasm and do not leak or are transported into the open and continuous periplasm in high quantity. A study by Brown and Rutenberg (2012) suggested that export occurs at significantly lower rate than import. In conclusion, the presented cytoplasmic channel closure appears to be the main mechanism avoiding cell death after fragmentation by molecular efflux.

5.4 Influence of filament fragmentation on intercellular communication

The influence of fragmentation on intercellular communication was investigated by FRAP measurements using 5-CFDA. Cells of strain CSDN28 were labelled with 5-CFDA, subjected to fragmentation and the recovery of fluorescence of cells within the filament followed over time. The fragmented filaments were identified by localising the SepJ-mTurquoise2 proteins at the termini. FRAP measurements reveal that 5-CFDA fluorescence recovers after fragmentation (Figure 42), indicating that the fluorophore remains mobile and diffuses between neighbouring cells. Accordingly, efflux of 5-CFDA would be possible if channel closure did not occur after cell breakage. These results also show that filament fragmentation does not cause channel closure between other cells within the filament, suggesting that the closure process is likely to be passive as a result of channel collapse caused by the applied sonication stress.

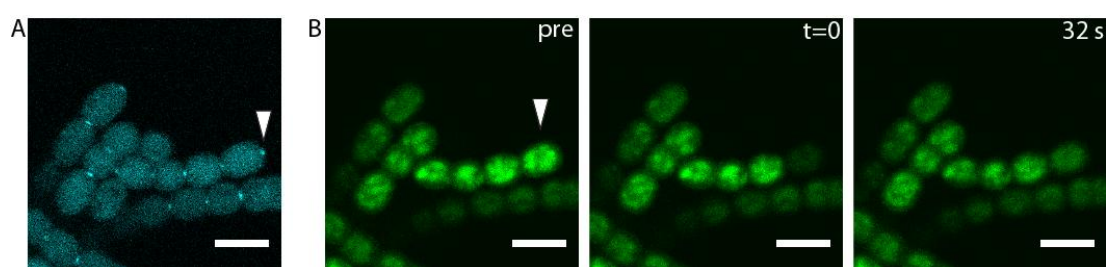


Figure 42. Recovery of 5-CFDA in CSDN28 after filament fragmentation by sonication.

The terminal cell of a fragmented filament was identified by the position of the SepJ-mTurquoise2 spot at the end (A). Panel B shows an exemplary FRAP experiment with a 5-CFDA labelled terminal cell (white arrow). After taking an initial image (pre), fluorescence of the terminal cell was bleached by increased laser intensity (t=0) and its recovery followed for 32 s. Scale bars, 5 μm .

5.5 Ultrastructure of fragmented filaments

Finally, we raised the question where cells break when they are fragmented by sonication. TEM images show that a part of the lysed cell remains attached to the intact filament, including the cytoplasmic membranes and the outer membrane of both cells with the peptidoglycan layer in between (Figure 43). A similar result was obtained by Nicolaisen *et al.* (2009) for cells which were fragmented by repeated passage through a syringe. Both results support the hypothesis of a tightly fused peptidoglycan layer in between neighbouring cells (Maldener *et al.*, 2014). The electron micrograph also shows that the membrane curvature at the terminal cell pole changes after fragmentation (Figure 43). The membranes are pushed outward (positive curvature) presumably as a result of osmotic changes.

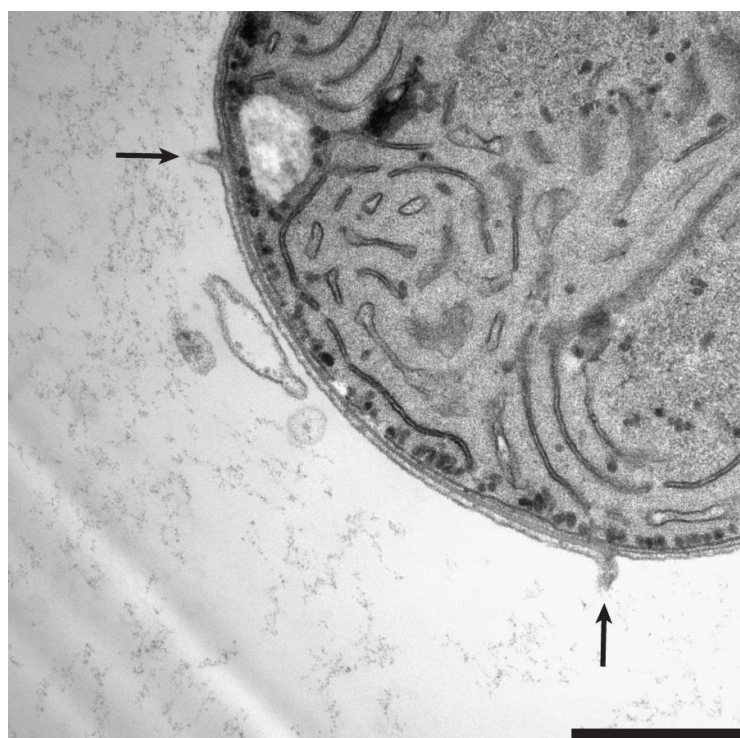


Figure 43. Electron micrograph of an ultra thin section through the septal region of *Anabaena* sp. PCC7120 after fragmentation by sonication.

Note that a part of the lysed cell remains attached to the part of the intact cell between the two arrows. Scale bar, 500 nm.

5.6 Influence of fragmentation on the localisation of SepJ

As shown earlier in this chapter, fragmentation leads to formation of short filaments that show a fluorescent SepJ spot at the new terminus facing the environment (Figure 41). SepJ is likely to be composed of three domains including a C-terminal permease domain which is predicted to possess 11 transmembrane helices spanning the cytoplasmic membrane (Flores *et al.*, 2007). Considering that cell breakage leaves the cytoplasmic membrane of the neighbouring cell attached to the shortened filament (Figure 43) it is likely that also the SepJ proteins from the detached cell remain localised at the pole. This question was addressed by using strain CSAM137 which possesses a GFP-tagged variant of SepJ, subjecting it to sonication and comparing the intensities of the SepJ-GFP spot between two cells with that found at the new terminus. A ratio of 1.21 ± 0.34 (n=32) was determined, indicating that slightly more GFP molecules are present in between two neighbouring cells than at the terminus. The nearly 1:1 ratio implies that after filament breakage the SepJ-GFP molecules of the former adjacent cell remain attached.

To determine the role of SepJ in this process further, the localisation of the SepJ-GFP spots after fragmentation was followed over time using confocal microscopy. Directly after fragmentation the SepJ-GFP remains at the new terminal pole of the vegetative cells, but disappears then within approximately 24 h from its initial position (Figure 44), suggesting that there exist mechanisms to recognise the position of filament breakage and remodel channel structure. An important factor for the redistribution of SepJ proteins is likely to be the altered membrane curvature at the cell pole (Figure 43). It has been reported that the specific localisation of some proteins depends on the membrane curvature in *Bacillus subtilis* and *E. coli* (see

5 Regulation, redistribution and remodelling of intercellular communication review by Ramamurthi (2010)). Hitherto, a changed curvature could either attract proteins important for the degradation of present SepJ molecules or alternatively lead to the redistribution of the proteins such as the division plane (Flores *et al.*, 2007).

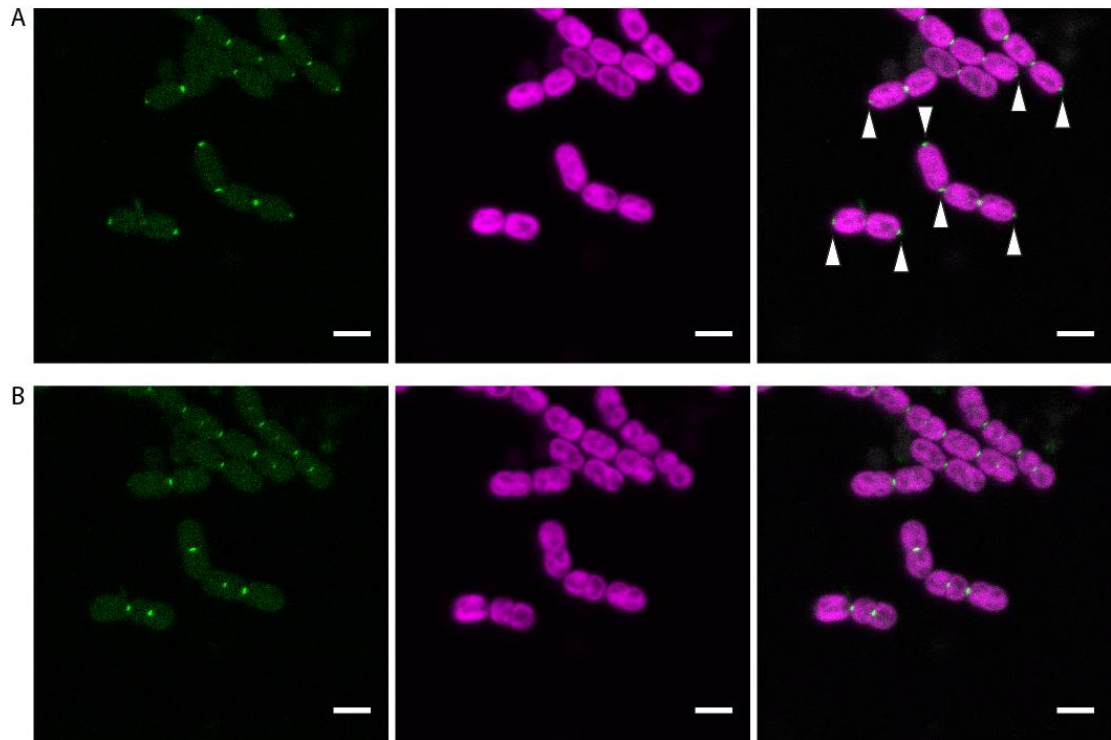


Figure 44. Redistribution of SepJ-GFP after fragmentation on strain CSAM137. SepJ-GFP (green) remains after fragmentation at the new cell terminus facing the environment (A), but disappears within 24 h (B). Terminal SepJ-GFP spots are highlighted by white arrows. Autofluorescence is shown in magenta. Scale bars, 5 μm .

5.7 Cell death in an aging culture of *Anabaena* sp. PCC 7120

In another approach the influence of naturally occurring filament fragmentation on channel closure and the role of SepJ was explored. The factors that lead to natural filament fragmentation are still poorly understood. It has been suggested that long-term starvation for sulphate reduces filament length which is mentioned by Bauer *et al.* (1995) based on personal communication with Bianca Brahmsha. In this work

5 Regulation, redistribution and remodelling of intercellular communication

cultures of *Anabaena* sp. PCC 7120 were grown to the stationary phase and left for several weeks standing on the bench at room temperature. This treatment produced cultures that showed dying filaments and filaments with dying cells within the filament (indicated by the absence of autofluorescence and their faded contrast in bright-field microscopy) (Figure 45; Figure 46). Filaments were then stained with 5-CFDA and visualised by confocal microscopy (Figure 45). As 5-CFDA is a live-cell stain which is added as a non-fluorescent and hydrophobic acetoxymethylester (AM) derivative that only becomes fluorescent after uptake into the cell and hydrolysis by esterases (Mullineaux *et al.*, 2008), it is possible to test whether the fluorophore diffuses from living stained cells into neighbouring dead cells. Confocal images reveal that the fluorophore does not diffuse into a dead cell from a living filament (Figure 45), indicating that channel closure occurs to avoid molecular efflux by a possible breakage of the filament at this position.

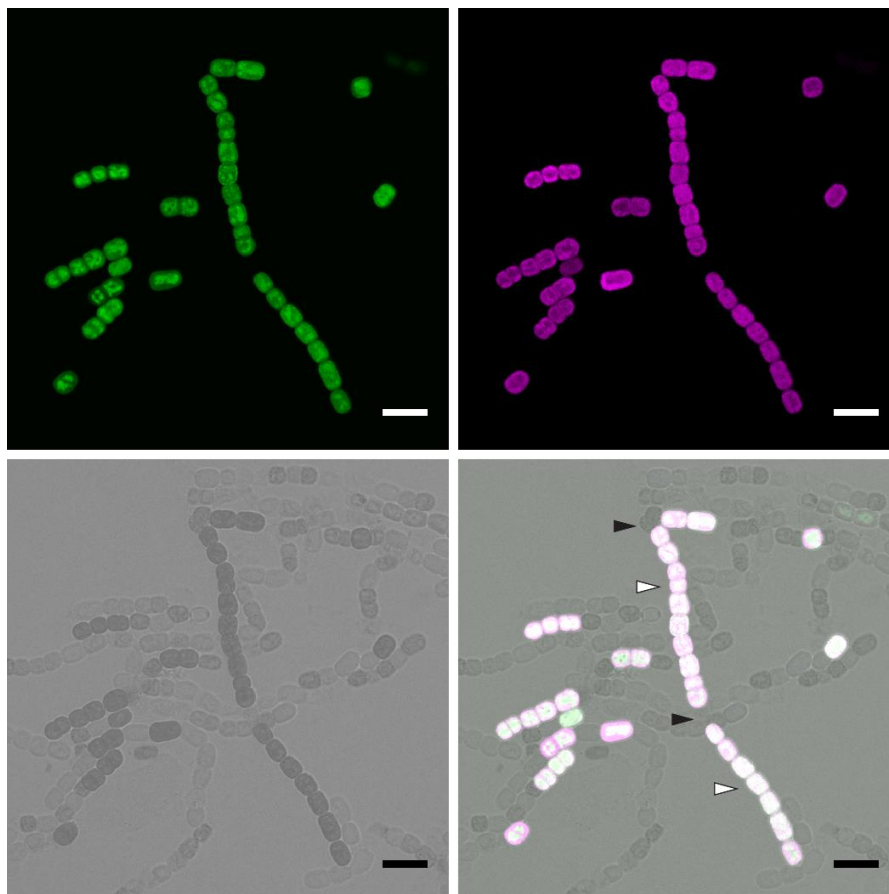


Figure 45. Labelling of an aging culture of *Anabaena* sp. PCC 7120 with 5-CFDA.

Images show 5-CFDA fluorescence (green), autofluorescence (magenta), a bright-field view (grey) and an overlay of all three channels. 5-CFDA labelled filaments (white arrow) show dead, unlabelled cells within the same filament (black arrows). Scale bars, 10 μm .

As shown earlier in this chapter filament fragmentation involves redistribution of SepJ. The influence of aging on the localisation was investigated using the *sepJ-gfp* expressing strain CSAM137 and visualising the fluorescent-tagged protein after keeping the culture standing for several weeks at room temperature. Images indicate no SepJ-GFP spots at the septa of dead and living cells while SepJ-GFP spots remain visible in between two living cells (Figure 46). These results support the hypothesis of redistribution and remodelling of the septal junctions during filament

5 Regulation, redistribution and remodelling of intercellular communication

fragmentation. Furthermore, they prove that the earlier presented results are not an artificial effect induced by the sonication procedure.

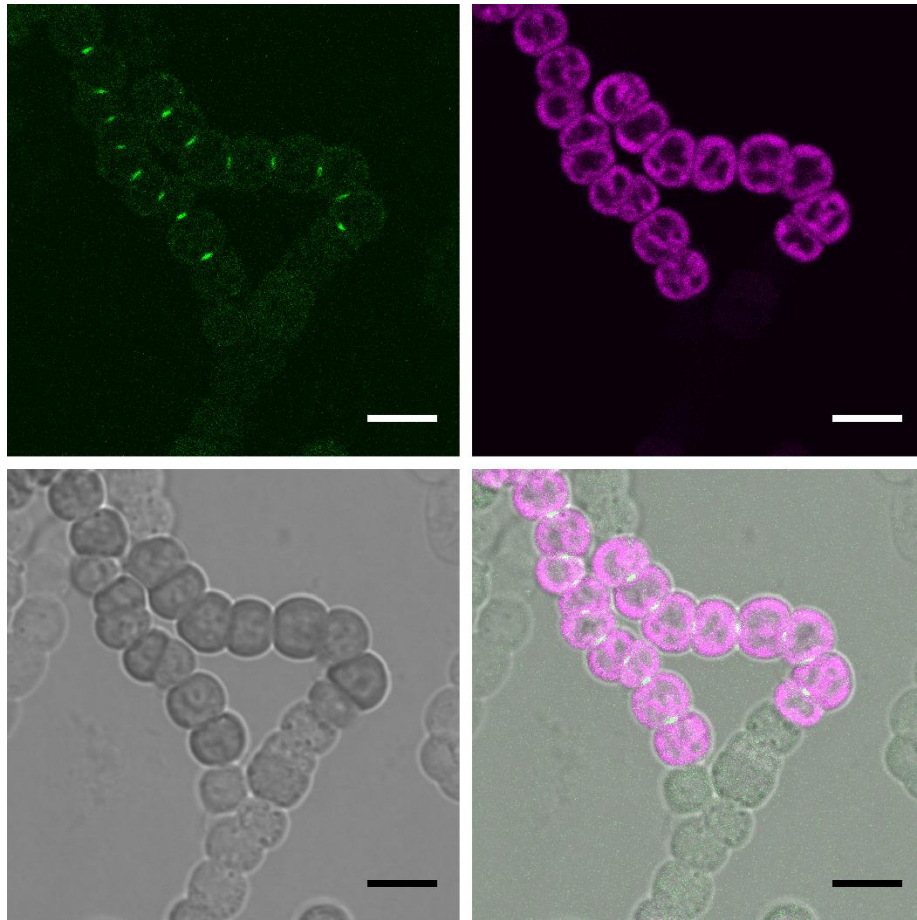


Figure 46. Localisation of SepJ-GFP in an aging culture of CSAM137.

Images show GFP fluorescence (green), autofluorescence (magenta), a bright-field view (grey) and an overlay of all three channels. Scale bars, 5 μm .

5.8 Conclusion

In this chapter the influence of filament fragmentation on intercellular communication was investigated, addressing the questions whether channels close after filament breakage and if there are remodelling processes of the septa involved. Mild sonication is a suitable method for inducing filament fragmentation in *Anabaena* sp. PCC 7120 without influencing filament and cell viability. Filaments

5 Regulation, redistribution and remodelling of intercellular communication

that were subjected to sonication continued dividing. After fragmentation the fluorescent tracer 5-CFDA remains in the cytoplasm of *Anabaena* sp. PCC 7120 indicating that channel closure occurs to prevent molecular efflux and subsequent cell death. The new terminus of the filament after fragmentation can be visualised by the presence of mTurquoise2-tagged version of the SepJ protein at the new pole of the cell in the presence of 5-CFDA. Both dyes exhibit different emission spectra when using a single excitation wavelength. After fragmentation remodelling of the septum occurs. SepJ is redistributed from the terminal cell pole by a yet unknown mechanism which could involve the altered membrane curvature observed at the new cell pole. Either degradation or diffusion processes could be possible mechanisms. Similar results were obtained for an aging culture of *Anabaena* sp. PCC 7120 where dead cells were visible in an intact filament. 5-CFDA and SepJ-GFP were only visible in the living part of the filament. Thus, channel closure occurs prior to fragmentation and possibly involves other mechanisms than simple channel collapse.

6 Morphological complexity and intercellular communication in the Section V cyanobacterium

Mastigocladus laminosus

While our understanding of multicellularity in Section IV cyanobacteria has deepened considerably by studying *Anabaena* sp. PCC 7120 as model organism, there is little known about cyanobacteria of Section V. The best understood organism within this section is probably *Mastigocladus laminosus*, which is a major component of epilithic microbial mats at White Creek, Yellowstone National Park, USA (Miller *et al.*, 2006), and can be found in geothermal sites and hot springs worldwide with an upper temperature limit of 63°C (Schwabe, 1960). The organism was first isolated and described by Cohn (1862) from hot springs in Carlsbad in the Czech Republic. Later reports document the presence of the organism in Costa Rica (Finsinger *et al.*, 2008), the Antarctic (Melick *et al.*, 1991), Greenland (Roeselers *et al.*, 2007), Myanmar (Soe *et al.*, 2011), New Zealand (Castenholz, 1976), Japan, and Chile (Schwabe, 1960; Mackenzie *et al.*, 2013).

Under most conditions, *M. laminosus* forms a dense network of intertwined narrow and wide trichomes (also known as type II (secondary) and type I (primary) trichomes respectively (Schwabe, 1960)). While cells of narrow trichomes have a uniform cylindrical shape, cells of wide trichomes are rounded and pleomorphic, usually giving rise to true branches, the characteristic feature for cyanobacteria of Section V (Anagnostidis and Komárek, 1990; Golubić *et al.*, 1996; Komárek *et al.*, 2003) (Figure 47). Microfossil records from Rhynie, Aberdeenshire, Scotland support the presence of this complex morphotype already around 400 million years

6 Morphological complexity and intercellular communication in *M. laminosus*

ago (Croft and George, 1959) and according to the phylogenetic analyses by Schirmer *et al.* (2011; 2013) multicellularity in cyanobacteria evolved possible as early as the Great Oxygenation Event that took place 2.48 to 2.32 billion years ago (Bekker *et al.*, 2004). True branching includes several different types, which have been named for simplicity after their morphological appearance, including ‘T’, ‘V’, ‘X’, and (reverse) ‘Y’ branching (Anagnostidis and Komárek, 1990; Golubić *et al.*, 1996) (Figure 47). Lateral ‘T’, ‘V’ and (reverse) ‘Y’ branches are formed of cylindrical cells (Desikachary, 1959; Fogg *et al.*, 1973; Golubić *et al.*, 1996). Branches can differentiate into motile hormogonia which are released from the main filament by death and disintegration of the branching point (Balkwill *et al.*, 1984) (Figure 47). The released hormogonia glide away from the parental colony, and form new colonies by differentiating into spherical cells, which give rise to new lateral branches (Hernandez-Muniz and Stevens, 1987; Robinson *et al.*, 2007).

According to ultrastructural investigations, cell division in *M. laminosus* and *Fischerella ambigua* differs from that seen in filamentous cyanobacteria of Sections III and IV (Thurston and Ingram, 1971; Martin and Wyatt, 1974; Nierzwicki *et al.*, 1982). It was suggested that rounded cells in wide trichomes became separated by the surrounding sheath (Martin and Wyatt, 1974). This would suggest that their filamentous character is maintained only by sheath material, so cyanobacteria of Section V may not represent the pinnacle of development among cyanobacteria but rather a primitive and basic form linking coccoid and filamentous forms (Martin and Wyatt, 1974). Under nitrogen deprivation almost every cell can differentiate into a heterocyst, following no regular spacing pattern, often forming multiple contiguous heterocysts (MCH) in wide trichomes (Nierzwicki-Bauer *et al.*, 1984a; Nierzwicki-

6 Morphological complexity and intercellular communication in *M. laminosus*

Bauer *et al.*, 1984b; Stevens *et al.*, 1985). This raises the question of how cells communicate in *M. laminosus*.

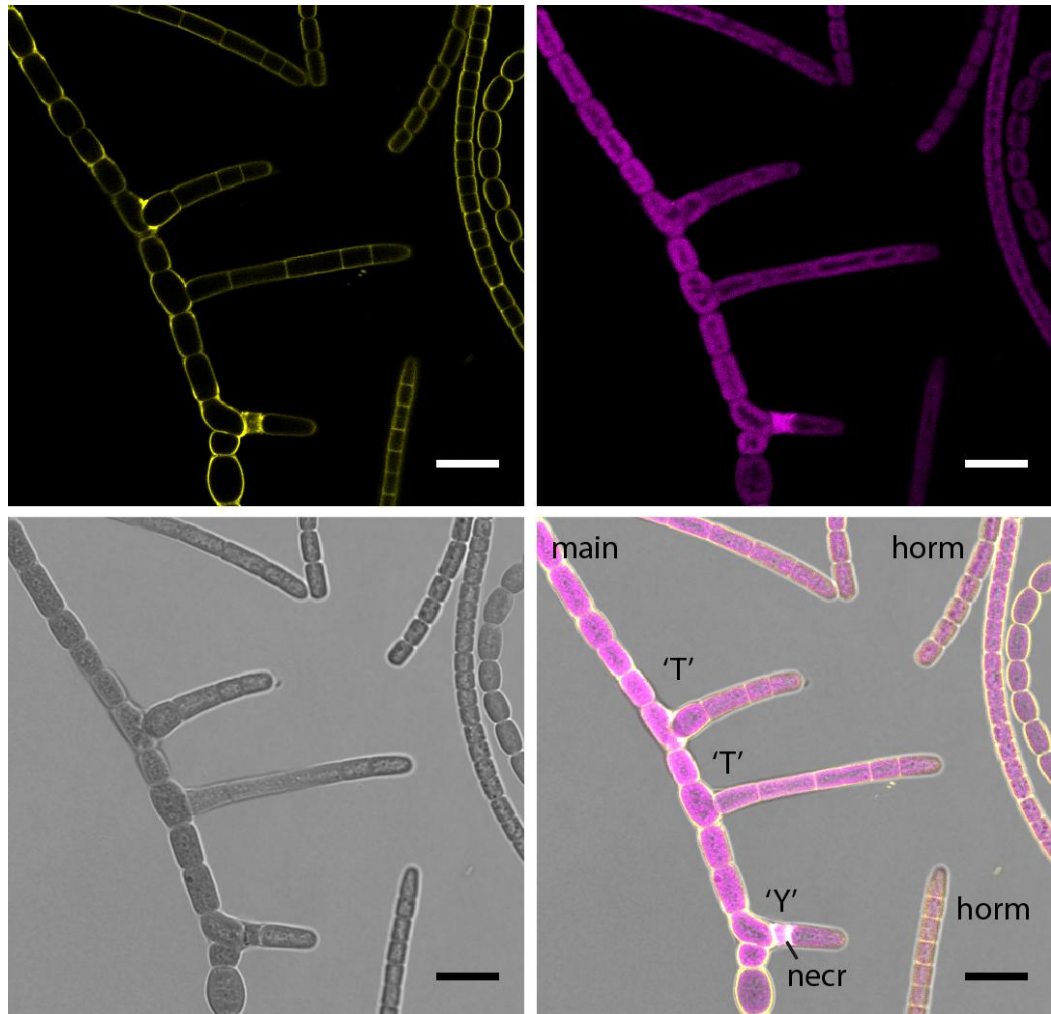


Figure 47. Morphological complexity of *M. laminosus*.

The main trichome is formed of rounded cells which give rise to 'T' and (reverse) 'Y' branches composed of cylindrical cells. Motile filaments (hormogonia (horm)) are released from the main trichome by formation of necridia (necr). Images show FM1-43FX staining (yellow), autofluorescence (magenta), the bright-field view (grey) and the merged image of the three channels. Scale bars, 10 μ m.

In this chapter intercellular communication in *M. laminosus* is investigated by loading the fluorescent tracer 5-CFDA into the cytoplasm, and performing FRAP experiments to observe intercellular exchange of dye molecules. The questions addressed are whether the branch and the main trichome communicate in *M.*

6 Morphological complexity and intercellular communication in *M. laminosus*

laminosus, and whether exchange depends on the cell morphotype. The development of different types of branches and the localisation of heterocysts is discussed. Furthermore, the role of SepJ in *M. laminosus* is investigated by identifying the gene, localising the protein and generating and characterising a *sepJ* inactivation mutant.

Work presented in this chapter has been partially published in Molecular Microbiology (Nürnberg *et al.*, 2014).

6.1 Development of different branching types in *M. laminosus*

As described in the paragraph above, *M. laminosus* forms mainly two morphologically distinct types of true branches with slight variations: (reverse) ‘Y’ (Figure 48A) and ‘T’ branches (Figure 48B). Both types of branches are not only present in the same culture, but even in the same filament (Figure 47), raising the question of whether the differences between the two branching types are merely superficial, or whether they arise from different developmental processes.

To approach this question the cytoplasmic membrane was visualised during branch formation using confocal microscopy and TEM. For confocal microscopy cells were stained with the fluorescent dye FM1-43FX, which highlights the cytoplasmic membrane in cyanobacteria (Schneider *et al.*, 2007). The results indicate that the (reverse) ‘Y’ and ‘T’ branches are topologically equivalent. In both cases branch formation is initiated by the growth of a cell in a direction other than the main axis of the filament (Figure 48A,C). This is generally followed by septum formation across the mid-line of the cell, as is the usual rule in bacteria (Meier and Goley, 2014) (Figure 48A). As a result of septum formation one of the daughter cells is connected to three cells: two in the main trichome and one in the developing branch (Figure 48A,B). A ‘T’ branch results from cell elongation in a direction roughly

6 Morphological complexity and intercellular communication in *M. laminosus*

perpendicular to the filament axis (Figure 48B), whereas a (reverse) ‘Y’ branch results from cell elongation at a more acute angle to the filament axis (Figure 48A,C), but the two cases are only superficially different. This implies that branching is the result of a randomisation of the direction of cell elongation. When cell elongation is constrained to occur along the filament axis, branch formation is repressed. A developmental switch leading to randomisation of the direction of cell elongation allows branches to form.

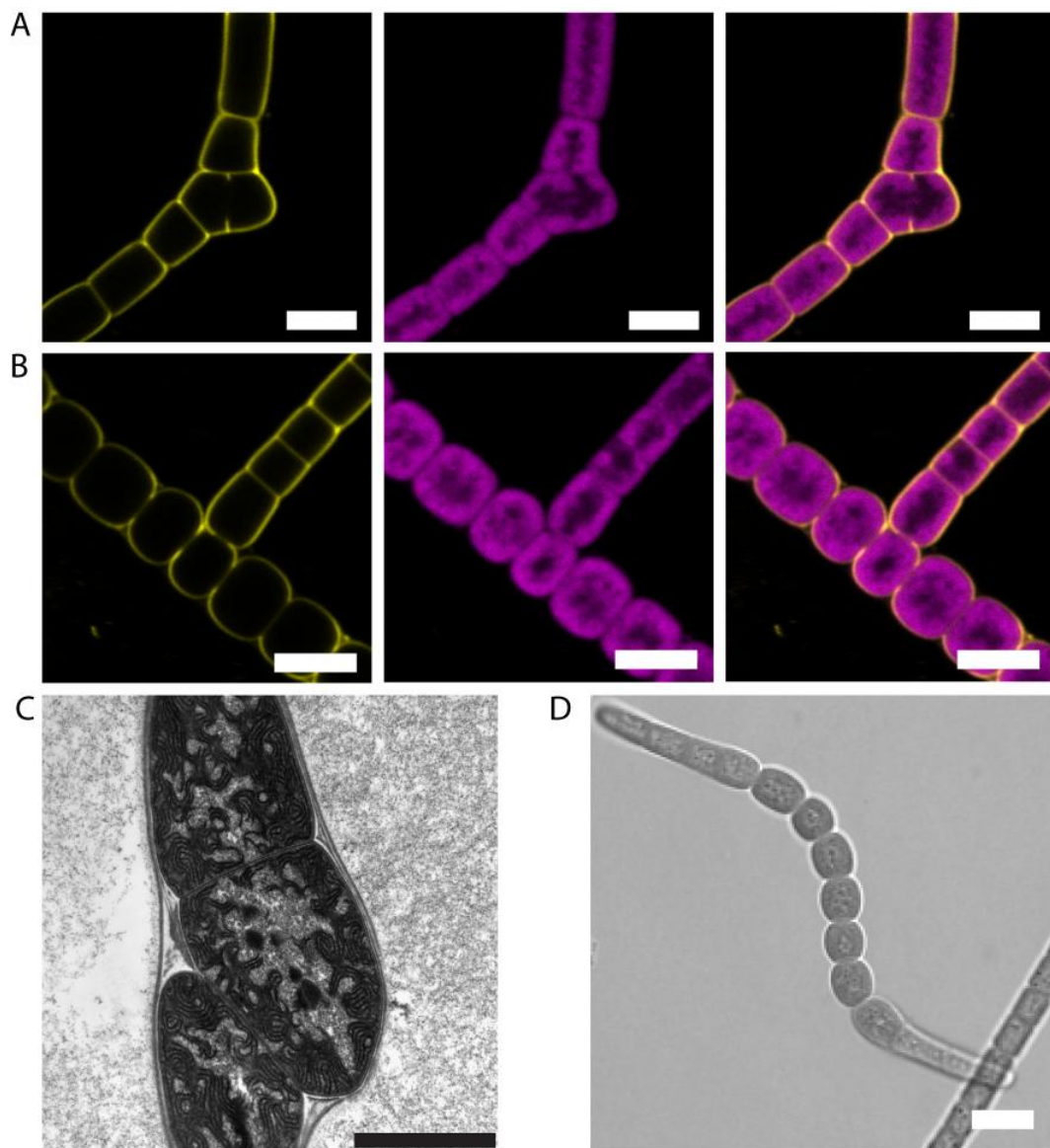


Figure 48. Different types of branching in *M. laminosus*, and their development revealed by confocal (A,B,D) and transmission electron microscopy (C).

Figure 48

Two main types of branching are present in *M. laminosus*, namely (reverse) ‘Y’- (A) and ‘T’-branching (B). While the division plane is localised parallel to the main filament axis in ‘T’-branching (B), it remains nearly transversal to the main filament axis during the formation of a (reverse) ‘Y’-branch (A,C). Cells at the terminus of the main trichome grow into the direction of the main filament but alter their cell shape (D). (A,B) The images show FM1-43 FX fluorescence (yellow; left), chlorophyll fluorescence (magenta, middle), and an overlay of both (right). Scale bars, 5µm. (C) Electron micrograph of a thin section prepared with KMnO₄. Scale bar, 2µm. (D) Bright field image. Scale bar, 5µm.

This conclusion is consistent with the message from recent genome sequence analyses of several cyanobacteria of Section V, which did not detect any specific signature protein for cyanobacteria of Section V (Dagan *et al.*, 2013; Shih *et al.*, 2013). Furthermore, it was shown by Singh and Tiwari (1969) that true branching can be induced in the non-branching filamentous cyanobacterium *Nostoc linckia* (Roth) Born. et Flah. (Section IV) by random mutagenesis using ultraviolet irradiation, which implies that branching can be induced by loss of gene function rather than being the result of a complex developmental programme. This fits with the conclusion that branching results from the selective relaxation of a stringent control over the direction of cell elongation. No obvious patterns in the spacing of branches were observed, even two adjacent cells start occasionally forming branches which remain either connected (Figure 49A) or separate (‘false branching’; Figure 49B). The role of the peptidoglycan layer during branch formation remains to be investigated. Images suggest that if the separation process of the peptidoglycan layers fails cells remain connected at the basis of an elongating branch (Figure 49C).

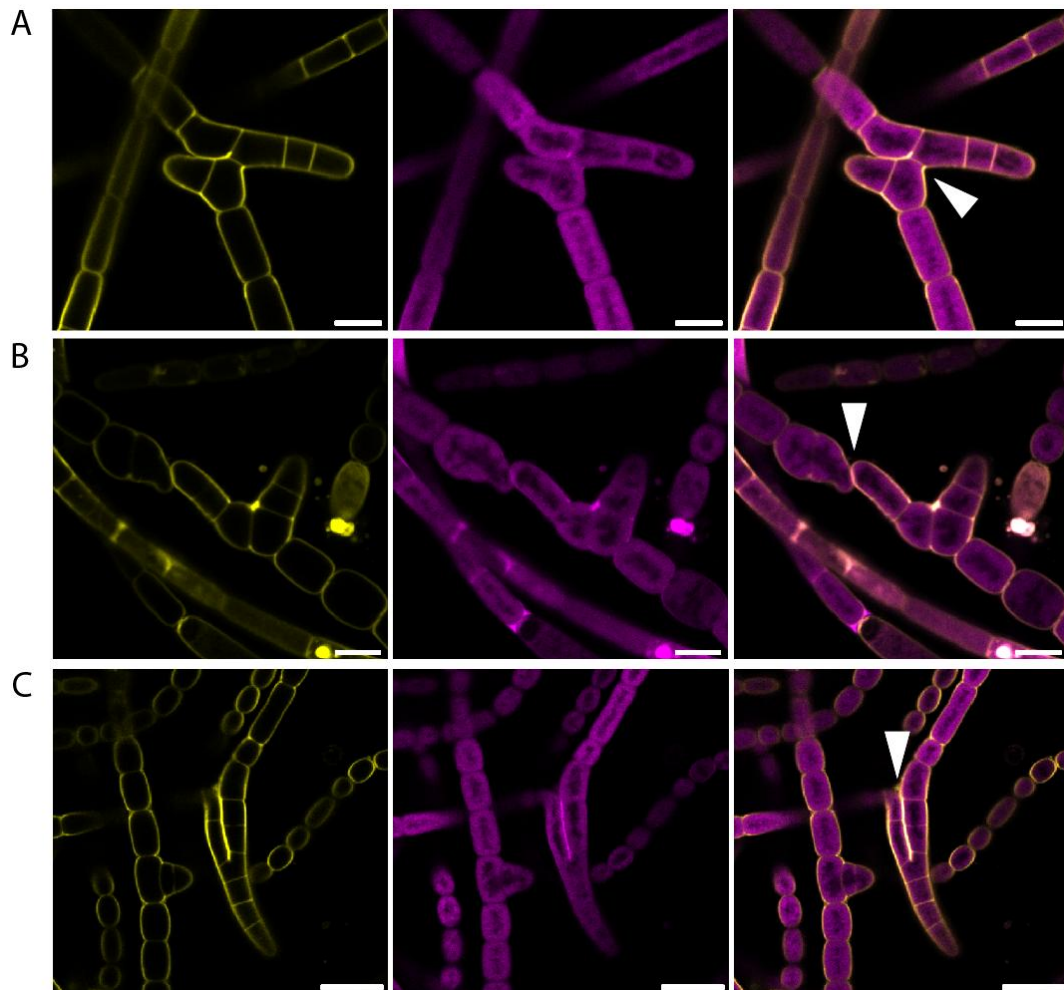


Figure 49. Variations of branching in *M. laminosus*.

No regular branching pattern is observed. Cells continue dividing next to an already formed branch, resulting in either connected (A) or separated double branches ((B); ‘false branching’). Occasionally, cells remain connected at the basis of a branch, forming an elongated (reverse) ‘Y’ branch (C). The images show FM1-43 FX fluorescence (yellow; left). autofluorescence (magenta, middle) and an overlay of both (right). Scale bars, 10 μm .

Terminal cells of wide trichomes do not branch and have a different, elongated shape (Figure 48D), which has been described as a ‘terminal hair’ by Anagnostidis and Komárek (1990). The attachment of another cell, or even a cell fragment, at the terminus of the filament is sufficient to inhibit cell elongation (Figure 50). A similar topology can be found e.g. in the filamentous cyanobacterium *Oscillatoria acuminata* (Section III; Geitler, 1960).

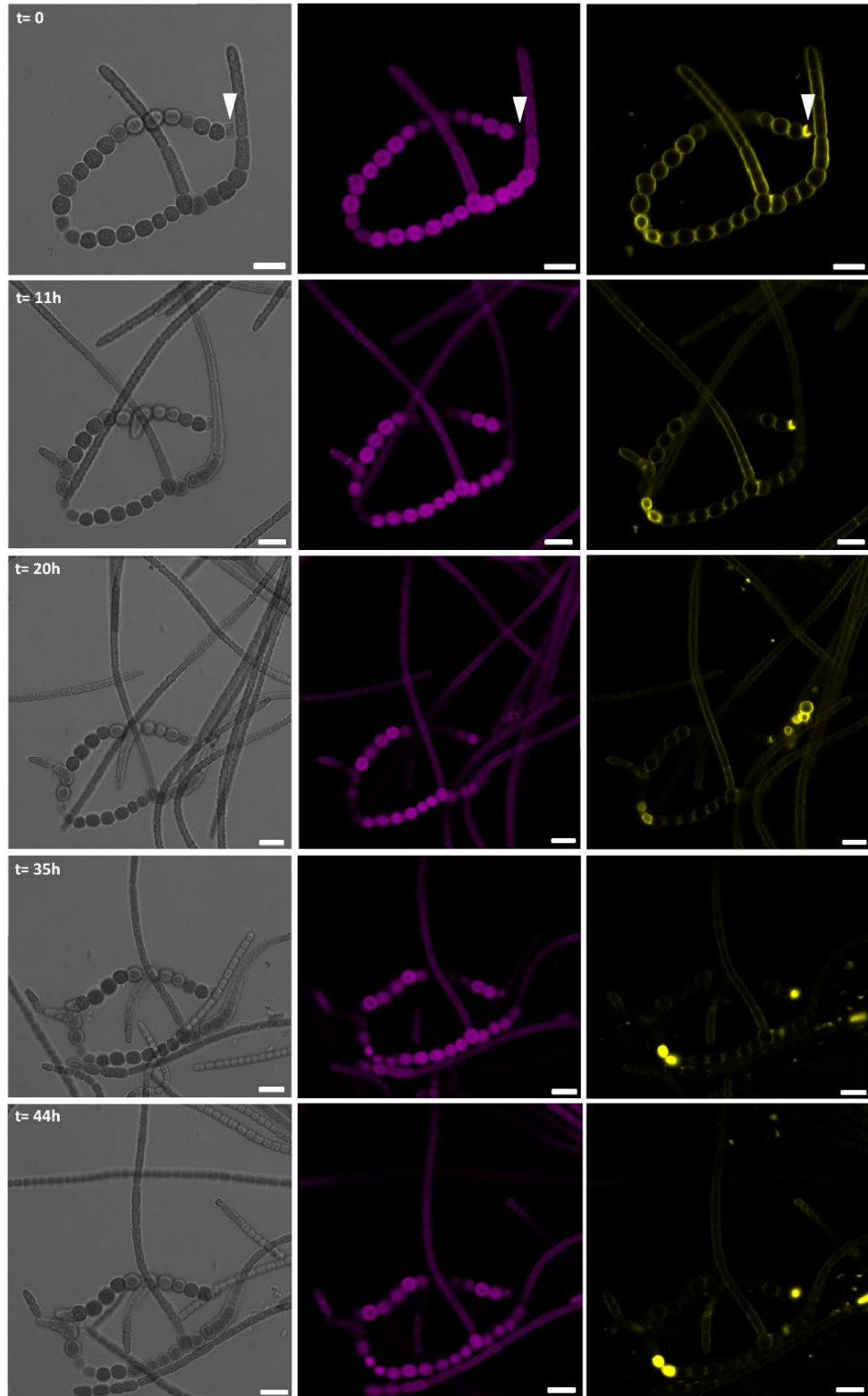


Figure 50. Inhibition of terminal filament growth by remaining cell fragments.

A remaining cell fragment at the terminus of a filament (arrow) inhibits further growth. Cells were monitored for 44 h. The images show bright field (left), autofluorescence (magenta, middle) and FM1-43 FX fluorescence (yellow; right). Scale bars, 10 μm .

6.2 Intercellular communication between branch and main trichome in *M. laminosus*

Until now it has remained unknown whether the branch and the main trichome communicate in cyanobacteria of Section V. A prerequisite for answering this question is to load a fluorescent molecule into the cytoplasm of cells of both the branch and the main trichome. In this study the fluorescent tracers 5-CFDA and calcein were tested for *M. laminosus*. The efficiency of cell labelling with 5-CFDA was much higher than that with calcein (data not shown), and hence suitable for further studies.

The question of connectivity between branch and main trichome cannot be answered simply by photobleaching and following fluorescence recovery of the cell at the branch point, as fluorescence recovery might be possible from three directions. Branch formation could be induced by transferring filaments of *M. laminosus* to fresh growth medium and agitating the culture for 24h. This is consistent with a previous observation by Thurston and Ingram (1971) that branch formation is induced by conditions favouring rapid growth. Cells were then loaded with 5-CFDA, and fluorescence of entire short branches bleached by scanning the region of the branch at increased laser intensity (Figure 51). All the cells in a branch, regardless whether they formed a 'T' (Figure 51) or (reverse) 'Y' branch (data not shown), showed recovery. A quantified analysis of recovery, shown for a specimen 'T' branch in Figure 51, in which the bleached out branch was defined as one region of interest (ROI), reveals that recovery is mediated by cells from both sides next to the branching point. The fluorescence intensity decreases in the adjacent cells over time. Accordingly our results demonstrate that trichomes of *M. laminosus* form a complex

6 Morphological complexity and intercellular communication in *M. laminosus*

interconnected cell communication network. A newly formed branch remains connected to its main trichome.

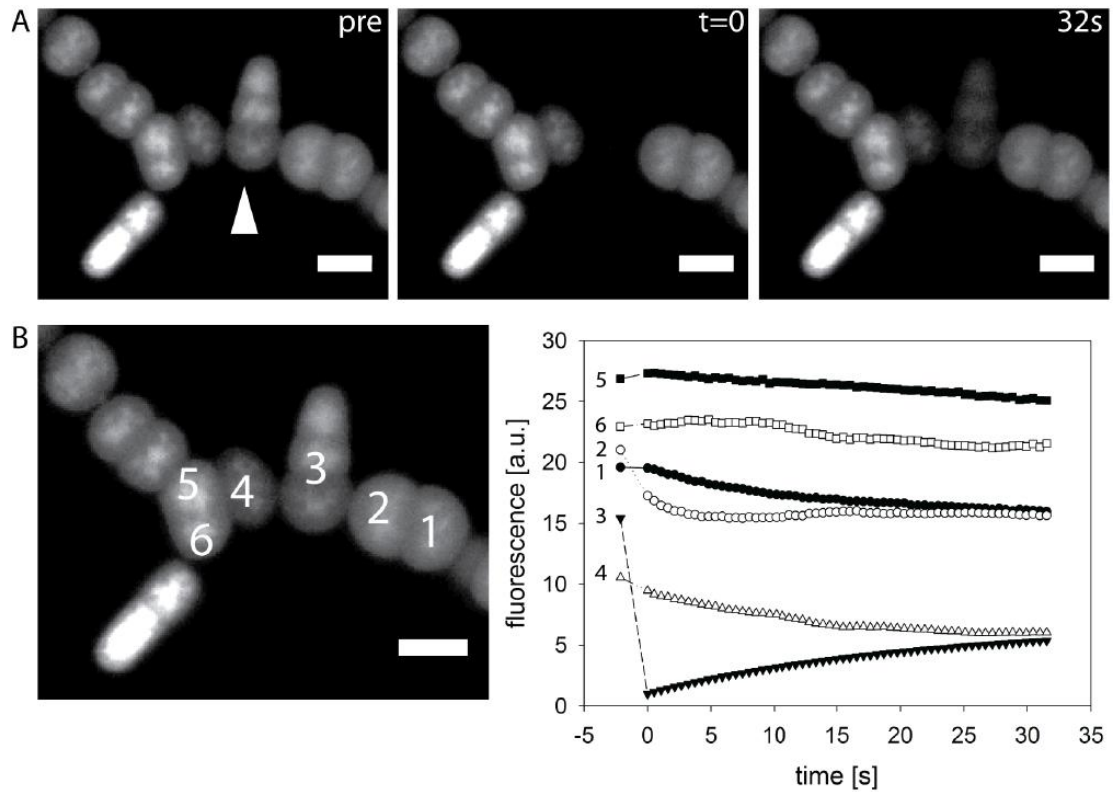


Figure 51. Intercellular transfer of 5-CFDA between branch and main trichome in a 'T'-branch of *M. laminosus*.

(A) FRAP image sequence. Only 5-CFDA fluorescence is shown. The left image was recorded prior to bleaching (pre). After bleaching out fluorescence in the branch ($t = 0$), the change in fluorescence intensity was followed over 32 s. Scale bars, 5 μm . (B) Quantitation of cell fluorescence of the FRAP sequence displayed in (A). Regions of interest (ROI) were defined as shown in the left image, the 'T'-branch formed of three cells was considered as one ROI ('cell 3'). The corresponding fluorescence recovery is indicated in the right graph. Scale bars, 5 μm .

6.3 Visualisation of septal junctions in *M. laminosus*

The exchange of molecules between the cytoplasm of cells requires the presence of cell-to-cell connecting structures penetrating the peptidoglycan layer and the plasma membranes of both cells. The occurrence of such structures, which have been termed

6 Morphological complexity and intercellular communication in *M. laminosus*

microplasmodesmata, septosoms or septal junctions, has been well characterized in *Anabaena* spp. by various methods, such as thin-section TEM (e.g. Wildon and Mercer, 1963), freeze-fracture EM (Giddings and Staehelin, 1978; Giddings and Staehelin, 1981) and electron tomography (Wilk *et al.*, 2011; Omairi-Nasser *et al.*, 2014), but it has remained unclear whether these structures exist in *M. laminosus*. A first indication of their presence in *M. laminosus* was given by Marcenko (1962), who could identify pores with an average diameter of 15 nm in the cross-walls of isolated cell wall sacculi. Electron micrographs of thin sections through the septal regions of *M. laminosus* clearly show structures pervading the septa between vegetative cells (Figure 52A) and between heterocysts and vegetative cells (Figure 52B). Different methods of sample preparation for TEM can also be used to reveal insights into the composition of intercellular channels (Wilk *et al.*, 2011). Our results are in good agreement with the proposed proteinaceous nature of the septal junctions found in *Anabaena* sp. PCC 7120 (Wilk *et al.*, 2011). While septal junctions appear as positively stained structures in a KMnO_4 -based preparation method (Figure 52A), they are negatively stained in an OsO_4 -based preparation (Figure 52B).

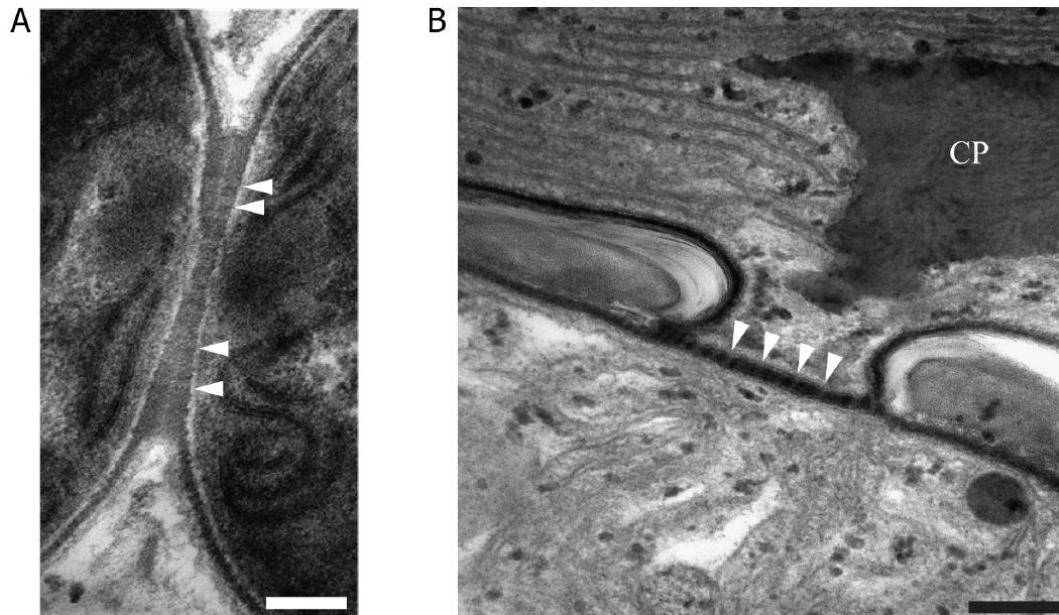


Figure 52. Electron micrographs of ultra thin sections through the septal region of *M. laminosus*.

Electron micrographs indicate the presence of structures connecting the cytoplasm of adjacent cells (arrows) in *M. laminosus*, using either a KMnO_4 - (A) or an OsO_4 -based preparation method (B). Septal junctions are present between vegetative cells (A), and between vegetative cells and heterocysts (B). Note that the outer membrane does not enter the septum. CP – cyanophycin. Scale bars, 200nm.

Although the presence of pores penetrating the septum was shown earlier in *Stigonema hormoides*, *Fischerella muscicola*, and *F. ambigua*, which belong to cyanobacteria of Section V, it has been suggested that these pores do not pierce the underlying plasma membranes, and accordingly do not mediate a direct connection of the protoplasts (Thurston and Ingram, 1971; Butler and Allsopp, 1972). The results from fluorescent dye exchange, however, show the continuity of the cytoplasm throughout the entire filament network, which is likely achieved by structures resembling septal junctions.

6.4 Identification and composition of SepJ in *M. laminosus*

A potential key player in the formation of septal junctions is the protein SepJ. In *Anabaena* sp. PCC 7120 SepJ is not only necessary for filament integrity (Flores *et al.*, 2007; Nayar *et al.*, 2007; Merino-Puerto *et al.*, 2010) but also essential for intercellular exchange of molecules (Mullineaux *et al.*, 2008; Mariscal *et al.*, 2011). Although a *sepJ* deletion mutant still exhibits septal junctions, the spacing between the two plasma membranes of the neighbouring vegetative cells is significantly reduced (Wilk *et al.*, 2011). The question arises whether SepJ is also present in *M. laminosus*. Due to the lack of a genome sequence for this cyanobacterium, primers were designed based on DNA sequence similarity between the *sepJ* and the *hetR* sequences deposited in the GenBank[®] database (Benson *et al.*, 2011). As *hetR* is usually located downstream of *sepJ* a highly conserved region between six cyanobacterial strains of Section V within this gene was selected, and defined it as primer rv_mlam_hetR (Figure 53A). The design of primer fw_mlam_sepJ was based on an alignment of the *sepJ* sequences from four species, which are filamentous and heterocyst forming (Figure 53B).

6 Morphological complexity and intercellular communication in *M. laminosus*

A

```

Chlo9212      CGGACGAGTGGGCACAGGCATGGGGCATT TTTTAGATGCAGCCGCAACCGC 50
Chlo6912      CGGACGAGTGGGCACAGGCATGGGGCATT TTTTAGATGCAGCCGCAACCGC 50
Fis7414       CGGACAAGTGGGCACAGGCATGGGGCCT TTTTAGATGCAGCCGCAACCGC 50
Fis1427       CGGACAAGTGGGCATAGACATGGGGCATT TTTTAGATGCAGCCGCAACCGC 50
Fis1829       CGGACAGGTGGGCATAGACATGGGGCCT TTTTAGATGCAGCCGCAACCGC 50
Fis7521       CGGACAAGTGGGCACAGACATGGGGCCT TTTTAGATGCAGCCGCAACAGC 50
                *****  *****  **  *****  *****  *****  *****  **

```

B

```

Avar          ATGGGGCGATTTGAGAAGCGACCAGACAACGACCCGCGAGTCCGAGGCGA--- 50
A7120        ATGGGGCGATTTGAGAAGCGACCAGACAACGACCCGCGAGTCCGAGGCGA--- 50
Nazol        ATGGGGCGATTTGAAAAGCGACCAGACA---ACCCACGAATCAGAGGCGACCT 50
Npun         ATGGGGCGATTCGAGAAGCAACCAGAAA---ACCCAAGAGTCAGAGGCGAGCT 50
                *****  **  ****  *****  *  ****  **  **  *****

```

Figure 53. Design of primers for the identification of *sepJ* in *M. laminosus* based on sequence alignments using ClustalW 2.1 (Larkin *et al.*, 2007).

(A) Reverse primer. Alignment of the first 50 nucleotides of *hetR* (partial) from different cyanobacteria of Section V. Chlo9212 - *Chlorogloeopsis* sp. PCC 9212; Chlo6912 - *C. fritschii* PCC 6912; Fis7414 - *Fischerella muscicola* PCC 7414; Fis1427 - *F. muscicola* SAG 1427-1; Fis1829 - *F. muscicola* UTEX 1829; Fis7521 - *F. thermalis* PCC 7521. The binding region of primer rv_mlam_hetR is underlined.

(B) Forward primer. Alignment of the first 50 nucleotides of *sepJ* from the cyanobacteria *Anabaena* sp. PCC 7120 (A7120), *A. variabilis* ATCC 29413 (Avar), '*Nostoc azollae*' 0708 (Nazol) and *N. punctiforme* PCC 73102 (Npun). Primer fw_mlam_sepJ is underlined. '*' indicates identity, '.' semi-conserved substitutions for panel (A) and (B).

The PCR with both primers generated a DNA product that contained a sequence with a high similarity to *sepJ*. The corresponding amino acid sequence revealed that SepJ of *M. laminosus* consists of three domains, including a coiled-coil domain, a highly repetitive linker region, and a permease domain which is found in nearly all filamentous, heterocyst-forming (and branching) cyanobacteria of Sections IV and V (see introduction 1.5, appendix: Table 26). Interestingly, the amino acid sequence of SepJ from *M. laminosus* SAG 4.84 is almost identical to that of *Fischerella*

6 Morphological complexity and intercellular communication in *M. laminosus muscicola* PCC 7414. This is especially interesting due to the great spatial separation of their origins of isolation. *M. laminosus* SAG 4.84 was originally collected from a thermal spring from Reyhjaness/Isafjord on Iceland, whilst *F. muscicola* PCC 7414 was isolated from a hot spring on New Zealand (Rippka *et al.*, 1979). It has been proposed that microbes which show a great tolerance of freezing and desiccation can facilitate long distance airborne dispersal, and might facilitate a cosmopolitan distribution; all characteristics which *Mastigocladus* spp. possess (Melick *et al.*, 1991; Castenholz, 1996; Roeselers *et al.*, 2007). Considering that the geologically diversification of the *M. laminosus* clade was a recent event, originating from a common ancestor associated with the western North American hot spot located below Yellowstone National Park (Miller *et al.*, 2007), and that intercontinental dispersal e.g. by transpacific winds is possible (Smith *et al.*, 2013), it might explain the presence of 'similar' strains of *M. laminosus* in widely separated habitats, such as New Zealand and Iceland.

A phylogenetic analysis based on 16S rRNA sequences (Figure 54) strongly supports the close relationship between *F. muscicola* PCC 7414 and *M. laminosus* SAG 4.84. Both strains form a distinct group with *M. laminosus* Greenland-8, *M. laminosus* CCMEE 5272, CCMEE 5321, CCMEE 5323, CCMEE 5324, and CCMEE 5326. Whilst most of the latter species originate from Iceland and Greenland (Figure 54), *M. laminosus* CCMEE 5272 was isolated from the Azores, Portugal, around 3,000 km south of Iceland, supporting the hypothesis of easy dispersal of *M. laminosus*. Although the amino acid sequence of SepJ from *M. laminosus* SAG 4.84 and *Fischerella* sp. PCC 7414 show a high similarity, it has to be pointed out that *sepJ* from *Fischerella* sp. PCC 7414 might exhibit a stop codon in the highly repetitive linker region.

6 Morphological complexity and intercellular communication in *M. laminosus*



Figure 54. 16S rRNA phylogenetic tree of *Mastigocladus/Fischerella* spp.

Figure 54

The BlastN search (Zhang *et al.*, 2000) was performed with the partial 16S rRNA sequence of *M. laminosus* SAG 4.84 as query. Only the first 100 BlastN results were used for the phylogenetic reconstruction using the Phylogeny.fr platform (Dereeper *et al.*, 2008). Nucleotide sequences were aligned with MUSCLE. Conserved blocks from the alignment were identified with Gblocks. Phylogenetic analyses were performed with PhyML using the substitution model GTR and the Approximate Likelihood-Ratio Test (aLRT; SH-like) to test branch support. The resulting tree was obtained with TreeDyn. Origin of strains forming the highlighted group in the phylogenetic are displayed next to the box according to Rippka *et al.* (1979), Ishida *et al.* (2001), Miller *et al.* (2007) and Roeselers *et al.* (2007).

6.5 Localisation of SepJ in *M. laminosus*

In order to localise SepJ in *M. laminosus* immunofluorescence labelling was performed using the antibody against the coiled-coil domain of SepJ from *Anabaena* sp. PCC 7120 (Mariscal *et al.*, 2011). The experiments show that SepJ is always located in the centre of intercellular septa of *M. laminosus* (Figure 55). There is also a dispersed background fluorescence signal in the cytoplasm. However this signal is also seen in the absence of the primary anti-SepJ antibody and therefore does not reflect SepJ localisation (Figure 55B,C). SepJ forms distinct spots not only in the main wide trichome (Figure 55A), but also in the narrow branch (Figure 55D). A newly-formed branching point shows three distinct regions of SepJ located to the adjacent cells (Figure 55A). The positioning of SepJ likely takes place during the cell division, when the protein forms a ring at the division plane (Figure 55D). These findings are in good agreement with those in *Anabaena* sp. PCC 7120 (Flores *et al.*, 2007) and support the importance of SepJ at the septal region of filamentous, heterocyst-forming cyanobacteria.

6 Morphological complexity and intercellular communication in *M. laminosus*

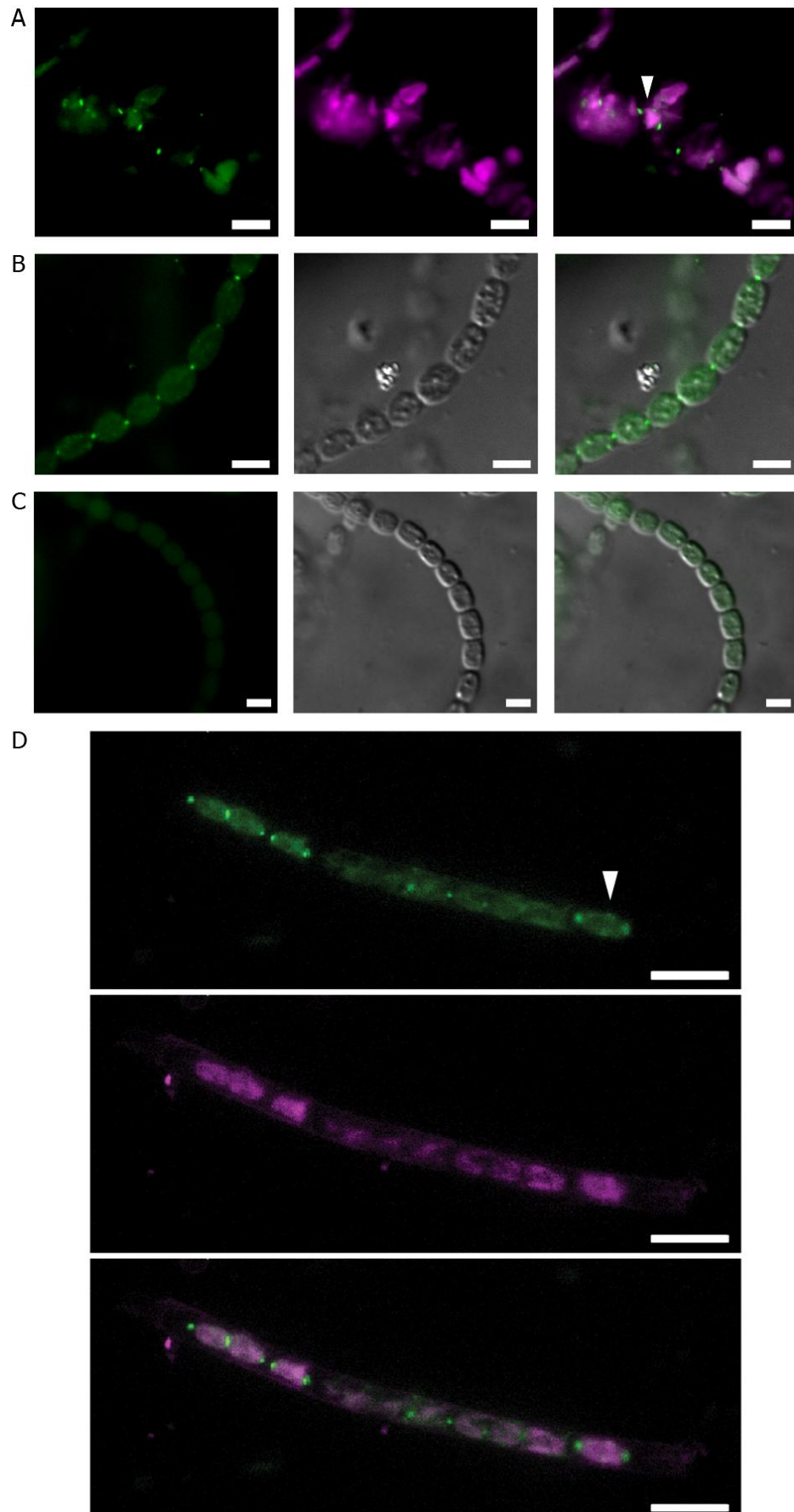


Figure 55. Localisation of SepJ by immunofluorescent labelling in *M. laminosus*.

Figure 55

SepJ is localised in distinct spots at the septa between two adjacent vegetative cells (A, B, D). A control experiment without incubation with the primary antibody (anti-SepJ) shows no fluorescent spots at the septum between cells (B). A branching point shows three distinct regions where SepJ is present (A; arrow). During cell division SepJ forms a ring at the division plane (D; arrow). The images show SepJ immunolabelling (green), autofluorescence (magenta), bright-field views (grey) and overlay images. Scale bars, 5 μm .

6.6 Generation and characterisation of a *sepJ* inactivation mutant of *M. laminosus*

To reveal further insights into the importance of *sepJ* for other cyanobacteria than *Anabaena* sp. PCC 7120 a *sepJ* inactivation mutant of *M. laminosus* was generated. Although it has been shown previously that foreign genes can be transferred into cyanobacteria of Section V (Flores and Wolk, 1985; Stucken *et al.*, 2012), a protocol for the generation of mutants by genome modification was lacking.

In order to introduce the resistance cassette into *sepJ*, a BamHI restriction site was generated within the gene by overlap PCR. DNA fragments of *sepJ* were amplified by PCR using primer fw_d_sepJ_ML_up_SpeI and rv_d_sepJ_ML_up_BamHI, and fw_d_sepJ_ML_down_BamHI and rv_d_sepJ_ML_down_PstI. Both products were used as DNA template for the overlap PCR with primers fw_d_sepJ_ML_up_SpeI and rv_d_sepJ_ML_down_PstI. The product was ligated into vector pRL271 (Black *et al.*, 1993) via SpeI and PstI, resulting in plasmid pDN40. In order to interrupt *sepJ* the kanamycin resistance cassette C.K1 from pRL161 (Elhai and Wolk, 1988a) was inserted in the BamHI restriction site of pDN40. The resulting vector pDN42 was transferred to *M. laminosus* by conjugation as described in the materials and methods section 2.4.6.2. The standard protocol normally used for plasmid transfer to

6 Morphological complexity and intercellular communication in *M. laminosus*

Anabaena sp. PCC 7120 was slightly modified by subjecting *M. laminosus* to homogenisation by several passages through a syringe needle and extensive washing with growth medium prior to conjugation. According to Stucken *et al.* (2012) an important step in transferring DNA to cyanobacteria of Section V is the partial removal of the exopolysaccharide sheath by salt washing. However, this was not the case for *M. laminosus*: salt washing did not lead to a higher conjugation frequency. In this study *M. laminosus* cultures were transferred from a resting state into an active growing state by changing medium, agitation and temperature. As described above changes in growth conditions lead to branching and the formation of narrow trichomes with less exopolysaccharides which could account for the observed transfer efficiency without salt washing. However, it also needs to be considered that cyanobacteria of Section V show a high morphological and metabolic variability (Anagnostidis and Komárek, 1990) and thus thickness of the exopolysaccharide sheath could vary naturally between different species.

Mutant strain MLDN42 was generated using double-crossover recombination. Gene *sepJ* was interrupted by the neomycin resistance cassette C.K1 in opposite direction to the gene and inserted after the predicted coiled-coil domain of *sepJ* (Figure 56A,B). A homologous region of 600 to 700 bp on each side of the desired position of insertion was sufficient to integrate the resistance cassette into the genome of *M. laminosus*. However, several attempts using single-crossover recombination to interrupt *sepJ* in *M. laminosus* failed. PCR with primers binding to sequences outside the inserted region confirmed that mutant MLDN42 was fully segregated, and hence no amplified product of the size of the wild type was present in MLDN42 (Figure 56C). The final verification by sequencing confirmed the correct position and sequence of the resistance cassette C.K1 in MLDN42.

6 Morphological complexity and intercellular communication in *M. laminosus*

Although a mutant of *M. laminosus* could be successfully generated in this work it is notable that the efficiency was quite low with approximately only one colony per 3 μg of chlorophyll *a*. It is likely that DNA is degraded by specific restriction endonucleases that are present in *Mastigocladus* spp. and *Fischerella* spp. (Duyvesteyn and de Waard, 1980; Lyra *et al.*, 2000; Stucken *et al.*, 2012). Identification and characterisation of these enzymes could help to design plasmids for the methylation of specific restriction sites and thus increase efficiency of transformation.

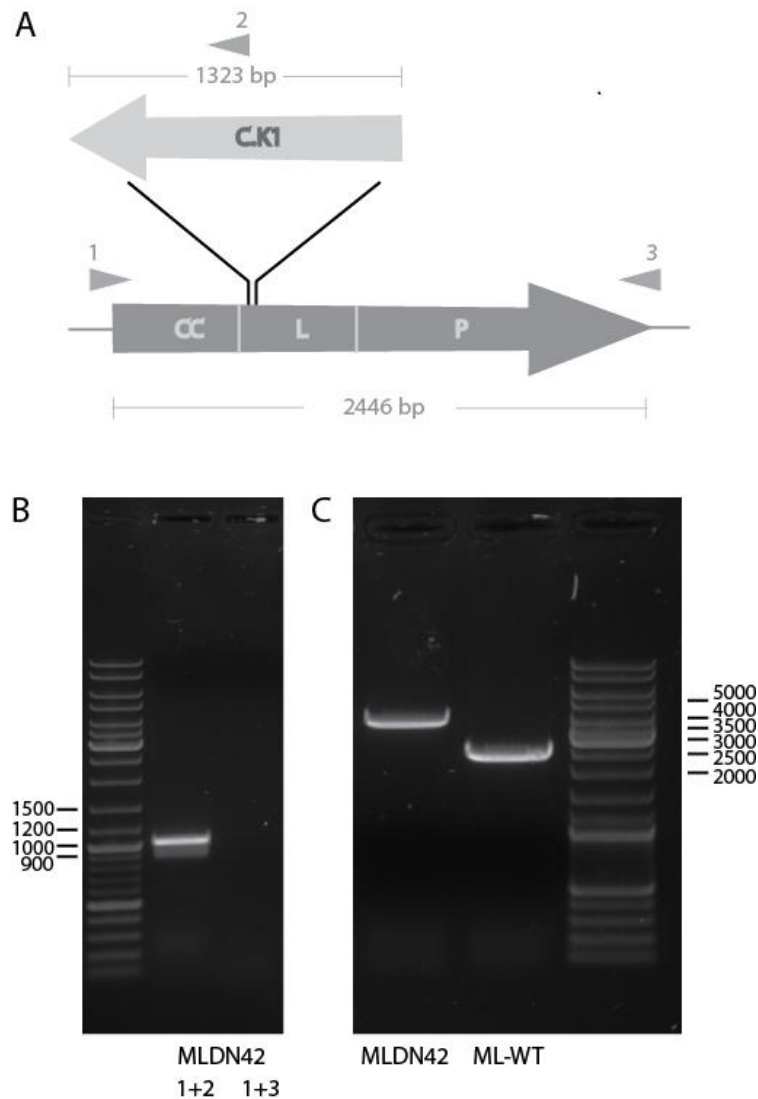


Figure 56. Generation and verification of the *sepJ* inactivation mutant MLDN42.

Figure 56

(A) Scheme of the final genetic construct. The C.K1 cassette bearing the neomycin transferase gene was inserted into the *sepJ* gene of *M. laminosus* in opposite direction after the coiled-coil domain (CC) encoding region of *sepJ*. Further domains of SepJ are the linker region (L) and the permease domain (P). (B) Orientation of the C.K1 cassette in MLDN42 confirmed by PCR using primers fw_mlam_sepJ (1), fw_neo (2) and rv_mlam_sepJ_seq (3). A PCR product was only obtained when using primers fw_mlam_sepJ and fw_neo (1+2) but not with primers fw_neo and rv_mlam_sepJ_seq (2+3). (C) Confirmation of full segregation of MLDN42. The amplified product from the genomic DNA of MLDN42 with primers binding outside the modified genomic region (fw_mlam_sepJ (1) and rv_mlam_sepJ_seq (3)) is ca. 1300 bp bigger than the product amplified from the genomic wild type DNA (ML-WT), corresponding to the length of the C.K1 cassette. C. Orientation of the C.K1 cassette in MLDN42 confirmed by PCR using primers fw_mlam_sepJ (1), fw_neo (2) and rv_mlam_sepJ_seq (3). A PCR product was only obtained when using primers fw_mlam_sepJ and fw_neo (1+2) but not with primers fw_neo and rv_mlam_sepJ_seq (2+3).

6.7 Characterisation of the *sepJ* inactivation mutant MLDN42

It has been shown earlier that SepJ in *Anabaena* sp. PCC 7120 is not only important for molecular communication between cells (Mullineaux *et al.*, 2008; Mariscal *et al.*, 2011), but also for filament integrity and diazotrophic growth (Flores *et al.*, 2007; Nayar *et al.*, 2007; Mariscal *et al.*, 2011). Interestingly, MLDN42 shows full morphological complexity, forming not only different types of branches and hormogonia, but also heterocysts under nitrogen deprivation (Figure 57A). FRAP experiments using the fluorescent tracers 5-CFDA and calcein revealed that MLDN42 is capable of exchanging both molecules between vegetative cells in different filament types (exemplarily shown for calcein for cells within a narrow trichome in (Figure 57B). indicating that SepJ does not inhibit intercellular

6 Morphological complexity and intercellular communication in *M. laminosus*

communication of molecules with these properties. In conclusion, *sepJ* seems to be less important for filament integrity, diazotrophic growth and intercellular communication in *M. laminosus*: Mutant MLDN42 misses the phenotypic characteristics found in a $\Delta sepJ$ mutant of *Anabaena* sp. PCC 7120.

Considering that *M. laminosus* is closely related to *Fischerella* sp. PCC 7414 (Figure 54) which possesses a *sepJ* with a stop codon in the linker region (Dagan *et al.*, 2013) but does not show the classical $\Delta sepJ$ phenotype neither, it would be interesting to investigate the function of the coiled-coil domain in *Anabaena* sp. PCC 7120.

Furthermore, it is likely, that an important component for maintaining filament integrity in *M. laminosus* is its ability to form a thick surrounding sheath which is consistent with the observation that filaments with heterocysts do not tend to fragment under nitrogen deprivation as reported for *Anabaena* sp. PCC 7120. No single heterocysts or short filaments with terminal heterocysts were observed for cultures of *M. laminosus* after nitrogen step-down.

In this context, it is also interesting to investigate the role of the N-Acetylmuramyl-L-alanine amidases (Ami), in particular AmiC1 and AmiC2, which are important for filament integrity, heterocyst development and nanopore formation in *Nostoc punctiforme* ATCC 29133 and *Anabaena* sp. PCC 7120 (Lehner *et al.*, 2011; Berendt *et al.*, 2012; Lehner *et al.*, 2013; Maldener *et al.*, 2014). Whether these proteins have a similar function in *M. laminosus* has yet to be investigated.

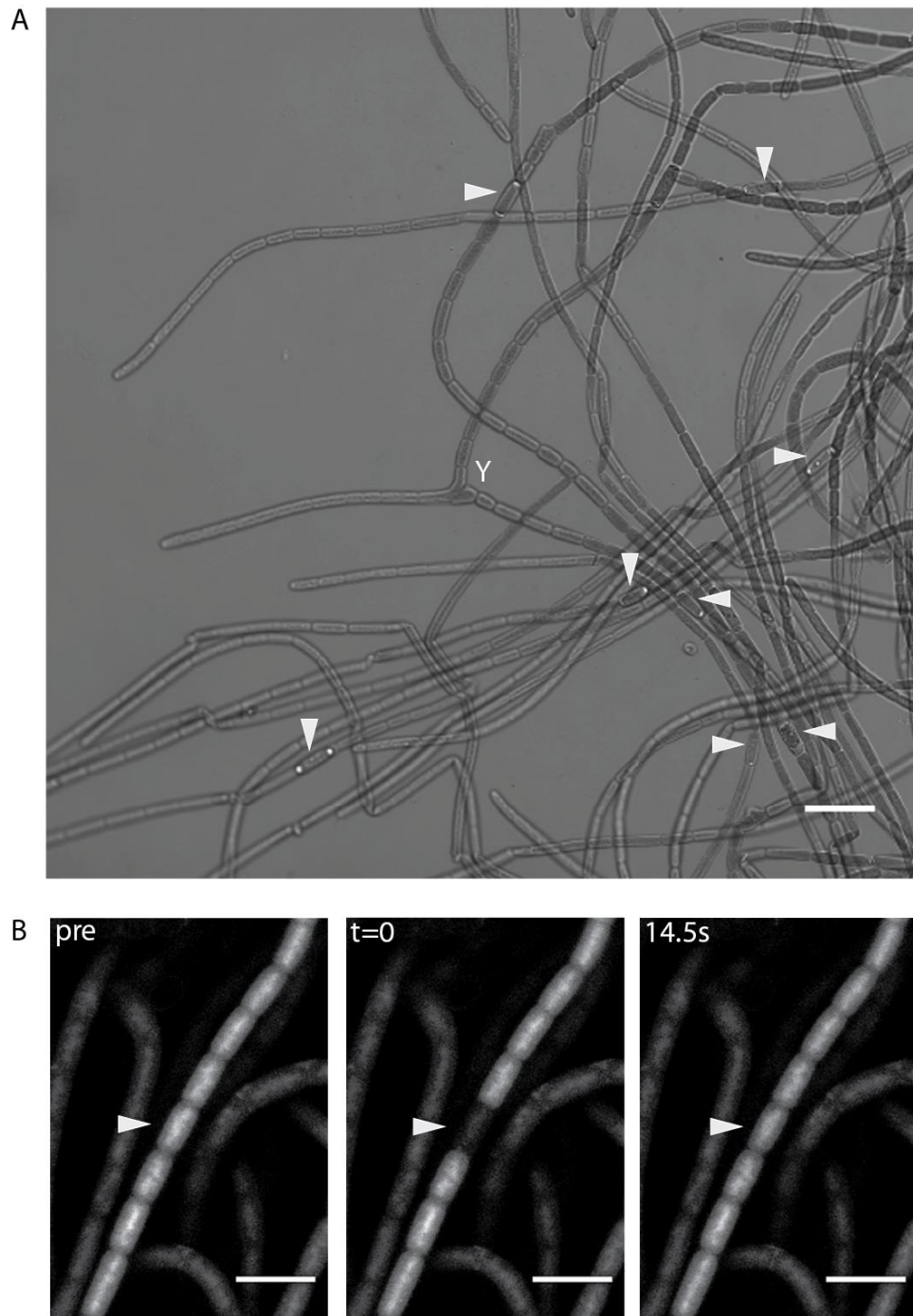


Figure 57. Characterisation of mutant MLDN42.

(A) Bright-field microscopy of MLDN42 grown in Castenholz ND medium. MLDN42 shows full morphological complexity under nitrogen deprivation, forming branches, e.g. a (reverse) ‘Y’-branch (Y), and heterocysts (arrow). Scale bar, 10 μm . (B) Calcein FRAP measurement on trichomes of MLDN42. The left image was recorded prior to bleaching (pre). After bleaching out fluorescence of a cell ($t = 0$), recovery was followed over 24 s. The region of interest is indicated with a white arrow. Scale bars, 5 μm .

6.8 Intercellular communication between cells of different trichome types in *M. laminosus*

While branches formed of long, narrow, cylindrical cells, main trichomes consist of large, rounded-up cells (e.g. Schwabe, 1960; Nierzwicki *et al.*, 1982). Although cells in branch and main trichomes show distinct differences in their cell shape, their ultrastructure is similar, varying mainly in the number of carboxysomes and peripherally located lipid bodies. Wide cells possess a higher number of these inclusions than narrow cells (Nierzwicki *et al.*, 1982; Nierzwicki-Bauer *et al.*, 1984b), and it has been suggested that they might be functionally active rather than being in a resting state (Balkwill *et al.*, 1984). To gain further information about the possible function of these different morphotypes, molecular exchange of 5-CFDA was investigated by FRAP experiments. A parameter to quantify the kinetics of dye exchange between cells is the ‘exchange coefficient’ (E), which can be calculated as previously described (Mullineaux *et al.*, 2008). E has units of s^{-1} and relates the rate of molecular flux between adjacent cells to the difference in dye concentration between the cells. However, E is not the best parameter to use for making comparisons of the connectivity of morphotypes with significantly different cell volumes, because the concentration changes resulting from flux of molecules across the cell junction depend on cell volume as well as the flux across the junction. Therefore a new parameter, the ‘flux coefficient’ F, defined as (E x cell volume), with units of $\mu m^3 s^{-1}$ was introduced. F corrects for the influence of cell volume on E, to give a value that allows comparison of molecular exchange activity at junctions between different morphotypes.

6 Morphological complexity and intercellular communication in *M. laminosus*

To take the influence of the high degree of cell polymorphism in *M. laminosus* on the cell volume into account, four different geometrical shapes, including cylinder, prolate spheroid, sphere, and oblate spheroid were chosen. While cylindrical cells were considered to represent cells in narrow trichomes, both spherical and spheroidal cells were considered to represent cells of wide trichomes. Our results indicate that cells in narrow trichomes exhibit significantly higher E and F values than cells in wide trichomes (Table 25), suggesting that not only the change in concentration of molecules but also the flux of molecules between cells depends on the trichome type. The mechanism which leads to the significant decrease in communication between cells during the process of maturation from a narrow to a wide trichome remains to be investigated.

Table 25. Exchange (E) and flux coefficients (F) for 5-CFDA in *M. laminosus*.

measurement	mean E [s^{-1}] (\pm s.d.)	mean F [$\mu m^3 s^{-1}$] (\pm s.d.)
1. cells in narrow trichomes	0.159 ± 0.072	7.65 ± 5.19
2. cells in wide trichomes	0.058 ± 0.044	3.60 ± 2.47
3. cells in hormogonia	0.132 ± 0.063	3.14 ± 1.04

t-tests indicate that E and F are significantly different in (1) and (2) ($P < 0.00001$). Number of experiments performed for (1) 27, (2) 57, and (3) 9.

A high degree of cell-cell communication might be essential to ensure a sufficient supply of nutrients and regulators within a fast-growing narrow trichome. To investigate this hypothesis, further cell differentiation processes in *M. laminosus*, which are supposed to require cell-cell communication, including the formation of heterocysts and motile hormogonia were considered.

6 Morphological complexity and intercellular communication in *M. laminosus*

Nitrogen limitation stimulates extensive heterocyst differentiation in *M. laminosus*. Almost any vegetative cell can differentiate into a heterocyst (Nierzwicki-Bauer *et al.*, 1984b; Stevens *et al.*, 1985). Heterocysts can be distinguished from vegetative cells by their diminished pigmentation and the presence of cyanophycin plugs at the cell poles. Bright-field microscopy revealed that any cell in the branching region is capable of undergoing cell differentiation, resulting in the formation of heterocysts in the branching point of a 'T'-branch and a (reverse) 'Y'-branch (Figure 58A-D). The position of the cyanophycin plugs in these cells is notable. Heterocysts at the origin of a branch show three cyanophycin plugs, while neighbouring heterocysts in the branching region of 'T' and (reverse) 'Y'-branches only possess two cyanophycin plugs (Figure 58B,C). These microscopic observations support the previous FRAP results that *M. laminosus* forms a complex network of various trichome types, which exchange metabolites, including products of nitrogen and carbon fixation. The key function of the main trichomes might be to provide the basis for growth of the organism under favourable environmental conditions.

Earlier observations by Nierzwicki-Bauer *et al.* (1984a) that *M. laminosus* forms multiple contiguous heterocysts in the main trichomes under nitrogen deprivation support this hypothesis. Although the formation of multiple contiguous heterocysts was rarely observed in the main trichome of *M. laminosus* SAG 4.84, double heterocysts could be regularly found in the branches (Figure 58E). It is possible that the different heterocyst localisation is caused either by the altered growth conditions or the diversity of *Mastigocladus* spp. and *Fischerella* spp. strains in general, even a strain of *M. laminosus* Cohn has been described which lacks the ability to form heterocysts (Melick *et al.*, 1991). The formation of double heterocysts is again interesting with regard to the position of cyanophycin plugs. Each heterocyst shows

two cyanophycin plugs, resulting in a double cyanophycin plug between both heterocysts (Figure 58E).

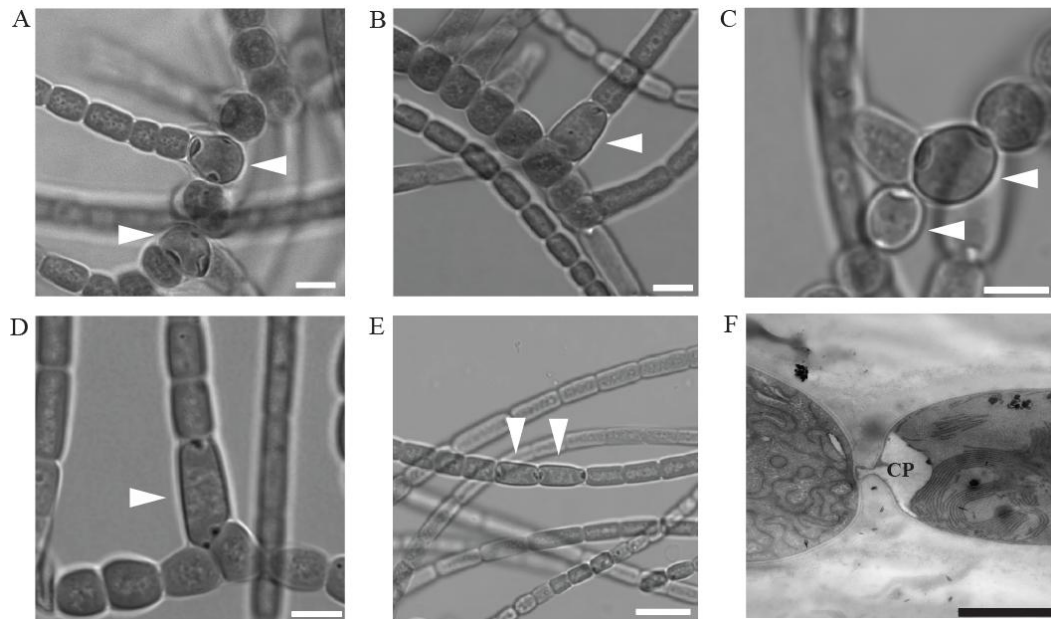


Figure 58. Position of heterocysts in filaments of *M. laminosus*.

(A-D) Heterocysts (arrows) can be found either in the branching start of ‘T’- (A) or (reverse) ‘Y’-branches (C), or in the new formed lateral branches (B and D, respectively). Note the position of cyanophycin granules in the heterocysts. They are always located close to cells they are connected with. Scale bars, 5 μm. (E) Double heterocyst in a narrow trichome of *M. laminosus* (arrows). Cyanophycin granules are located at each pole of the cell, resulting in two cyanophycin plugs between two heterocysts. Scale bar, 10 μm. (F) Electron micrograph of an ultra-thin section of a heterocyst in *M. laminosus*. A cyanophycin plug (CP) is present in the neck region. Rearrangements of thylakoid membranes are visible. The sample was prepared using the KMnO_4 method. Scale bar, 1 μm.

To characterise the heterocyst-heterocyst connection further the fluorescent dye FM1-43FX was used to highlight the cytoplasmic membrane (Schneider *et al.*, 2007). Confocal images indicate that both heterocysts are connected via two neck regions (Figure 59).

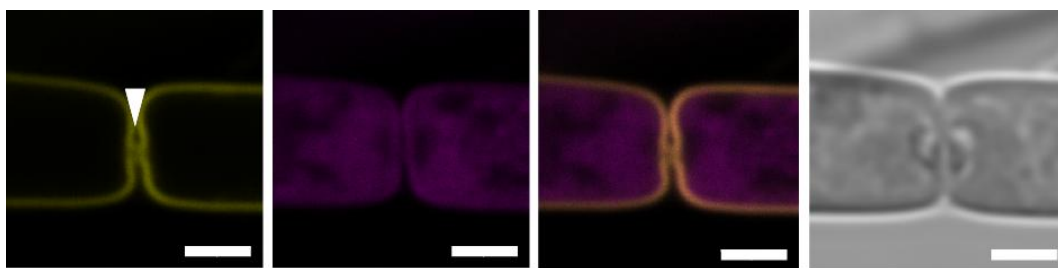


Figure 59. Heterocyst-heterocyst connection in a narrow trichome of *M. laminosus*.

Adjacent heterocysts are connected via two neck regions (arrow). The images show FM1-43 FX fluorescence (yellow), autofluorescence (magenta), an overlay of both fluorescent images, and the bright field view (grey). Scale bars, 2 μm .

Another important stage in the life cycle of *M. laminosus* is the formation of hormogonia, motile filaments which glide slowly away from the parental filament, before finally differentiating into a sedentary wide trichome and forming a new colony (Hernandez-Muniz and Stevens, 1987; Robinson *et al.*, 2007). Hormogonia show a high variability in surface velocity, which differs not only between hormogonia but also for the same hormogonium over time, and a high variability in the directions they move (Hernandez-Muniz and Stevens, 1987). Their ability to reverse the direction of gliding (Hernandez-Muniz and Stevens, 1987) suggests a high degree of cell-cell communication. In order to determine the exchange and flux coefficient for hormogonia the cell dimensions of a moving hormogonium were measured and correlated to the tracer exchange data represented earlier. This ensures that also hormogonia are considered which were not moving during the FRAP experiments. As hormogonia are formed by cell division without biomass increase, they can be distinguished from other filament types by their distinctly smaller cell size (Campbell and Meeks, 1989). Accordingly, hormogonia of *M. laminosus* were defined by cell diameter, cell length, and the diameter to length ratio, resulting in a group of cells characterised by an average cell diameter of $2.76 \pm 0.31 \mu\text{m}$, an

6 Morphological complexity and intercellular communication in *M. laminosus* average cell length of $3.61 \pm 0.88 \mu\text{m}$, and a diameter to length ratio of 0.80 ± 0.19 ($n = 80$). While the mean exchange coefficient E is similar to that found between cells in narrow trichomes ($E = 0.159 \pm 0.072 \text{ s}^{-1}$) and meets the expectation that cellular communication is fast in hormogonia, the flux coefficient F is significantly lower, showing a value similar to that found in wide trichomes ($F = 3.60 \pm 2.47 \mu\text{m}^3 \text{ s}^{-1}$) (Table 25). Therefore communication between cells in hormogonia is rapid in the sense that intercellular diffusion of molecules is fast enough to lead to rapid changes in the cytoplasmic concentration of putative signalling molecules. However, as compared to cells in the parental filament, this rapid communication is achieved by reducing the cell volume rather than by accelerating the flux of molecules across the cell junctions. Therefore signal transduction to coordinate movement (and possibly other aspects of the biology) of hormogonia is probably accelerated by the reduction of the cell volume rather than by increased flux of signalling molecules across the cell junctions.

6.9 Barriers to cell-cell communication in the life cycle of *M.*

laminosus

The release of a hormogonium from its parental trichome is mediated by the formation of releasing, dead cells, called necridia, which are possibly best studied in *Oscillatoria/Microcoleus* spp. (Kohl, 1903; Lamont, 1969; Brown *et al.*, 2010). Beside heterocysts (Meeks *et al.*, 2002), necridia are one of the few known developmental ‘dead ends’ among prokaryotes, and can be seen as a basic form of programmed cell death (apoptosis). Since a necridium can be found early after the branching event in the growing narrow trichome (Figure 60A-C), it was investigated whether exchange of molecules is still possible between the branch and the main

6 Morphological complexity and intercellular communication in *M. laminosus*

trichome. After loading the fluorescent tracer 5-CFDA into the cytoplasm, the fluorescence of the part of the branch which was separated by the necridium was bleached out and its change in fluorescence intensity recorded (Figure 60A). The bleached region did not show any recovery within 24 s (Figure 60A) indicating that a necridium inhibits cell-cell communication completely. Accordingly, the fate of a trichome is determined early after branch formation; molecular exchange not being possible once a necridium is formed.

To get an impression of the complexity of this event and its importance for the filamentous network, the position of necridium formation was explored. Necridia can be easily detected by enhanced red fluorescence in the region of formation, possibly as a result of degradation of the photosynthetic apparatus (Figure 60B-D, Figure 61A). Necridia also show brighter staining with the membrane dye FM1-43FX (Figure 60B-D), probably because leakiness of the cytoplasmic membrane allows the dye to penetrate to the interior of the cell. Necridia are not only located in the branching point, as reported in an earlier study (Balkwill *et al.*, 1984), but also in various other positions within narrow trichomes, such as the beginning of the recently formed branch (Figure 60C), indicating that almost any cell within a filament can differentiate into a necridium. Even within the same filament several necridia can be found, contiguous or separated only by a single cell (Figure 60D), suggesting that necridia formation in *M. laminosus* seems to follow no regular pattern of spacing and distribution.

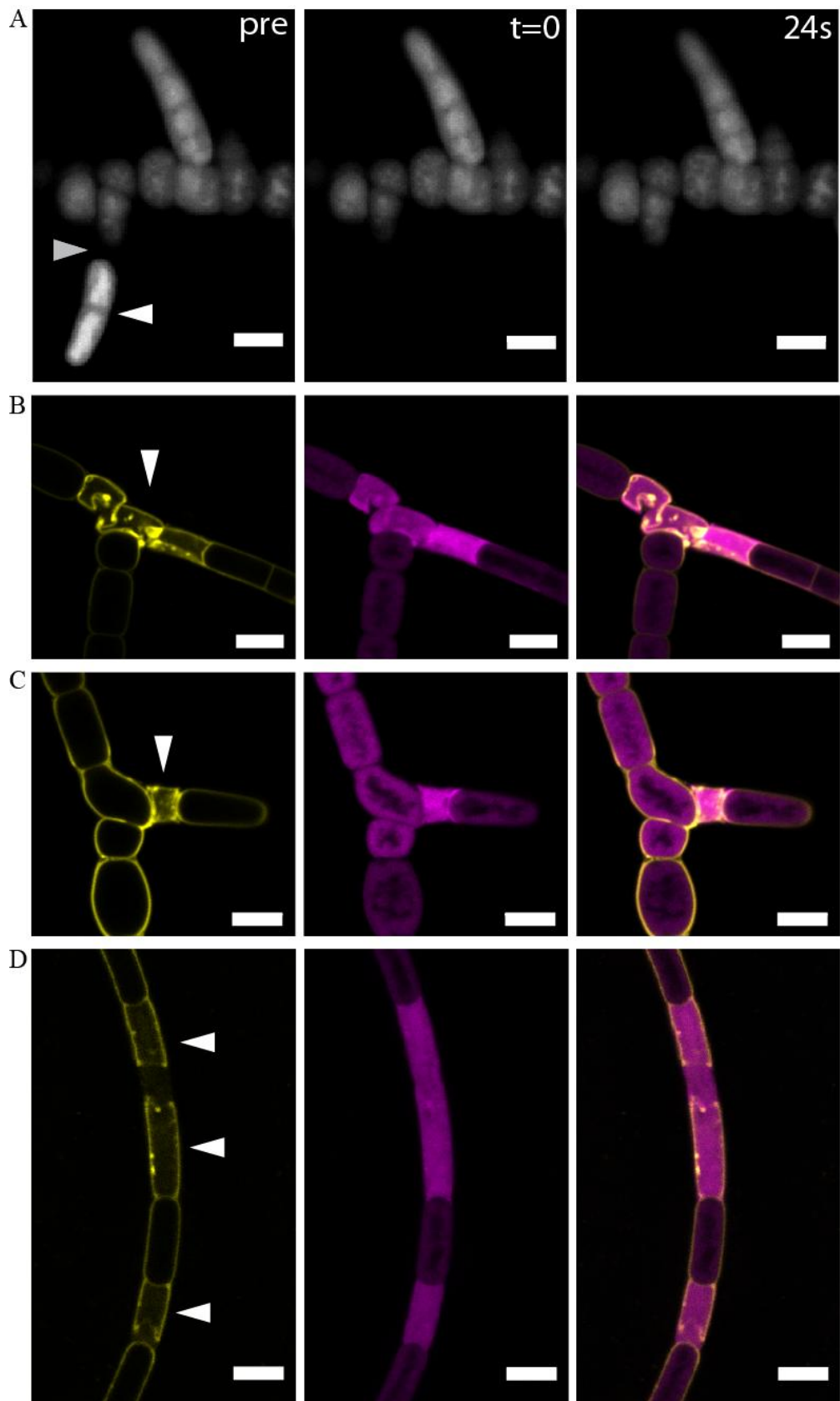


Figure 60. Function of necridia in intercellular communication, and their localisation in filaments of *M. laminosus*.

Figure 60

(A) FRAP image sequence of 5-CFDA loaded cells. Intercellular transfer is inhibited between main trichome and branch by the formation necridium (grey arrow). The left image was recorded prior to bleaching (pre). After bleaching out fluorescence in the branch ($t = 0$), recovery was followed over 24 s. The ROI is indicated with a white arrow. Scale bars, 5 μm . (B-D) Position of necridia and reorganisation of membranes in filaments of *M. laminosus*. Necridia (arrows) can be found in the branching start (B), at the beginning of a recently formed branch (C), or at various positions within a narrow trichome (D). Their position follows no regular pattern. Two necridia can be even found in a single filament, separated only by one vegetative cell (D). The images show FM1-43 FX fluorescence (yellow; left), autofluorescence (magenta, middle) and an overlay of both (right). Scale bars, 5 μm .

The final release involves remodelling the septal region on both sides of the necridium. To avoid cell death of the entire cellular network by efflux of molecules, the membranes of the neighbouring cells have to stay intact, and the channels must be closed (see chapter 5). Electron micrographs confirm that the plasma membrane and outer membrane are sealed at the terminal cell (Figure 60B). Although it was observed that necridia usually consist only of a single cell, they can be formed by two cells (Figure 60B,D). A possible mechanism to prevent efflux of molecules in other cyanobacteria, e.g. *Symploca muscorum* and *M. vaginatus* might be by the synthesis of an additional cell wall layer at the new terminus ('calyptra'; Pankratz and Bowen, 1963; Lamont, 1969). It remains to be investigated whether this structure also exists in *M. laminosus*.

Filament breakage, however, is only possible by the disintegration of the membranes of the necridium. To investigate this process the cytoplasmic membrane stain FM1-43FX (Figure 60B-D) and the DNA stain Hoechst 33258 (Figure 61A) were used. The fluorescence micrographs indicate that during necridium formation the

6 Morphological complexity and intercellular communication in *M. laminosus*

cytoplasmic membrane of the necridium deteriorates mainly from one terminus of the cell (Figure 61B-D), leaving an ‘open’ and empty (DNA-free) cell attached to the released filament (Figure 61), while only a small part of membranes remains at the terminus of the parental filament.

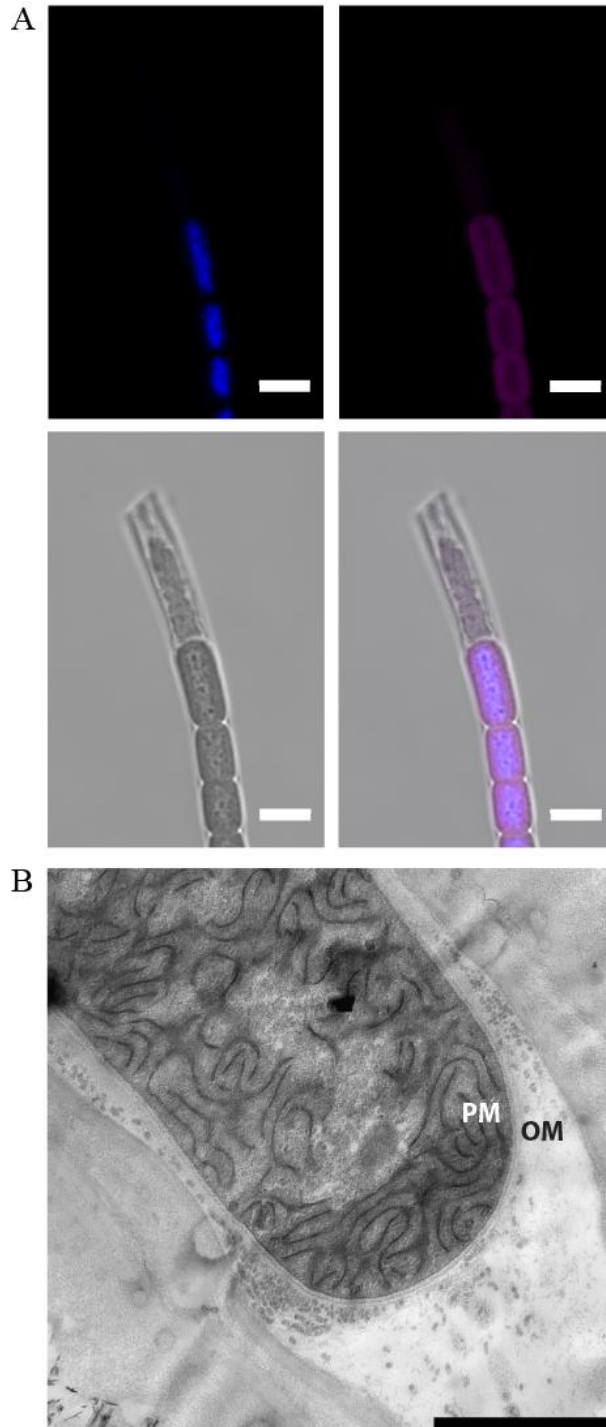


Figure 61. Appearance of necridia after filament release.

Figure 61

(A) Localisation of DNA in a hormogonium of *M. laminosus*. DNA was visualised by staining cells with Hoechst 33258 (blue). Autofluorescence is shown in magenta. An overlay with the bright-field image illustrates the position of DNA in the hormogonium, while a dead part remains at the end of the released filament (arrow). Scale bars, 5µm. (B) Electron micrograph of an ultra-thin section of a branch terminus after filament breakage via necridium formation. Note that plasma membrane (PM) and outer membrane (OM) are sealed at the terminal cell to prevent cell death by molecule efflux. The sample was prepared with the method based on KMnO₄. Scale bar, 1 µm.

6.10 Conclusion

M. laminosus forms a complex cellular network, in which the main trichome and branches communicate via intercellular connections which resemble septal junction complexes. Furthermore, FRAP measurements revealed that exchange between cells within a culture is regulated, depending on cell morphology. Young, narrow trichomes exhibited faster exchange rates among cells than older, wider trichomes showed reduced rates. Accordingly, wide trichomes might not only provide a platform for the outgrowth of branches, but they might also support the growth of branches by supplying metabolites in the presence and absence of a combined nitrogen source. Under nitrogen deprivation heterocysts can be found frequently in the branching region, sometimes even in the branching start, forming a heterocyst with three cyanophycin plugs. The integrity of the filament network is only interrupted by the formation of necridia, which inhibit further molecular exchange, and, hence, determining the fate of a developing branch, likely to become a hormogonium, early after the branching event. Interestingly, signal transduction to coordinate movement of the released hormogonia might be accelerated by the reduction in cell volume.

6 Morphological complexity and intercellular communication in *M. laminosus*

Cell differentiation seems to be generally less regulated than in Section IV cyanobacteria; the formation of heterocysts (Nierzwicki-Bauer *et al.*, 1984a; Nierzwicki-Bauer *et al.*, 1984b; Stevens *et al.*, 1985) and necridia (this work) seem to follow no regular spacing and distribution pattern. The analyses of different types of branches also suggest a degree of randomness in cell development, leading to the hypothesis that ‘T’ and (reverse) ‘Y’ branches are basically equivalent: the different forms simply result from loose control of the positioning of the cell elongation machinery.

As a possible component of the cell-cell connecting structures SepJ was identified in *M. laminosus*. The protein consists of the typical three domain architecture found in other filamentous, heterocyst-forming cyanobacteria such as *Anabaena* sp. PCC 7120 (Section IV), and immunofluorescence labelling revealed its localisation at the septa. A cell in the branching point exhibits three SepJ spots, suggesting that although *M. laminosus* shows branching, the septa are similar to those described in *Anabaena* sp. PCC 7120. However, SepJ seems to be less important for filament integrity, intercellular communication and diazotrophic growth in *M. laminosus* as a generated *sepJ* inactivation mutant did not show the phenotype observed in *Anabaena* sp. PCC 7120.

Earlier studies had suggested that rounded cells in wide trichomes seem to be completely separated by their surrounding sheath (Thurston and Ingram, 1971; Martin and Wyatt, 1974; Nierzwicki *et al.*, 1982) which would imply a lack of communication between these cells. According to ultrastructural and FRAP analyses this is however not the case. *M. laminosus* shows intercellular communication and highly-structured cell junctions between cells of various shapes, forming a complex network of cell communication. The hypothesis that cyanobacteria of Section V

6 Morphological complexity and intercellular communication in *M. laminosus* represent a primitive and basic form linking coccoid and filamentous forms (Martin and Wyatt, 1974), is not supported by this study. Overall, the presented results from cell division and intercellular communication experiments indicate that Section V cyanobacteria are similar to cyanobacteria of Section IV, but show the highest degree of morphological complexity and diversity within the phylum.

7 Summary and outlook

Development of true multicellularity involves three major and mutually-dependent processes: cell-cell adhesion, intercellular communication and cell differentiation (Flores and Herrero, 2010). This study focussed on investigating intercellular communication in the well-established model organism of Section IV cyanobacteria, *Anabaena* sp. PCC 7120 (chapter 3-5) and the Section V cyanobacterium, *Mastigocladus laminosus* (chapter 6).

When cells of *Anabaena* sp. PCC 7120 and *M. laminosus* are deprived of combined nitrogen, photosynthetically-active vegetative cells differentiate into nitrogen-fixing heterocysts, making intercellular communication essential for maintaining filament viability. This study revealed that molecular exchange in both organisms occurs mainly via septal junctions, connecting the cytoplasm of neighbouring cells (chapter 3 and 6). FRAP experiments on filaments of *Anabaena* sp. PCC 7120 showed that a range of fluorescent molecules is cytoplasmically exchanged between vegetative cells and heterocysts, including the fluorophores calcein (Mullineaux *et al.*, 2008; Mariscal *et al.*, 2011; chapter 3.3 and 4.3.1), BCECF (chapter 3.3), 5-CFDA (Merino-Puerto *et al.*, 2010; Mariscal *et al.*, 2011; Merino-Puerto *et al.*, 2011b; chapter 3.3 and 4.3.1), 2- and 6-NBDG (chapter 3.2) and esculin (chapter 3.1). However, it cannot be excluded at this stage that a fraction of molecules diffuses from cell to cell via a continuous periplasm (Flores *et al.*, 2006; Mariscal *et al.*, 2007). Further studies using fluorescent tracers, specifically located to the periplasmic space, are required to resolve the question of periplasmic transport.

For the first time transfer of physiologically-important molecules was shown. In contrast to the ‘artificial’ fluorescein variants, calcein, 5-CFDA and BCECF, uptake of the fluorescent sucrose analogue esculin and the fluorescent glucose derivatives 2- and 6-NBDG is mediated by specific transporters. Addition of sucrose reduces the rate of esculin uptake, while import of glucose-derivatives was increased by expressing genes from *Nostoc punctiforme* ATCC 29133, encoding the glucose permease GlcP (Npun_R5323) and the OprB-like porin Npun_R5320 in *Anabaena* sp. PCC 7120. These results support earlier studies, suggesting the importance of sucrose and glucose as carbon carriers (Haury and Spiller, 1981; Jüttner, 1983; Schilling and Ehrnsperger, 1985; Wolk *et al.*, 1994; Curatti *et al.*, 2002; Cumino *et al.*, 2007; Marcozzi *et al.*, 2009; López-Igual *et al.*, 2010; Vargas *et al.*, 2011). Whether fructose is additionally transferred between cells as suggested by Haury and Spiller (1981) and Jüttner (1983) remains to be investigated. This question could be addressed by using the fluorescent fructose variant 1-NBDF which has been introduced to label breast cancer cells (Levi *et al.*, 2007). Although it has been shown recently that *Anabaena* sp. PCC 7120 grows chemo-organoheterotrophically in the presence of high concentrations of fructose (Stebegg *et al.*, 2012), using an *Anabaena* sp. PCC 7120 mutant that expresses the *frtRABC* genes from *A. variabilis* ATCC 29413 might be more efficient as fructose uptake occurs at much higher level in this strain than in the wild-type (Ungerer *et al.*, 2008).

Further studies should also investigate which metabolites function as nitrogen carriers. It has been suggested that ammonia or a substance derived from it such as glutamine (Fogg, 1949; Wolk *et al.*, 1976; Thomas *et al.*, 1977) and the amino acids which form the storage compound cyanophycin, i.e. aspartate, arginine, or its smallest subunit β -aspartyl-arginine (Carr, 1988; Richter *et al.*, 1999; Ke and

Haselkorn, 2013; Burnat *et al.*, 2014) are transferred between heterocysts and vegetative cells in *Anabaena* spp. Fusing arginine, aspartic acid or β -aspartyl-arginine to a fluorescent tag such as NBD (nitrobenzoxadiazole) could not only reveal insights into the role of these molecules in intercellular communication but also into their function in the metabolism of cyanophycin. Although it has been shown for *Anabaena* sp. PCC 7120 that aspartic acid and arginine are taken up by specific transporters (Pernil *et al.*, 2008), it remains unknown whether the fluorescent amino acids are taken up by the same transporters or whether *Anabaena* sp. PCC 7120 possesses a specific transporter for β -aspartyl-arginine.

But intercellular communication in *Anabaena* sp. PCC 7120 requires not only exchange of nutritional compounds. In order to establish the regular heterocyst spacing pattern, regulators need to be transferred between cells. It has been suggested that the spacing pattern is a result of periodic concentration gradients of an inhibitor along the filament that allows heterocyst formation only at the position of the lowest concentration (Fogg, 1949). In *Anabaena* sp. PCC 7120 this inhibitor is likely to be the product of the gene *patS* (Yoon and Golden, 1998). Although *patS* encodes a polypeptide of 17 amino acids (Corrales-Guerrero *et al.*, 2013), a shortened PatS variant of 5 C-terminal amino acids (RGSGR (PatS5)) is sufficient to inhibit heterocyst differentiation when added to the growth medium (Yoon and Golden, 1998; Huang *et al.*, 2004; Wu *et al.*, 2004). Recent immunofluorescence localisation studies by Corrales-Guerrero *et al.* (2013) showed that RGSGR-containing peptides such as PatS accumulate in cells adjacent to the differentiating proheterocysts, suggesting that these peptides are transferred between cells. However, direct transfer of the potential inhibitor has not been visualised yet. In collaboration with Prof Jason Micklefield, Dr Anna-Winona Struck and Matthew Bennett I was able to undertake a

preliminary study using a fluorescent-labelled version of PatS5 which is shown in this chapter due to its preliminary nature. In our approach an NBD-molecule was attached to the N-terminus of the pentapeptide, generating the fluorophore NBD-PatS5. Confocal microscopy revealed that the fluorescent pentapeptide is incorporated into the cytoplasm of *Anabaena* sp. PCC 7120 filaments (Figure 62A,B) and FRAP experiments confirmed that NBD-PatS5 diffuses cytoplasmically between vegetative cells (Figure 62C).

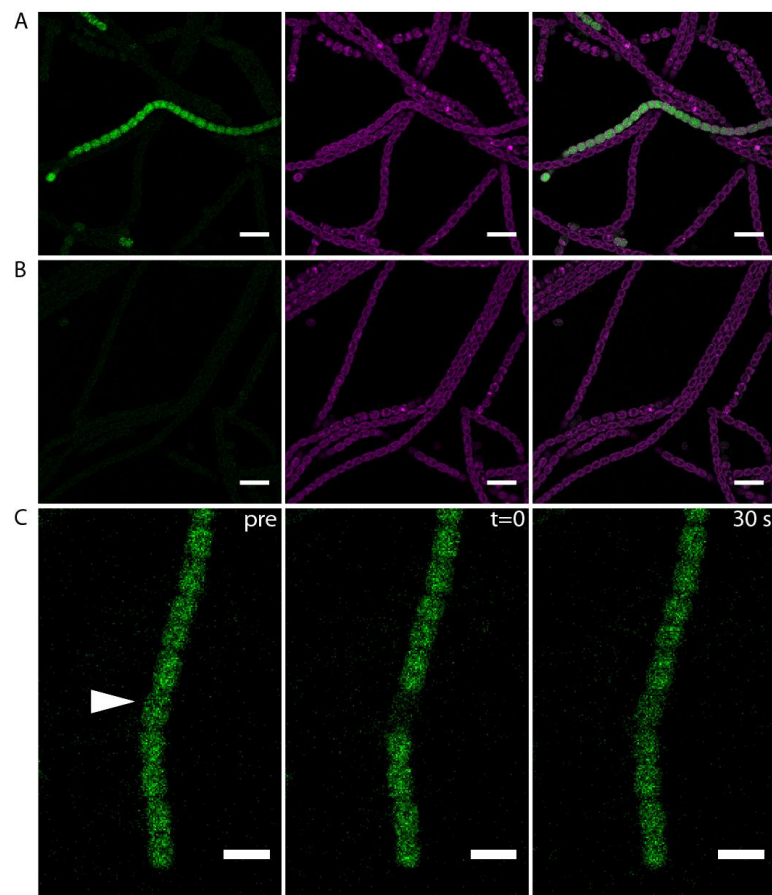


Figure 62. Uptake and diffusion of NBD-PatS5 in *Anabaena* sp. PCC 7120 grown in BG11.

(A) Uptake of NBD-PatS5. Filaments were incubated for 30 min with NBD-PatS5 and visualised by confocal microscopy using an excitation wavelength of 476 nm and an emission range of 520-540 nm for detection. Images show NBD-PatS5 fluorescence (green), chlorophyll fluorescence (magenta) and overlays. Control with unlabeled cells is shown in (B). (C) FRAP time-series. NBD-PatS5 fluorescence

prior to the bleach (pre), immediately after bleaching out fluorescence in the highlighted cell ($t = 0$), and 30 s later. Scale bars, 5 μm .

To test whether attaching the NBD molecule to PatS5 influences its physiological function, NBD-PatS5 was added to *Anabaena* sp. PCC 7120 cultures after nitrogen step-down. While the control culture (same culture without NBD-PatS5) showed fully developed heterocysts after 36 h of incubation (Figure 63A), no heterocysts were observed after adding NBD-PatS5 (Figure 63B) or PatS5 (Figure 63C). Thus, NBD-PatS5 is considered as functional.

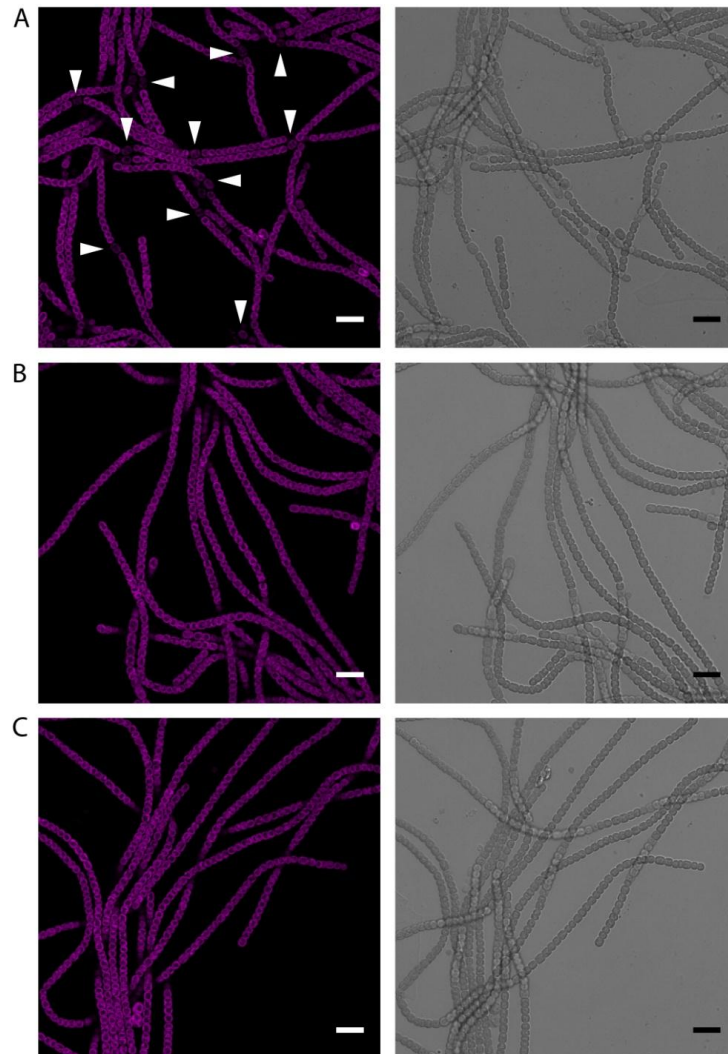


Figure 63. Physiological importance of NBD-PatS-5.

Under nitrogen deprivation *Anabaena* sp. PCC 7120 forms mature heterocysts within 36 h after nitrogen deprivation (A). Addition of 5 μ M NBD-PatS-5 (B) and 5 μ M PatS-5 (C) inhibit heterocyst formation in the absence of a combined nitrogen source. Scale bars, 10 μ m.

Further FRAP experiments are required to quantitate the rate of molecular exchange between vegetative cells and between vegetative cells and heterocysts. In addition, the influence of the septal proteins SepJ, FraC and FraD could be tested by using the corresponding mutants for FRAP measurements. Although these experiments are preliminary, they show that molecules even bigger than calcein (730 Da in comparison to 622 Da) can be transferred between cells via septal junction complexes. However, the size exclusion limit for molecules in cyanobacteria remains to be determined.

The expansion of the range of molecular probes for intercellular communication described in this work, revealed insights into the selectivity of the septal junction complexes mediating transfer between cells in *Anabaena* sp. PCC 7120 (chapter 3). In the presence of a combined nitrogen source, charge and size are important properties of the transferred molecules. Calcein and BCECF exhibit significantly slower recovery rates than the smaller and less charged molecules 5-CFDA, 2-NBDG and esculin. When cultures of *Anabaena* sp. PCC 7120 are deprived of combined nitrogen, exchange of calcein increases significantly in comparison to conditions when a combined nitrogen source is present. As no significant differences were observed between plus and minus N conditions for the smaller but partly similar charged fluorophores BCECF, 5-CFDA, 2-NBDG and esculin, it is hypothesised that molecule size is the main property that affects diffusion between vegetative cells in the absence of combined nitrogen. Comparison of the recovery

rates of all tested molecules under minus N conditions reveals that the smallest molecule, esculin, is exchanged fastest between vegetative cells.

In *Anabaena* sp. PCC 7120 the septal proteins FraC, FraD and SepJ are important components mediating intercellular transfer of calcein and 5-CFDA (Mullineaux *et al.*, 2008; Mariscal *et al.*, 2011; Merino-Puerto *et al.*, 2011b). Comparison of all published FRAP data and data obtained in this study revealed that deletion of SepJ strongly impairs transfer of calcein (ca. 24 % of wild-type) while transfer of BCECF, 5-CFDA, 2-NBDG and esculin is reduced to a lesser extent (approximately 61 - 72 %), indicating that SepJ is a key protein for transfer of bigger molecules independent of their charge. Furthermore, overexpression of *sepJ* led to an increase of calcein transfer between vegetative cells and heterocysts and an altered heterocyst spacing pattern with more vegetative cells between two heterocysts (chapter 4). It is likely that the additional SepJ molecules allow faster diffusion of inhibitors such as PatS from heterocysts into neighbouring vegetative cells. FRAP experiments using NBD-PatS5 could clarify this question. Increasing the rate of molecular exchange between heterocysts and vegetative cells could also be an interesting possibility of enhancing the productivity of heterocysts as anaerobic cell factories, producing hydrogen and combined nitrogen.

Loss of FraC and FraD in *Anabaena* sp. PCC 7120 reduces transfer of all tested molecules dramatically with smaller and neutral molecules being less impaired in diffusion. Additional deletion of *sepJ* in this mutant does not reduce transfer of molecules further, suggesting that additional proteins are involved in mediating transfer between cells which remain to be identified. Overexpression studies of *fraC* and *fraD* might reveal further insights into the importance of both proteins for

intercellular communication and the formation of a regular heterocysts spacing pattern in *Anabaena* sp. PCC 7120.

Diffusion of all tested molecules into heterocysts was always much slower than between vegetative cells. Exchange of calcein, 5-CFDA and 2-NBDG remains at around 25 % while exchange of BCECF is slightly slower and exchange of esculin is slightly faster. According to Giddings and Staehelin (1978) the number of septal junctions is reduced between vegetative cells and heterocysts by 80 % which is in good agreement with the observed reduction of molecule transfer. As heterocysts are unable to undergo cell division, they represent one of the few developmental ‘dead ends’ among prokaryotes (Meeks *et al.*, 2002). To avoid death of the entire filament after death of a single heterocyst, the channels between vegetative cells and heterocysts need to be closed after the fragmentation event. A first indication that channel closure occurs, was given by the loss of intercellular transfer of esculin in a significant fraction of older heterocysts in *Anabaena* sp. PCC 7120 (chapter 3.1.5). Further studies using fragmented filaments and confocal microscopy revealed that 5-CFDA labelled filaments remained fluorescent after filament fragmentation by sonication and that SepJ is redistributed or degraded within 24 h after the fragmentation event (chapter 5). Thus, it is hypothesised that *Anabaena* sp. PCC 7120 exhibits mechanisms to regulate intercellular communication to avoid filament death.

Regulation of intercellular transfer was also observed in *M. laminosus* (chapter 6). Morphologically different filament types exhibit different rates of molecular exchange. Cells in young, narrow trichomes and hormogonia exhibited faster exchange rates than cells in older, wider trichomes. Although SepJ is present and

localised in distinct spots at the septa, the protein seems to be less important for cell differentiation, filament integrity and cell communication than in *Anabaena* sp. PCC 7120. A *sepJ* inactivation mutant did not show the phenotype observed for CSV34. Further experiments should investigate the role of FraC and FraD in *M. laminosus*. Inactivation mutants and localisation studies could give new insights into the importance of the proteins for cyanobacteria.

8 Appendix

Table 26. Distribution and composition of SepJ-like proteins and DME-family permeases among cyanobacteria (Nürnberg *et al.*, 2014).

	organism	Sequence length [aa]	no. of domains	pred. TMHs [#]	CC [§]	L ⁺	P
Section I	<i>Acaryochloris marina</i> MBIC11017 ^T	312	1	10			1
	<i>Acaryochloris marina</i> MBIC11017 ^T	291	1	10			1
	<i>Acaryochloris</i> sp. CCMEE 5410	315	1	11			1
	<i>Acaryochloris</i> sp. CCMEE 5410	291	1	10			1
	<i>Cyanothece</i> sp. PCC 7425	316	1	10			1
	<i>Dactylococcopsis salina</i> PCC 8305	305	1	10			1
	<i>Gloeocapsa</i> sp. PCC 7428	316	1	11			1
	<i>Halothece</i> sp. PCC 7418	312	1	10			1
	<i>Synechococcus</i> sp. PCC 7335	332	1	10			1
	<i>Synechocystis</i> sp. GT-S, PCC 6803	329	1	10			1
	<i>Synechocystis</i> sp. PCC 6803	329	1	10			1
	<i>Synechocystis</i> sp. PCC 6803, GT-I	329	1	10			1
	<i>Synechocystis</i> sp. PCC 6803, PCC-N	329	1	10			1
II	<i>Chroococcidiopsis thermalis</i> PCC 7203	321	1	10			1
	<i>Pleurocapsa</i> sp. PCC 7327	318	1	10			1
Section III	<i>Arthrospira maxima</i> CS-328	574	2	11	1		1
	<i>Arthrospira platensis</i> C1	574	2	11	1		1
	<i>Arthrospira platensis</i> NIES-39	566	2	10	1		1
	<i>Arthrospira platensis</i> Paraca	566	2	10	1		1
	<i>Arthrospira</i> sp. PCC 8005	574	2	11	1		1
	<i>Crinalium epipsammum</i> PCC 9333	560	2	10	1		1
	<i>Cyanobacterium</i> sp. JSC-1	642	3	10	1	1	1
<i>Cyanobacterium</i> sp. ESFC-1	566	2	10	1		1	

organism	Sequence length [aa]	no. of domains	pred. TMHs[#]	CC[§]	L⁺	P
<i>Cyanobacterium</i> sp. ESFC-1	573	2	11	1		1
<i>Geitlerinema</i> sp. PCC 7105	596	2	10	1		1
<i>Geitlerinema</i> sp. PCC 7407	317	1	10			1
<i>Geitlerinema</i> sp. PCC 7407	602	3	9	1	1	1
<i>Leptolyngbya boryana</i> PCC 6306	387	1	10			1
<i>Leptolyngbya</i> sp. PCC 6406	318	1	10			1
<i>Leptolyngbya</i> sp. PCC 6406	598	2	10	1		1
<i>Leptolyngbya</i> sp. PCC 7375	558	2	10	1		1
<i>Leptolyngbya</i> sp. PCC 7375	327	1	9			1
<i>Leptolyngbya</i> sp. PCC 7376	563	2	10	1		1
<i>Lyngbya</i> sp. CCY 8106	569	2	11	1		1
<i>Microcoleus chthonoplastes</i> PCC 7420	579	2	11	1		1
<i>Microcoleus</i> sp. PCC 7113	568	2	11	1		1
<i>Microcoleus</i> sp. PCC 7113	314	1	10			1
<i>Microcoleus vaginatus</i> FGP-2	592	2	10	1		1
<i>Nodosilinea nodulosa</i> PCC 7104	310	1	10			1
<i>Nodosilinea nodulosa</i> PCC 7104	627	3	9	1	1	1
<i>Oscillatoria acuminata</i> PCC 6304	613	3	9	1	1	1
<i>Oscillatoria acuminata</i> PCC 6304	330	1	10			1
<i>Oscillatoria formosa</i> PCC 6407	588	2	10	1		1
<i>Oscillatoria nigro-viridis</i> PCC 7112	591	2	10	1		1
<i>Oscillatoria</i> sp. PCC 10802	627	3	11	1	1	1
<i>Oscillatoria</i> sp. PCC 6506	588	2	10	1		1
<i>Oscillatoriales</i> sp. JSC-1	312	1	10			1
<i>Oscillatoriales</i> sp. JSC-1	642	3	10	1	1	1
<i>Oscillatoriales</i> sp. JSC-12	614	3	10	1	1	1
<i>Prochlorothrix hollandica</i> PCC 9006	199	1	4			1

organism	Sequence length [aa]	no. of domains	pred. TMHs[#]	CC[§]	L⁺	P
<i>Prochlorothrix hollandica</i> PCC 9006	624	3	9	1	1	1
<i>Pseudanabaena</i> sp. PCC 6802	555	2	10	1		1
<i>Pseudanabaena</i> sp. PCC 7367	565	2	10	1		1
<i>Pseudanabaena</i> sp. PCC 7429	348	1	10			1
<i>Pseudanabaena</i> sp. PCC 7429	584	2	11	1		1
<i>Spirulina major</i> PCC 6313	556	2	10	1		1
<i>Spirulina major</i> PCC 6313	314	1	10			1
<i>Spirulina subsalsa</i> PCC 9445	573	2	10	1		1
<i>Spirulina subsalsa</i> PCC 9445	588	2	9	1		1
<i>Trichodesmium erythraeum</i> IMS101	583	2	10	1		1
<i>Trichodesmium erythraeum</i> IMS101	315	1	10			1
<i>Anabaena cylindrica</i> PCC 7122	791	3	9	1	1	1
<i>Anabaena</i> sp. PCC 7108	770	3	9	1	1	1
<i>Anabaena variabilis</i> ATCC 29413	751	3	11	1	1	1
<i>Anabaena variabilis</i> ATCC 29413	316	1	10			1
<i>Calothrix desertica</i> PCC 7102	704	3	10	1	1	1
<i>Calothrix</i> sp. PCC 6303	628	3	10	1	1	1
<i>Calothrix</i> sp. PCC 7103	703	3	10	1	1	1
<i>Calothrix</i> sp. PCC 7507	301	1	10			1
<i>Calothrix</i> sp. PCC 7507	806	3	9	1	1	1
<i>Cylindrospermopsis raciborskii</i> CS-505	79	1	1			1
<i>Cylindrospermopsis raciborskii</i> CS-505	529	3	6	1	1	1
<i>Cylindrospermum stagnale</i> PCC 7417	847	3	9	1	1	1
<i>Microchaete</i> sp. PCC 7126	750	3	9	1	1	1
<i>Nodularia spumigena</i> CCY9414	853	3	9	1	1	1
<i>Nostoc azollae</i> 0708	728	3	9	1	1	1
<i>Nostoc punctiforme</i> PCC 73102	779	3	10	1	1	1

Section IV

organism	Sequence length [aa]	no. of domains	pred. TMHs [#]	CC [§]	L ⁺	P
<i>Nostoc</i> sp. PCC 7107	737	3	10	1	1	1
<i>Nostoc</i> sp. PCC 7120	751	3	11	1	1	1
<i>Nostoc</i> sp. PCC 7524	747	3	9	1	1	1
<i>Raphidiopsis brookii</i> D9	677	3	10	1	1	1
<i>Rivularia</i> sp. PCC 7116	634	3	10	1	1	1
<i>Scytonema hofmanni</i> PCC 7110	637	3	10	1	1	1
<i>Scytonema hofmanni</i> UTEX 2349	812	3	10	1	1	1
<i>Chlorogloeopsis fritschii</i> PCC 6912	633	3	10	1	1	1
<i>Chlorogloeopsis fritschii</i> PCC 9212	633	3	10	1	1	1
unidentified cyanobacterium PCC 7702	607	2	10	1		1
<i>Fischerella muscicola</i> PCC 73103	760	3	10	1	1	1
<i>Fischerella muscicola</i> PCC 7414	213	1*	0	1		
<i>Fischerella muscicola</i> PCC 7414	359	1	10			1
Section V <i>Fischerella</i> sp. JSC-11	650	3	10	1	1	1
<i>Fischerella</i> sp. PCC 9339	821	3	10	1	1	1
<i>Fischerella</i> sp. PCC 9431	818	3	10	1	1	1
<i>Fischerella</i> sp. PCC 9605	690	3	10	1	1	1
<i>Fischerella thermalis</i> PCC 7521	231	1*	0	1		
<i>Fischerella thermalis</i> PCC 7521	407	1	10			1
<i>Mastigocladopsis repens</i> PCC 10914	647	3	10	1	1	1
<i>Mastigocladus laminosus</i> SAG 4.84	699	3	11	1	1	1

* Sequences show a stop codon after the predicted CC domain. [#]Transmembrane helices (TMHs) were identified using the TMHMM server 2.0 (<http://www.cbs.dtu.dk/services/TMHMM/>). [§]Potential CC domains were identified using Coils/PCoils (<http://toolkit.tuebingen.mpg.de/pcoils>). ⁺Internal repeats were detected using TRUST (Szklarczyk and Heringa, 2004).

9 Bibliography

- Abràmoff MD, Magalhães PJ, Ram SJ** (2004) Image Processing with ImageJ. *Biophotonics Int* **11**: 36–42
- Altschul SF, Madden TL, Schäffer a a, Zhang J, Zhang Z, Miller W, Lipman DJ** (1997) Gapped BLAST and PSI-BLAST: a new generation of protein database search programs. *Nucl Acids Res* **25**: 3389–3402
- Anagnostidis K, Komárek J** (1990) Modern approach to the classification system of Cyanophytes. 5 - Stigonematales. *Algol Stud* **59**: 1–73
- Balkwill DL, Nierzwicki-Bauer SA, Stevens SEJ** (1984) Modes of cell division and branch formation in the morphogenesis of the cyanobacterium *Mastigocladus laminosus*. *J Gen Microbiol* **130**: 2079–2088
- Bauer CC, Buikema WJ, Black K, Haselkorn R** (1995) A short-filament mutant of *Anabaena* sp. strain PCC 7120 that fragments in nitrogen-deficient medium. *J Bacteriol* **177**: 1520–1526
- Bauersachs T, Compaoré J, Hopmans EC, Stal LJ, Schouten S, Sinnighe Damsté JS** (2009) Distribution of heterocyst glycolipids in cyanobacteria. *Phytochemistry* **70**: 2034–2039
- Bekker A, Holland HD, Wang P-L, Rumble D, Stein HJ, Hannah JL, Coetzee LL, Beukes NJ** (2004) Dating the rise of atmospheric oxygen. *Nature* **427**: 117–20
- Bell K, Oparka K** (2011) Imaging plasmodesmata. *Protoplasma* **248**: 9–25
- Benson DA, Karsch-Mizrachi I, Lipman DJ, Ostell J, Sayers EW** (2011) GenBank. *Nucl Acids Res* **39**: D32–D37
- Berendt S, Lehner J, Zhang YV, Rasse TM, Forchhammer K, Maldener I** (2012) Cell wall amidase AmiC1 is required for cellular communication and heterocyst development in the cyanobacterium *Anabaena* PCC 7120 but not for filament integrity. *J Bacteriol* **194**: 5218–27
- Berg H, Ziegler K, Piotukh K, Baier K, Lockau W, Volkmer-Engert R** (2000) Biosynthesis of the cyanobacterial reserve polymer multi-L-arginyl-poly-L-aspartic acid (cyanophycin): mechanism of the cyanophycin synthetase reaction studied with synthetic primers. *Eur J Biochem* **267**: 5561–5570
- Bergman B, Carpenter EJ** (1991) Nitrogenase confined to randomly distributed trichomes in the marine cyanobacterium *Trichodesmium thiebautii*. *J Phycol* **27**: 158–165

- Bergman B, Sandh G, Lin S, Larsson J, Carpenter EJ** (2013) Trichodesmium - a widespread marine cyanobacterium with unusual nitrogen fixation properties. *FEMS Microbiol Rev* **37**: 286–302
- Berman-Frank I, Lundgren P, Chen Y-B, Küpper H, Kolber Z, Bergman B, Falkowski P** (2001) Segregation of nitrogen fixation and oxygenic photosynthesis in the marine cyanobacterium Trichodesmium. *Science* **294**: 1534–1537
- Berntzon L, Erasmie S, Celepli N, Eriksson J, Rasmussen U, Bergman B** (2013) BMAA Inhibits Nitrogen Fixation in the Cyanobacterium *Nostoc* sp. PCC 7120. *Mar Drugs* **11**: 3091–3108
- Bethesda Research Laboratories** (1986) BRL pUC host: *E. coli* DH5 α TM competent cells. *Bethesda Res Lab Focus* **8**: 9–12
- Billi D, Friedmann EI, Helm RF, Potts M** (2001) Gene Transfer to the Desiccation-Tolerant Cyanobacterium Chroococcidiopsis. *J Bacteriol* **183**: 2298–2305
- Bisalputra T, Oakley BR, Walker DC, Shields CM** (1975) Microtubular Complexes in Blue-Green Algae. *Protoplasma* **86**: 19–28
- Black TA, Cai Y, Wolk CP** (1993) Spatial expression and autoregulation of *hetR*, a gene involved in the control of heterocyst development in *Anabaena*. *Mol Microbiol* **9**: 77–84
- Black TA, Wolk CP** (1994) Analysis of a Het- Mutation in *Anabaena* sp. Strain PCC 7120 Implicates a Secondary Metabolite in the Regulation of Heterocyst Spacing. *J Bacteriol* **176**: 2282–2292.
- Blanco-Rivero A, Leganés F, Fernández-Valiente E, Calle P, Fernández-Piñas F** (2005) *mrpA*, a gene with roles in resistance to Na⁺ and adaptation to alkaline pH in the cyanobacterium *Anabaena* sp. PCC7120. *Microbiology* **151**: 1671–1682
- Blank CE, Sánchez-Baracaldo P** (2010) Timing of morphological and ecological innovations in the cyanobacteria - a key to understanding the rise in atmospheric oxygen. *Geobiology* **8**: 1–23
- Bloemendal S, Kück U** (2013) Cell-to-cell communication in plants, animals, and fungi: a comparative review. *Naturwissenschaften* **100**: 3–19
- Borck K, Beggs JD, Brammar WJ, Hopkins AS, Murray NE** (1976) The construction in vitro of transducing derivatives of phage lambda. *Mol Gen Genet* **146**: 199–207
- Borthakur PB, Orozco CC, Young-Robbins SS, Haselkorn R, Callahan SM** (2005) Inactivation of *patS* and *hetN* causes lethal levels of heterocyst

- differentiation in the filamentous cyanobacterium *Anabaena* sp. PCC 7120. *Mol Microbiol* **57**: 111–123
- Borzi A** (1887) Le comunicazioni intracellulari delle Nostochinee. *Malpighia* **1**: 28–74
- Boyer HW, Roulland-Dussoix D** (1969) A Complementation Analysis of the Restriction and Modification of DNA in *Escherichia coli*. *J Mol Biol* **41**: 459–472
- Branton D, Bullivant S, Gilula NB, Karnovsky MJ, Moor H, Mühlethaler K, Northcote DH, Packer L, Satir B, Satir P, et al** (1975) Freeze-Etching Nomenclature. *Science* **190**: 54–56
- Brown AI, Rutenberg AD** (2012) Reconciling cyanobacterial fixed-nitrogen distributions and transport experiments with quantitative modelling. *Phys Biol* **9**: 016007
- Brown II, Bryant DA, Casamatta D, Thomas-Keprta KL, Sarkisova SA, Shen G, Graham JE, Boyd ES, Peters JW, Garrison DH, et al** (2010) Polyphasic characterization of a thermotolerant siderophilic filamentous cyanobacterium that produces intracellular iron deposits. *Appl Env Microbiol* **76**: 6664–6672
- Buikema WJ, Haselkorn R** (1991) Isolation and Complementation of Nitrogen Fixation Mutants of the Cyanobacterium *Anabaena* sp. Strain PCC 7120. *J Bacteriol* **173**: 1879–1885
- Burnat M, Herrero A, Flores E** (2014) Compartmentalized cyanophycin metabolism in the diazotrophic filaments of a heterocyst-forming cyanobacterium. *Proc Natl Acad Sci USA* **111**: 3823–3828
- Butler RD, Allsopp A** (1972) Ultrastructural investigations in the Stigonemataceae (Cyanophyta). *Arch Microbiol* **82**: 283–299
- Cai YP, Wolk CP** (1990) Use of a Conditionally Lethal Gene in *Anabaena* sp. Strain PCC 7120 To Select for Double Recombinants and To Entrap Insertion Sequences. *J Bacteriol* **172**: 3138–3145
- Callahan SM, Buikema WJ** (2001) The role of HetN in maintenance of the heterocyst pattern in *Anabaena* sp. PCC 7120. *Mol Microbiol* **40**: 941–950
- Campbell EL, Christman H, Meeks JC** (2008) DNA Microarray Comparisons of Plant Factor- and Nitrogen Deprivation-Induced Hormogonia Reveal Decision-Making Transcriptional Regulation Patterns in *Nostoc punctiforme*. *J Bacteriol* **190**: 7382–7391
- Campbell EL, Meeks JC** (1989) Characteristics of Hormogonia Formation by Symbiotic *Nostoc* spp. in Response to the Presence of *Anthoceros punctatus* or Its Extracellular Products. *Appl Env Microbiol* **55**: 125–131

- Campbell EL, Summers ML, Christman H, Martin ME, Meeks JC** (2007) Global Gene Expression Patterns of *Nostoc punctiforme* in Steady-State Dinitrogen-Grown Heterocyst-Containing Cultures and at Single Time Points during the Differentiation of Akinetes and Hormogonia. *J Bacteriol* **189**: 5247–5256
- Canfield DE, Glazer AN, Falkowski PG** (2010) The Evolution and Future of Earth's Nitrogen Cycle. *Science* **330**: 192–196
- Capone DG, Neil JMO, Zehr J, Carpenter EJ** (1990) Basis for Diel Variation in Nitrogenase Activity in the Marine Planktonic Cyanobacterium *Trichodesmium thiebautii*. *Appl Env Microbiol* **56**: 3532–3536
- Carr NG** (1988) Nitrogen Reserves and dynamic reservoirs in cyanobacteria. *In* LJ Rodgers, JR Gallon, eds, *Biochem. Algae Cyanobacteria*. Oxford University Press, Oxford, UK, pp 13–21
- Castenholz RW** (1969) Thermophilic Blue-Green Algae and the Thermal Environment. *Bacteriol Rev* **33**: 476–504
- Castenholz RW** (1988) Culturing methods for cyanobacteria. *Methods Enzym* **167**: 68–93
- Castenholz RW** (1976) The effect of sulfide on the bluegreen algae of hot springs. New Zealand and Iceland. *J Phycol* **12**: 54–68
- Castenholz RW** (1996) Endemism and biodiversity of thermophilic cyanobacteria. *Nov Hedwigia* **112**: 33–47
- Chanal A, Santini C-L, Wu L-F** (2003) Specific Inhibition of the Translocation of a Subset of *Escherichia coli* TAT Substrates by the TorA Signal Peptide. *J Mol Biol* **327**: 563–570
- Cohen Y, Jørgensen BB, Padan E, Shilo M** (1975) Sulphide-dependent anoxygenic photosynthesis in the cyanobacterium *Oscillatoria limnetica*. *Nature* **257**: 489–492
- Cohen Y, Jørgensen BB, Revsbech NP, Poplawski R** (1986) Adaptation to Hydrogen Sulfide of Oxygenic and Anoxygenic Photosynthesis among Cyanobacteria. *Appl Env Microbiol* **51**: 398–407
- Cohn F** (1862) Über die Algen des Karlsbader Sprudels, mit Rücksicht auf die Bildung des Sprudelsinesters. *Abhandlungen der schlesischen Gesellschaft für vaterländische Kult* **5**: 37–55
- Corrales-Guerrero L, Mariscal V, Flores E, Herrero A** (2013) Functional dissection and evidence for intercellular transfer of the heterocyst-differentiation PatS morphogen. *Mol Microbiol* **88**: 1093–1105

- Corrales-Guerrero L, Mariscal V, Nürnberg DJ, Elhai J, Mullineaux CW, Flores E, Herrero A** (2014) Subcellular localization and clues for the function of the HetN factor influencing heterocyst distribution in *Anabaena* sp. strain PCC 7120. *J Bacteriol* pii: JB.01922–14
- Corvini PFX, Gautier H, Rondags E, Vivier H, Goergen JL, Germain P** (2000) Intracellular pH determination of pristinamycin-producing *Streptomyces pristinaespiralis* by image analysis. *Microbiology* **146**: 2671–2678
- Couté A** (1982) Ultrastructure d'une cyanophycée aérienne calcifiée cavernicole: *Geitleria calcarea* Friedmann. *Hydrobiologia* **97**: 255–274
- Croft WN, George EA** (1959) Blue-green algae from the Middle Devonian of Rhynie, Aberdeenshire. *Bull Br Museum Nat Hist Geol* 341–353
- Crowe S a, Døssing LN, Beukes NJ, Bau M, Kruger SJ, Frei R, Canfield DE** (2013) Atmospheric oxygenation three billion years ago. *Nature* **501**: 535–538
- Cumino AC, Marcozzi C, Barreiro R, Salerno GL** (2007) Carbon Cycling in *Anabaena* sp. PCC 7120 . Sucrose Synthesis in the Heterocysts and Possible Role in Nitrogen Fixation. *Plant Physiol* **143**: 1385–1397
- Curatti L, Flores E, Salerno G** (2002) Sucrose is involved in the diazotrophic metabolism of the heterocyst-forming cyanobacterium *Anabaena* sp. *FEBS Lett* **513**: 175–178
- Dagan T, Roettger M, Stucken K, Landan G, Koch R, Major P, Gould SB, Goremykin V V, Rippka R, Tandeau de Marsac N, et al** (2013) Genomes of stigonematalean cyanobacteria (Subsection V) and the evolution of oxygenic photosynthesis from prokaryotes to plastids. *Genome Biol Evol* **5**: 31–44
- Damuth JD** (2001) Evolution : Tempo and Mode. *Encycl Life Sci* 1–7
- Dereeper A, Guignon V, Blanc G, Audic S, Buffet S, Chevenet F, Dufayard J-F, Guindon S, Lefort V, Lescot M, et al** (2008) Phylogeny.fr: robust phylogenetic analysis for the non-specialist. *Nucl Acids Res* **36**: 465–469
- Desikachary T V** (1959) *Cyanophyta*. Indian Council of Agricultural Research, New Dehli
- Donze M, Haveman J, Schiereck P** (1972) Absence of photosystem 2 in heterocysts of the blue-green alga *Anabaena*. *Biochim Biophys Acta* **256**: 157–161
- Drawert H, Metzner I** (1956) Fluoreszenz- u. elektronenmikroskopische Beobachtungen an *Cylindrospermum* und einigen anderen Cyanophyceen. *Ber Dtsch Bot Ges* **69**: 291–300

- Drews G, Weckesser J** (1982) Function, structure and composition of cell walls and external layers. In NG Carr, BA Whitton, eds, *The Biology of Cyanobacteria*. Blackwell Scientific Publications, Oxford, pp 333–357
- Duyvesteyn M, de Waard A** (1980) A new sequence-specific endonuclease from a thermophilic cyanobacterium, *Mastigocladus laminosus*. *FEBS Lett* **11**: 2–5
- Dzelzkalns VA, Owens GC, Bogorad L** (1984) Chloroplast promoter driven expression of the chloramphenicol acetyl transferase gene in a cyanobacterium. *Nucl Acids Res* **12**: 8917–8925
- Ekman M, Picossi S, Campbell EL, Meeks JC, Flores E** (2013) A *Nostoc punctiforme* sugar transporter necessary to establish a Cyanobacterium-plant symbiosis. *Plant Physiol* **161**: 1984–1992
- Elfgang C, Eckert R, Lichtenberg-Fraté H, Butterweck A, Traub O, Klein RA, Hülser DF, Willecke K** (1995) Specific Permeability and Selective Formation of Gap Junction Channels in Connexin-transfected HeLa Cells. *J Cell Biol* **129**: 805–817
- Elhai J, Vepritskiy A, Muro-Pastor AM, Flores E, Wolk CP** (1997) Reduction of conjugal transfer efficiency by three restriction activities of *Anabaena* sp. strain PCC 7120. *J Bacteriol* **179**: 1998–2005
- Elhai J, Wolk CP** (1988a) Conjugal transfer of DNA to cyanobacteria. *Methods Enzym* **167**: 747–754
- Elhai J, Wolk CP** (1988b) A versatile class of positive-selection vectors based on the nonviability of palindrome-containing plasmids that allows cloning into long polylinkers. *Gene* **68**: 119–138
- El-Shehawey R, Lugomela C, Ernst A, Bergman B** (2003) Diurnal expression of *hetR* and diazocyte development in the filamentous non-heterocystous cyanobacterium *Trichodesmium erythraeum*. *Microbiology* **149**: 1139–1146
- Ernst A, Black T, Cai Y, Panoff J-M, Tiwari DN, Wolk CP** (1992) Synthesis of Nitrogenase in Mutants of the Cyanobacterium *Anabaena* sp. Strain PCC 7120 Affected in Heterocyst Development or Metabolism. *J Bacteriol* **174**: 6025–6032
- Espinosa J, Castells MA, Laichoubi KB, Forchhammer K, Contreras A** (2010) Effects of spontaneous mutations in PipX functions and regulatory complexes on the cyanobacterium *Synechococcus elongatus* strain PCC 7942. *Microbiology* **156**: 1517–1526
- Fan Q, Lechno-Yossef S, Ehira S, Kaneko T, Ohmori M, Sato N, Tabata S, Wolk CP** (2006) Signal Transduction Genes Required for Heterocyst Maturation in *Anabaena* sp. Strain PCC 7120. *J Bacteriol* **188**: 6688–6693

- Fay P** (1992) Oxygen Relations of Nitrogen Fixation in Cyanobacteria. *Microbiol Rev* **56**: 340–373
- Fay P, Walsby AE** (1966) Metabolic Activities of Isolated Heterocysts of the Blue-green Alga *Anabaena cylindrica*. *Nature* **209**: 94–95
- Fay P, Stewart WDP, Walsby AE, Fogg GE** (1968) Is the heterocyst the site of nitrogen fixation in blue-green algae? *Nature* **220**: 810–812.
- Feldmann EA, Ni S, Sahu ID, Mishler CH, Risser DD, Murakami JL, Tom SK, McCarrick RM, Lorigan GA, Tolbert BS, et al** (2011) Evidence for Direct Binding between HetR from *Anabaena* sp. PCC 7120 and PatS-5. *Biochemistry* **50**: 9212–9224
- Finsinger K, Scholz I, Serrano A, Morales S, Uribe-lorio L, Mora M, Sittenfeld A, Weckesser J, Hess WR** (2008) Characterization of true-branching cyanobacteria from geothermal sites and hot springs of Costa Rica. *Env Microbiol* **10**: 460–473
- Flores E** (2012) Restricted cellular differentiation in cyanobacterial filaments. *Proc Natl Acad Sci USA* **109**: 15080–15081
- Flores E, Herrero A** (2010) Compartmentalized function through cell differentiation in filamentous cyanobacteria. *Nat Rev Microbiol* **8**: 39–50
- Flores E, Herrero A, Wolk CP, Maldener I** (2006) Is the periplasm continuous in filamentous multicellular cyanobacteria? *Trends Microbiol* **14**: 439–43
- Flores E, Pernil R, Muro-Pastor AM, Mariscal V, Maldener I, Lechno-Yossef S, Fan Q, Wolk CP, Herrero A** (2007) Septum-localized protein required for filament integrity and diazotrophy in the heterocyst-forming cyanobacterium *Anabaena* sp. strain PCC 7120. *J Bacteriol* **189**: 3884–3890
- Flores E, Wolk CP** (1985) Identification of facultatively heterotrophic, N₂-fixing cyanobacteria able to receive plasmid vectors from *Escherichia coli* by conjugation. *J Bacteriol* **162**: 1339–41
- Fogg GE** (1949) Growth and Heterocyst Production in *Anabaena Cylindrica* Lemm. *Ann Bot* **13**: 241–259
- Fogg GE, Stewart WDP, Fay P, Walsby AE** (1973) *The Blue-Green Algae*. Academic Press, London and New York
- Frank H, Lefort M, Mertin HH** (1962) Elektronenoptische und chemische Untersuchungen an Zellwänden der Blaualge *Phormidium unicum*. *Z Naturforsch* **17b**: 262–268
- Fredriksson C, Bergman B** (1997) Ultrastructural characterisation of cells specialised for nitrogen fixation in a non-heterocystous cyanobacterium, *Trichodesmium* spp. *Protoplasma* **197**: 76–85

- Geitler L** (1960) Schizophyceen. Gebrüder Borntraeger, Berlin-Nikolassee
- Giddings THJ, Staehelin LA** (1978) Plasma membrane architecture of *Anabaena cylindrica*: occurrence of microplasmodesmata and changes associated with heterocyst development and the cell cycle. *Cytobiologie* **16**: 235–249
- Giddings THJ, Staehelin LA** (1981) Observation of microplasmodesmata in both heterocyst-forming and non-heterocyst forming filamentous cyanobacteria by freeze-fracture electron microscopy. *Arch Microbiol* **129**: 295–298
- Goedhart J, von Stetten D, Noirclerc-Savoie M, Lelimosin M, Joosen L, Hink M a., van Weeren L, Gadella TWJ, Royant A** (2012) Structure-guided evolution of cyan fluorescent proteins towards a quantum yield of 93%. *Nat Commun* **3**: 751
- Golden JW, Whorff LL, Wiest DR** (1991) Independent Regulation of nifHDK Operon Transcription and DNA Rearrangement during Heterocyst Differentiation in the Cyanobacterium *Anabaena* sp. Strain PCC 7120. *J Bacteriol* **173**: 7098–7105
- Golecki JR** (1988) Electron Microscopy of Isolated Microbial Membranes. *Methods Microbiol* **20**: 261–281
- Golecki JR, Drews G** (1974) Zur Struktur der Blaualgen-Zellwand. Gefrierätzuntersuchungen an normalen und extrahierten Zellwänden von *Anabaena variabilis*. *Cytobiologie* **8**: 213–227
- Golubić S, Hernandez-Marine M, Hoffmann L** (1996) Developmental aspects of branching in filamentous Cyanophyta/Cyanobacteria. *Arch Hydrobiol Suppl Algal Stud* **83**: 303–329
- Gora PJ, Reinders A, Ward JM** (2012) A novel fluorescent assay for sucrose transporters. *Plant Methods* **8**: 13
- Gorelova OA, Baulina OI** (2009) Ultrastructure of Cyanobacterium *Nostoc* sp. f. *Blasia* Cell Forms in Persisting Populations. *Microbiology* **78**: 674–683
- Gould SB, Waller RF, McFadden GI** (2008) Plastid evolution. *Annu Rev Plant Biol* **59**: 491–517
- Gruber N, Galloway JN** (2008) An Earth-system perspective of the global nitrogen cycle. *Nature* **451**: 293–296
- Hagedorn H** (1961) Untersuchungen über die Feinstruktur der Blaualgenzellen. *Z Naturforsch* **16b**: 825–829
- Halfen LN, Castenholz RW** (1971) Gliding motility in the blue-green alga *Oscillatoria princeps*. *J Phycol* **7**: 133–145

- Han J, Burgess K** (2010) Fluorescent indicators for intracellular pH. *Chem Rev* **110**: 2709–28
- Hanahan D** (1983) Studies on Transformation of *Escherichia coli* with Plasmids. *J Mol Biol* **166**: 557–580
- Haselkorn R** (2008) Cell–cell communication in filamentous cyanobacteria. *Mol Microbiol* **70**: 783–785
- Haselkorn R** (1978) Heterocysts. *Ann Rev Plant Physiol* **29**: 319–344
- Haury JF, Spiller H** (1981) Fructose Uptake and Influence on Growth of and Nitrogen Fixation by *Anabaena variabilis*. *J Bacteriol* **147**: 227–235
- Haystead A, Robinson R, Stewart WDP** (1970) Nitrogenase Activity in Extracts of Heterocystous and Non-Heterocystous Blue-Green Algae. *Arch Microbiol* **74**: 235–243
- Heidrich C, Templin MF, Ursinus A, Merdanovic M, Berger J, Schwarz H, de Pedro MA, Höltje J-V** (2001) Involvement of N-acetylmuramyl-L-alanine amidases in cell separation and antibiotic-induced autolysis of *Escherichia coli*. *Mol Microbiol* **41**: 167–178
- Herdman M, Rippka R** (1988) Cellular Differentiation: Hormogonia and Baeocytes. *Methods Enzym* **167**: 232–242
- Hernández-Mariné M, Asoncio AD, Canals A, Ariño X, Aboal M, Hoffmann L** (1999) Discovery of populations of the lime-incrusting genus *Loriella* (Stigonematales) in Spanish caves. *Algol Stud* **94**: 121–138
- Hernandez-Muniz W, Stevens SEJ** (1987) Characterization of the motile hormogonia of *Mastigocladus laminosus*. *J Bacteriol* **169**: 218–223
- Higa KC, Rajagopalan R, Risser DD, Rivers OS, Tom SK, Videau P, Callahan SM** (2012) The RGSGR amino acid motif of the intercellular signalling protein, HetN, is required for patterning of heterocysts in *Anabaena* sp. strain PCC 7120. *Mol Microbiol* **83**: 682–693
- Hirschberg J, McIntosh L** (1983) Molecular Basis of Herbicide Resistance in *Amaranthus hybridus*. *Science* **222**: 1346–1349
- Holland D, Wolk CP** (1990) Identification and characterization of *hetA*, a gene that acts early in the process of morphological differentiation of heterocysts. *J Bacteriol* **172**: 3131–3137
- Holland HD** (2006) The oxygenation of the atmosphere and oceans. *Phil Trans R Soc B* **361**: 903–915

- Huang X, Dong Y, Zhao J** (2004) HetR homodimer is a DNA-binding protein required for heterocyst differentiation, and the DNA-binding activity is inhibited by PatS. *Proc Natl Acad Sci USA* **101**: 4848–4853
- Inoue H, Nojima H, Okayama H** (1990) High efficiency transformation of *Escherichia coli* with plasmids. *Gene* **96**: 23–28
- Ionescu D, Voss B, Oren A, Hess WR, Muro-Pastor AM** (2010) Heterocyst-Specific Transcription of NsiR1, a Non-Coding RNA Encoded in a Tandem Array of Direct Repeats in Cyanobacteria. *J Mol Biol* **398**: 177–188
- Ishida T, Watanabe MM, Sugiyama J, Yokota A** (2001) Evidence for polyphyletic origin of the members of the orders of Oscillatoriales and Pleurocapsales as determined by 16S rDNA analysis. *FEMS Microbiol Lett* **201**: 79–82
- Jensen BB, Cox RP** (1983) Effect of oxygen concentration on dark nitrogen fixation and respiration in cyanobacteria. *Arch Microbiol* **135**: 287–292
- Jones KM, Buikema WJ, Haselkorn R** (2003) Heterocyst-Specific Expression of patB, a Gene Required for Nitrogen Fixation in *Anabaena* sp. Strain PCC 7120. *J Bacteriol* **185**: 2306–2314
- Jüttner F** (1983) ¹⁴C-Labeled Metabolites in Heterocysts and Vegetative Cells of *Anabaena cylindrica* Filaments and Their Presumptive Function as Transport Vehicles of Organic Carbon and Nitrogen. *J Bacteriol* **155**: 628–633
- Ke S, Haselkorn R** (2013) The Sakaguchi reaction product quenches phycobilisome fluorescence, allowing determination of the arginine concentration in cells of *Anabaena* strain PCC 7120. *J Bacteriol* **195**: 25–28
- Kibbe WA** (2007) OligoCalc: an online oligonucleotide properties calculator. *Nucl Acids Res* **35**: W43–46
- Kim WH, Lee J, Jung D-W, Williams DR** (2012) Visualizing Sweetness: Increasingly Diverse Applications for Fluorescent-Tagged Glucose Bioprobes and Their Recent Structural Modifications. *Sensors* **12**: 5005–5027
- Kohl FG** (1903) Über die Organisation und Physiologie der Cyanophyceenzelle und die mitotische Teilung ihres Kernes. Gustav Fischer, Jena
- Komárek J, Kling H, Komárková J** (2003) Filamentous cyanobacteria. In JD Wehr, RG Sheath, eds, *Freshwater Algae of North America*. Elsevier Inc., pp 117–196
- Di Lallo G, Fagioli M, Barionovi D, Ghelardini P, Paolozzi L** (2003) Use of a two-hybrid assay to study the assembly of a complex multicomponent protein machinery: bacterial septosome differentiation. *Microbiology* **3353–3359**

- Lamont HC** (1969) Sacrificial cell death and trichome breakage in an Oscillatoriacean blue-green alga: the role of murein. *Arch Microbiol* **69**: 237–259
- Lamprinou V, Hernández-Mariné M, Canals T, Kormas K, Economou-Amilli A, Pantazidou A** (2011) Morphology and molecular evaluation of *Iphinoe spelaebios* gen. nov., sp. nov. and *Loriellopsis cavernicola* gen. nov., sp. nov., two stigonematalean cyanobacteria from Greek and Spanish caves. *IJSEM* **61**: 2907–2915
- Lang NJ, Fay P** (1971) The Heterocysts of Blue-Green Algae. II. Details of Ultrastructure. *Proc R Soc B* **178**: 193–203
- Larkin MA, Blackshields G, Brown NP, Chenna R, McGettigan P a, McWilliam H, Valentin F, Wallace IM, Wilm A, Lopez R, et al** (2007) Clustal W and Clustal X version 2.0. *Bioinformatics* **23**: 2947–2948
- Lee D-Y, Rhee G-Y** (1997) Kinetics of cell death in the cyanobacterium *Anabaena flos-aquae* and the production of dissolved organic carbon. *J Phycol* **33**: 991–998
- Lee D-Y, Rhee G-Y** (1999) Circadian rhythm in growth and death of *Anabaena flos-aquae* (cyanobacteria). *J Phycol* **35**: 694–699
- Lee MH, Scherer M, Rigali S, Golden JW** (2003) PlmA, a New Member of the GntR Family, Has Plasmid Maintenance Functions in *Anabaena* sp. Strain PCC 7120. *J Bacteriol* **185**: 4315–4325
- Lehner J, Berendt S, Dörsam B, Pérez R, Forchhammer K, Maldener I** (2013) Prokaryotic multicellularity: a nanopore array for bacterial cell communication. *FASEB J* **27**: 1–8
- Lehner J, Zhang Y, Berendt S, Rasse TM, Forchhammer K, Maldener I** (2011) The morphogene AmiC2 is pivotal for multicellular development in the cyanobacterium *Nostoc punctiforme*. *Mol Microbiol* **79**: 1655–1669
- Levi J, Cheng Z, Gheysens O, Patel M, Chan CT, Wang Y, Namavari M, Gambhir SS** (2007) Fluorescent fructose derivatives for imaging breast cancer cells. *Bioconjug Chem* **18**: 628–34
- Liu D, Golden JW** (2002) hetL overexpression stimulates heterocyst formation in *Anabaena* sp. strain PCC 7120. *J Bacteriol* **184**: 6873–6881
- López-Igual R, Flores E, Herrero A** (2010) Inactivation of a heterocyst-specific invertase indicates a principal role of sucrose catabolism in heterocysts of *Anabaena* sp. *J Bacteriol* **192**: 5526–5533
- Louzao MC, Espiña B, Vieytes MR, Vega F V, Rubiolo JA, Baba O, Terashima T, Botana LM** (2008) “Fluorescent glycogen” formation with sensibility for in vivo and in vitro detection. *Glycoconj J* **25**: 503–510

- Luft JH** (1956) Permanganate-A New Fixative for Electron Microscopy. *J Biophys Biochem Cytol* **2**: 799–802
- Lyra C, Halme T, Torsti A-M, Tenkanen T, Sivonen K** (2000) Site-specific restriction endonucleases in cyanobacteria. *J Appl Microbiol* **89**: 979–991
- Mackenzie R, Pedrós-Alió C, Díez B** (2013) Bacterial composition of microbial mats in hot springs in Northern Patagonia: variations with seasons and temperature. *Extremophiles* **17**: 123–36
- Maldener I, Muro-Pastor AM** (2010) Cyanobacterial Heterocysts. *Encycl Life Sci*. doi: 10.1002/9780470015902.a0000306.pub2
- Maldener I, Summers ML, Sukenik A** (2014) Cellular differentiation in filamentous cyanobacteria. In E Flores, A Herrero, eds, *Cell Biology of Cyanobacteria*. Caister Academic Press, pp 263–292
- Mannan RM, Whitmarsh J, Nyman P, Pakrasi HB** (1991) Directed mutagenesis of an iron-sulfur protein of the photosystem I complex in the filamentous cyanobacterium *Anabaena variabilis* ATCC 29413. *Proc Natl Acad Sci USA* **88**: 10168–10172
- Marcenko E** (1962) Licht- und elektronenmikroskopische Untersuchungen an der Thermalalge *Mastigocladus laminosus* Cohn. *Acta Bot Coratica* **20/21**: 47–74
- Marcozzi C, Cumino AC, Salerno GL** (2009) Role of NtcA, a cyanobacterial global nitrogen regulator, in the regulation of sucrose metabolism gene expression in *Anabaena* sp. PCC 7120. *Arch Microbiol* **191**: 255–263
- Mariscal V** (2014) Cell–Cell Joining Proteins in Heterocyst-Forming Cyanobacteria. In E Flores, A Herrero, eds, *Cell Biology of Cyanobacteria*. Caister Academic Press, pp 293–304
- Mariscal V, Herrero A, Flores E** (2007) Continuous periplasm in a filamentous, heterocyst-forming cyanobacterium. *Mol Microbiol* **65**: 1139–1145
- Mariscal V, Herrero A, Nenninger A, Mullineaux CW, Flores E** (2011) Functional dissection of the three-domain SepJ protein joining the cells in cyanobacterial trichomes. *Mol Microbiol* **79**: 1077–1088
- Markowitz VM, Chen I-MA, Palaniappan K, Chu K, Szeto E, Grechkin Y, Ratner A, Jacob B, Huang J, Williams P, et al** (2012) IMG: the Integrated Microbial Genomes database and comparative analysis system. *Nucl Acids Res* **40**: D115–D122
- Martin TC, Wyatt JT** (1974) Comparative physiology and morphology of six strains of Stigonematacean blue-green algae. *J Phycol* **10**: 57–65

- Martín-Figueroa E, Navarro F, Florencio FJ** (2000) The GS-GOGAT pathway is not operative in the heterocysts. Cloning and expression of *glsF* gene from the cyanobacterium *Anabaena* sp. PCC 7120. *FEBS Lett* **476**: 282–286
- Maryan PS, Eady RR, Chaplin AE, Gallon JR** (1986) Nitrogen Fixation by *Gloeotheca* sp. PCC 6909: Respiration and Not Photosynthesis Supports Nitrogenase Activity in the Light. *J Gen Microbiol* **132**: 789–796
- Meeks JC, Campbell EL, Summers ML, Wong FC** (2002) Cellular differentiation in the cyanobacterium *Nostoc punctiforme*. *Arch Microbiol* **178**: 395–403
- Meier EL, Goley ED** (2014) Form and function of the bacterial cytokinetic ring. *Curr Opin Cell Biol* **26**: 19–27
- Melick DR, Broady PA, Rowan KS** (1991) Morphological and physiological characteristics of a non-heterocystous strain of the cyanobacterium *Mastigocladus laminosus* Cohn from fumarolic soil on Mt Erebus, Antarctica. *Polar Biol* 81–89
- Mella-Herrera RA, Neunuebel MR, Golden JW** (2011) *Anabaena* sp. strain PCC 7120 *conR* contains a LytR-CpsA-Psr domain, is developmentally regulated, and is essential for diazotrophic growth and heterocyst morphogenesis. *Microbiology* **157**: 617–626
- Merino V, Hernández-Mariné M, Fernández M** (1994) Ultrastructure of *Mastigladopsis repens* (Stigonematales, Cyanophyceae). *Cryptogam Algal* **15**: 37–46
- Merino-Puerto V, Herrero A, Flores E** (2013) A cluster of genes that encode positive and negative elements influencing filament length in a heterocyst-forming cyanobacterium. *J Bacteriol* **195**: 3957–3966
- Merino-Puerto V, Mariscal V, Mullineaux CW, Herrero A, Flores E** (2010) Fra proteins influencing filament integrity, diazotrophy and localization of septal protein SepJ in the heterocyst-forming cyanobacterium *Anabaena* sp. *Mol Microbiol* **75**: 1159–70
- Merino-Puerto V, Mariscal V, Schwarz H, Maldener I, Mullineaux CW, Herrero A, Flores E** (2011a) FraH Is Required for Reorganization of Intracellular Membranes during Heterocyst Differentiation in *Anabaena* sp. Strain PCC 7120. *J Bacteriol* **193**: 6815–6823
- Merino-Puerto V, Schwarz H, Maldener I, Mariscal V, Mullineaux CW, Herrero A, Flores E** (2011b) FraC/FraD-dependent intercellular molecular exchange in the filaments of a heterocyst-forming cyanobacterium, *Anabaena* sp. *Mol Microbiol* **82**: 87–98
- Metzner I** (1955) Zur Chemie und zum submikroskopischen Aufbau der Zellwände, Seiden und Gallerten von Cyanophyteen. *Arch Microbiol* **22**: 45–77

- Miller SR, Castenholz RW, Pedersen D** (2007) Phylogeography of the Thermophilic Cyanobacterium *Mastigocladus laminosus*. *Appl Env Microbiol* **73**: 4751–4759
- Miller SR, Purugganan MD, Curtis SE** (2006) Molecular Population Genetics and Phenotypic Diversification of Two Populations of the Thermophilic Cyanobacterium *Mastigocladus laminosus*. *Appl Env Microbiol* **72**: 2793–2800
- Morin N, Vallaeyts T, Hendrickx L, Natalie L, Wilmotte A** (2010) An efficient DNA isolation protocol for filamentous cyanobacteria of the genus *Arthrospira*. *J Microbiol Methods* **80**: 148–154
- Moronta-Barrios F, Espinosa J, Contreras A** (2013) Negative control of cell size in the cyanobacterium *Synechococcus elongatus* PCC 7942 by the essential response regulator RpaB. *FEBS Lett* **587**: 504–509
- Mullineaux CW, Mariscal V, Nenninger A, Khanum H, Herrero A, Flores E, Adams DG** (2008) Mechanism of intercellular molecular exchange in heterocyst-forming cyanobacteria. *EMBO J* **27**: 1299–1308
- Nayar AS, Yamaura H, Rajagopalan R, Risser DD, Callahan SM** (2007) FraG is necessary for filament integrity and heterocyst maturation in the cyanobacterium *Anabaena* sp. strain PCC 7120. *Microbiology* **153**: 601–607
- Nicolaisen K, Hahn A, Schleiff E** (2009a) The cell wall in heterocyst formation by *Anabaena* sp. PCC 7120. *J Basic Microbiol* **49**: 5–24
- Nicolaisen K, Mariscal V, Bredemeier R, Pernil R, López-igual R, Maldener I, Herrero A, Schleiff E, Flores E** (2009b) The outer membrane of a heterocyst-forming cyanobacterium is a permeability barrier for uptake of metabolites that are exchanged between cells. *Mol Microbiol* **74**: 58–70
- Nierzwicki SA, Maratea D, Balkwill DL, Hardie LP, Mehta VB, Stevens SEJ** (1982) Ultrastructure of the cyanobacterium, *Mastigocladus laminosus*. *Arch Microbiol* **133**: 11 – 19
- Nierzwicki-Bauer SA, Balkwill DL, Stevens SEJ** (1984a) Heterocyst differentiation in the cyanobacterium *Mastigocladus laminosus*. *J Bacteriol* **157**: 514–525
- Nierzwicki-Bauer SA, Balkwill DL, Stevens SEJ** (1984b) Morphology and ultrastructure of the cyanobacterium *Mastigocladus laminosus* growing under nitrogen-fixing conditions. *Arch Microbiol* **137**: 97–103
- Ning S-B, Guo H-L, Wang L, Song Y-C** (2002) Salt stress induces programmed cell death in prokaryotic organism *Anabaena*. *J Appl Microbiol* **93**: 15–28
- Nürnberg DJ, Mariscal V, Parker J, Mastroianni G, Flores E, Mullineaux CW** (2014) Branching and intercellular communication in the Section V

- cyanobacterium *Mastigocladus laminosus*, a complex multicellular prokaryote. *Mol Microbiol* **91**: 935–949
- Ohki K, Fujita Y** (1988) Aerobic nitrogenase activity measured as acetylene reduction in the marine non-heterocystous cyanobacterium *Trichodesmium* spp. grown under artificial conditions. *Mar Biol* **98**: 111–114
- Omairi-Nasser A, Haselkorn R, Austin II J** (2014) Visualization of channels connecting cells in filamentous nitrogen-fixing cyanobacteria. *FASEB J* 1–7
- Palinska KA, Krumbein WE** (2000) Perforation patterns in the peptidoglycan wall of filamentous cyanobacteria. *J Phycol* **36**: 139–145
- Pankratz HS, Bowen CC** (1963) Cytology of Blue-Green Algae. I. The Cells of *Symploca muscorum*. *Am J Bot* **50**: 387–399
- Peat A, Whitton BA** (1968) Vegetative cell structure in *Anabaenopsis* sp. *Arch Microbiol* **63**: 170–176
- Pernil R, Herrero A, Flores E** (2010) Catabolic function of compartmentalized alanine dehydrogenase in the heterocyst-forming cyanobacterium *Anabaena* sp. strain PCC 7120. *J Bacteriol* **192**: 5165–5172
- Pernil R, Picossi S, Mariscal V, Herrero A, Flores E** (2008) ABC-type amino acid uptake transporters Bgt and N-II of *Anabaena* sp. strain PCC 7120 share an ATPase subunit and are expressed in vegetative cells and heterocysts. *Mol Microbiol* **67**: 1067–80
- Picossi S, Valladares A, Flores E, Herrero A** (2004) Nitrogen-regulated genes for the metabolism of cyanophycin, a bacterial nitrogen reserve polymer: expression and mutational analysis of two cyanophycin synthetase and cyanophycinase gene clusters in heterocyst-forming cyanobacterium *Anabaena* sp. PCC 7120. *J Biol Chem* **279**: 11582–11592
- Porra RJ, Thompson WA, Kriedemann PE** (1989) Determination of accurate extinction coefficients and simultaneous equations for assaying chlorophylls a and b extracted with four different solvents: verification of the concentration of chlorophyll standards by atomic absorption spectroscopy. *Biochim Biophys Acta* **975**: 384–394
- Ramamurthi KS** (2010) Protein localization by recognition of membrane curvature. *Curr Opin Microbiol* **13**: 753–757
- Reddy KJ, Haskell JB, Sherman DM, Sherman LA** (1993) Unicellular, Aerobic Nitrogen-Fixing Cyanobacteria of the Genus *Cyanothece*. *J Bacteriol* **175**: 1284–1292
- Reinders A, Sivitz AB, Ward JM** (2012a) Evolution of plant sucrose uptake transporters. *Front Plant Sci* **3**: 00022

- Reinders A, Sun Y, Karvonen KL, Ward JM** (2012b) Identification of amino acids important for substrate specificity in sucrose transporters using gene shuffling. *J Biol Chem* **287**: 30296–30304
- Reynolds ES** (1963) The use of lead citrate at high pH as an electron-opaque stain in electron microscopy. *J Cell Biol* **17**: 208–212
- Richter R, Hejazi M, Kraft R, Ziegler K, Lockau W** (1999) Cyanophycinase, a peptidase degrading the cyanobacterial reserve material multi-L-arginyl-poly-L-aspartic acid (cyanophycin). *Eur J Biochem* **263**: 163–169
- Rink TJ, Tsien RY, Pozzan T** (1982) Cytoplasmic pH and Free Mg^{2+} in Lymphocytes. *J cell Biol* **95**: 189–196
- Rippka R, Deruelles J, Waterbury JB, Herdman M, Stanier RY** (1979) Generic assignments, strain histories and properties of pure cultures of cyanobacteria. *J Gen Microbiol* **111**: 1–61
- Risser DD, Callahan SM** (2009) Genetic and cytological evidence that heterocyst patterning is regulated by inhibitor gradients that promote activator decay. *Proc Natl Acad Sci USA* **106**: 19884–19888
- Risser DD, Wong FCY, Meeks JC** (2012) Biased inheritance of the protein PatN frees vegetative cells to initiate patterned heterocyst differentiation. *Proc Natl Acad Sci USA* **109**: 15342–15347
- Robinson WB, Mealar AE, Stevens SEJ, Ospeck M** (2007) Measuring the force production of the hormogonia of *Mastigocladus laminosus*. *Biophys J* **93**: 699–703
- Roeselers G, Norris TB, Castenholz RW, Rysgaard S, Glud RN, Kühl M, Muyzer G** (2007) Diversity of phototrophic bacteria in microbial mats from Arctic hot springs (Greenland). *Env Microbiol* **9**: 26–38
- Salerno GL, Curatti L** (2003) Origin of sucrose metabolism in higher plants: when, how and why? *Trends Plant Sci* **8**: 63–69
- Sambrook J, Russel DW** (2001) *Molecular Cloning - A laboratory manual.*, Third Edit. Cold Spring Harbor Laboratory Press, Cold Spring Harbor, New York
- Sánchez-Baracaldo P, Ridgwell A, Raven JA** (2014) A Neoproterozoic Transition in the Marine Nitrogen Cycle. *Curr Biol* **24**: 1–6
- Schilling N, Ehrnsperger K** (1985) Cellular Differentiation of Sucrose Metabolism in *Anabaena variabilis*. *Z Naturforsch* **70**: 776–779
- Schirrmeister BE, Antonelli A, Bagheri HC** (2011) The origin of multicellularity in cyanobacteria. *BMC Evol Biol* **11**: 45

- Schirrmeister BE, de Vos JM, Antonelli A, Bagheri HC** (2013) Evolution of multicellularity coincided with increased diversification of cyanobacteria and the Great Oxidation Event. *Proc Natl Acad Sci USA* **110**: 1791–1796
- Schmetterer G, Wolk CP** (1988) Identification of the region of cyanobacterial plasmid pDU1 necessary for replication in *Anabaena* sp. strain M-131. *Gene* **62**: 101–109
- Schneider D, Fuhrmann E, Scholz I, Hess WR, Graumann PL** (2007) Fluorescence staining of live cyanobacterial cells suggest non-stringent chromosome segregation and absence of a connection between cytoplasmic and thylakoid membranes. *BMC Cell Biol* **10**: 1–10
- Schwabe GH** (1960) Über den thermobionten Kosmopoliten *Mastigocladus laminosus* Cohn. *Hydrology* 759–792
- Severs NJ** (2007) Freeze-fracture electron microscopy. *Nat Protoc* **2**: 547–576
- Sherman DM, Tucker D, Sherman LA** (2000) Heterocyst development and localization of cyanophycin in N₂-fixing cultures of *Anabaena* sp. PCC 7120 (Cyanobacteria). *J Phycol* **36**: 932–941
- Shih PM, Wu D, Latifi A, Axen SD, Fewer DP, Talla E, Calteau A, Cai F, Tandeau de Marsac N, Rippka R, et al** (2013) Improving the coverage of the cyanobacterial phylum using diversity-driven genome sequencing. *Proc Natl Acad Sci USA* **110**: 1053–1058
- Simon RD** (1971) Cyanophycin granules from the blue-green alga *Anabaena cylindrica*: a reserve material consisting of copolymers of aspartic acid and arginine. *Proc Natl Acad Sci USA* **68**: 265–267
- Simon RD, Weathers P** (1976) Determination of the structure of the novel polypeptide containing aspartic acid and arginine which is found in cyanobacteria. *Biochim Biophys Acta* **420**: 165–176
- Singh RN, Tiwari DN** (1969) Induction by Ultraviolet Irradiation of Mutation in the Blue-Green Alga *Nostoc linckia* (Roth) Born. et Flah. *Nature* **221**: 62–64
- Sivitz AB, Reinders A, Johnson ME, Krentz AD, Grof CPL, Perroux JM, Ward JM** (2007) Arabidopsis sucrose transporter AtSUC9. High-affinity transport activity, intragenic control of expression, and early flowering mutant phenotype. *Plant Physiol* **143**: 188–198
- Slavík J** (1997) Applications of fluorescent probes in cellular biology. Measurement of intracellular pH. *JOL* **72-74**: 575–577
- Smith DJ, Timonen HJ, Jaffe D a, Griffin DW, Birmele MN, Perry KD, Ward PD, Roberts MS** (2013) Intercontinental dispersal of bacteria and archaea by transpacific winds. *Appl Env Microbiol* **79**: 1134–1139

- Soe KM, Yokoyama A, Yokoyama J, Hara Y** (2011) Morphological and genetic diversity of the thermophilic cyanobacterium, *Mastigocladus laminosus* (Stigonematales, Cyanobacteria) from Japan and Myanmar. *Phycol Res* **59**: 135–142
- Stal LJ** (1995) Physiological ecology of cyanobacteria in microbial mats and other communities. *New Phytol* **131**: 1–32
- Stal LJ, Krumbein WE** (1985) Nitrogenase activity in the non-heterocystous cyanobacterium *Oscillatoria* sp. grown under alternating light-dark cycles. *Arch Microbiol* **143**: 67–71
- Staras K, Mikulincer D, Gitler D** (2013) Monitoring and quantifying dynamic physiological processes in live neurons using fluorescence recovery after photobleaching. *J Neurochem* **126**: 213–222
- Stebegg R, Wurzinger B, Mikulic M, Schmetterer G** (2012) Chemoheterotrophic Growth of the Cyanobacterium *Anabaena* sp. *J Bacteriol* **194**: 4601–4607
- Stephens N, Flynn KJ, Gallon JR** (2003) Interrelationships between the pathways of inorganic nitrogen assimilation in the cyanobacterium *Gloeothece* can be described using a mechanistic mathematical model. *New Phytol* **160**: 545–555
- Stevens SEJ, Nierzwicki-Bauer SA, Balkwill DL** (1985) Effect of nitrogen starvation on the morphology and ultrastructure of the cyanobacterium *Mastigocladus laminosus*. *J Bacteriol* **161**: 1215–8
- Stewart WDP, Haystead A, Pearson HW** (1969) Nitrogenase Activity in Heterocysts of Blue-Green Algae. *Nature* **224**: 226–228
- Stucken K, Ilhan J, Roettger M, Dagan T, Martin WF** (2012) Transformation and conjugal transfer of foreign genes into the filamentous multicellular cyanobacteria (Subsection V) *Fischerella* and *Chlorogloeopsis*. *Curr Microbiol* **65**: 552–560
- Szklarczyk R, Heringa J** (2004) Tracking repeats using significance and transitivity. *Bioinformatics* **20**: 311–317
- Thomas J** (1970) Absence of the Pigments of Photosystem II of Photosynthesis in Heterocysts of a Blue-Green Alga. *Nature* **228**: 181–183
- Thomas J, Meeks JC, Wolk CP, Shaffer PW, Austin SM** (1977) Formation of glutamine from [¹³N]ammonia, [¹³N]dinitrogen, and [¹⁴C]glutamate by heterocysts isolated from *Anabaena cylindrica*. *J Bacteriol* **129**: 1545–1555
- Thurston EL, Ingram LO** (1971) Morphology and fine structure of *Fischerella ambigua*. *J Phycol* **7**: 203–210

- Tomitani A, Knoll AH, Cavanaugh CM, Ohno T** (2006) The evolutionary diversification of cyanobacteria: molecular-phylogenetic and paleontological perspectives. *Proc Natl Acad Sci USA* **103**: 5442–5447
- Tucker EB** (1982) Translocation in the Staminal Hairs of *Setcreasea purpurea*. I. A Study of Cell Ultrastructure and Cell-to-Cell Passage of Molecular Probes. *Protoplasma* **113**: 193–201
- Tuit C, Waterbury J, Ravizza G** (2004) Diel variation of molybdenum and iron in marine diazotrophic cyanobacteria. *Limnol Ocean* **49**: 978–990
- Ungerer JL, Pratte BS, Thiel T** (2008) Regulation of fructose transport and its effect on fructose toxicity in *Anabaena* spp. *J Bacteriol* **190**: 8115–25
- Valladares A, Rodríguez V, Camargo S, Martínez-Noël GMA, Herrero A, Luque I** (2011) Specific role of the cyanobacterial PipX factor in the heterocysts of *Anabaena* sp. strain PCC 7120. *J Bacteriol* **193**: 1172–1182
- Vargas WA, Nishi CN, Giarrocco LE, Salerno GL** (2011) Differential roles of alkaline/neutral invertases in *Nostoc* sp. PCC 7120: Inv-B isoform is essential for diazotrophic growth. *Planta* **233**: 153–162
- Vincent WF** (2007) Cold Tolerance in Cyanobacteria and Life in the Cryosphere. *In* J Seckbach, ed, *Algae and Cyanobacteria in Extreme Environments*. Springer Netherlands, pp 287–301
- Walsby AE** (1985) The permeability of heterocysts to the gases nitrogen and oxygen. *Proc R Soc B* **226**: 345–366
- Walsby AE** (2007) Cyanobacterial heterocysts: terminal pores proposed as sites of gas exchange. *Trends Microbiol* **15**: 340–349
- Weare NM, Benemann JR** (1974) Nitrogenase Activity and Photosynthesis in *Plectonema boryanum*. *J Bacteriol* **119**: 258–265
- Wilcox M, Mitchison GJ, Smith RJ** (1973) Pattern formation in the blue-green alga, *Anabaena*. *J Cell Sci* **12**: 707–723
- Wildon DC, Mercer F V** (1963a) The Ultrastructure of the Heterocyst and Akinete of the Blue-Green Algae. *Arch Microbiol* **47**: 19–31
- Wildon DC, Mercer F V** (1963b) The ultrastructure of the vegetative cell of blue-green algae. *Aust J Biol Sci* **16**: 585–596
- Wilk L, Strauss M, Rudolf M, Nicolaisen K, Flores E, Kühlbrandt W, Schleiff E** (2011) Outer membrane continuity and septosome formation between vegetative cells in the filaments of *Anabaena* sp. PCC 7120. *Cell Microbiol* **49**: 1–12

- Wolk C, Ernst A, Elhai J** (1994) Heterocyst metabolism and development. In D Bryant, ed, *Molecular Biology of Cyanobacteria*. Kluwer Academic Publishers, Dordrecht, The Netherlands, pp 769–823
- Wolk CP** (1996) Heterocyst formation. *Annu Rev Genet* **30**: 59–78
- Wolk CP** (1968) Movement of carbon from vegetative cells to heterocysts in *Anabaena cylindrica*. *J Bacteriol* **96**: 2138–2143
- Wolk CP** (1973) Physiology and Cytological Chemistry of Blue-Green Algae. *Bacteriol Rev* **37**: 32–101
- Wolk CP, Cai Y, Cardemil L, Flores E, Hohn B, Murry M, Schmetterer G, Schrautemeier B, Wilson R** (1988) Isolation and Complementation of Mutants of *Anabaena* sp. Strain PCC 7120 Unable to Grow Aerobically on Dinitrogen. *Microbiology* **170**: 1239–1244
- Wolk CP, Thomas J, Shaffer PW, Austin SM, Galonsky A** (1976) Pathway of nitrogen metabolism after fixation of ¹³N-labeled nitrogen gas by the cyanobacterium, *Anabaena cylindrica*. *J Biol Chem* **251**: 5027–5034
- Wu X, Lee DW, Mella RA, Golden JW** (2007) The *Anabaena* sp. strain PCC 7120 *asr1734* gene encodes a negative regulator of heterocyst development. *Mol Microbiol* **64**: 782–794
- Wu X, Liu D, Lee MH, Golden JW** (2004) patS Minigenes Inhibit Heterocyst Development of *Anabaena* sp. Strain PCC 7120. *J Bacteriol* **186**: 6422–6429
- Yanisch-Perron C, Vieira J, Messing J** (1985) Improved M13 phage cloning vectors and host strains: nucleotide sequences of the M13mp18 and pUC19 vectors. *Gene* **33**: 103–119
- Yin Z-H, Hüve K, Heber U** (1996) Light-dependent proton transport into mesophyll vacuoles of leaves of C3 plants as revealed by pH-indicating fluorescent dyes : a reappraisal. *Planta* **199**: 9–17
- Yoon H-S, Golden JW** (1998) Heterocyst Pattern Formation Controlled by a Diffusible Peptide. *Science* **282**: 935–938
- Yoon H-S, Golden JW** (2001) PatS and Products of Nitrogen Fixation Control Heterocyst Pattern. *J Bacteriol* **183**: 2605–2613
- Yoshioka K, Saito M, Oh K-B, Nemoto Y, Matsuoka H, Natsume M, Abe H** (1996) Intercellular Fate of 2-NBDG, a Fluorescent Probe for Glucose Uptake Activity, in *Escherichia coli* Cells. *Biosci Biotech Biochem* **60**: 1899–1901
- Zhang J-Y, Chen W-L, Zhang C-C** (2009) *hetR* and *patS*, two genes necessary for heterocyst pattern formation, are widespread in filamentous nonheterocyst-forming cyanobacteria. *Microbiology* **155**: 1418–1426

- Zhang L-C, Chen Y-F, Chen W-L, Zhang C-C** (2008a) Existence of periplasmic barriers preventing green fluorescent protein diffusion from cell to cell in the cyanobacterium *Anabaena* sp. strain PCC 7120. *Mol Microbiol* **70**: 814–823
- Zhang L-C, Risoul V, Latifi A, Christie JM, Zhang C-C** (2013) Exploring the size limit of protein diffusion through the periplasm in cyanobacterium *Anabaena* sp. PCC 7120 using the 13 kDa iLOV fluorescent protein. *Res Microbiol* **164**: 710–717
- Zhang Y, Li J, Dong L, Li Y, Chen X** (2008b) Characterization of interaction between esculin and human serum albumin in membrane mimetic environments. *J Mol Struct* **889**: 119–128
- Zhang Z, Schwartz S, Wagner L, Miller W** (2000) A Greedy Algorithm for Aligning DNA Sequences. *J Comp Biol* **7**: 203–214
- Zhu J, Jäger K, Black T, Zarka K, Koksharova O, Wolk CP** (2001) HcwA, an Autolysin, Is Required for Heterocyst Maturation in *Anabaena* sp. Strain PCC 7120. *J Bacteriol* **183**: 6841–6851
- Ziegler K, Diener A, Herpin C, Richter R, Deutzmann R, Lockau W** (1998) Molecular characterization of cyanophycin synthetase, the enzyme catalyzing the biosynthesis of the cyanobacterial reserve material multi-L-arginyl-poly-L-aspartate (cyanophycin). *Eur J Biochem* **254**: 154–159
- Ziegler K, Stephan DP, Pistorius EK, Ruppel HG, Lockau W** (2001) A mutant of the cyanobacterium *Anabaena variabilis* ATCC 29413 lacking cyanophycin synthetase : growth properties and ultrastructural aspects. *FEMS Microbiol Lett* **196**: 13–18